



GRADUATE THESIS/DISSERTATION APPROVAL FORM AND SIGNATURE PAGE

Instructions: This form must be completed by all master's and doctoral students with a thesis or dissertation requirement. Please type or print clearly as this form MUST be included as page 1 of your thesis or dissertation via electronic submission to ProQuest. All theses and dissertations must be formatted according to the University and department/program requirements. **Reminder:** It is the responsibility of the student to submit any/all edits requested by the Examining Committee to the Faculty Mentor or Supervising Professor for final approval and signature via the Graduate Program Completion Form.

Type: Master's Thesis PhD/Doctoral Thesis or Dissertation

Thesis or Dissertation Title: Investigation of Modular Taper Material and Design Factors That Affect Mechanically-Assisted Crevice Corrosion at the Femoral Head-Stem Interfaces in Total Hip Arthroplasty

Author's Name: Sevi Berna Kocagoz

Month and Year: June 2020


The signatures below certify that this thesis / dissertation (circle one) is complete and approved by the Examining Committee.

Committee Chairperson's Name: Sriram Balasubramanian, PhD

Title: Associate Professor

Department: BIOMED

Institution (if other than Drexel University): Drexel


Signature: 

Committee Member's Name: Kenneth Barbee, PhD

Title: Professor, Senior Associate Dean, and Associate Dean for Research

Department: The School of Biomedical Engineering, Science and Health Systems

Institution (if other than Drexel University): _____


Signature: 

Committee Member's Name: Adrian Shieh, PhD

Title: Associate Teaching Professor

Department: BIOMED

Institution (if other than Drexel University): Drexel


Signature: 

Committee Member's Name: Steven Kurtz

Title: Research Professor

Department: BIOMED

Institution (if other than Drexel University): _____

Signature: 

Committee Member's Name: Richard Underwood, PhD

Title: Senior Associate

Department: Exponent/Imperial College, London

Institution (if other than Drexel University): Exponent/Imperial College, London

Signature: Richard Underwood

Committee Member's Name: _____

Title: _____

Department: _____

Institution (if other than Drexel University): _____

Signature: _____

**Investigation of Modular Taper Material and Design Factors That
Affect Mechanically Assisted Crevice Corrosion at the Femoral Head-
Stem Junctions in Total Hip Arthroplasties**

A dissertation

Submitted to the Faculty

of

Drexel University

by

Sevi Berna Kocagöz

In partial fulfillment of the

Requirements for the degree

Of

Doctor of Philosophy

June 2020



© Copyright 2020
Sevi B. Kocagoz. All rights reserved.

Dedicated to my parents, Sesin and Tanil

And to my sister, Sezgi

And to my dearest grandmother, Sebahat, who always gives the best advice

Acknowledgements

"Ars longa, vita brevis, occasio praeceps, experimentum periculosum, iudicium difficile."

- *Hippocrates*

This has been one phrase that has resonated with me over the years. Loosely translated into “life is short, and art (craft) long, opportunity fleeting, experimentations perilous and judgement difficult” rings so true to those in the ranks of academia. I greatly appreciate the scientific community in working so tirelessly and building a shared body of knowledge over generations. I am grateful to be part of this community of scientists, past and present. I have had the privilege to work with part of this community of curious and brilliant minds at Drexel University and the Kurtz lab (aka the Implant Research Core).

An optimistic and very important supplement to the quote above is conveyed by Carl Sagan: “science is more than a body of knowledge; it is a way of thinking”. For this I’d like to thank my advisor Dr. Steve Kurtz for encouraging this kind of critical thinking. I’d also like to thank him for his patience over these years in guiding me to become a better engineer, scientist, statistician and writer/communicator. I’d like to thank Dr. Richard Underwood from Exponent Inc. for teaching me everything I know about metrology and failure analysis inspection techniques and providing guidance to navigate grad school.

I’d like to thank the rest of my committee members Dr. Adrian Shieh, Dr. Sriram Balasubramanian and Dr. Kenneth Barbee for their time and feedback in helping shape this dissertation into a tangible, peer-reviewed work.

I’d like to thank Dr. Jeremy Gilbert (and his students Sachin Mali, Shiril Silvan and Eric Ouellette) for hosting my visit at Syracuse University and his deep-dive conversations about implants, corrosion and more. Thank you to Tina Arnholt, my lab mate from the

Implant Research Center, for traveling with me to Syracuse and for your contributions to implant analysis over the years.

Thank you to all my resourceful lab-mates at the IRC whom I've worked and traveled together. They have been my family throughout this process, and they are what made the Implant Research Center a home away from home. Thank you Mariya Tohfafarosh, Tina Arnholt, Dan MacDonald, Genymphas Higgs, Eliza Bober, Sai Veruva, Josa Hanzlik, Alex Sevit, Doruk Baykal and Dave Jaekel! Thank you for the support!

I would also like to acknowledge Dr. Banu Onaral, Dr. Sriram Balasubramanian and Prof. Mike Glaser who encouraged applying human centered design thinking. They helped shape my vision of a project-based, interdisciplinary and social innovation targeted, creative learning space, dLab: the makerspace at Drexel University. I'd also like to thank the College of Engineering at Drexel University for providing the resources for this makerspace and the students who joined!

I'd also like to thank Dr. Judd Day, Dr. Marta Villagra and Ryan Siskey from Exponent, Inc. in Philadelphia for always providing an alternative perspective.

Finally, thank you to my parents and sister for their continued support.

Abstract and Specific Aims

Modularity in total hip arthroplasty (THA) designs allows intraoperative flexibility for the surgeon to adapt leg length and femoral offset to the individual anatomy and gives the option to keep a well-fixed femoral stem and revise femoral head and acetabulum, as needed. In early designs, modularity was only used in the femoral head-stem tapers. In the 1980s-1990s, researchers detected corrosion at this interface; however, the clinical significance was unclear at this time, and the use of modularity continued. Recent design changes to THA include the use of multiple modular interfaces on the stem, and adapter sleeves for additional intraoperative flexibility. Large head metal on metal (LHMOM) bearings had gained popularity to eliminate polyethylene debris from the articulating surfaces and provide improved range of motion. The clinical use of these designs led to increased reports of adverse local tissue reactions (ALTRs), and release of metallic material and corrosion at the modular tapers became a clinical concern. ALTR due to corrosion is also observed in total knee arthroplasty cases. Taper corrosion still poses a clinical risk for all components that employ any modular connections. There is a need to systematically investigate the factors that increase the risk of taper corrosion.

The process leading to corrosion and metallic particle release from modular connections is mechanically assisted crevice corrosion (MACC). The severity of MACC depends on a combination of mechanical, electrochemical, geometrical, material and solution conditions. Previous researchers have investigated the device design and material factors that may lead to variations in these conditions; however, there still does not exist any manufacturing standards for the design and materials of tapers. The goals for this doctoral research were to:

1. Investigate the difference of visual fretting-corrosion damage in the femoral head-stem taper in a matched cohort study comparing THA with ceramic and CoCrMo femoral heads.
2. Develop a method for measuring taper angle clearance. Use developed method to measure retrievals and compare taper corrosion between ceramic and CoCr heads in retrievals using a matched cohort study design as a function of taper angle clearance.
3. Develop and validate a quantitative method to estimate volumetric material lost from the taper surfaces. Use developed method to compare taper corrosion between ceramic and CoCr heads in retrievals using a matched cohort study design as a function of volumetric material loss.
4. Investigate fretting-corrosion behavior of PEEK-metal interfaces and compare with metal-metal interfaces using a previously developed in vitro pin-on-disk fretting-corrosion test system. Explore potential mitigation of taper fretting-corrosion using alternative materials.

The key findings of this research have shown that there was no correlation between taper angle clearance and volumetric material loss. There was a significant correlation between femoral head material and volumetric material loss. Using ceramic heads reduced the total volumetric material loss from femoral head-stem taper junctions. The volumetric material loss from femoral head taper surfaces was higher compared to their mated femoral stem taper surfaces in THAs using CoCrMo alloy femoral heads. Lastly, the fretting currents generated between PEEK-metal material couples was lower

compared to metal-metal material couples tested in vitro using a tribocorrosion pin-on-disk test setup.

Table of Contents

Acknowledgements.....	iv
Abstract and Specific Aims	vi
Abbreviations/Symbols.....	iv
List of Tables	v
List of Figures.....	vii
1__ Overview.....	1
1.1 Motivation.....	1
1.2 Structure of Dissertation.....	5
1.3 Specific Aims and Hypothesis	8
1.4 Background and Significance.....	11
1.4.1 Osteoarthritis	11
1.4.2 Modularity	13
1.4.3 Retrieval Analysis – A systematic review of the clinical significance of corrosion at the head-stem taper of single modular stems in non-MoM THA.....	23
1.4.4 In Vitro Test Methods.....	41
1.5 Need for Quantitative Evaluation of Tapers	54
References	56
2__ Ceramic Biomaterials.....	63
2.1 History.....	63

2.2 Zirconia Toughened Alumina	66
2.2.1 Zirconia phase transformation	68
2.3 Experimental Methods	75
2.3.1 Study Design and Matched Cohort Selection.....	75
2.3.2 Evaluation of Fretting-Corrosion Damage	80
2.4 Results	82
2.5 Discussion	87
References	94
3__Taper Angle Clearance Measurement.....	98
3.1 Introduction	98
3.2 Experimental Methods	113
3.2.1 Study Design, Cohort Selection, and Clinical Information	113
3.2.2 Taper Angle Measurement Method Development	114
3.2.3 Repeatability Study.....	122
3.3 Results	123
3.4 Discussion	130
References	135
4__Volumetric Material Loss	138
4.1 Background and Significance.....	138
4.2 Experimental Methods	142

4.2.1 Study Design.....	142
4.2.2 Estimation of Material Loss From Head Bore Tapers.....	143
4.2.3 Gravimetric validation of volumetric material loss method	148
4.2.3 Estimation of Material Loss from Stem Cone Tapers	154
4.3 Results.....	158
4.4 Discussion	164
References	176
5__ In vitro comparison of PEEK/metal and metal/metal fretting-corrosion.....	179
5.1 Introduction	179
5.1.1 Modified Pin-on-Disk Tribocorrosion Testing.....	181
5.2 Experimental Methods	182
5.3 Results.....	188
5.4 Discussion	202
References	210
6__ Synthesis and Future Directions	212
6.1 Summary of work.....	212
6.2 Observed damage modes and proposed mechanisms of fretting-corrosion	217
6.3 Factors that influence fretting crevice corrosion and recommendations for surgeons and designers	231
6.3.1 Factors that influence MACC.....	231

6.3.2 Recommendations for Assisting Surgical Technique.....	246
6.3.3 Recommendations for Improving Modular Taper Design	248
6.4 Future Directions.....	250
6.4.1 Improving Predictive Capabilities of New Designs	252
6.4.2 Preventing Micromotion.....	254
6.4.3 Understanding the Role of Alloy Metallurgy	257
References	260
Appendix.....	269
References.....	285

Abbreviations/Symbols

ALTR – Adverse Local Tissue Reaction (terminology used in the USA to describe same wide range of biological events as ARMD)

ARMD – Adverse Reaction to Metal Debris (terminology used in Europe to describe same wide range of biological events as ALTR)

THA – total hip arthroplasty

THR – total hip replacement

TJR – total joint replacement

CoCrMo – cobalt, chromium and molybdenum alloy

Ti6Al4V – titanium alloy with aluminum and vanadium

TMZF - titanium-molybdenum-zirconium-iron alloy

OxZr – oxidized zirconium

CoC – ceramic on ceramic bearing articulation

CoP – ceramic on polyethylene bearing articulation

MoP – metal on polyethylene bearing articulation

MoM – metal on metal bearing articulation (usually exists as LHMoM unless it's a hemiarthroplasty)

LHMoM – large head metal on metal bearing articulation

CMM – coordinate measuring machine

MACC – Mechanically assisted crevice corrosion

ZTA – zirconia toughened alumina

List of Tables

Table I: Summary of corrosion resistance, oxidative stress induction, immunogenicity, and carcinogenicity of main transition metals used in manufacturing of metallic devices [84, 233].....	4
Table II: Visual fretting-corrosion scoring method and selection criteria.....	25
Table III: Summary of risk factors investigated in the literature related to fretting-corrosion damage at the taper surfaces.	39
Table IV: ZTA manufacturers and material compositions [142].....	67
Table V: Patient and device information for ceramic and CoCr cohorts. Cohorts were matched previously [143].	114
Table VI: Comparison of visual appearance and score of femoral heads with a single selected axial trace measured from the inside of that femoral head taper and the estimated wear parameters calculated using the axial traces.	139
Table VII: Method to quantify volumetric material loss from retrieval female taper surfaces with fretting-corrosion damage using in-vitro simulated surfaces for method validation.....	144
Table VIII: Method to quantify volumetric material loss from retrieval male taper surfaces with fretting-corrosion damage.....	155
Table IX: Estimated total volumetric material loss and rate of volumetric material loss for CoCr and ceramic cohorts.....	160
Table X: List of correlation between cumulative rate of volumetric material loss from head-stem CoCr cohort and device and patient factors.	163

Table XI: Reported values of quantified material loss from head-stem tapers in previous studies.	171
Table XII: Fretting-scars and other surface changes on the disks and pins post-testing.	200
Table XIII: Patient and device information corresponding to the ceramic-metal cohort in Section 2.3.1.....	269
Table XIV: Patient and device information corresponding to the metal-metal cohort in Section 2.3.1.....	271

List of Figures

Figure 1: Monoblock hip joint replacement with femoral head fixed to the femoral stem.	
Modular hip joint replacement with removable and interchangeable femoral head and stem.	14
Figure 2: Schematic of <i>possible</i> locations of modularity and commercially available examples. Modularity is available at the shell-liner, head-neck, neck-stem, modular-body tapers in total hip arthroplasty designs where MACC may occur. MACC may also occur at Metal-on-Metal articulating surfaces and implant-bone or cement interfaces [6, 109].	15
Figure 3: Figure showing some device design factors that affects the biomechanics of the head-stem modular taper.	18
Figure 4: The taper dimensions that are used in taper angle definition.	19
Figure 5: The expected contact location between the head and stem taper based on the taper angle clearance value.	20
Figure 6: Figure showing 3 different examples of retrieval stem tapers, photographed at the same scale to show the difference of available stem taper size and surface finish.	21
Figure 7: The contact type based on offset and taper size. Type 1 contact has as-manufactured surfaces on both the distal and proximal end. Type 2 contact only has as-manufactured surfaces available on the proximal end of the head taper. More as-manufactured surfaces that are available enable improved as-manufactured surface approximation for data fitting. Type 1 contact is more accurate than Type 2 because linear fitting is improved with available data spaced apart.	22
Figure 8: An example each of a micro-grooved and smooth stem taper. The figure is showing the photo of a micro-grooved stem (A) and corresponding surface profile with a	

typical grooved topography (B). The bottom row is showing a photo of representative smooth stem taper (C) and corresponding surface profile with a typical smooth topography (D) [7].	23
Figure 9: Screening of articles obtained from compiled database searches. The exclusion criteria at different levels is shown and the final number of articles included were 34. ..	28
Figure 10: The equilibrium oxidation and reduction reactions taking place at the surface of a metal. Ion dissolution and anodic and cathodic currents are generated during the formation of the protective oxide film [84].	45
Figure 11: Summary of factors that may contribute to MACC in a total joint arthroplasty.	49
Figure 12: Wear scar section on stationary disk measured using stylus profilometer [207].	50
Figure 13: Page from the standard ASTM F1875 showing test system setup.	53
Figure 14: Summary possible device, surgical and patient factors and the potential revision outcome due to severe fretting-corrosion.	55
Figure 15: Scanning electron microscopy image of ZTA composite after polishing and thermal etching the surface. Alumina grains are the larger grains in grey and zirconia grains are smaller and white [210].	71
Figure 16: Crack propagation in a ZTA ceramic progressing at the alumina grain boundaries (a) and halting at the zirconia region (white – tetragonal phase) due to stress induced phase transformation and increased zirconia grain volume (red – monoclinic) (b).	72

Figure 17: Crack propagation and halting in a ZTA ceramic with strontium aluminate (gold) and tetragonal zirconia (white) reinforcing particles present among the dark grey alumina grains.	74
Figure 18: The flow of retrieved implants and deidentified patient data in the Repository.	76
Figure 19: The femoral stem taper fretting and corrosion damage scores for the matched ceramic and CoCr head cohorts are shown. The damage scores were significantly lower for the ceramic cohort ($p = 0.03$).	84
Figure 20: Some examples of stem taper fretting and corrosion scores for the ceramic-metal cohort (median score 2) and metal-metal cohort (median score 3).	85
Figure 21: A boxplot illustrating femoral stem taper fretting and corrosion score versus stem alloy for the ceramic and metal head cohorts is presented.	85
Figure 22: SEM images of five different design and materials for the stem tapers implanted with ceramic heads (A) TMZF (Stryker Orthopedics, Mahwah, NJ, USA) 9 35 BEC, (B) Ti-6Al-4V (Zimmer, Inc, Warsaw, IN, USA) 9 100 SEI, (C) Ti-6Al-4V (Wright Medical Technology, Inc, Arlington, TN, USA) 9 220 BEC, (D) Co-Cr-Mo (DePuy Orthopedics, Inc, Warsaw, IN, USA) 9 100 BEC, (E) Co-Ni-Cr-Mo (Zimmer) 9 100 BEC. SEI = secondary electron imaging; BEC = backscattered electron contrast image. A is a ground surface, whereas B–E have machining grooves present. Also shown are fretting scars and corrosion and biological debris present. For grooved implants, only the groove tips show evidence of fretting corrosion damage.	86
Figure 23: Backscattered electron micrographs of (A) TMZF, (B) Ti-6Al-4V, (C) Co-Cr-Mo, and (D) CoNiCrMo alloy tapers used in conjunction with ceramic femoral heads.	

Backscattered evaluation makes corrosion deposits appear black and help identify fretting damage and some corrosion debris present. In C, the damage has a distinctly corrosion-like appearance emanating from a machining ridge. 87

Figure 24: Illustration of hypothesized toggling mechanism of the femoral head due to applied cyclic loading and mismatched stem taper. Asymmetric damage mode may be seen in proximal-superior and distal-inferior regions. 99

Figure 25: Stylus types available on the Talyrond 585 a) 5µm diameter tip diamond stylus, b) 4mm diameter ruby sphere. 107

Figure 26: Measurement of the internal taper of a femoral head using a diamond stylus and a ruby stylus. There are clear resolution differences between the two measurements even though measurements with both styli collected the same number of data points. Each surface map is comprised of 720 profiles, 160001 points per profile and 11.5 million data points. Axial profiles 108

Figure 27: Distortion of a measured profile due to finite dimensions of stylus tip [232]. 109

Figure 28: Distortion of a measured profile due to finite dimensions of stylus tip [232]. 110

Figure 29: Example axial trace from a ceramic (BioloX Delta) head taper. 112

Figure 30: Axial profiles showing differences in surface topography for a smooth and micro-grooved stem taper. The bell-shaped curve of the profile is due to manufacturing form. 112

Figure 31: Process showing the preliminary axial (a) and circumferential (b) traces measured for inspection and determination of regions with material loss and corrosion.

The Talyrond 585 software allows the manual exclusion of user defined regions and does least squares fitting only on the as-manufactured sections of the profile. The axial profile shows exclusion of material loss and the circumferential profile shows the exclusion of debris.....	116
Figure 32: Stem taper axial profiles taken from the same stem at different locations 360° around the circular axis. The profile taken at 0° shows irregular changes in the profile which has been determined to be material loss due. For the profiles taken at 30° and 150°, the change in the profile seen in the proximal end is an example of change of form during implantation due to stem taper proximal end getting fitted into the head taper and getting compressed in the proximal region.	118
Figure 33: Schematic diagram showing the taper angle clearance, a) shows positive taper angle clearance and proximal head/stem contact, b) shows negative taper angle clearance and distal head/stem contact. These figures are only representatives of the theoretical contact at the taper-trunnion junction. In vivo, while the overall contact area will be located proximally or distally, the contact surfaces may not be axisymmetric and may have a contact area larger on the superior or inferior side with only a point contact on the other side.....	119
Figure 34: The radius and relative height of each LS circle was compiled in a spreadsheet and the linear slope of the 5-7 profiles were used to calculate the angle. Areas with corrosion debris were excluded from the measurements. Measurements were only taken in as-manufactured surfaces.....	121
Figure 35: Examples of Talyrond traces for components with observable regions of material loss proximally (a), distally (b) and in both proximal and distal locations (c). The	

red lines on the schematic of the femoral heads represent the orientation of the profiles being measured. These profiles provide information about the taper-trunnion junction in addition to the clearance values observed for the metal cohort. 122

Figure 36: Examples of Talyrond traces for components with observable regions of material loss proximally (a), distally (b) and in both proximal and distal locations (c). The red lines on the schematic of the femoral heads represent the orientation of the profiles being measured. These profiles provide information about the taper-trunnion junction in addition to the clearance values observed for the metal cohort. 123

Figure 37: Taper angle measurements for the ceramic and metal head-stem pairs. There is no overlap in the taper and trunnion angle measurements for the ceramic cohort, while there is overlap in the metal cohort. 124

Figure 38: Taper angle clearance distribution for the ceramic and metal cohorts. The taper angle clearance for the ceramic cohort is always greater than zero (indicating proximal contact), while the metal cohort has clearance values that are greater and smaller than zero (indicating a mixture of proximal and distal contact). 125

Figure 39: Metal transfer was observed on the proximal ends of the internal tapers of ceramic heads, providing visual confirmation for clearance values greater than zero for the ceramic cohort. 125

Figure 40: Distribution of measured ceramic and metal cohorts according to a) trunnion fretting corrosion score, and metal cohort according to b) metal head fretting corrosion score. 126

Figure 41: SEM image taken in distal portion of metal head taper showing fretting in regions with horizontal bands of material loss. Bands of material loss most likely

corresponded to regions in contact with trunnion as-manufactured grooves (370x, BEC).

..... 127

Figure 42: A component showing pitting corrosion (marked in white circles) initiated preferentially in a crevice formed due to fretting abrasion (5-40µm scratches), imaged midway between proximal and distal ends on the taper (left, BEC, 1400x). A different component showing scratches (50-500µm) throughout head taper, with preferential pitting inside the scratches, imaged midway between proximal and distal ends on the taper (right, BEC, 600x). Corrosion by-products (biological and electrochemical deposits) have accumulated inside the scratches..... 127

Figure 43: Axial profile of a metal head implanted with a trunnion with a “smooth” finish (left). Regions corresponding to the material loss, marked A and B were imaged using the SEM (right). Both regions of material loss on the Talyrond profile showed evidence of change to the as-manufactured surface. 128

Figure 44: Axial profile of a metal head implanted with a “microgrooved” trunnion finish (left). Regions corresponding to the material loss, marked C and D were imaged using the SEM (right). Both regions of material loss on the Talyrond profile showed evidence of change to the as-manufactured surface. 128

Figure 45: Schematic diagram showing the taper-trunnion interface and typical SEM image and measured profiles from head taper mated with microgrooved trunnion. The red dotted lines represent locations used for roundness profile measurements. 129

Figure 46: An example femoral head axial profile inspected using the Talyrond software. The regions with material removal and in this case appear like imprinting on the femoral

head had a significantly higher surface roughness. The Ra value of the as-manufactured surface was $0.99\mu\text{m}$, and the region with material removal had an Ra value of $2.3\mu\text{m}$.	129
Figure 47: The profile of the regions that appear like imprinting on the femoral head was compared with the stem axial profile. They had very similar profiles, both with a topography amplitude of $\pm 4\mu\text{m}$ and similar surface roughness. The region with material removal on the femoral head (same from Figure 46) had an Ra value of $2.3\mu\text{m}$ and the stem profile had an Ra value of $2.3\mu\text{m}$.	130
Figure 48: There is a large variability in the range of estimated volumetric material loss in components with severe (4) visual fretting-corrosion scores.	139
Figure 49: Example of an imported axial trace and analysis in custom MATLAB R2016a. The user is prompted to select limits on the proximal and distal ends to select region to exclude during least squares fitting to identified as-manufactured surfaces.	144
Figure 50: Exemplar taper adapter sleeves and femoral heads used for gravimetric validation.	149
Figure 51: Example cylinder map of one of the most severe cases of material loss among the retrieval tapers.	150
Figure 52: Summary of gravimetric material removal using a lathe and Dremel.	151
Figure 53: In vitro material removal using lathe and Dremel setup to simulate axisymmetric material loss. The low amount of depth of material loss ($20\mu\text{m}$) and the high amount of depth of material loss ($60\mu\text{m}$) are within the range of in vivo material loss observed in the retrieval cohorts also evaluated earlier in Chapter 4.	151
Figure 54: In vitro material removal using lathe and Dremel setup simulating asymmetric material loss. Asymmetric material loss is speculated to occur due to toggling.	152

Figure 55: Linear fitting calculated volumetric removal data using our previously described method with a customized Matlab script and the gravimetric material removal measurement. There is very good fit (>95%) between the two sets of data showing >99% reliability of the volumetric removal estimation method.....	152
Figure 56: Sensitivity analysis comparing number of axial profiles and normalized volumetric material loss. With this analysis we were looking for the minimum number of profiles needed to stay within 1% accuracy of 144 profile measurements and 24 profiles meets this requirement and saves >2hrs in measurement time.	153
Figure 57: Box plots showing the rate of material loss from the metal and ceramic cohorts. The median and the maximum value seen for the CoCr cohort (median = 0.1 mm ³ , maximum = 9 mm ³) are an order of magnitude greater compared to the ceramic cohort (median = 0.0 mm ³ , maximum = 0.4 mm ³). Outliers with asterisks indicate a value taken from a Type 2 pattern of material loss.	159
Figure 58: A region of metal transfer was observed on the proximal end of 42/50 of the ceramic tapers. For ceramic heads, the head bore taper and matching stem cone taper geometry is designed to have highest contact pressure at the proximal end.	159
Figure 59: The box plots for rate of material loss at CoCr head bore and stem cone tapers show a difference between head and stem surfaces. Outliers with asterisks indicate a value taken from a Type 2 pattern of material loss.....	161
Figure 60: Correlation between visual fretting corrosion score and estimated volumetric material loss in the CoCr cohort.	161
Figure 61: Correlation between visual fretting corrosion score and estimated volumetric material loss in the CoCr cohort.	166

- Figure 62: Stylus tip evidence of plastic deformation on the taper surface of one of our measured CoCrMo femoral heads. This deformation does not affect the results and the effects are negligible. The same area is shown with different magnifications to give an idea of the plastic deformation relative to the size of other features, a) mag 65x, showing machining marks, b) mag 200x, showing machining marks and stylus tip plastic deformation, c) mag 500x showing plastic deformation up close. 167
- Figure 63: Flat circular disk and cone-shaped flat bottom pin (tip diameter ranging from 0.35 to 0.8 mm) combinations tested in triplicate..... 183
- Figure 64: “PEEK pellet sandwich” testing setup where a thin and small PEEK disk is placed between a CoCrMo pin and disk and variable load pin-on-disk testing was carried out in this configuration. 184
- Figure 65: Microscopic examination and optical profiling of surfaces of each sample using the KH-8700, HIROX optical microscope..... 184
- Figure 66: Previously published tribocorrosion test set-up schematic and photo [226]. Test solution PBS (pH 7.4). Fretting is simulated by the piezoelectric actuator. Motion of pin relative to disk is captured with the DVRT. 186
- Figure 67: Pin tips and disks inspected using scanning electron microscopy (JEOL JSM-5600) and optical microscopy (KH-8700, HIROX) for quantification of contact area. Area calculation feature is available on the KH-8700 by selecting the worn area. 188
- Figure 68: Pin tips and disks inspected using scanning electron microscopy (JEOL JSM-5600) and optical microscopy (KH-8700, HIROX) for quantification of contact area. Area calculation feature is available on the KH-8700 by selecting the worn area. 189

Figure 69: Pin tips and disks inspected using scanning electron microscopy (JEOL JSM-5600) and optical microscopy (KH-8700, HIROX) for quantification of contact area.

Area calculation feature is available on the KH-8700 by selecting the worn area. 190

Figure 70: Fretting-current density ($I(\text{Amps}/\text{cm}^2)$) vs. time depicts the orders of magnitude difference in currents generated between the Ti/CoCr material couple (in black) and the Ti/PEEK couple. Arrows show fretting initiation. The spikes in fretting-current at the initiation of fretting (where the arrows are) and sometimes at the end of fretting are noise and were excluded from analysis. 191

Figure 71: Average fretting current density vs. work done per cycle of fretting for all four material couples. Work done and average fretting current density is significantly higher for metal-metal couples compared to PEEK-metal. Average values obtained from triplicate tests for each material couple is compiled. 192

Figure 72: Coefficient of friction during sliding motion (left) vs. sticking (right). 193

Figure 73: Representative tangential force vs. displacement graph for CoCrMo/Ti6Al4V. At each applied load, fretting motion exhibits a hysteresis loop behavior. The maximum tangential force increases, and displacement decreases during fretting with increasing applied normal load F_N . At the maximum normal load of 30N in this case, there is no displacement, sticking is achieved. The F_t seen is elastic behavior and for that fretting loop, the work is equal to zero. 194

Figure 74: Representative tangential force vs. displacement graph for a) PEEK/Ti6Al4V and b) PEEK/CoCrMo. At each applied load, fretting motion exhibits a hysteresis loop behavior. The maximum tangential force increases, and displacement decreases during fretting with increasing applied normal load F_N . The maximum normal load where stick

happens is reached at 12N for (a) and 16N for (b) which is lower than the maximum load for metal/metal couples.....	195
Figure 75: Work per cycle of fretting vs. real normal stress is reported for all material couples. Sticking of the pin on the disk begins at the peak work value. Average values obtained from triplicate tests for each material couple is compiled.	197
Figure 76: Example damage zones identified on the optical microscope (KH-8700, HIROX) for CoCrMo and PEEK post testing. Damage zones identified based on scratches in different appearance than machining marks. The surface area calculation feature on the microscope is used to find real contact area.	197
Figure 77: Coefficient of friction (COF) values vs. real normal stress for all material couples. Irrespective of material couple, COF values start higher and decreases quickly in a small range of applied stress and reaches a plateau value. Average values obtained from triplicate tests for each material couple is compiled.	198
Figure 78: PEEK pellet SEM scratching seen after test 1 and test 2. Different pellets were used for each test. The images above are the same region with different magnification, focusing on the most damaged area.	201
Figure 79: Representative surface scratching for CoCrMo post-test. Representative galling damage for Ti6Al4V post-test.	201
Figure 80: Discrepancy between the true asperity-asperity contact area and the nominal contact area. The nominal contact area is equal to the area of the observed fretting-wear scar post-testing [225].....	204

- Figure 81: Schematic representation of the pin on disk contact of the pin tip and disk. A) ideal smooth, nominal contact is in brown. B) real asperity-asperity contact area in brown. 204
- Figure 82: Characteristic elastic-sliding response hysteresis loop (right image, [170]) was observed in the current study (left image). The sliding amplitude at a given normal load can be directly measured from the F_t vs. displacement graph. 206
- Figure 83: SEM images from a study investigating the effect of load and pH on fretting-corrosion [170]. They have observed tribofilm formation at high loads. 208
- Figure 84: SEM and HIROX microscopy of PEEK pin surface after testing. There appears to be some type of film formation surrounding the surface that has evidence of mechanical wear. The exact composition and process of formation of this film is unknown, let alone the role it plays during the fretting-corrosion tests. We would like to note; however, that we observed this film on all three PEEK pins post testing and on none of the metal surfaces. 209
- Figure 85: Also Figure 41 from Chapter 3, SEM image taken in distal portion of metal head taper showing fretting in regions with horizontal bands of material loss. Bands of material loss most likely corresponded to regions in contact with trunnion as-manufactured grooves (370x, BEC). 220
- Figure 86: Also Figure 42 from Chapter 3, a component showing pitting corrosion (marked in white circles) initiated preferentially in a crevice formed due to fretting abrasion (5-40 μ m scratches), imaged midway between proximal and distal ends on the taper (left, BEC, 1400x). A different component showing scratches (50-500 μ m) throughout head taper, with preferential pitting inside the scratches, imaged midway

between proximal and distal ends on the taper (right, BEC, 600x). Corrosion by-products (biological and electrochemical deposits) have accumulated inside the scratches. 221

Figure 87: Also Figure 43 from Chapter 3, axial profile of a metal head implanted with a trunnion with a “smooth” finish (left). Regions corresponding to the material loss, marked A and B were imaged using the SEM (right). Both regions of material loss on the Talyrond profile showed evidence of change to the as-manufactured surface. 222

Figure 88: Also Figure 44 from Chapter 3, axial profile of a metal head implanted with a “microgrooved” trunnion finish (left). Regions corresponding to the material loss, marked C and D were imaged using the SEM (right). Both regions of material loss on the Talyrond profile showed evidence of change to the as-manufactured surface. 223

Figure 89: Also figure 46 from Chapter 3, an example femoral head axial profile inspected using the Talyrond software. The regions with material removal and in this case appear like imprinting on the femoral head had a significantly higher surface roughness. The Ra value of the as-manufactured surface was $0.99\mu\text{m}$, and the region with material removal had an Ra value of $2.3\mu\text{m}$ 224

Figure 90: Schematic diagram showing the taper-trunnion interface and typical SEM image and measured profiles from head taper mated with microgrooved trunnion. The red dotted lines represent locations used for roundness profile measurements. The profile of the regions that appear like imprinting on the femoral head was compared with the stem axial profile. They had very similar profiles, both with a topography amplitude of $\pm 4\mu\text{m}$ and similar surface roughness. The region with material removal on the femoral head (same from Figure 46) had an Ra value of $2.3\mu\text{m}$ and the stem profile had an Ra value of $2.3\mu\text{m}$ 226

- Figure 91: Published by Hall et al. 2018 [98], comparison of the initial stem taper topography (black) with the head taper topography (blue) showing imprinting has shown matching of the imprinting pattern with the stem taper topography. They also observed higher imprinting damage in the distal end of the taper and gradual decrease along the axis towards the proximal end. 226
- Figure 92: Published by Hall et al. 2018 [95], a) SEM micrograph of column damage on a femoral head taper that is characterized by deep grooves or troughs in proximal distal direction. (b) Close up image on column damage showing the etched appearance within the troughs of the damage pattern. Locally, organic residue has accumulated within the troughs..... 230
- Figure 93: The occurrence of fretting-corrosion damage is multifactorial, dependent on taper design (implant), assembly (surgical technique) and patient factors. The current workflow includes observing these damage mechanisms using retrieval analysis, replicating damage modes and verifying mechanisms using in vitro testing and making modifications to taper designs based on results from retrieval analyses and in vitro tests. 232
- Figure 94: A) Accolade TMZF femoral stem retrieval taper without any signs of GTF, B) Accolade TMZF stem retrieval taper with impending GTF, C) Accolade TMZF stem retrieval taper with a severe case of GTF. Images B and C were published by Urish et al. [239] and image A is from our retrieval studies in chapters 3 and 4. 239
- Figure 95: Also published in [143] SEMs of five different design and materials for the male taper of ceramic-metal trunnions. (A) TMZF (Stryker Orthopaedics, Mahwah, NJ, USA) \times 35 BEC, (B) Ti-6Al-4V (Zimmer, Inc, Warsaw, IN, USA) \times 100 SEI, (C) Ti-

6Al-4V (Wright Medical Technology, Inc, Arlington, TN, USA) \times 220 BEC, (D) Co-Cr-Mo (DePuy Orthopaedics, Inc, Warsaw, IN, USA) \times 100 BEC, (E) Co-Ni-Cr-Mo (Zimmer) \times 100 BEC. SEI = secondary electron imaging; BEC = backscattered electron contrast image. (A) is a ground surface, whereas (B–E) have machining grooves present. Also shown are fretting scars and corrosion and biological debris present. For grooved implants, only the groove tips show evidence of fretting corrosion damage..... 243

1 Overview

1.1 Motivation

Metallic biomaterials are used in a wide variety of biomedical applications including orthopedic, spinal, dental, urological, and cardiovascular applications. Metals provide desired mechanical properties, unique electrical properties for cardiac leads, ease of manufacturing and overall satisfactory performance in biomedical device applications. However, there is concern about metals susceptibility to corrode and release ions and particles over the lifetime of being implanted. These degradation products may lead to an inflammatory reaction and potentially elicit adverse local tissue reactions and in rare cases, failure by fracture due to compromised structural integrity of the implant [84]. Biocompatibility of metals has been associated with their corrosion resistance in vitro and this has been a useful guide for material selection for implants. However, looking only at corrosion resistance is a limited and incomplete view of the electrochemical interaction of metals in the body.

The in-situ fretting-wear and corrosion of metallic biomaterials in total hip arthroplasty have been observed through retrieval studies on modular connection surfaces. The incidence of femoral head and stem taper fretting and corrosion is not new [85]; however, the clinical significance of these observations was unclear. The rise in attention to this problem is observed by the increase in publications per year focusing on modular taper corrosion in the late 2000s. The increased concern in this time frame is due to the clinical significance of the adverse local tissue reactions (ALTRs) reported in total hip arthroplasty (THA) with large head metal-on-metal (LHMoM) bearing combinations [237]. The reported ALTRs are a wide range of biological events that may include

pseudotumor formation and other inflammatory reactions and have a high reported incidence in LHMOM (head diameter ≥ 36 mm) bearing designs. The higher than expected revision rate of LHMOM bearings compared to other bearing combinations has raised concern about the release of metal wear particles and corrosion products from any THA with modular tapers because there was a higher than expected incidence of taper corrosion observed during revision surgery for LHMOM bearings [231].

Prior to the new millennium, the biggest challenge for total hip and knee replacements was reducing the wear particles generated from the bearing surfaces of cobalt chromium molybdenum (CoCrMo) alloy articulating against conventional polyethylene (PE). In THA CoCrMo femoral heads articulating against PE liners have led to severe cases of osteolysis and adverse local tissue reactions and have a higher cumulative revision rate compared to newer material combinations using highly crosslinked polyethylene (XLPE) or ceramic acetabular liners [10] [135]. Hence, the use of conventional PE liners has been replaced with new generation materials and the potential threat for the longevity of next generation total joint replacements (TJR) are wear particles and corrosion products from modular tapers.

Over the years, metallic biomaterial alloys used in orthopedic implants have evolved to improve wear and corrosion resistance. Early designs of orthopedic biomaterials used 316 L Stainless Steel (nominal composition, in weight %, 17-20% Cr, 10-14% Ni, 2-3% Mo, approx. 65% Fe) and cast Vitallium (nominal 64-31-5 Co-Cr-Mo) [40, 52]. Current orthopedic implants use a fine-tuned composition of CoCrMo alloy (ASTM F 75 alloy (UNS R30075), nominal 62-26-5 Co-Cr-Mo) like the Vitallium composition. For both stainless steels and cobalt alloys, the addition of chromium (Cr)

enhances passivity in aqueous media and encourages the formation of protective oxide films in addition to the strengthening effect of forming stable metal carbides at the grain boundaries. Addition of molybdenum (Mo), acts by increasing lattice strain, thus increasing the energy required to dissolve out iron atoms from the surface [63].

In 1984, titanium alloys were introduced for use in total joint replacements [161]. Titanium alloys were originally developed for the aerospace industry in the early 1950s because of their high strength-to-density ratios. In addition to this attractive property, recognition of the excellent resistance of titanium to many highly corrosive environments, particularly oxidizing and chloride-containing process streams, has led to widespread non-aerospace (industrial) applications. The high corrosion resistance of titanium alloys results from the formation of very stable, continuous, highly adherent, and protective surface oxide films. Because titanium metal itself is highly reactive and has an extremely high affinity for oxygen, these beneficial surface oxide films form spontaneously and instantly when fresh metal surfaces are exposed to air and/or moisture. Damaged oxide film can re-heal itself instantaneously if at least traces of oxygen or water are present in the environment [64].

In vitro studies have tested the commonly used biomedical metals, namely 316 stainless steel (ASTM F55-56), Co–Cr alloys (ASTM F75) and Ti6Al4V (ASTM F 136) alloys under clinically relevant simulated electrochemical conditions [221, 250]. Even though these biomaterials are highly corrosion resistant in vitro, the overwhelming evidence from retrieval studies show that all modular interlocking surfaces in total hip arthroplasty (THA) have the potential to release corrosion products due to the mechanical and solution conditions in vivo that may lead to mechanically assisted crevice corrosion

(MACC). This is concerning because corrosion products may lead to adverse systemic and periprosthetic adverse reactions [42]. Table I summarizes the potential immunogenic and carcinogenic effect of the ions that may be released during corrosion of commonly used Co and Ti alloys for orthopedic applications. Additionally, it is known that any metal particles and ions may lead to acute or chronic inflammation resulting in osteolysis [84]. In future generations of THA, the biomechanical loads and geometry of the design must be considered in addition to the corrosion resistance of the materials to minimize the wear particles and degradation products in vivo.

Table I: Summary of corrosion resistance, oxidative stress induction, immunogenicity, and carcinogenicity of main transition metals used in manufacturing of metallic devices [84, 233]

	Corrosion resistance	Oxidative stress induction	Immunogenicity	Carcinogenicity
Cobalt	High due to CoO. Passive layer stable in neutral and alkaline environment.	Yes. Co ²⁺ can generate reactive oxygen species (ROS) by Fenton reaction (FR).	Yes, can induce different mechanisms of immune response.	Yes. Co can induce chromosome aberration in bone marrow.
Chromium	High due to Cr ₂ O ₃ , also CrO ₃ , CrOOH	Yes. Cr ⁶⁺ more harmful than Cr ³⁺ but unstable. ROS generated by FR.	Yes, can induce different mechanisms of immune response.	Yes. Genotoxicity of Cr ⁶⁺ in vitro and in vivo well documented. Implicated in lung and small intestine cancers.
Iron	Poor due to unstable passive layer.	Yes	Not documented	No

Table I (continued):

Molybdenum	High due to mostly MoO ₂ . MoO ₃ in acidic solutions. Stable in neutral and acidic solutions.	No	Yes	No
Nickel	High due to NiO, Ni ₂ O ₃ , Ni(OH) ₂ . Stable in alkali environment.	Yes. Ni ²⁺ /Ni ³⁺	Yes. Is the most common metal sensitizer for humans. Well documented.	Yes but in vitro
Titanium	Excellent. Due to TiO ₂ , highly adherent. Stable in acidic environment.	Controversial	Yes	Not documented
Vanadium	Strong due to VO, V ₃ O, V ₂ O ₃	Yes	Yes	Yes. V ⁵⁺ and V ⁴⁺ have induced micronuclei, aneuploidies, and chromosome aberrations.

1.2 Structure of Dissertation

The first chapter, the overview, includes the introduction and motivation for conducting this research on taper corrosion. It also presents a detailed systematic review of the clinical performance of total hip arthroplasty with modular head-stem taper junctions through retrieval studies. This review asked what clinical and device factors were identified in retrieval studies as the possible causes leading to corrosion in modular

tapers and what treatments/solutions were most utilized during revision surgery. Studies that conducted in vitro testing were excluded from the systematic review; however, relevant in vitro studies are presented later in the chapter to introduce the reader to possible design and material screening methods for future generation implants.

The systematic review performed in Chapter 1 shows that revision of metal femoral heads to ceramic femoral heads (and either polyethylene or ceramic liners) are a clinically significant solution to taper corrosion. Chapter 2 gives an overview of history and performance of ceramic biomaterials, specifically zirconia toughened alumina (ZTA), being used for total hip arthroplasty. The information in the first section of Chapter 2 was published in *Journal of the Mechanical Behavior of Biomedical Materials* titled “Advances in Zirconia Toughened Alumina Biomaterials for Total Joint Replacement”. The next section of Chapter 2 details the matched cohort study design we utilized to investigate the incidence of taper corrosion in THA with ceramic femoral heads compared to metal femoral heads. The information in this section was published as a manuscript in *Clinical Orthopedics and Related Research* titled “Do Ceramic Femoral Heads Reduce Taper Fretting Corrosion in Hip Arthroplasty? A Retrieval Study”.

Chapter 3 is an introduction to metrology and profilometry techniques and the details of a newly developed taper angle clearance measurement method for retrieved head- stem taper junctions. The measurement technique is used to measure the taper angle of the femoral heads and stems of the same matched retrieval cohort mentioned in Chapter 2. The findings are printed as a single manuscript in *Seminars in Arthroplasty* titled “Does taper angle clearance influence fretting and corrosion damage at the head–stem interface? A matched cohort retrieval study”.

Chapter 4 presents a novel method to estimate volumetric material loss from femoral head tapers and stem trunnions. Some of the work that went into the development and validation of the material loss estimation method has been published in the *ASTM STP 1560: Metal-on-Metal Total Hip Replacement Devices* (2013) issue as a technical publication titled “A Protocol to Assess the Wear of Head/Neck Taper Junctions in Large Head Metal-on-Metal (LHMoM) Hips”. The retrieval study completed in Chapter 4 uses the same devices in Chapters 2 & 3 for the matched ceramic and CoCrMo femoral head cohorts. This chapter also used never implanted femoral heads and sleeves to gravimetrically validate the novel volumetric material loss method. The findings in this chapter have been previously used for the manuscript titled “Ceramics Heads Decrease Metal Release Caused by Head-Taper Fretting and Corrosion” published in *Clinical Orthopedics and Related Research*.

Chapter 5 in vitro electrochemical pin-on-disk fretting-corrosion testing of metal/metal and PEEK/metal interfaces. This chapter gives some information about the basic electrochemical and mechanical forces interacting and influencing fretting-corrosion. The findings in this chapter show that the fretting currents, which is an established measurable metric for corrosion processes, are significantly lower for PEEK/metal interfaces compared to metal/metal interfaces. The information in this chapter is being prepared as a separate peer-reviewed publication for *Journal of Biomedical Materials Research - Part B Applied Biomaterials* or similar relevant journal.

1.3 Specific Aims and Hypothesis

Specific Aim 1

Investigate the difference of visual fretting-corrosion damage in the femoral head-stem taper in a matched cohort study comparing total hip arthroplasty with ceramic femoral heads and CoCrMo femoral heads.

Rationale: Modular head-neck taper corrosion is a clinical concern; however, there is little information known about the taper corrosion ceramic femoral heads.

Hypothesis: Implants using ceramic heads will have less taper corrosion compared to CoCrMo femoral heads.

Specific Aim 2

Develop method for measuring taper angle clearance. Use method to measure retrievals and compare taper corrosion between ceramic and CoCr heads in retrievals using a matched cohort study design as a function of taper angle clearance.

Rationale: Taper angle mismatch between the femoral head and stem has been an associated clinical risk factor for taper corrosion due to the possibility of toggling motion. It is assumed that this toggling motion will initiate fretting-corrosion; however, the direct relationship between taper angle mismatch and clinical performance has not been studied.

Hypothesis: Femoral head-stem contact location will be different for hips with ceramic heads compared to CoCrMo heads. Contact location will directly be correlated with fretting-corrosion damage location.

Specific Aim 3

Develop and validate a quantitative method to estimate volumetric material lost from the taper surfaces. Use method to measure retrievals and compare taper corrosion between ceramic and CoCr heads in retrievals using a matched cohort study design as a function of **volumetric material loss**.

Rationale: The visual semi-quantitative fretting-corrosion method has been a useful resource to compare damage severity within and between publications and identify correlations between damage scores and other factors. It is especially useful for identifying risk factors associated with components with consistently high scores. However, the relationship between volumetric material loss and corrosion scores in LHMOM implant tapers show a wide variation for high damage scores. Visual scoring methods are not as reliable as quantitative methods and there is a need for a practical quantitative method to evaluate volumetric material loss from tapers.

Hypothesis: The highly accurate measurement method of using a roundness machine will enable the development of a reliable and repeatable taper angle clearance measurement method for both femoral head and stem tapers provided they have sufficient as-manufactured surfaces to allow linear fitting.

Specific Aim 4

Investigate fretting-corrosion behavior of PEEK-metal interfaces and compare with metal-metal interfaces using a previously developed in vitro pin-on-disk fretting-corrosion test system as a mitigation solution to taper fretting-corrosion using **alternative materials**.

Rationale: PEEK biomaterials have been a viable solution for spinal orthopedic applications. Its in vivo chemical stability and strength to weight ratio make it an attractive option for THA.

Hypothesis: PEEK/metal interfaces will decrease the fretting currents generated during the pin on disk testing compared to metal/metal test couples.

1.4 Background and Significance

1.4.1 Osteoarthritis

Osteoarthritis of the joint is a debilitating condition which affects healthy tissue around the hip socket leading to degeneration of articular cartilage, narrowing of the joint space and development of bone spurs. Osteoarthritis of the hip and knee may cause pain and stiffness and affect the ability to do everyday activities like walking, climbing stairs and bending. Osteoarthritis develops slowly and the pain worsens over time. There is no specific cause for the development of osteoarthritis; however, certain factors such as increasing age, family history of osteoarthritis, previous injury to the joint, obesity, and developmental dysplasia lead to higher risk. Osteoarthritis most of the time is seen in patients older than 50 years of age; yet may be seen in younger patients too. In the US, more than 28 million people were estimated to have osteoarthritis in 2011, and this number is projected to increase with the aging baby-boomer population [146]. Non-surgical treatments including lifestyle modifications, anti-inflammatory medications and physical therapy may help alleviate pain, slow down the progression of osteoarthritis, increase motion and improve strength. Removing bone spurs using arthroscopy, realigning long bones of the arms or legs to take pressure off the joint with osteotomy and joint fusion are also options to alleviate symptoms; however, total joint replacements currently provide the most successful treatment option that alleviates pain and restores function.

Osteoarthritis is the principal diagnosis for total hip replacement procedures (88.5%), followed by fractured neck of femur (4.1%), osteonecrosis (3.4%), developmental dysplasia (1.3%) and rheumatoid arthritis (1.1%) [10]. In 2013, an

estimated 399,700 primary hip replacement procedures and 61,400 (15%) revision hip replacement procedures were performed in the US [176] and is expected to increase to an estimate of 572,000 primary procedures and 96,700 (14%) revision hip replacement procedures by the year 2030 [146]. According to the Orthopedic Research Network 15.2% of the hip procedures in 2013 were revision hip procedures. This statistic is referred to as the “revision burden” and is compared in many international registries as the percentage of cases that are revisions compared to primary and revision procedures [176]. The Australian registry in 2014 reported the cumulative percent revision of primary (1st) revisions at 10 years is 21.6% [135]. This percentage of revision surgeries is similar in the US and was found to be between 15-20% of the primary surgeries between 1990 and 2002 in the National Hospital Discharge Survey [135].

The five most common types of revision recorded by the Australian Registry are femoral only (31.4%), acetabular only (22.7%), head and insert (19.1%), THR (femoral/acetabular) (12.0%) and head only (5.1%). The most common reason for revision is loosening/lysis (28.0%), followed by prosthesis dislocation (24.2%), fracture (18.2%) and infection (17.3%) [10]. Loosening/osteolysis is caused by chronic inflammatory reactions to wear particles of any kind. Metallic corrosion products can also induce osteolysis even when there are not any other types of particles present and have both immunogenic and inflammatory effects [84]. Hence, to minimize the revision burden for next generation THA the greatest challenge is to eliminate the wear particles and corrosion of modular taper surfaces.

1.4.2 Modularity

1.4.2.1 History and Current Use

Early designs of hip joint replacements were monoblock and did not have the option of changeability of the femoral head over the femoral stem (Figure 1) [44]. Modular designs (Figure 1), introduced later, allow intraoperative flexibility for the surgeon to adapt leg length and femoral offset to the individual anatomy and gives the option to keep a well-fixed femoral stem and revise femoral head and acetabulum as needed. Also, modularity allows the use of the optimal material for each part of the hip implant for best performance and easier manufacturing. For example, titanium alloy (Ti-6Al-4V) is best suited as the femoral stem due to lower modulus relative to CoCr and high fatigue resistance; however, it lacks the high wear resistance exhibited by CoCrMo alloy or ceramic necessary for the femoral head [85]. It may also facilitate revision, if needed, during which a well-fixed stem that does not have any damage can remain while only the femoral head can be replaced. In addition to material and intraoperative advantages, modularity reduces the hospital's inventory by making combinations of size and materials that best fit the patient available with less number of devices, thereby reducing costs [81]. According to data from the Australian joint registry and the National Joint Registry of England and Wales, use of monoblock designs has decreased by 60.1% since 2003 and currently the most popular design is unipolar modular with either ceramic or CoCr femoral head articulating on highly crosslinked UHMWPE [10, 177, 231].

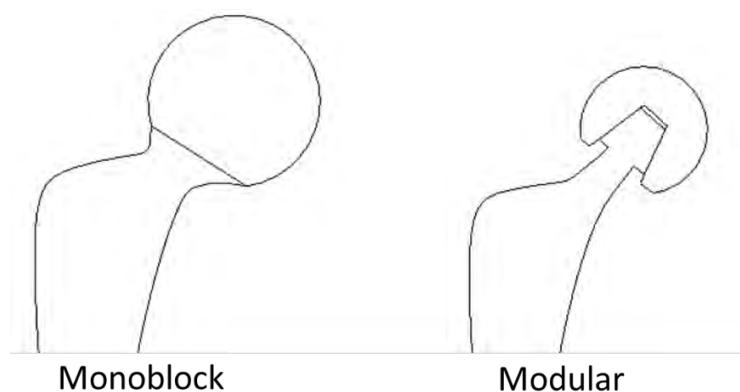


Figure 1: Monoblock hip joint replacement with femoral head fixed to the femoral stem. Modular hip joint replacement with removable and interchangeable femoral head and stem.

In the 1980s-1990s, researchers identified fretting-corrosion at the head-neck taper in retrievals [87, 91, 171]; however, the clinical significance was unclear at this time and the use of modularity continued. Recent design changes to THA include additional modular connections (Figure 2) for increased intraoperative flexibility and a second generation of metal-on-metal (MoM) bearings introduced in the 1990s. Compared to their counterparts in the 1960s, the new generation of MoM bearings were improved to address revision due to osteolysis from polyethylene wear particles. They are also typically referred to as large head size MoM (LHMoM) bearings due to head sizes $\geq 36\text{mm}$ for improved range of motion. However, clinical use of these designs led to increased reports of adverse local tissue reactions (ALTRs) attributed to release of metallic wear and corrosion particles. Designs with additional modularity at the neck-stem taper and LHMoM bearings had severe corrosion and reports of pseudotumor formation [42, 91, 109]. Certain designs of LHMoM bearings have been recalled due to higher than expected revision rates and designs with modularity at the neck-stem are used less often [10].

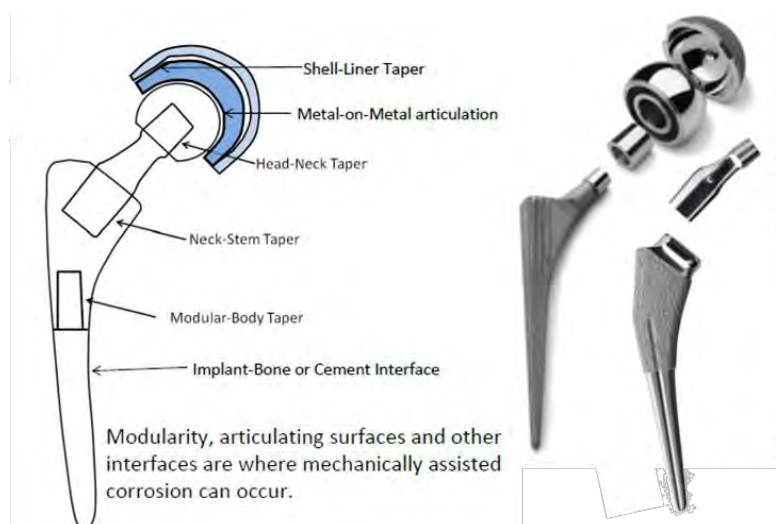


Figure 2: Schematic of *possible* locations of modularity and commercially available examples. Modularity is available at the shell-liner, head-neck, neck-stem, modular-body tapers in total hip arthroplasty designs where MACC may occur. MACC may also occur at Metal-on-Metal articulating surfaces and implant-bone or cement interfaces [6, 109].

As described in a report by the National Joint Registry of England and Wales, the higher than expected revision rate for implants with LHMOM bearings is associated with design, such as head size. They report that the differences in the reasons for revision between LHMOM and MoP are more evident in the LHMOM prostheses with a head size greater than or equal to 34mm. Metal related pathology is largely confined to head sizes greater than 32mm. The cumulative incidence of metal related pathology at 10 years is 9.9% for head sizes greater than 32mm and 0.4% for head sizes 32mm or less. The incidence of metal related pathology is potentially higher as it is possible that undiagnosed metal related pathology contributes to the increased rate of loosening/lysis and infection reported in metal on metal articulations with larger head sizes. The Registry

has also identified that lysis, as the sole diagnosis for revision, is reported with the highest frequency in metal on metal articulations [10, 231].

Upon closer examination of retrieval MoM systems, studies have shown that biomechanical factors that arise from the longer neck moment arm due to lateral offset and larger head sizes are correlated with higher corrosion at the taper [113]. Additionally, higher number of modular connections for the LHMoM is also associated with higher risk of damage at tapers [109]. It has been established that certain designs, such as LHMoM or other systems using femoral stems with multiple modular junctions, pose a higher risk for revision in a shorter time-frame due to taper corrosion. The reasons per corrosion still may manifest and pose a clinical risk for all components that uses any modular connection. Modularity at the head-neck taper in designs with non-LHMoM bearings provides a lot of benefits for the surgeon and the patient. Modularity allows the surgeon to adjust for excess femoral anteversion, offset and leg length when necessary and to restore the biomechanics of the hip joint independent of femoral fixation [243]. To keep benefitting from modularity at the femoral head-stem junction, we must understand and manufacture better modular interfaces.

In the next section, 1.5.3 Retrieval Analysis, a systematic review on the patient, surgical and device factors that have been reported to affect fretting-corrosion of the femoral head-stem taper is presented. During the literature search for this review, we have encountered inconsistent terminology and lack of specificity when referring to modular geometries and observations of corrosion. In our research, we have made the effort to stay consistent with the definitions established in international standards for testing and measurement (American Society for Testing and Materials (ASTM))

International), the American Academy of Orthopedic Surgeons (AAOS) and American Association of Hip and Knee Surgeons (AAHKS). It is important to recognize and adopt standardized terminology for effective communication of findings and identification of the cause and effect of corrosion. Before moving onto the systematic review, I have put together the definitions and terminology relevant to this dissertation which is intended to provide clarity and reference for the discussion throughout this document.

1.4.2.2 Taper Geometry Definitions and Terminology

Throughout this document we will often refer to the femoral head taper, which is the female connection of the femoral head-stem junction. The male connection at this interface will be referred to as the stem taper or trunnion. The studies in this dissertation have included components with only this singular modularity at the head-stem intersection. Femoral stems with additional modular connections at the stem-neck or further down the stem body have been excluded. Components that have LHMOM bearing surfaces have also been excluded from studies. The following are factors specific to variability at the head-stem interface based on commercially available designs.

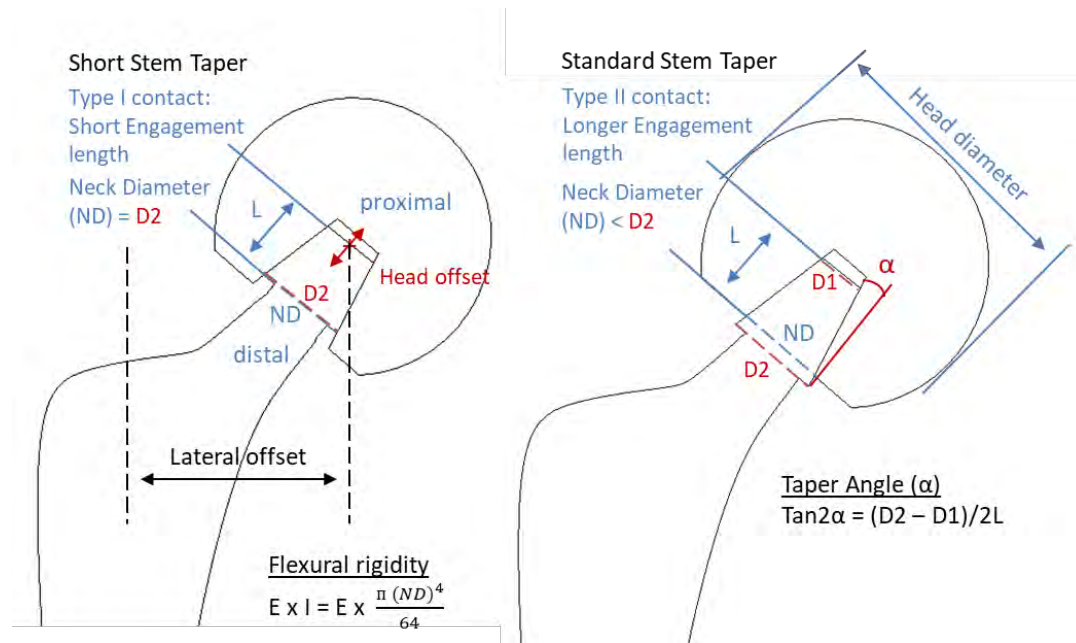


Figure 3: Figure showing some device design factors that affects the biomechanics of the head-stem modular taper.

Head size: Head diameters can range from 22mm up to >50mm in modular THA with heads ≥ 36 mm being considered large [121, 144]. The size of the femoral head plays an important role in providing a full range of motion without the issues of impingement of the stem neck on the rim of the acetabular liner, as well as reducing the potential for dislocation. Impingement may lead to edge loading of the head on the liner and may increase surface wear damage, creep and in the case of ceramic liners, risk of fracture. Larger head sizes is a risk factor that has been considered as a possible cause for increased taper corrosion because of the larger diameters leading to increased moments at the taper junction due to the larger moment arm for frictional forces at the bearing surface.

Head-stem offset: is the relative position of the center of the femoral head and the most proximal stem taper location. A head-offset of 0mm refers to the condition in which the top of the trunnion is located at the geometric center of the head. Offsets are referred to only in positive magnitude in terms of the displacement of the stem taper from the head center. In Figure 3, it is the position of the red crosshatch which can be moved proximally or distally depending on the intraoperative need for soft-tissue balancing and to avoiding leg-length discrepancies. This parameter is also critical to align the acetabular and femoral rotation centers and avoid subluxation, micro-separation or dislocation of the joint.

Taper angle (α) and Taper Angle Clearance: Taper angle is defined by the taper conical dimensions D_1 and D_2 , top and bottom width of the cone and L , the length of the cone. $\tan\alpha = (D_2 - D_1) / 2L$. Most commonly the target taper angle is $2\alpha = 5^\circ 40'$; however, taper angles are proprietary information. Commercially available taper angles are typically in the range from 5° to 6° and are machined to very high tolerances (to within a few minutes of the target angle). Some commonly available stem tapers are marketed using their D_1 and D_2 dimensions in mm (12/14, 11/13, 9/10), see Figure 4.

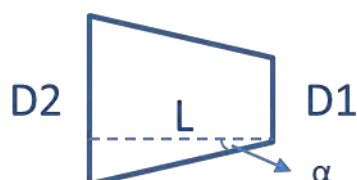


Figure 4: The taper dimensions that are used in taper angle definition.

Taper angle clearance (also referred to as taper angle mismatch) is the difference between the head taper angle and the stem taper (trunnion) angle. As shown in figure 5, taper angle clearance determines the type of contact (proximal, distal or neutral if they are perfectly matched) that is likely to be expected. The details about the effect of taper angle clearance on MACC is discussed in Chapter 3.

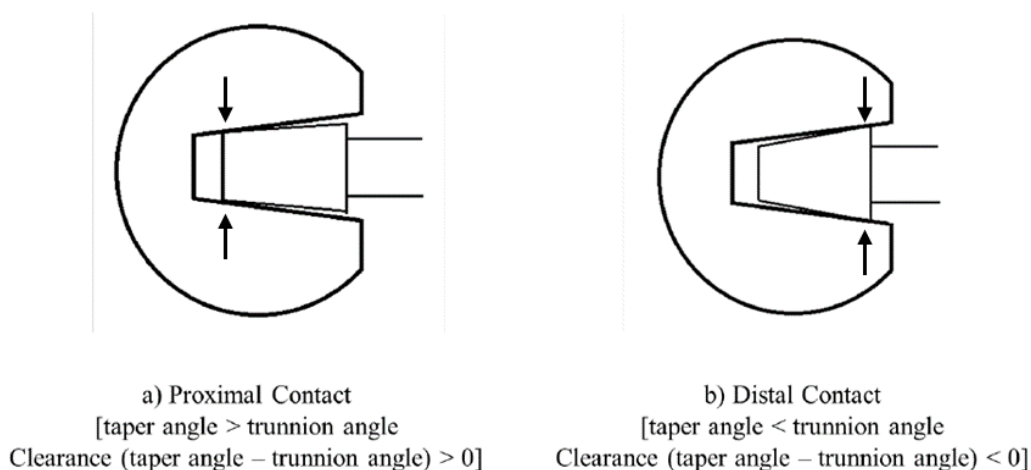


Figure 5: The expected contact location between the head and stem taper based on the taper angle clearance value.

Stem flexural rigidity: This is a parameter that has been deemed potentially critical for the development of MACC in taper junctions. Flexural rigidity is the product of the Young's modulus, E (GPa), the stiffness of the alloy material and the second moment of area (I). The second moment of area is a measure of the spread of the area of the cross-section about its bending axis (the center of the stem taper). The calculation of the second moment of area uses the neck diameter (ND) raised to the fourth power (as seen in figure 3, $I = (\pi (ND)^4)/64$). Flexural rigidity (EI) is smaller with titanium alloys (110 GPa

modulus compared with 230 GPa for CoCrMo), or with smaller diameters (e.g., 9/10 versus 12/14).

Stem taper length: Depending on the manufacturer, the size of the cone dimensions is variable for D_1 and D_2 and L , the length of the taper. It has been shown that modern tapers have been getting shorter and smaller and this factor has been speculated as a risk factor for increased taper fretting-corrosion. Figure 6 shows pictures of stem tapers with 3 different sizes (note the images are in the same scale). Stem taper length and the head offset will determine the final engagement length of the head-stem interface. Stem taper length and offset also determine the type of contact that will occur at the head-stem taper junction. As seen in Figure 7, the entire stem cone could be inside the head taper with as-manufactured surfaces of the head taper present on both the proximal and distal ends (Type I) or the stem taper could be extending out of the head taper with as-manufactured surface of the head taper being only present in the proximal end (Type II). The importance of contact type will be discussed further in chapters 3 and 4 because this will be important for linear fitting as-manufactured surfaces.

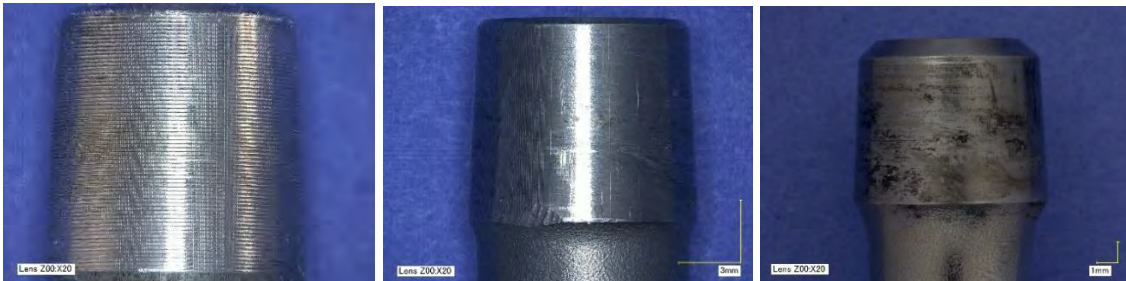


Figure 6: Figure showing 3 different examples of retrieval stem tapers, photographed at the same scale to show the difference of available stem taper size and surface finish.

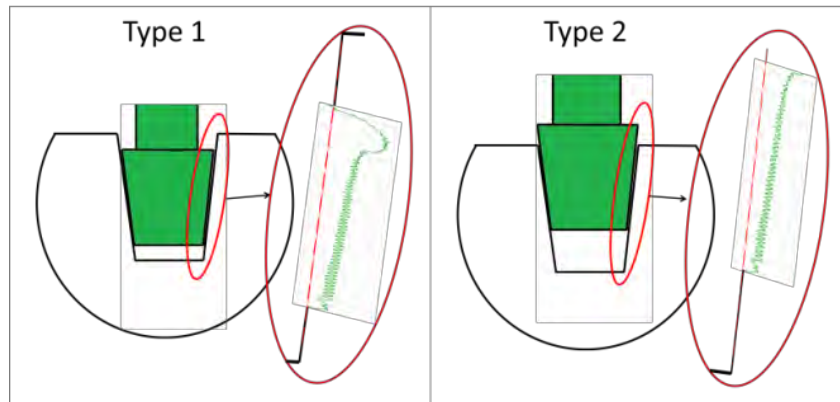


Figure 7: The contact type based on offset and taper size. Type 1 contact has as-manufactured surfaces on both the distal and proximal end. Type 2 contact only has as-manufactured surfaces available on the proximal end of the head taper. More as-manufactured surfaces that are available enable improved as-manufactured surface approximation for data fitting. Type 1 contact is more accurate than Type 2 because linear fitting is improved with available data spaced apart.

Stem taper roughness and machining finish: Manufacturers have varied designs available with smooth or micro-grooved surface finishes available. Stem tapers are defined as micro-grooved if their surface profile measured with a roundness machine precision stylus tip exhibits a periodic profile with a wavelength $>100\mu\text{m}$ and an amplitude of $>4\mu\text{m}$ [4, 7]. Some representative smooth and micro-grooved stem tapers are shown in Figure 8. The variation in topography is designed on purpose to accommodate different femoral head types. The ridges are present on stem tapers to enable plastic deformation when a ceramic head is fitted and to distribute the load evenly. Even load distribution is important for ceramic heads to avoid the risk of fracture due to concentrated loads on a localized area on the taper surface. The variable topography of stem tapers implanted with ceramic femoral heads will be discussed further in Chapter 2.

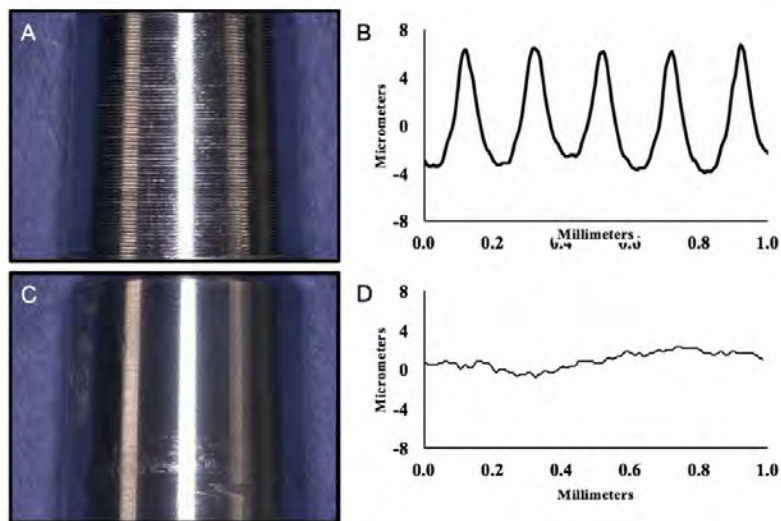


Figure 8: An example each of a micro-grooved and smooth stem taper. The figure is showing the photo of a micro-grooved stem (A) and corresponding surface profile with a typical grooved topography (B). The bottom row is showing a photo of representative smooth stem taper (C) and corresponding surface profile with a typical smooth topography (D) [7].





1.4.3 Retrieval Analysis – A systematic review of the clinical significance of corrosion at the head-stem taper of single modular stems in non-MoM THA

There are currently >100 femoral and acetabular design combinations actively being used in the clinic [10, 231]. Retrieval studies completed at our lab, the Implant Research Core at Drexel University, and other institutions have aimed at identifying, analyzing and documenting the damage mechanisms seen in excised implants. National registries such as those in England and Wales, Sweden and Australia also serve an important role in understanding which implants perform better among the large variety of designs available. As was seen in the case for LHMOM designs, the alarmingly high percentage of revisions at 10 years raised concerns about this implant design and was

reflected in the registries. However, registries do not provide the reason why components fail, only the outcome. Retrieval studies have been and continue to be very helpful to observe damage mechanisms understand the material and design factors that may be leading to the failure of total joint replacement components [22, 53, 152, 172, 173, 237].

Observation of taper corrosion in retrievals dates back to the early 1980s, soon after the introduction of modularity to total hip arthroplasties [85, 171]. Evaluation of retrievals have been conducted using visual observations (including visual scoring methods with a scale of 1 through 4 where 1 is least severe and 4 is most severe (Table II)[94, 110, 131]), optical microscopy, scanning electron microscopy (SEM), energy dispersive analysis (EDS) and focused ion beam (FIB). Biomechanical analysis for bending moment calculations were completed when radiographs and patient information were available using specialized software and component size information [109]. Quantitative measurements of the material loss from head-stem or stem neck modular junctions and characterization of the damage using surface profilometry techniques, white light interferometry and coordinate measurement machines (CMM) [152, 173, 236] are utilized for retrieval analysis. Finally, impedance spectroscopy has been used to determine the change in open circuit potential and debris accumulation on retrievals [249]. Using all or some of these evaluation methods retrieval studies have documented whether factors such as implantation time, use of different alloys for the head and stem, head material, head diameter, flexural rigidity of the femoral neck, lateral offset and femoral stem neck modularity (single vs. dual modularity) are predictors of corrosion of the femoral head and stem tapers [55, 94, 109, 143].

Table II: Visual fretting-corrosion scoring method and selection criteria.

Severity of Corrosion	Score	Criteria	Visual Appearance
None	1	No visible corrosion observed No visible signs of fretting observed	
Mild	2	<30% of taper surface discolored or dull Single band or bands of fretting scars involving three or fewer machine lines on taper surface	
Moderate	3	> 30% of taper surface discolored or dull, or <10% of taper surface containing black debris, pits, or etching Several bands of fretting scars or single band involving more than three machine lines	
Severe	4	>10% of taper surface containing black debris, pits or etching Several bands of fretting scars involving several adjacent machine lines, or flattened areas with nearby fretting scars	

Early retrieval studies have shown that corrosion at modular connections are ubiquitous and the causes are likely multifactorial including patient, surgeon and device factors affecting the severity of damage [29, 57-59]. Clinical factors are considered and controlled for when possible to isolate the effect of device factors. The dual modular hip arthroplasty, including a modular stem neck in addition to modular head-stem, has been associated with increased fretting-corrosion damage at the femoral head-stem interface [109]. However, the variation in device design factors are not limited only the number of modular junctions as shown in Figure 2. As manufacturers have offered systems with increased number of modular connections for intraoperative flexibility, they have changed other design and material factors in the past and continue to do so today. Femoral head and stem taper designs vary in features including head diameter, stem neck diameter, trunnion contact length on head taper surface, stem lateral offset, flexural

rigidity, head and stem material and taper machining surface finish. There are reasons behind each design modifications in commercially available total hip replacement femoral heads and stems. For example, stems with grooved taper surfaces, compared to a smooth taper finish, were released to improve mechanical locking and even contact load distribution between femoral heads and stem tapers [4, 100]. There is a need to examine and understand the effect of these material and design factors on the effect of taper corrosion.

Literature Search and Screening

For this purpose, we have conducted a systematic review of the literature for retrieval studies that looked at the clinical and device factors associated with risk of taper corrosion to understand the clinical significance and reported damage mechanisms observed. We looked for studies that had significantly large sample sizes, controlled for isolated effect of each factor investigated and the solutions proposed for revision. A literature search was performed with use of Ovid MEDLINE, SCOPUS, PubMed, ISI Web of Science, (from inception of each database to April 28, 2020). Articles were identified using an electronic search of the following keyword terms: hip AND corrosion AND ("taper junction" OR "taper" OR "modular") AND ("total hip replacement" OR "total hip prosthesis") AND (("head and neck" OR "head-neck") OR ("corrosion and adverse tissue reaction" OR "total hip arthroplasty and adverse tissue reaction" OR "total hip replacement and adverse tissue reaction") OR ("trunnion and corrosion" OR "trunnion and corrosion")). The combined number of results were 1087 articles for this

search in the mentioned databases. This number dropped to 846 when the duplicates were removed.

The remaining 846 articles were screened by a single reviewer (SBK) and eliminated further based on the titles and abstracts. Other review articles, studies performing only in vitro testing or finite element simulations were excluded from further analysis. Articles looking at in vivo performance and retrieval analysis of systems with dual modular stems (modularity at the stem-neck interface), modularity at acetabular shell, or any LHMOM THA studies, spine and knee arthroplasty articles were also excluded. This review only focused on metal-on-polyethylene, ceramic-on-polyethylene and ceramic-on-ceramic bearings with a single modular junction at the femoral stem, located at the femoral head-stem taper. The final exclusion criteria were based on the level of evidence in the article. This review included articles with level III or level IV of information available in the article: well documented clinical and device information such as implantation time, articulation type, device manufacturer, taper type, head size, gross or microscopic description of corrosion. The year range of the articles included in the review is 1993 – 2019. The screening process is summarized in Figure 9. The next section is a summary of their findings and highlights from some of the key technical papers in chronological order of publication.

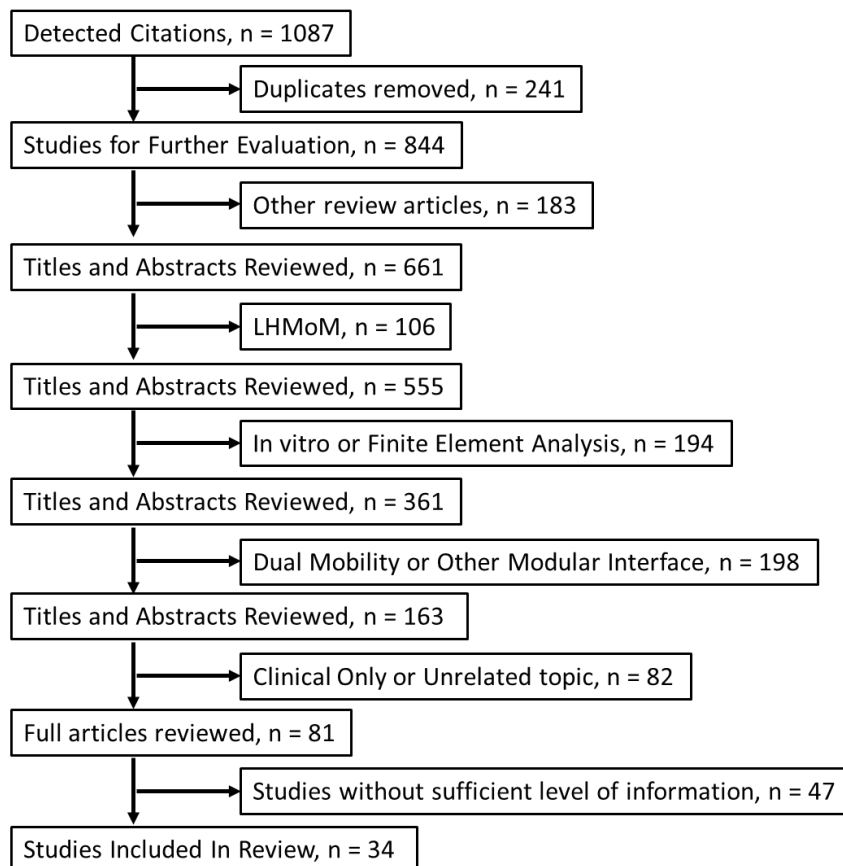


Figure 9: Screening of articles obtained from compiled database searches. The exclusion criteria at different levels is shown and the final number of articles included were 34.

Summary of Findings from Systematic Review

The earliest retrieval studies by Collier et al. they used optical microscopy to examine 139 femoral heads and stems and found implantation time and mixed alloy combinations were directly correlated with extent of corrosion. There was no semi-qualitative or quantitative method to compare the severity of corrosion in 1992. They were looking for evidence of pitting corrosion and used a profilometer for parts with extensive corrosion. As they did not observe any fretting and only pitting they concluded that the corrosion mechanism must be galvanically-accelerated crevice corrosion [55].

Retrieval studies shortly following Collier et al. [37, 85, 171] found evidence of corrosion damage in the head-stem modular taper junctions of both mixed (Ti6Al4V/CoCrMo) and similar (CoCrMo/CoCrMo) metal combinations. The theory of galvanic corrosion leading to corrosion at the modular tapers was replaced with the demonstration of in vivo fretting initiated crevice corrosion. Gilbert et al. [85] looked at 148 retrieved modular hip prosthesis that had either a Ti6A4V stem and CoCrMo head, or both CoCrMo stem and head. They found evidence of corrosion in 16% of stems and 35% of heads in mixed-metal combinations and corrosion in 14% of stems and 23% heads for similar metal cases. They also found that the severity of corrosion was correlated with duration of implantation and concluded this must be an event that progresses over-time. Inspection of SEM and x-ray energy dispersive analysis (EDS) analysis revealed a variety of corrosion and damage modes including etching, fretting, pitting, selective leaching, interfacial layer formation and intergranular attack. They saw evidence of all in mixed-metal hip samples except for intergranular attack and the similar metal samples showed evidence of etching, fretting, pitting, selective leaching, and intergranular attack. They also note that the onset of moderate to severe corrosion in this sample group was seen in prior to 10 months of implantation time for mixed metal combinations and prior to 20 months. In this study, Gilbert et al. also describe the mechanically assisted crevice corrosion process theory in detail (which is developed further over the years and mentioned in depth in the next section) and mention that independent of fretting, cyclic strains in the metals are also a possible cause for the disruption oxide passive protective films and initiators of the positive feedback loop that leads to MACC.

Cook et al. [57, 58] inspected 108 uncemented femoral stems with modular heads retrieved for reasons other than loosening. They also observed evidence of corrosion in both mixed alloy systems (35%) and single alloy systems (9%) at an average of 25 months implantation time. They did not find any correlation between corrosion presence or extent with implantation time, initial diagnosis, reason for removal (which already excluded cases with loosening, and this study included well affixed stems), patient age or weight. They observed that stems with mechanical wear damage and corrosion were less likely to show histological bony ingrowth. Collier et al. [54] also confirmed corrosion in both mixed and similar alloy combinations in a later study that looked at 701 head/neck tapers. 7% of the all-cobalt alloy components had corrosion and 33% of the mixed-alloy components had corrosion.

The findings in the early retrieval studies of both mixed and similar alloy combinations led to a consensus on fretting-initiated crevice corrosion. The studies thereafter are designed to confirm findings and started to look at specific factors that may lead to higher instability at the head-stem modular interface. Lieberman et al.[159] investigated 48 implants of three different designs retrieved from the same medical center. They evaluated the modular taper surfaces for evidence of corrosion and the quality of the taper lock. Group I (Omnifit) had a CoCr/CoCr head-stem interface (n=26), Group II (Harris Galante, Bias) had a CoCr/Ti alloy head-stem interface (n=10) and Group III had a CoCr/Ti alloy head-stem interface that was coupled in the factory via a shrink fit. They did not see any evidence of corrosion in Group I and III, while Group II did show evidence of corrosion. Group III implants required a significantly greater pull-off force compared to Group I. They concluded that improving the tolerances of the

mating surfaces may reduce micromotions and be a key factor in preventing corrosion. Similarly, Brown et al. used visual scoring to evaluate 79 retrievals with similar and mixed metal alloy modular combinations and concluded that devices with press fit interfaces (regardless of alloy combination) are likely to produce a stable fit that minimizes relative motion and thus reduces the amount of fretting corrosion. Other studies have also supported that instability at the head-stem taper and toggling due to angular mismatch may be the cause that initiated MACC [37, 56]. This dependence on biomechanical stability has also brought up other factors such as patient weight and head offset that contribute to the increased bending moment and initiation of MACC [111].

The multicenter retrieval analysis of 231 modular hip implants conducted by Goldberg et al. [94] was specifically designed to investigate the effects of material combination, metallurgic condition, flexural rigidity, head and neck moment arm, neck length and implantation time on corrosion and fretting of modular taper surfaces. It is also the publication that made the visual scoring system used in the study the gold standard for evaluating corrosion damage and a modified Goldberg-Higgs scoring method is still used commonly today to evaluate fretting-corrosion damage [110]. Scores for corrosion and fretting were assigned to medial, lateral, anterior, and posterior quadrants of the necks, and proximal and distal regions of the heads. They reported greater head-neck corrosion damage scores for stem trunnions with a lower flexural rigidity, mixed alloy combinations and higher implantation time. They recommended that larger diameter necks will increase neck stiffness and may reduce fretting and subsequent corrosion of the taper interface regardless of the alloy used.

Studies conducted more recently still agree with the assessment that lower flexural rigidity and taper angle mismatch is likely leading to higher corrosion [125]. Huot Carlson et al. [120] also concluded that the severely corroded and fractured 7 out of 78 components in their study were due to the higher stresses thinner stem neck diameters (less flexural rigidity) with high offsets. Their study also had taper adapter sleeves and they saw corrosion at both the head-neck junction (54% showing corrosion; 88% showing fretting) and at the stem-sleeve junction (88% corrosion; 65% fretting). Corrosion correlated to in vivo duration, patient activity, and metal (vs ceramic) femoral heads. Porter et al. [202] conducted a dual-center retrieval analysis of 85 modular femoral stems released between 1983 and 2012 was performed, and the flexural rigidity and length of the femoral trunnions were determined. There was a negative correlation between flexural rigidity and length of the trunnion and release date of the stem confirming that there is a trend in recent years to release shorter/smaller stem tapers. They found a wide variability in flexural rigidity of various taper designs, with a trend toward trunnions becoming shorter and less rigid with time. They suggested this new trend may partly explain why taper corrosion is being seen with increasing frequency in modern THAs. Tan et al. also found that taper design affected fretting corrosion scoring especially at the base of the stem [229]. Siljander et al. also looked at taper design for a retrieval group of only CoP systems and found that taper design also had a statistically significant affect with V40 and 16/18 tapers showing greater corrosion compared to 12/14 [217].

Femoral head diameter has been widely investigated for its effect on fretting-corrosion. Kurtz et al. [144] looked at 508 CoCr alloy heads and 216 metallic femoral stems (CoCrMo, Ti6Al4V, TiMoZrFe) from MoP THA using a visual fretting-corrosion

score and found mild to severe taper fretting and corrosion (≥ 2) in 78% head tapers and 53% of stem tapers. They looked at the effect of femoral head diameter (with heads ≥ 36 mm being considered large diameter) and they found no increased risk of fretting-corrosion in larger heads compared to smaller diameter femoral heads. The only positive correlation found in this study was between fretting-corrosion scores and implantation time. Previously Dyrkacz et al. [74] had found a positive correlation between larger head sizes (36mm) and higher corrosion compared to a smaller head size (28mm). Del Balso et al. [70] observed higher fretting scores for 32mm heads compared to 28mm heads; however, there was no effect on the overall corrosion scores due to head size. Hothi et al. [114] looked at group of MoP with large head size and did not find the effect from head size to be clinically significant. Recent studies have even found a negative correlation between head size and fretting corrosion with larger femoral heads correlated with less severe head corrosion and head fretting compared to smaller heads [216].

Surface topography has been suggested as a factor in fretting corrosion and there are some very meticulous studies that looked at the effect of this factor. Arnholt et al. [4] examined 398 stems paired with CoCrMo alloy heads that were collected as part of a multicenter, institutional review board-approved retrieval program. Stems were fabricated from CoCrMo or Ti6Al4V alloys and were used in a metal-on-polyethylene bearing total hip device. Surface topography of stems were quantified using roundness machine profiles using average surface roughness, amplitude and wavelength of microgrooves (if any). From here they categorized the stem taper surfaces as smooth or microgrooved and it ended up being a 50%-50% ratio. Surface topography was not correlated with fretting

corrosion scores. The findings from a later, smaller matched cohort of 120 retrieval head-stem pairs also supported the same conclusion [7].

Some retrieval studies compared the taper corrosion based on femoral head material [41, 73, 103, 127, 228]. These studies have made the effort to design a matched cohort study by controlling other design and patient factors when possible between the groups with CoCrMo heads and ceramic heads. Designing retrieval studies with ceramic heads is difficult because they are less readily available due to their good clinical performance. Researchers found suitable hips with ceramic heads and matched with CoCrMo femoral head hips from their collection. Three of these studies used only visual fretting-corrosion scoring [103, 127, 228] and two used both visual and quantitative material loss [41, 73]. Three studies, one quantitative and two visual only, looked at hips with Oxinium femoral heads, a femoral head with a zirconium base and thin oxidized layer of oxidized zirconia (OxZr) covering the bearing surface. The ceramic surface of Oxinium material provides increased scratch resistance and is more wettable and provides lower UHMWPE wear in hip simulators compared to CoCrMo femoral heads. Additionally, since it has a ductile zirconia alloy substrate, this product combines the bearing wear properties of a ceramic material without the negative risks associated with ceramic fracture. The other studies compared zirconia and CoCrMo heads and BioloX Delta (zirconia-toughened alumina) and CoCrMo heads.

Cartner et al. [41] found differences in corrosion scores based on femoral head offset and head material with oxidized zirconium (OxZr) heads leading to lower material loss and lower scores compared to CoCr heads. They also found a positive correlation with fretting corrosion with greater head offsets, concluding that reducing the moment

arm at the head-neck junction may reduce fretting corrosion damage. They did not find any effect of head size or implantation time with fretting-corrosion in this retrieval study with 210 femoral head tapers. This study by Cartner et al. [41] also utilized a roundness machine to take vertical straightness profiles of femoral heads with high visual fretting corrosion scores (scores of 3 or 4). For CoCr heads chromium-rich precipitates and other artifacts were found on the femoral head tapers associated with high corrosion scores and deviations from vertical straightness in this study. These features were absent from OxZr femoral head tapers, which displayed lower scores and no measurable material loss. The other studies that compared OxZr and CoCrMo heads with visual scoring both also saw significantly lower fretting-corrosion scores for the OxZr group [103, 229].

Di Laura et al. [73] prepared a matched cohort between Biolox Delta heads, which are commercially available zirconia toughened alumina (ZTA) ceramic heads and a group with CoCrMo heads. I describe in detail the microstructure and performance of ZTA ceramics in Chapter 2; however, briefly, they are the newest generation of orthopedic ceramics with the highest fracture toughness currently in the market. In the study by Di Laura et al. all the heads in both groups were implanted with a single stem design (Stryker Rejuvenate, V40 taper angle). They later reveal that this is a recalled femoral stem model with dual modularity (it has a modular junction also at the stem-neck). They use a roundness machine to take vertical profiles of the head-stem taper junction; but not the stem-neck tapers. They calculate material loss from the head-stem junctions with median taper material loss rates of $0.210 \text{ mm}^3/\text{year}$ (0.030 to 0.448) for the metal head group and $0.084 \text{ mm}^3/\text{year}$ (0.059 to 0.108) for the ceramic group. The difference was not significant ($p = 0.58$). The dual-modularity is a confounding factor,

and they mention in the discussion that severe corrosion was observed at the stem-neck interface at the of time of revision and retrieval examination. Increased modularity has been associated as a risk factor for fretting-corrosion damage [109]. Using a ceramic head will not lower the risk of revision if other high risk factors that lead to fretting-corrosion and metallic material loss are used in the components selected for the THA.

Kim et al. [127] examined a matched cohort of 78 femoral heads each of zirconia and CoCrMo and all with the same diameter of 32mm. In this study, they only scored and compared the stem tapers (trunnions) and do not report the fretting-corrosion score for the CoCrMo heads. They did not find a significant difference between the stem taper fretting-corrosion scores of the two groups. This is not entirely surprising as it has been shown in other studies that most of the material loss due to fretting-corrosion at the head-stem taper junction is from the head taper of CoCrMo heads. This will be discussed in further detail in Chapter 4 of this dissertation; however, researchers have also observed damage mechanisms in vivo that lead to the majority of material loss from the head tapers [98].

Conclusions from Systematic Review

The numerous retrieval studies that investigated corrosion at modular connections over the past decades show that there are no metallic biomaterials or modular interface designs by any manufacturer that are immune to fretting corrosion. This review of single modularity at the head-stem of non-LHMoM systems also show that this problem is prevalent and may lead to revision even in MoP hip replacements. The factors evaluated in the articles that met the selection criteria are summarized in Table III. Most of these articles in the review used visual methods of examining fretting corrosion and used the

semi-qualitative visual scoring method in correlating the device factors and severity of corrosion. We found 5 articles that looked at quantitative material loss from the head-stem interface of retrievals from non-MoM bearing systems. One of them only measured stems and the other used a non-contact replicator method and used roundness machine measurements as verification [30, 242]. The third study used a CMM and looked at the material loss from a single design and calculated material loss up to 20.8mm^3 [183]. Two studies used a roundness machine to take vertical axial traces around the taper surfaces; however, one of the studies only measured the most severe components [41] and the other study looked at THA with a dual modular stem, but, only quantified the material loss from the head-stem surface even though they reported severe corrosion also at the stem-neck modular interface [73]. There is a need for practical quantitative methods for the evaluation of material loss from taper surfaces.

The findings about the effect of head size seem to be mixed, with some studies finding a correlation and others not reporting an effect for this particular design factor or seeing even the reverse with larger heads showing less fretting corrosion. The corrosion processes at the modular interfaces are complex and varied and we know that a few factors are affecting these fretting-corrosion mechanisms at the same time. Other factor such as head-taper engagement and geometry rather than head size may be affecting rates of fretting corrosion. Also, most studies have used visual fretting-corrosion scoring methods which are useful for categorizing the severity of damage; but do not provide accurate information about metallic material loss compared to quantitative methods. However, neither estimation of material loss nor visual scoring explain the mechanism and damage mode of fretting-corrosion at the taper, only the severity of damage. For

damage modes other techniques such as SEM are recommended [98]. Overall, the findings from retrieval studies suggest that design factors that make it biomechanically easier for vibrations, bending or motion to occur will most likely lead to higher corrosion damage and there are some factors with greater effect (flexural rigidity) compared to others (head size).

Another significant consensus from these retrieval studies has been that ceramic heads are likely to protect from corrosion [31, 120, 228] especially since CoCrMo femoral head tapers corrode more than stem tapers [43, 94]. Reports show that CoP has surpassed use of MoP [107] and surgeons performing revision for ALTR and corrosion at the head-stem taper prefer replacing the CoCrMo with a ceramic head at revision and place a titanium adapter sleeve on the stem taper [132]. Ceramic heads with titanium adapter sleeves show good survivability [160, 163] but the long term survivability of ceramic heads with titanium stems needs to be investigated [205]. Additionally, a new study has shown that tribocorrosion at the articulating surfaces, in addition to the head-neck junction, may be contributing to release of metal particles [244]. Another factor that also needs to be understood and prevented is the increasing evidence of inflammatory cell induced corrosion as a contributing mechanism to metal release from taper and articulating surfaces [90, 98, 134].

Distinguishing between the numerous possible damage mechanisms and determination of the correct mechanism is important in retrieval analyses to isolate possible causes of device, patient and surgical factors that lead to MACC. Some of the retrieval studies have identified specific damage mechanisms using SEM [85, 98] which is a necessary supplemental technique to visual scoring and profilometry. Retrieval

studies give valuable information about the direct clinical significance of device factors and has at times shown disagreement with in vitro or modeling (finite element method) publications. For example, while Arnholt [4] did not find any effect of surface finish of stem tapers on fretting corrosion, in vitro studies have reported the opposite [8, 194]. However, even matched cohort retrieval studies have limitations, and in vitro studies are a necessary supplemental test technique for factors that retrieval studies are not able to isolate such as surgical techniques (assembly load, taper cleanliness). Additionally, retrieval studies are an investigation of existing designs and failed samples, in vitro studies can provide significant insights for new designs as will be discussed in the next section of this document.

Table III: Summary of risk factors investigated in the literature related to fretting-corrosion damage at the taper surfaces.

Factor	Studies	Consensus? (Y/N) and Summary of Findings
Femoral head size (higher frictional torque)	[41, 69, 70, 74, 144]	N- There is not consensus between studies, the conclusion varies with some finding an effect and others not. Needs further investigation, depends on study design and other confounding factors.
Dissimilar metal combinations	[37, 53, 54, 85, 94, 111]	Y - There is consensus that fretting-corrosion damage is seen in both similar and mixed-metal alloy combination tapers. Galvanic corrosion has been contested but also all studies reported higher percent of mixed alloy couples exhibit fretting and corrosion compared to similar alloy pairs.
Head material (metal vs. ceramic)	[41, 73, 75, 103, 120, 228]	N – some studies found significant difference between the metal and ceramic femoral head cohorts and others did not; however, the studies that did not find a significant difference had some confounding factors that they did not account for. Also, some used visual scoring only and others used quantitative methods. Further investigation is needed.

Table III (continued):

Flexural rigidity	[94, 120, 183, 202]	Y – There is consensus that lower flexural rigidity leads to higher fretting corrosion in tapers due to more movement and bending under loading. This is also related to patient BMI and activity level.
Head offset (moment arm)	[41]	Larger offsets in both negative and positive direction which potentially leads to higher bending was shown to be positively correlated with fretting corrosion. Neutral head offsets showed the least fretting-corrosion damage.
Stem taper length (contact length/area), taper type	[43, 111, 125, 217, 229]	Y – There is consensus that taper type (9/10,11/13, 12/14, V40...and so on) lead to significant differences in fretting-corrosion damage in vivo. While the consensus seems to be towards the conclusion that thinner and smaller tapers lead to more fretting-corrosion, the conclusion about this factor was not entirely clear and further investigation is needed.
Stem taper surface finish (smooth vs. grooved)	[4, 7]	Y – taper surface finish did not affect taper fretting-corrosion in vivo
Taper fit tolerances/Taper angle clearance	[37, 56, 98, 159]	Y – stable and well fitted tapers to minimize movement at the head-stem taper is a conclusion recommended in the studies referenced.
Implantation time	[85, 94, 111, 144]	Y – There is consensus that longer implantation time is positively correlated with fretting-corrosion.
Patient activity	[120]	This was shown as a factor positively correlated with risk of fretting corrosion. Needs to be investigated further; however, supports the hypothesis that higher flexural bending due to low rigidity is a risk factor
Patient weight (BMI)	[111]	This was shown as a factor positively correlated with risk of fretting corrosion. Needs to be investigated further; however, supports the hypothesis that higher flexural bending due to low rigidity is a risk factor

1.4.4 In Vitro Test Methods

There currently are no national or international standards for the design, materials, and manufacture of modular interfaces in total joint replacement (TJR). New modular designs are introduced by medical device manufacturers with the expectation of improved patient outcome based on retrieval studies of previous designs. As mentioned in the previous sections, these designs have a wide range of design parameters for taper geometry and surface finish on both the femoral head and stem. There is a need to systematically investigate the factors that increase the risk of taper corrosion and find ways to mitigate and eliminate this phenomenon in total joint replacements. As shown in the literature review in section 1.4.3, the ideal factors for modular taper angle, stem flexural rigidity, taper material, surface finish, assembly mechanics and related conditions are currently unknown. Matched cohort retrieval studies useful to learn about the clinical performance of some of these factors; but these studies do not allow to test and control surgical factors such as assembly force.

There is a need to develop appropriate in vitro tests to evaluate designs, material and surgical factors to address the continued concern about MACC. In vitro studies are designed to evaluate the electrochemical changes in crevice conditions due to mechanical loading. They have tested the effects of assembly conditions, cyclic load magnitude, number of load cycles, material combinations, variations in taper geometry and surface finish/topography/preparation methods. The factors being monitored are usually fretting currents, open circuit potential, changes in crevice solution chemistry (pH, oxygen depletion, [Cl⁻]) and metal ion levels in the solution.

1.4.4.1 Mechanically Assisted Crevice Corrosion Model (MACC)

Mechanical wear leading to corrosion in metallic materials has been a concern for over a century in various industries [72]. The term ‘fretting-corrosion’ was coined by the English physicist Tomlinson as early as 1927 while studying machine components [72, 234]. Fretting-corrosion takes place at closely fitted interfaces subjected to micromotions, vibrations and compressive loads. Contacts which seem to be devoid of relative movement, such as interference fits, do in fact allow sliding on the scale of 1µm when alternating and oscillating loads are carried. It is very difficult to eliminate such movements and the resultant fretting damage. Fretting wear and fretting fatigue are present in almost all machinery and are the cause of total failure of some otherwise robust components. In biomedical applications, which experience cyclic and compressive loads, fretting-corrosion and crevice corrosion was first seen at the screw-plate interfaces of stainless steel fracture fixation plates [38, 40, 51, 227]. It was not until the early 90s that researchers provided evidence that it was fretting that was initiating corrosion on modular taper surfaces [37, 85, 174].

In an aqueous environment, the surface of the orthopedic alloys forms a protective oxide layer and remains in an equilibrium state of oxidation and reduction reactions. The passivating behavior of a metal surface in solution has been extensively studied for alloys used in orthopedics which are typically 316 stainless steel (ASTM F55-56), CoCrMo alloy (ASTM F75) and Ti6Al4V alloy (ASTM F 136) [122, 221]. The passivation in vivo depends on thermodynamic driving forces of oxidation and reduction defined by the free energy change in equation 1:

$$\Delta G_{\text{red}} = -\Delta G_{\text{ox}} = -nFE \quad (1)$$

where n is the valence of the metallic ion (number of electrons), F is Faraday's constant, $96\,500\text{ C/mol}$ and E is the half-cell potential. A reaction will occur, in this case the surface of the metal will oxidize, only if there is negative free energy change. The half-cell potential exists because of the difference in the neutral state compared to the oxidized state, such as Fe/Fe^{2+} and at the cathode, the difference between the neutral state and the reduced state as in H^+/H_2 . For an experimental metal, these reduction-oxidation (redox) potentials are measured relative to a reference half-cell potential, usually the standard hydrogen electrode (SHE) or silver, Ag/AgCl .

$$E = \text{Cathode half-cell} - \text{Anode half-cell} \quad (2)$$

During equilibrium conditions the rate of oxidation and reduction reactions are the same and we get the following balance, also known as the Nernst equation:

$$E^{eq} = E^o + \frac{RT}{nF} \ln \left[\frac{[\text{Ox}]}{[\text{Red}]} \right] \quad (3)$$

where R is the ideal gas constant, T is temperature and $[\text{Ox}]$ and $[\text{Red}]$ are the concentration of oxidation and reduction reactions. E^{eq} is the equilibrium potential for the half-cell reaction and E^o is the standard cell potential (cathode). The larger the potential difference, the greater the driving force for the reaction. The greater the chemical driving force for oxidation, the more negative this potential. Metals used for biomaterials have a negative electromotive force that lead them to form a passive oxide protective layer instantaneously when placed in an aqueous medium such as in vivo conditions.

In a crevice environment, body fluids enter and remain stagnant. Monitoring the chemistry at rest without the application of cyclic load, the following was observed: drop in pH, increase in chloride and decrease in oxygen [87]. It is possible that crevices alone drive changes in the solution due to the very slow rate of metal ion transport through the

oxide layer even with stable passive oxide layer. Applying fretting-wear at the surface in a crevice further accelerates the oxidation and reduction reactions and solution changes. Fretting or cyclic loading strains leads to repeated abrasion of the protective oxide layer and dissolution of ions from the taper surface. When abrasion occurs in a crevice, non-passivated metal is exposed to an initially oxygen rich aqueous crevice fluid. The highly reactive underlying metal quickly oxidizes, consuming some oxygen from the fluid and with repeated fretting-corrosion eventually depleting O_2 . Once the O_2 is depleted, the concentration of free metal ions starts to increase in the crevice as fretting continues. This may lead to the formation of metal-chlorides, the next preferred reaction in the absence of O_2 . Subsequently, the metal chlorides react with water to form metal hydroxide and hydrochloric acid which lowers the pH in the crevice leading to highly acidic conditions [85].

When fretting-corrosion occurs, there is a shifting of the corrosion potential of the implant to more cathodic potentials. Increased anodic activity (oxidation) releases increased number of electrons which are accumulated until consumed in corresponding reduction reactions (cathodic) (Figure 10). These anodic and cathodic reactions change the potential and pH conditions within the crevice, as detailed above. The change in conditions within the crevice will change the potential across the interface (E) and change the rate of repassivation. When the surface is scratched, oxidation reactions result in oxide film formation and form a barrier that limits ion release, and the currents drop significantly. However, if the voltage across the interface reaches the breakdown potential (E_b) due to some of the changes observed in the solution conditions in a crevice environment, then the metal will lose its ability to reform an oxide layer [84, 92, 93]. The

open circuit potential is dependent on the rate of oxidation and reduction reactions, which are dependent on oxide stability and pH.

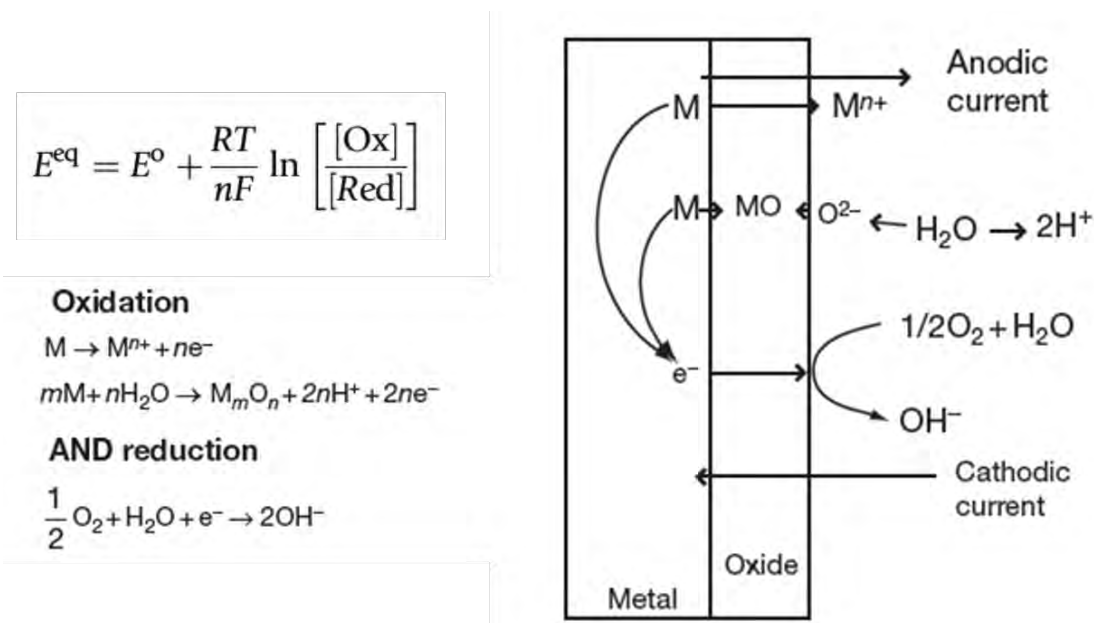


Figure 10: The equilibrium oxidation and reduction reactions taking place at the surface of a metal. Ion dissolution and anodic and cathodic currents are generated during the formation of the protective oxide film [84].

In summary, the rate of corrosion in THA modular junctions is dependent on the rate of disruption of the protective oxide film due to mechanical abrasion or changes in the solution condition in the crevice that disturbs the chemical stability of the film.

Swaminathan and Gilbert have developed the model of mechanically assisted crevice corrosion with an equation that relates fretting currents (I_{film}) to the metal oxide properties, mechanical forces, asperity contact, sliding speed and electrochemical potential, multiplied by two due to the back and forth motion [89, 225]:

$$I_{film} = 2 \frac{\rho n F}{M_w} \frac{A_{nom}}{\Delta} m (E - E^{onset}) \frac{d\delta}{dt} \quad (4)$$

where:

ρ = the oxide density,

n = the charge per cation,

F = Faraday's constant (96,500 C/mol),

M_w = the molecular weight of the oxide,

A_{nom} = the nominal area,

m = the anodization rate for oxide growth (typically 1.8 to 2 nm/V for Ti and CoCr oxides),

E = the voltage across the interface,

E_{onset} = the onset potential above which oxide films will regrow and below which they will not,

$d\delta/dt$ = the sliding speed, and

Δ = the average inter-asperity distance in the sliding direction.

The term Δ , the average inter-asperity distance in the sliding direction, is a normal-load dependent parameter and a Hertzian contact mechanics quantity that links the distance between asperities to the applied load. Hertzian analysis defines area of contact:

$$A_{contact} = k(F_N)^{2/3} \quad (5)$$

From here, inter-asperity distance can be defined as [164, 226]:

$$\Delta = c(F_N)^{-\alpha} \quad (6)$$

Where F_N is normal load and c is a constant dependent on material and surface parameters (such as roughness, hardness...etc.). The exponential term α is also dependent on material properties and will have values in the 2/3 to 1 range. If the I_{film} is measured experimentally between two sliding contacts, it is possible to use Equation 4 to get a close estimation of Δ if all the other material and experimental parameters are known.

There is greater error in this experimental approximation of inter-asperity contact when a

mixed metal combination is used as the exact contribution of each metal type to the total current is unknown. While these limitations exist, Equation 4 and studies that have contributed to its development show a tangible way of estimating and measuring the electrochemical and mechanical interactions that take place during fretting-corrosion [226]. In his dissertation, Mali [164] has estimated the inter-asperity distance Δ based on measured fretting-currents for a total of 6 metal contact combinations (CoCrMo-CoCrMo, CoCrMo-Ti6Al4V, Ti6Al4V-Ti6Al4V, CoCrMo-SS316L, Ti6Al4V-SS316L and SS316L-SS316L). The contribution towards fretting currents for each material in an alloy couple was assumed arbitrarily. He showed that as the normal load increases, the inter-asperity distance decreases. Lower inter-asperity distance indicates increased amount of real contact area established between the fretting interfaces.

As mentioned in the literature review in section 1.4.3 of this document, evidence from decades of retrieval and in vitro studies [4, 37, 42, 85, 88, 94, 100, 143, 171] have shown that the mechanism leading to degradation at the taper junctions is a combination of factors related; but not limited to, the following [4, 89, 226]:

- 1) Solution electrochemistry: pH, repassivation potential and speed, proteins present;
- 2) Material chemical properties: oxide resistance and capacitance, oxide abrasion resistance;
- 3) Bulk mechanical properties: resistance to bending, plastic deformation, compression and shear;
- 4) Interface mechanics: taper angle clearance, crevice geometry, transport of fluids, surface finish, contact area and stresses, micromotion;

- 5) Biological Interactions: inflammatory cell induced (ICI) corrosion, ion and particle toxicity.
- 6) Surgical and patient factors: assembly force and seating mechanics as well as the initial taper cleanliness conditions during the operation are thought to be operative factors contributing to fretting-corrosion. Patient activity level and BMI have been assumed to effect loading conditions and potentially also influence taper fretting-corrosion.

Gilbert et al. has characterized the combined process leading to corrosion and metallic particle release from modular connections as mechanically assisted crevice corrosion (MACC) [87, 226]. Fretting continuously disrupts the passivation layer on metal taper surfaces due to cyclic loading and/or micromotion ($<100\mu\text{m}$). The severity of MACC depends on a combination of mechanical, electrochemical, geometrical, material and solution conditions (Figure 11). Previous studies have already illustrated the mechanism of MAC in great detail [4, 226]. In order to make optimal adjustments to the taper design and reduce the volumetric material loss due to fretting-corrosion, we need to understand the interplay and influence the factors mentioned above have on each other and the rate of degradation in vivo.

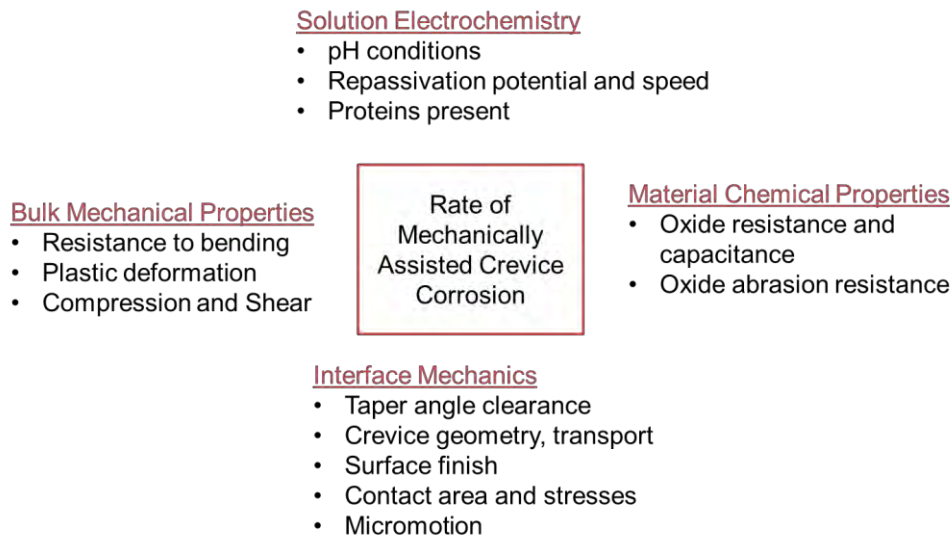


Figure 11: Summary of factors that may contribute to MACC in a total joint arthroplasty.

1.4.4.2 In vitro Tribocorrosion Testing

Tribology encompasses the study of friction and wear when two materials slide over each other. For two materials in dynamic contact, the coefficient of friction, μ , is defined as the ratio of the tangential force, F_T , and the normal force, F_N , as follows:

$$\mu = F_T/F_N \quad (7)$$

In a sliding contact some guiding principles are that the tangential force is proportional to the normal load and independent of the apparent area of contact and independent of the sliding velocity. Tribological testing of orthopedic implant materials began with the need to understand the wear performance of the first bearing materials in THA. Wear testing first began with a custom wear tester built by Charnley to screen the wear performance of PTFE and UHMWPE in the 1960s [135]. Later, wear testing has been standardized in the form of pin on disk testing (ASTM 732 – Standard Test Method for Wear Testing of Polymeric Materials Used in Total Joint Prosthesis). This standardized configuration

allows for testing different material combinations under controlled loading and environmental conditions in a physiologically relevant solution. Pin-on-disk testing uses cylindrical pins with flat, truncated conical or spherical cap ends. Usually the polymer material is machined as pin and test against a flat metal surface. Wear testing using pin-on-disk tester enables testing combinations of materials for millions of cycles and measure wear rate and compare performance of different material combinations [20, 21, 145]. During pin-on-disk testing, the pin is rotating on the same track on the stationary disk for a predetermined number of cycles, and at the end of the test wear rate can be measured gravimetrically or through the use of profilometry (Figure 12) [207]. The use of profilometry for the analysis of material wear and surface deviations are used in more detail in Chapters 3 and 4.

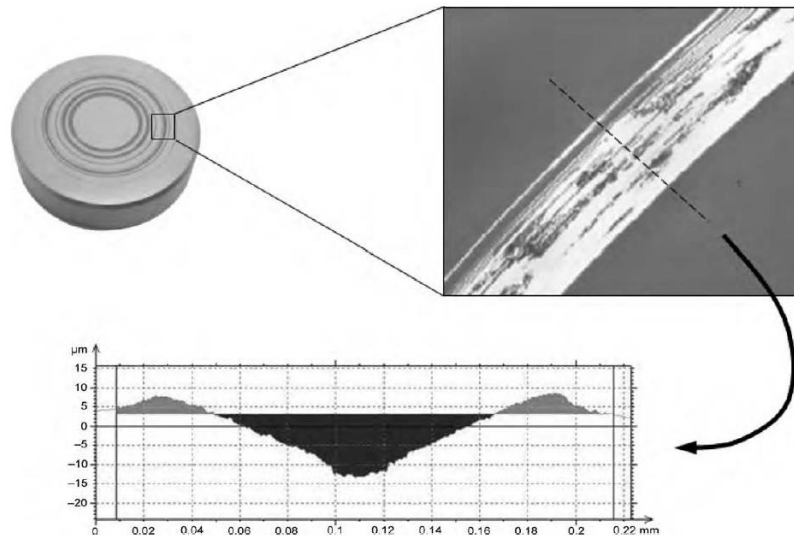


Figure 12: Wear scar section on stationary disk measured using stylus profilometer [207].

Standardized pin-on-disk test methods are only for evaluating the mechanical wear and coefficient of friction of materials in sliding contact. Tribocorrosion is defined as a material degradation process that is due to the combined effect of corrosion and mechanical wear. While tribocorrosion phenomena may affect many materials, they are most critical for metals, especially the normally corrosion resistant, so-called passive metals. As described in the previous section under the MACC model, all the metals used for total joint replacement implants fall under the category of passivating metals. The term biotribocorrosion can be used to describe tribological systems exposed to biological environments. Commercially available pin-on-disk tribometers modified for tribocorrosion testing with liquid cell and contacts for electrodes are available. These tests are designed to monitor the open-circuit potential (OCP) throughout the wear test as an indicator for corrosion/passivation or deterioration of a surface coating, if any, due to mechanical wear. The tests are also designed to monitor the evolution of the corrosion current during wear testing while a fixed potential is maintained or a potential scan, also known as potentiodynamic test, is performed to evaluate changes as a function of applied potential [207].

In some cases, the conditions that lead to fretting-corrosion does not correspond to a rotating pin-on-disk configuration and may be closer to a linear reciprocating motion. Examples of this is the deployment of a stent into an artery, the movement of a catheter or cardiac leads or the modular femoral head and stem taper micromotion. There are not commercially available linear reciprocating biotribocorrosion test setups capable of monitoring and controlling all the relevant factors pertaining to MACC in THA, hence, Swaminathan et al. built a test system used to develop and validate the MACC model in

the previous section [226]. This is a versatile test system that enables testing of any material combination (with user determined starting roughness) under variable load or potentiodynamic conditions while monitoring fretting currents, normal and tangential loads and moments. The direct movement of the pin is also monitored and they found that the observed sliding contact regimes under variable loading is consistent with previously defined fretting-wear maps [241]. Under increasing loads, fretting currents increase as asperity contacts increase and the pin is slipping across the surface of the disk, and eventually the pin sticks (no more movement under high normal loads) and the fretting-currents drop and fretting stops. We have used this test setup for the study conducted in Chapter 5.

Pin-on-disk biotribocorrosion test systems are useful for fundamental understanding of the fretting corrosion behavior of interfacing materials under variable loading and potential conditions; however, they do not give insights into the behavior of an assembled taper. Modular interfaces in orthopedic devices form a crevice interface. Standardized electrochemical test methods exist to evaluate implant materials for their susceptibility to corrode under crevice like conditions. These are ASTM F746 – Standard Test Method for Pitting and Crevice Corrosion of Metallic Surgical Implant Materials and ASTM F2129 – Standard Test Method for Conducting Cyclic Potentiodynamic Polarization Measurements to Determine the Corrosion Susceptibility of Small Implant Devices. A recent study compared these two test methods and found ASTM F2129 more effective overall at evaluating crevice corrosion compared to ASTM F746 [219]. These standardized tests for crevice corrosion are conducted under static conditions and do not account for fretting. This had led to the release of ASTM F1875 - Standard Practice for

Fretting Corrosion Testing of Modular Implant Interfaces: Hip Femoral Head-Bore and Cone Taper Interface. ASTM F1875 is the currently accepted voluntary consensus standard used to evaluate fretting corrosion of head-neck modular tapers (Figure 13).

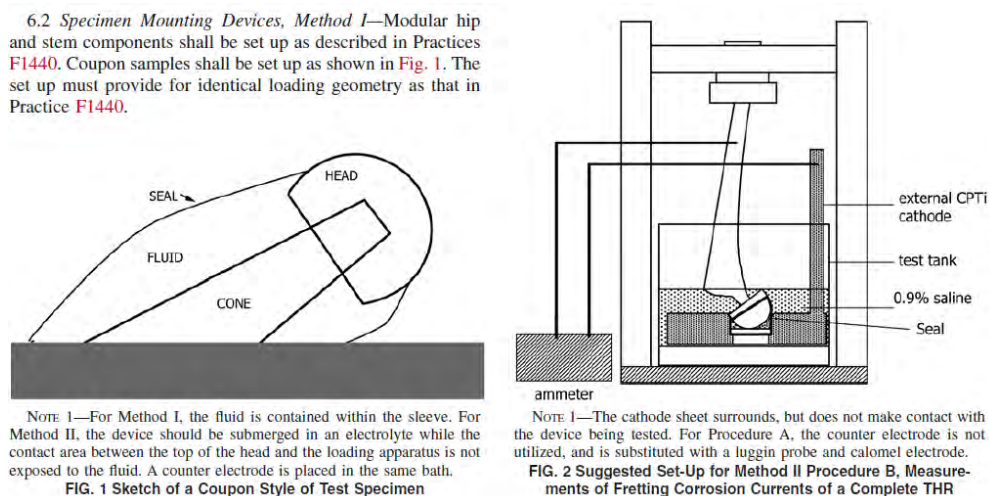


Figure 13: Page from the standard ASTM F1875 showing test system setup.

A similar test system to ASTM F1875, yet with some important differences to compensate for the factors that limit the ability of F1875 to quantitatively assess the differences in fretting corrosion of head-neck modular tapers was developed by Mali et al [165]. Compared to the system in F1875, the adjustments Mali et al. made were designed to be able to better relate motion measurements to fretting currents, hence, linking the mechanical and electrochemical processes present during testing certain material or taper designs. In addition, their test setup also includes potentiostatic measurements, incremental loading, higher maximum cyclic loads and incorporated the use of noncontact micron-scale motion sensors that were used in electrochemical solutions to

obtain concurrent information on corrosion currents and micromotions. The test to be described in this study brings together simultaneous measurement of subsidence and micromotion of the head on the neck with fretting current response. This is lacking in the F1875 test system and is important to measure because of the direct relationship between oxide abrasion, dictated by mechanics, and corrosion, dictated by electrochemical repassivation. This incremental cyclic fretting corrosion test method [165] is a versatile means of assessing potential new taper designs in the future and was used to evaluate the short-term corrosion and micromechanical behavior of 32 unique head-neck taper design/material/assembly conditions [191].

1.5 Need for Quantitative Evaluation of Tapers

The comprehensive literature review of taper corrosion in retrieval studies and the following examination of modular junctions in vitro have established that the materials and designs being used in THA are prone to undergoing MACC. Additionally, it has been shown that modular taper fretting corrosion is the most likely initiator of other damage modes seen such as etching, pitting corrosion, intergranular corrosion, imprinting and widening of the crevice leading to subsequent fluid infiltration. Surgical and patient factors may exacerbate existing risk factors due to device design and lead to increased severity of the damage due to fretting and corrosion. There are still unknowns about the best strategy to mitigate modular fretting-corrosion; however, modularity is an asset and the factors that contribute to the MACC phenomenon further need to be investigated. Figure 14 summarizes the risk factors identified in the literature review and the potential reasons for revision if there is severe fretting-corrosion damage.

Retrieval analyses and in vitro studies each provide different ways of gaining further insight about the device, surgical and patient factors that may be contributing to MACC. There has been an effort to improve evaluation methods of retrievals and while visual semi-qualitative methods are widely used, quantitative methods are used less often. The studies provided in this document detail the efforts to develop practical quantitative evaluation methods of retrieval taper surfaces. Retrieval studies help evaluate existing designs and their clinical performance; however, future materials and designs developed need to be tested using in vitro methods that accurately simulate the conditions in vivo.

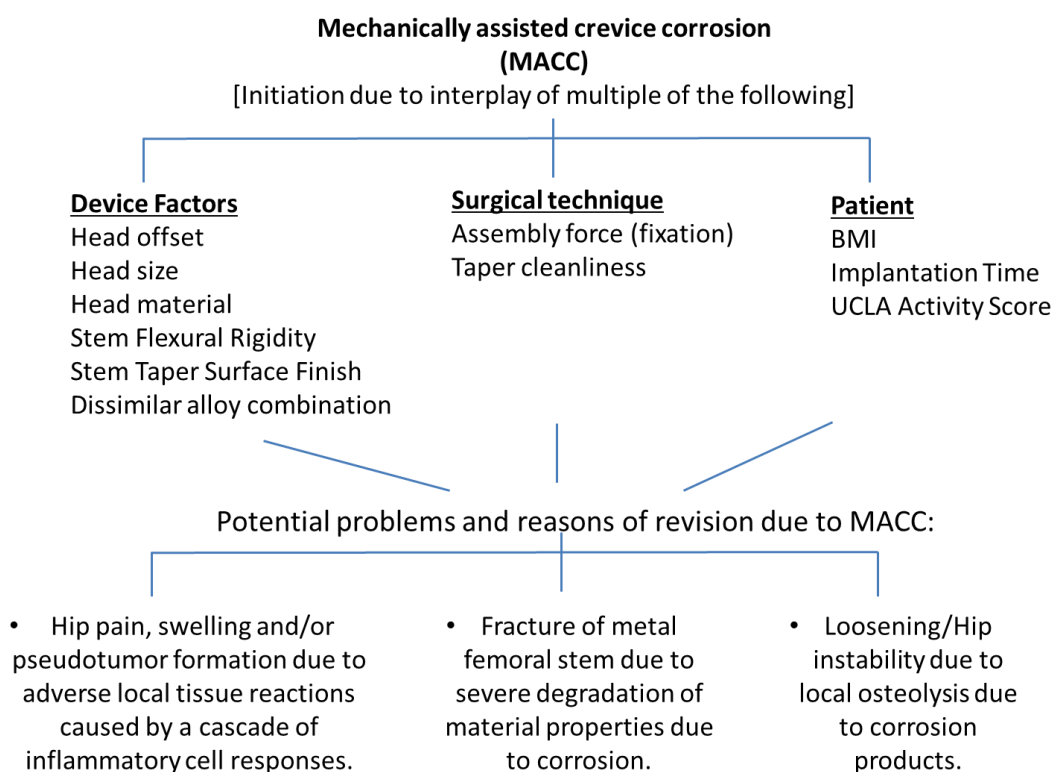


Figure 14: Summary possible device, surgical and patient factors and the potential revision outcome due to severe fretting-corrosion.

References

4. Arnholt C, Underwood R, MacDonald D, Higgs G, Chen A, Klein G, Hamlin B, Lee G, Mont M, Cates H, Malkani A, Kraay M, Rimnac C, Kurtz S. Microgrooved Surface Topography Does Not Influence Fretting Corrosion of Tapers in THA: Classification and Retrieval Analysis. *Modularity and Tapers in Total Joint Replacement Devices*. Conshohocken PA: American Society of Testing Materials (ASTM); 2015.
6. Arnholt CM, MacDonald DW, Tohfafarosh M, Gilbert JL, Rimnac CM, Kurtz SM, Implant Research Center Writing C, Klein G, Mont MA, Parvizi J, Cates HE, Lee GC, Malkani A, Kraay M. Mechanically assisted taper corrosion in modular TKA. *Journal of Arthroplasty*. 2014;29:205-208.
7. Arnholt CM, MacDonald DW, Underwood RJ, Guyer EP, Rimnac CM, Kurtz SM, Implant Research Center Writing C, Mont MA, Klein GR, Lee GC, Chen AF, Hamlin BR, Cates HE, Malkani AL, Kraay MJ. Do Stem Taper Microgrooves Influence Taper Corrosion in Total Hip Arthroplasty? A Matched Cohort Retrieval Study. *Journal of Arthroplasty*. 2017;32:1363-1373.
8. Ashkanfar A, Langton DJ, Joyce TJ. Does a micro-grooved trunnion stem surface finish improve fixation and reduce fretting wear at the taper junction of total hip replacements? A finite element evaluation. *Journal of Biomechanics*. 2017;63:47-54.
10. Australian Orthopaedic Association. *Australian Orthopaedic Association National Joint Replacement Registry. Annual Report. Adelaide:AOA; 2019*.
20. Baykal D, Siskey RS, Haider H, Saikko V, Ahlroos T, Kurtz SM. Advances in tribological testing of artificial joint biomaterials using multidirectional pin-on-disk testers. *Journal of the mechanical behavior of biomedical materials*. 2014;31:117-134.
21. Baykal D, Siskey RS, Underwood RJ, Briscoe A, Kurtz SM. The Biotribology of PEEK-on-HXLPE Bearings Is Comparable to Traditional Bearings on a Multidirectional Pin-on-disk Tester. *Clinical orthopaedics and related research*. 2016;474:2384-2393.
22. Bishop N, Witt F, Pourzal R, Fischer A, Rutschi M, Michel M, Morlock M. Wear patterns of taper connections in retrieved large diameter metal-on-metal bearings. *Journal of orthopaedic research : official publication of the Orthopaedic Research Society*. 2013;31:1116-1122.
29. Bobyn JD, Tanzer M, Krygier JJ, Dujovne AR, Brooks CE. Concerns with modularity in total hip arthroplasty. *Clinical orthopaedics and related research*. 1994:27-36.
30. Bone MC, Sidaginamale RP, Lord JK, Scholes SC, Joyce TJ, Nargol AVF, Langton DJ. Determining material loss from the femoral stem trunnion in hip arthroplasty using a coordinate measuring machine. *Proceedings of the Institution of Mechanical Engineers Part H-Journal of Engineering in Medicine*. 2015;229:69-76.
31. Bonner B, Arauz P, Klemm C, Kwon YM. Outcome of Re-Revision Surgery for Adverse Local Tissue Reaction in Metal-on-Polyethylene and Metal-on-Metal Total Hip Arthroplasty. *The Journal of arthroplasty*. 2020.
37. Brown SA, Flemming CA, Kawalec JS, Placko HE, Vassaux C, Merritt K, Payer JH, Kraay MJ. Fretting corrosion accelerates crevice corrosion of modular hip tapers. *Journal of Applied Biomaterials (New York)*. 1995;6:19-26.
38. Brown SA, Simpson JP. Crevice and fretting corrosion of stainless-steel plates and screws. *Journal of biomedical materials research*. 1981;15:867-878.
40. Cahoon JR, Paxton HW. Metallurgical Analyses of Failed Orthopedic Implants *Journal of biomedical materials research*. 1968;2:1-22.

41. Cartner J, Aldinger P, Li C, Collins D. Characterization of Femoral Head Taper Corrosion Features Using a 22-Year Retrieval Database. *HSS Journal*. 2017;13:35-41.
42. Chana R, Esposito C, Campbell PA, Walter WK, Walter WL. Mixing and matching causing taper wear: corrosion associated with pseudotumour formation. *The Journal of bone and joint surgery. British volume*. 2012;94:281-286.
43. Chaplin RPS, Lee AJC, Hooper RM. Assessment of wear on the cones of modular stainless steel Exeter hip stems. *Journal of Materials Science: Materials in Medicine*. 2004;15:977-990.
44. Charnley J. Arthroplasty of the hip. A new operation. *Lancet*. 1961;1:1129-1132.
51. Cohen J, Lindenbaum B. Fretting corrosion in orthopedic implants. *Clinical orthopaedics and related research*. 1968;61:167-175.
52. Colangelo VJ, Greene ND. Corrosion and fracture of type 316 SMO orthopedic implants. *Journal of biomedical materials research*. 1969;3:247-265.
53. Collier JP, Mayor MB, Jensen RE, Surprenant VA, Surprenant HP, McNamar JL, Belec L. Mechanisms of failure of modular prostheses. *Clinical orthopaedics and related research*. 1992:129-139.
54. Collier JP, Mayor MB, Williams IR, Surprenant VA, Surprenant HP, Currier BH. The tradeoffs associated with modular hip prostheses. *Clinical orthopaedics and related research*. 1995:91-101.
55. Collier JP, Surprenant VA, Jensen RE, Mayor MB, Surprenant HP. Corrosion between the components of modular femoral hip prostheses. *The Journal of bone and joint surgery. British volume*. 1992;74:511-517.
56. Cook RB, Bolland BJ, Wharton JA, Tilley S, Latham JM, Wood RJ. Pseudotumour formation due to tribocorrosion at the taper interface of large diameter metal on polymer modular total hip replacements. *The Journal of arthroplasty*. 2013;28:1430-1436.
57. Cook SD, Barrack RL, Baffes GC, Clemow AJ, Serekian P, Dong N, Kester MA. Wear and corrosion of modular interfaces in total hip replacements. *Clinical orthopaedics and related research*. 1994:80-88.
58. Cook SD, Barrack RL, Clemow AJ. Corrosion and wear at the modular interface of uncemented femoral stems. *The Journal of bone and joint surgery. British volume*. 1994;76:68-72.
59. Cook SD, Manley MT, Kester MA, Dong NG. Torsional resistance and wear of a modular sleeve-stem hip system. *Clinical materials*. 1993;12:153-158.
63. Cramer SD, Covino BS, Jr. 14. Corrosion of Cobalt and Cobalt-Base Alloys. *ASM Handbook, Volume 13B - Corrosion: Materials*: ASM International; 2005.
64. Cramer SD, Covino BS, Jr. 19. Corrosion of Titanium and Titanium Alloys. *ASM Handbook, Volume 13B - Corrosion: Materials*: ASM International; 2005.
69. de Steiger RN, Hatton A, Peng Y, Graves S. What Is the Risk of THA Revision for ARMD in Patients with Non-metal-on-metal Bearings? A Study from the Australian National Joint Replacement Registry. *Clinical orthopaedics and related research*. 2020.
70. Del Balso C, Teeter MG, Tan SC, Howard JL, Lanting BA. Trunnionosis: Does Head Size Affect Fretting and Corrosion in Total Hip Arthroplasty? *Journal of Arthroplasty*. 2016;31:2332-2336.
72. DeVilliers T, ed. *STP 144: Symposium on Fretting Corrosion*. Philadelphia, PA: American Society for Testing Materials; 1952.

73. Di Laura A, Hothi H, Henckel J, Swiatkowska I, Liow MHL, Kwon YM, Skinner JA, Hart AJ. Retrieval analysis of metal and ceramic femoral heads on a single CoCr stem design. *Bone & joint research*. 2017;6:345-350.
74. Dyrkacz RMR, Brandt JM, Ojo OA, Turgeon TR, Wyss UP. The influence of head size on corrosion and fretting behaviour at the head-neck interface of artificial hip joints. *Journal of Arthroplasty*. 2013;28:1036-1040.
75. Eichler D, Barry J, Lavigne M, Masse V, Vendittoli PA. No radiological and biological sign of trunnionosis with Large Diameter Head Ceramic Bearing Total Hip Arthroplasty after 5 years. *Orthopaedics & traumatology, surgery & research : OTSR*. 2020.
81. Flemming CAC, Brown SA, Payer JH. Mechanical testing for fretting corrosion of modular total hip tapers. In: Kambic HE, Yokobori JAT, ed. *Biomaterials' Mechanical Properties*. Philadelphia: American Society for Testing and Materials; 1994.
84. Gilbert JL. Electrochemical Behavior of Metals in the Biological Milieu. In: Ducheyne P, ed. *Comprehensive Biomaterials*: Elsevier; 2011:21-48.
85. Gilbert JL, Buckley CA, Jacobs JJ. In vivo corrosion of modular hip prosthesis components in mixed and similar metal combinations. The effect of crevice, stress, motion, and alloy coupling. *Journal of biomedical materials research*. 1993;27:1533-1544.
87. Gilbert JL, Jacobs JJ. The Mechanical and Electrochemical Processes Associated with Taper Fretting and Crevice Corrosion: A Review. In: Marlowe DE, Parr JE, Mayor MB, ed. *STP1301: Modularity of Orthopedic Implants*. West Conshohocken, PA: American Society for Testing and Materials; 1997.
88. Gilbert JL, Mali S, Urban RM, Silverton CD, Jacobs JJ. In vivo oxide-induced stress corrosion cracking of Ti-6Al-4V in a neck-stem modular taper: Emergent behavior in a new mechanism of in vivo corrosion. *Journal of biomedical materials research. Part B, Applied biomaterials*. 2011;100:584-594.
89. Gilbert JL, Mali SA, Sivan S. Corrosion of Modular Tapers in Total Joint Replacements: A Critical Assessment of Design, Materials, Surface Structure, Mechanics, Electrochemistry, and Biology. In: Greenwald S, Kurtz SM, ed. *STP1591: Modularity and Tapers in Total Joint Replacement Devices*. West Conshohocken, PA: ASTM International; 2015.
90. Gilbert JL, Sivan S, Liu Y, Kocagöz SB, Arnholt CM, Kurtz SM. Direct in vivo inflammatory cell-induced corrosion of CoCrMo alloy orthopedic implant surfaces. *Journal of Biomedical Materials Research - Part A*. 2015;103:211-223.
91. Gill IP, Webb J, Sloan K, Beaver RJ. Corrosion at the neck-stem junction as a cause of metal ion release and pseudotumour formation. *The Journal of bone and joint surgery. British volume*. 2012;94:895-900.
92. Goldberg JR, Gilbert JL. In vitro corrosion testing of modular hip tapers. *Journal of biomedical materials research. Part B, Applied biomaterials*. 2003;64:78-93.
93. Goldberg JR, Gilbert JL. The electrochemical and mechanical behavior of passivated and TiN/AlN-coated CoCrMo and Ti6Al4V alloys. *Biomaterials*. 2004;25:851-864.
94. Goldberg JR, Gilbert JL, Jacobs JJ, Bauer TW, Paprosky W, Leurgans S. A multicenter retrieval study of the taper interfaces of modular hip prostheses. *Clinical orthopaedics and related research*. 2002:149-161.
98. Hall DJ, Pourzal R, Lundberg HJ, Mathew MT, Jacobs JJ, Urban RM. Mechanical, chemical and biological damage modes within head-neck tapers of CoCrMo and Ti6Al4V contemporary hip replacements. *Journal of Biomedical Materials Research. Part B, Applied Biomaterials*. 2018;106:1672-1685.

100. Hallab NJ, Messina C, Skipor A, Jacobs JJ. Differences in the fretting corrosion of metal-metal and ceramic-metal modular junctions of total hip replacements. *Journal of orthopaedic research : official publication of the Orthopaedic Research Society*. 2004;22:250-259.
103. Hampton C, Weitzler L, Baral E, Wright TM, Bostrom MPG. Do oxidized zirconium heads decrease tribocorrosion in total hip arthroplasty? A study of retrieved components. *Bone and Joint Journal*. 2019;101 B:386-389.
107. Heckmann ND, Sivasundaram L, Stefl MD, Kang HP, Basler ET, Lieberman JR. Total Hip Arthroplasty Bearing Surface Trends in the United States From 2007 to 2014: The Rise of Ceramic on Polyethylene. *Journal of Arthroplasty*. 2018;33:1757-1763.e1751.
109. Higgs GB, Hanzlik JA, MacDonald DW, Gilbert JL, Rimnac CM, Kurtz SM. Is increased modularity associated with increased fretting and corrosion damage in metal-on-metal total hip arthroplasty devices?: a retrieval study. *The Journal of arthroplasty*. 2013;28:2-6.
110. Higgs GB, Hanzlik JA, MacDonald DW, Kane WM, Day JS, Klein GR, Parvizi J, Mont MA, Kraay MJ, Martell JM, Gilbert JL, Rimnac CM, Kurtz SM. Method of characterizing fretting and corrosion at the various taper connections of retrieved modular components from metal-on-metal total hip arthroplasty. In: *ASTM Symposium on Metal-on-Metal Total Hip Replacement Devices, May 8, 2012 - May 8, 2012*. Phoenix, AZ, United states: ASTM International: 2013:146-156.
111. Higgs GB, MacDonald DW, Gilbert JL, Rimnac CM, Kurtz SM, Implant Research Center Writing C. Does Taper Size Have an Effect on Taper Damage in Retrieved Metal-on-Polyethylene Total Hip Devices? *The Journal of arthroplasty*. 2016;31:277-281.
113. Hothi HS, Eskelinen AP, Henckel J, Kwon YM, Blunn GW, Skinner JA, Hart AJ. Effect of Bearing Type on Taper Material Loss in Hips From 1 Manufacturer. *Journal of Arthroplasty*. 2018;33:1588-1593.
114. Hothi HS, Kendoff D, Lausmann C, Henckel J, Gehrke T, Skinner J, Hart A. Clinically insignificant trunnionosis in large-diameter metal-on-polyethylene total hip arthroplasty. *Bone and Joint Research*. 2017;6:52-56.
120. Huot Carlson JC, Van Citters DW, Currier JH, Bryant AM, Mayor MB, Collier JP. Femoral stem fracture and in vivo corrosion of retrieved modular femoral hips. *The Journal of arthroplasty*. 2012;27:1389-1396.e1381.
121. Jacobs JJ. Corrosion at the Head-Neck Junction: Why Is This Happening Now? *Journal of Arthroplasty*. 2016;31:1378-1380.
122. Jacobs JJ, Gilbert JL, Urban RM. Corrosion of Metal Orthopaedic Implants*. *Journal of Bone & Joint Surgery - American Volume*. 1998;80:268-282.
125. Kao YYJ, Koch CN, Wright TM, Padgett DE. Flexural Rigidity, Taper Angle, and Contact Length Affect Fretting of the Femoral Stem Trunnion in Total Hip Arthroplasty. *Journal of Arthroplasty*. 2016;31:254-258.
127. Kim YH, Park JW, Kim JS. There is no significant difference in fretting and corrosion at the trunnion of metal and ceramic heads. *Orthopedics*. 2019;42:e99-e103.
131. Kocagoz SB, Underwood RJ, Sivan S, Gilbert JL, Macdonald DW, Day JS, Kurtz SM. Does Taper Angle Clearance Influence Fretting and Corrosion Damage at the Head-Stem Interface? A Matched Cohort Retrieval Study. *Semin Arthroplasty*. 2013;24:246-254.
132. Koch CN, Figgie M, Jr., Figgie MP, Elpers ME, Wright TM, Padgett DE. Ceramic Bearings with Titanium Adapter Sleeves Implanted During Revision Hip Arthroplasty Show Minimal Fretting or Corrosion: a Retrieval Analysis. *HSS Journal*. 2017;13:241-247.

134. Kubacki GW, Gilbert JL. The effect of the inflammatory species hypochlorous acid on the corrosion and surface damage of Ti-6Al-4V and CoCrMo alloys. *Journal of biomedical materials research. Part A*. 2018;106:3185-3194.
135. Kurtz SM, ed. *UHMWPE Biomaterials Handbook: Ultra-High Molecular Weight Polyethylene in Total Joint Replacement and Medical Devices*: Elsevier; 2009.
143. Kurtz SM, Kocagoz SB, Hanzlik JA, Underwood RJ, Gilbert JL, MacDonald DW, Lee GC, Mont MA, Kraay MJ, Klein GR, Parvizi J, Rimnac CM. Do ceramic femoral heads reduce taper fretting corrosion in hip arthroplasty? A retrieval study. *Clinical orthopaedics and related research*. 2013;471:3270-3282.
144. Kurtz SM, MacDonald DW, Gilbert JL, Mont MA, Klein G, Chen A, Kraay M, Hamlin B, Rimnac CM. Is Taper Fretting Corrosion a Threat to the Clinical Performance of Large-Diameter Hips with Highly Crosslinked Polyethylene Bearings? In: Greenwald S, Kurtz SM, ed. *STP1591: Modularity and Tapers in Total Joint Replacement Devices*. West Conshohocken, PA: ASTM International; 2015.
145. Kurtz SM, MacDonald DW, Kocagoz S, Tohfafarosh M, Baykal D. Can pin-on-disk testing be used to assess the wear performance of retrieved UHMWPE components for total joint arthroplasty? *BioMed research international*. 2014;2014:581812.
146. Kurtz SM, Ong KL, Schmier J, Mowat F, Saleh K, Dybvik E, Karrholm J, Garellick G, Havelin LI, Furnes O, Malchau H, Lau E. Future clinical and economic impact of revision total hip and knee arthroplasty. *The Journal of bone and joint surgery. American volume*. 2007;89 Suppl 3:144-151.
152. Langton DJ, Sidaginamale R, Lord JK, Nargol AV, Joyce TJ. Taper junction failure in large-diameter metal-on-metal bearings. *Bone & joint research*. 2012;1:56-63.
159. Lieberman JR, Rimnac CM, Garvin KL, Klein RW, Salvati EA. An analysis of the head-neck taper interface in retrieved hip prostheses. *Clinical orthopaedics and related research*. 1994:162-167.
160. Lim S-JMD, Jang S-PMD, Kim D-WMD, Moon Y-WMD, Park Y-SMDa. Primary Ceramic-on-ceramic Total Hip Arthroplasty Using a 32-mm Ceramic Head With a Titanium-alloy Sleeve. *Clinical Orthopaedics & Related Research*. 2015;473:3781-3787.
161. Lombardi AV, Jr., Mallory TH, Vaughn BK, Drouillard P. Aseptic loosening in total hip arthroplasty secondary to osteolysis induced by wear debris from titanium-alloy modular femoral heads. *The Journal of bone and joint surgery. American volume*. 1989;71:1337-1342.
163. MacDonald DW, Chen AF, Lee GC, Klein GR, Mont MA, Kurtz SM, Taper Corrosion Writing C, Cates HE, Kraay MJ, Rimnac CM. Fretting and Corrosion Damage in Taper Adapter Sleeves for Ceramic Heads: A Retrieval Study. *The Journal of arthroplasty*. 2017;32:2887-2891.
164. Mali SA. MECHANICALLY ASSISTED CORROSION PERFORMANCE OF METALLIC BIOMATERIALS: IMPLANT RETRIEVAL, MATERIAL ANALYSES AND DEVICE TESTING. Syracuse University; 2015.
165. Mali SA, Gilbert JL. Correlating fretting corrosion and micromotions in modular tapers: Test method development and assessment. In: *ASTM Special Technical Publication*. 2015:259-282.
171. Mathiesen EB, Lindgren JU, Blomgren GG, Reinholt FP. Corrosion of modular hip prostheses. *The Journal of bone and joint surgery. British volume*. 1991;73:569-575.
172. Matthies A, Underwood R, Cann P, Ilo K, Nawaz Z, Skinner J, Hart AJ. Retrieval analysis of 240 metal-on-metal hip components, comparing modular total hip replacement with hip resurfacing. *The Journal of bone and joint surgery. British volume*. 2011;93:307-314.

173. Matthies AK, Racasan R, Bills P, Blunt L, Cro S, Panagiotidou A, Blunn G, Skinner J, Hart AJ. Material loss at the taper junction of retrieved large head metal-on-metal total hip replacements. *Journal of orthopaedic research : official publication of the Orthopaedic Research Society*. 2013;31:1677-1685.
174. McKellop HA, Sarmiento A, Brien W, Park SH. Interface corrosion of a modular head total hip prosthesis. *The Journal of arthroplasty*. 1992;7:291-294.
176. Mendenhall S. 2014 Hip and Knee Implant Review. *Orthopedic Network News*. 2014;25.
177. Mendenhall S. Hospital resources and implant cost management—a 2013 update. *Orthopedic Network News*. 2014;25:9-15.
183. Morlock MM, Dickinson EC, Günther KP, Bünte D, Polster V. Head Taper Corrosion Causing Head Bottoming Out and Consecutive Gross Stem Taper Failure in Total Hip Arthroplasty. *Journal of Arthroplasty*. 2018;33:3581-3590.
191. Ouellette ES, Mali SA, Kim J, Grostefon J, Gilbert JL. Design, Material, and Seating Load Effects on In Vitro Fretting Corrosion Performance of Modular Head-Neck Tapers. *The Journal of arthroplasty*. 2019;34:991-1002.
194. Panagiotidou A, Meswania J, Hua J, Muirhead-Allwood S, Hart A, Blunn G. Enhanced wear and corrosion in modular tapers in total hip replacement is associated with the contact area and surface topography. *Journal of orthopaedic research : official publication of the Orthopaedic Research Society*. 2013;31:2032-2039.
202. Porter DA, Urban RM, Jacobs JJ, Gilbert JL, Rodriguez JA, Cooper HJ. Modern trunnions are more flexible: a mechanical analysis of THA taper designs. *Clinical orthopaedics and related research*. 2014;472:3963-3970.
205. Pourzal R, Lundberg HJ, Hall DJ, Jacobs JJ. What Factors Drive Taper Corrosion? *Journal of Arthroplasty*. 2018;33:2707-2711.
207. Randall NX. Tribological Characterization of Biomaterials. In: Narayan R, ed. *ASM Handbook, Volume 23: Materials for Medical Devices*: ASM International; 2012.
216. Siljander MP, Baker EA, Baker KC, Salisbury MR, Thor CC, Verner JJ. Fretting and Corrosion Damage in Retrieved Metal-on-Polyethylene Modular Total Hip Arthroplasty Systems: What Is the Importance of Femoral Head Size? *Journal of Arthroplasty*. 2018;33:931-938.
217. Siljander MP, Gehrke CK, Wheeler SD, Sobh AH, Moore DD, Flierl MA, Baker EA. Does Taper Design Affect Taper Fretting Corrosion in Ceramic-on-Polyethylene Total Hip Arthroplasty? A Retrieval Analysis. *Journal of Arthroplasty*. 2019;34:S366-S372.e362.
219. Sivan S, Rahman E, Weaver JD, Di Prima M. Comparison of ASTM F2129 and ASTM F746 for Evaluating Crevice Corrosion. *Journal of Testing and Evaluation*. 2019;47.
221. Songur M, Calikkan H, Gokmese F, Simsek SA, Altun NS, Aksu ML. Electrochemical corrosion properties of metal alloys used in orthopaedic implants. *J Appl Electrochem*. 2009;39:1259–1265.
225. Swaminathan V. FRETTING CREVICE CORROSION OF METALLIC BIOMATERIALS: INSTRUMENT DEVELOPMENT AND MATERIALS ANALYSIS. *Biomedical and Chemical Engineering*. Syracuse, NY, USA: Syracuse University; 2012:224.
226. Swaminathan V, Gilbert JL. Fretting corrosion of CoCrMo and Ti6Al4V interfaces. *Biomaterials*. 2012;33:5487-5503.
227. Syrett BC, Acharya A, ed. *STP 684: Corrosion and Degradation of Implant Materials*. Philadelphia, PA: American Society for Testing and Materials; 1978.
228. Tan SC, Lau ACL, Del Balso C, Howard JL, Lanting BA, Teeter MG. Tribocorrosion: Ceramic and Oxidized Zirconium vs Cobalt-Chromium Heads in Total Hip Arthroplasty. *Journal of Arthroplasty*. 2016;31:2064-2071.

229. Tan SC, Teeter MG, Del Balso C, Howard JL, Lanting BA. Effect of Taper Design on Trunnionosis in Metal on Polyethylene Total Hip Arthroplasty. *The Journal of arthroplasty*. 2015;30:1269-1272.
231. The National Joint Registry [NJR] for England W, Northern Ireland and the Isle of Man. *National Joint Registry 15th Annual Report 2018*.
233. Tkaczyk C, Tabrizian M. Biocompatibility, Metals Ions, and Corrosion Products. In: Narayan R, ed. *ASM Handbook, Volume 23: Materials for Medical Devices*: ASM International; 2012.
234. Tomlinson GA, Thorpe PL, Gough HJ. An Investigation of the Fretting Corrosion of Closely Fitting Surfaces. *Proceedings of the Institution of Mechanical Engineers*. 1939;141:223-249.
236. Underwood RJ, Kocagoz SB, Smith R, Sayles RS, Siskey R, Kurtz SM, Cann PM. A Protocol to Assess the Wear of Head/Neck Taper Junctions in Large Head Metal-on-Metal (LHMoM) Hips. In: Kurtz SM, Greenwald AS, Mihalko WM, Lemons JE, ed. *Metal-on-Metal Total Hip Replacement Devices*; 2013:209-234.
237. Underwood RJ, Kocagoz SB, Smith R, Sayles RS, Siskey R, Kurtz SM, Cann PM. A protocol to assess the wear of head/neck taper junctions in large head metal-on-metal (LHMoM) hips. In: *ASTM Symposium on Metal-on-Metal Total Hip Replacement Devices, May 8, 2012 - May 8, 2012*. Phoenix, AZ, United states: ASTM International: 2013:209-234.
241. Vingsbo O, Soderberg S. On Fretting Maps. *Wear*. 1988;126:131-147.
242. Walton K, Petrucci M, Racasan R, Blunt L, Hart A, Bills P. Focus variation measurement and advanced analysis of volumetric loss at the femoral head taper interface of retrieved modular replacement hips in replica. In: *Journal of Physics: Conference Series*. 2019.
243. Waly F, Abduljabbar FH, Gascoyne T, Turgeon TR, Huk O. Stem-Sleeve Junction Failure of a Modular Femoral Hip System: a Retrieval Analysis. *HSS Journal*. 2015;11:285-290.
244. Wang Q, Eltit F, Garbuz D, Duncan C, Masri B, Greidanus N, Wang R. CoCrMo metal release in metal-on-highly crosslinked polyethylene hip implants. *Journal of Biomedical Materials Research - Part B Applied Biomaterials*. 2020;108:1213-1228.
249. Wiegand MJ, Shenoy AA, Littlejohn SE, Gilbert JL. Sensing Localized Surface Corrosion Damage of CoCrMo Alloys and Modular Tapers of Total Hip Retrievals Using Nearfield Electrochemical Impedance Spectroscopy. *ACS Biomaterials Science & Engineering*. 2020;6:1344-1354.
250. Williams RL, Brown SA, Merritt K. Electrochemical studies on the influence of proteins on the corrosion of implant alloys. *Biomaterials*. 1988;9:181-186.

2 Ceramic Biomaterials

Ceramic components are an attractive option for biomaterial components due to their advantageous properties in biocompatibility, wear resistance, low friction and wettability [116] and they do not corrode. The high wear rate in the gold standard metal-on-polyethylene (MoP) bearings, especially prior to highly-crosslinked polyethylene led to the introduction of ceramic components in joint replacement implants [65, 148]. The first total hip arthroplasty (THA) used an alumina-on-polyethylene bearing combination and was performed in 1970 in France by Boutin et al. [33, 35] and the use of alumina for joint replacements was later followed by researchers in Japan in both hips and knees in the late 1970s [188, 215]. These studies with alumina-on-polyethylene bearings had promising results with lower polyethylene mechanical wear and the alumina showed high chemical durability and biocompatibility [34, 35]; however, early applications were associated with high fracture rates of ceramic components [119, 128, 142]. This section outlines the advancements made in the orthopedic ceramic materials and their clinical performance today evaluated in a matched cohort retrieval study as an alternative to mitigate taper fretting and corrosion.

2.1 History

Since the first use of alumina in 1970 for THA, advances in manufacturing techniques and introduction of new materials have significantly improved the fracture-toughness of ceramics used in orthopedics [142], [116]. Improvements in manufacturing techniques includes the introduction of hot-isostatic pressing (HIP), proof testing and laser marking. HIP, introduced in 1995, improved fracture strength by creating denser

ceramics with lower porosity and smaller grain sizes. Proof testing, started in the 1990s, replaced destructive burst testing of 2-3% of each lot as a more reliable method of quality control by exposing 100% of the components temporarily to stress state above the physiological requirements. Engravings of manufacturer and lot numbers, which may have been a possible stress riser, were replaced by laser markings further reducing the risk of fracture [230]. Improvements in manufacturing processes have shown a clear decrease in the incidence of fracture for alumina ceramics. BioloX-forte (CeramTec Inc., Germany), 3rd generation alumina implants, were manufactured using HIP and had 6 times less fracture rates compared to the 1st generation of alumina according to manufacturer statistics (rate 0.004%) [230].

Prior to the widespread use and successful manufacturing of alumina, engineered zirconia, ZrO_2 , was introduced in the late 1980's, as a more reliable alternative to alumina ceramics with higher fracture toughness and mechanical strength. Unfortunately, there are mixed reports as to the success of zirconia in the clinic [47] which was attributed to its metastable nature and the manufacturing process. Zirconia owes its higher fracture toughness to a stress induced phase transformation from its metastable tetragonal phase to its stable monoclinic phase at ambient temperatures. During the 1990s, stabilized zirconia was widely used as ceramic femoral heads in COP bearings because of its higher toughness and strength relative to alumina. However, depending on the manufacturing conditions and hydrothermal effects in vivo, the monolithic tetragonal zirconia may be too unstable and transform catastrophically into the monoclinic phase [50].

Looking at the history of the ceramic materials market and their late adoption is important to understand how metal femoral heads and the MoM hard-on-hard bearings became so prevalent in the orthopedics. Unfortunately, the rise of the zirconia femoral heads led to the increase in demand and to meet the market need, a change in the manufacturing process by one of the leading zirconia femoral head manufacturers also led to this materials decline. St. Gobain Desmarquest, the largest manufacturer of zirconia femoral heads, switched their production from a batch furnace process to a serial line furnace, which led to instability in the microstructure of the ceramic material. These batches produced with the new method led to zirconia femoral heads that underwent catastrophic phase transformation in vivo [168]. In 2001, St. Gobain Desmarquest announced a worldwide recall of selected batches due to deviations in thermal processing during their manufacture. While zirconia is still being used clinically in Europe and Japan [83, 149] the controversial clinical success has shown that this is not the optimal material for orthopedic applications. Shortly after this recall, alumina ceramic-on-ceramic (CoC) bearings were approved in the United States in 2003, but the clinical adoption faced another road-block due to increasing reports of bearing noise (squeaking) appeared in the scientific literature as well as the lay press. Unfortunately, this made the large diameter, metal-on-metal (MoM) bearings the primary alternative to articulations incorporating polyethylene.

To address the issues with the existing orthopedic ceramics performance, two promising CoC alternatives to zirconia were introduced. The first option addresses the fracture concerns by using zirconium metal alloy with a proprietary method to generate a ceramicized surface a few microns thick through oxidation. This oxidized zirconium was

marketed under the trade name Oxinium™ by Smith and Nephew Orthopedics (Memphis, TN) [214]. The ceramic surface of Oxinium material provides increased scratch resistance and is more wettable leads to lower UHMWPE wear in hip simulators compared to CoCrMo femoral heads. Additionally, since it has a ductile zirconia alloy substrate, this product combines the bearing wear properties of a ceramic material without the negative risks associated with ceramic fracture.

Other commercially available options, more broadly available than Oxinium, are ceramic composites which use the phase transformation of zirconia to their advantage as a toughening mechanism. Fabricated from mixtures of alumina and zirconia and known as zirconia-toughened alumina (ZTA), or alumina-toughened zirconia (ATZ) ceramic composites are suitable for both CoP and CoC applications. ATZ comprises 80% tetragonal zirconia polycrystals (ZrO_2 -TZP) and 20% alumina (Al_2O_3) and is reported to have superior mechanical and tribological properties compared to alumina [45].

2.2 Zirconia Toughened Alumina

Zirconia toughened alumina (ZTA), an alumina matrix composite ceramic, in which alumina is the primary or continuous phase (70–95%) and zirconia is the secondary phase (30% to 5%), is a material that combines the advantageous properties of monolithic alumina and zirconia. Under the condition that most of the zirconia is retained in the tetragonal phase, the addition of zirconia to alumina results in higher strength and fracture toughness with little reduction in hardness and elastic modulus compared to monolithic alumina ceramics. Additionally, the excellent wear characteristics and low susceptibility to stress assisted degradation of high performance, alumina ceramics is also preserved in zirconia toughened alumina ceramics. Higher fracture toughness allows for

the manufacture of thinner liners to reduce risk of impingement and dislocation and improve stability.

ZTA components are comprised of an alumina-rich composition where zirconia is evenly dispersed in the alumina matrix. ZTA composites have mechanical properties that are often better than monolithic alumina or stabilized zirconia. They achieve these properties by using several mechanisms: controlling the phase transformation in the zirconia particles, blocking crack growth by controlling grain shape, and strengthening the alumina phase itself through control of grain size and various additions. Advances in material properties led to FDA approval of ceramic-on-polyethylene (CoP) combinations in 1989 and alumina inserts in 2003 for ceramic-on-ceramic (CoC) combinations [230]. The final improvement for ceramic component materials was the introduction of alumina toughened zirconia materials, the generation of BioloX Delta (CeramTec, Medical Products, Plochingen, Germany) and AZ209 (Kyocera Medical, Osaka, Japan). Each manufacturer has their own composition for this product which is given in Table IV.

Table IV: ZTA manufacturers and material compositions [142].

Manufacturer	Product Name	Availability	% Zirconia	% Alumina	Stabilizers	%Additives
CeramTec AG	BioloX Delta	On the market worldwide	22.5 wt%	76.1 wt%	Yttria	1.4 wt% (chromium, strontium and others)
Kyocera Medical	Bioceram, AZ209	On the market in Japan	19 wt%	79 wt%	No stabilizers for zirconia	2 wt% other

2.2.1 Zirconia phase transformation

Zirconia is a metastable ceramic, consisting of monoclinic, tetragonal, and cubic phases and undergoes transformation depending on temperature, stress and moisture. Under controlled conditions, the metastable nature leads to an inherent transformation toughening mechanism that creates a high stress intensity factor threshold for crack growth. Medical grade zirconia is sintered at temperatures in the range 1350° to 1550° which is in the range where the tetragonal phase is stable (1170° to 2370°, above 2370° zirconia is stable in cubical form). Post-sintering, without stabilizers, the zirconia ceramic transforms to the monoclinic phase when it cools to temperatures below 1170° [199]. The phase transformation leads to an increase in volume of the material at the transformation sites and increases local stresses in that region. To prevent temperature driven phase transformation at room temperature, yttria is added as a stabilizing agent. Yttria-stabilized tetragonal zirconia phase (Y-TZP) does not transform to the monoclinic phase under physiological temperatures and is the material that is in clinical use in THR. The chemical composition of Y-TZP is about 5% yttria (Y_2O_3) and 93-94% zirconia (ZrO_2) [135].

The stabilization with yttria limits phase transformation under conditions of stress such as crack propagation. The stress-induced phase transformation from the metastable tetragonal phase to the monoclinic phase at ambient temperatures results in a 3–5% volume expansion and approximately 7% shear strain [68]. The induced volume change and strain oppose crack propagation, thereby improving the fracture toughness of the ceramic [50]. This phase transformation may also lead to microcracking, which enhances fracture toughness by effectively distributing the stress ahead of the main crack. However, microcracking is beneficial only if it remains limited; extensive microcracking

will reduce strength [220]. This is the mechanism in zirconia that combats delayed failure due to slow crack growth and leads to superior toughness under mechanical loads compared to alumina. There are risks and limitations to this phase transformation mechanism in monolithic zirconia. Even with a controlled manufacturing process, the factors that contribute to the phase transformation are complex and still not well understood.

During operation *in vivo*, it has been observed that an aqueous environment has deleterious effects on the performance of zirconia especially in regions of continuous contact at the bearing surface. This vulnerability, also known as low temperature degradation or ageing, leads to hydrothermally induced degradation of hardness and strength on the surface because of higher frictional stresses. The monoclinic phase of zirconia has lower hardness and lower resistance to crack formation compared to the tetragonal phase, making the post-transformation component more susceptible to damage and surface roughening. When tetragonal to monoclinic phase transformation occurs at the bearing surface of the zirconia, the surface roughness may increase due to the increase in volume resulting from phase transformation. Increased roughness at this interface leads to an increase in the wear rate [158]. When phase transformation occurs at the head–trunnion interface, it can initiate fracture [50]. Additionally, the effects of the phase transformation toughening mechanism become unusable for prevention of crack propagation as the tetragonal phase becomes consumed by hydrothermal degradation [212].

Zirconia toughened alumina ceramics make use of the same toughening mechanisms; however, there are some important differences between the transformation

mechanism seen in monolithic zirconia and zirconia toughened composites. As shown in Table IV, ZTA composites contain a significant percent of zirconia in their composition. Figure 15 is an SEM image of a ZTA composite showing the alumina grains (in grey) inter-dispersed with the submicron zirconia particles (in white). Figure 16 shows the schematic representation of a crack propagation being halted by the tetragonal to monoclinic stress induced phase transformation of the zirconia in a ZTA composite ceramic [142]. This mechanism has been confirmed in vitro for ZTA ceramics [49]. The main difference of this mechanism taking place in a matrix composite ceramic compared to monolithic zirconia is that the grains with the stable structure, alumina, prevent the run-away effect of chemisorption accelerated self-induced transformation that may occur in the long-term usage of zirconia ceramic components. In zirconia, once a grain has transformed the change in volume puts stress on neighboring grains which makes them prone to transformation as well. In a ZTA ceramic, the alumina grains contain the transformation and limits it to the local zirconia grains and retains stability while exhibiting high toughness. When transformation is not contained as in zirconia, progressive tetragonal-to-monoclinic transformation initiated at the surface due to penetration of water may result in surface roughening and microcracking. Surface roughening will lead to higher bearing surface wear and potentially cause other problems in the THA.

The run-away transformation can take place only for connected zirconia grains. In the manufacturing of ZTA and the determination of the composition, obtaining toughness while keeping the zirconia isolated among the alumina grains helped establish the recipes given in Table IV and enabled zirconia regions to be dispersed as shown in Figure 15.

However, beyond composition, the processing of ZTA ceramics has been shown to be another important factor in their superior toughness and generally higher mechanical properties. Researchers were concerned that the hydrothermal degradation seen in zirconia would also affect the properties of ZTA ceramics during use. However, experiments have shown that decrease in toughness values with cyclic loading due to low temperature degradation only occurs in ZTA materials if their composite grain structure is not nano and micro sized for the zirconia and alumina grains respectively. The values of toughness and threshold of stress for crack propagation for nano and micro composite ZTAs are above the values for monolithic alumina and zirconia [142].

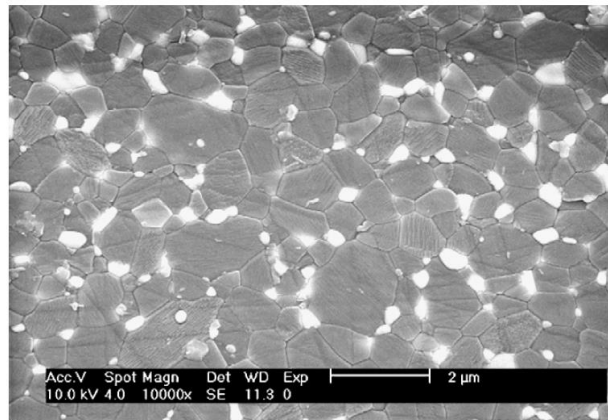


Figure 15: Scanning electron microscopy image of ZTA composite after polishing and thermal etching the surface. Alumina grains are the larger grains in grey and zirconia grains are smaller and white [210].

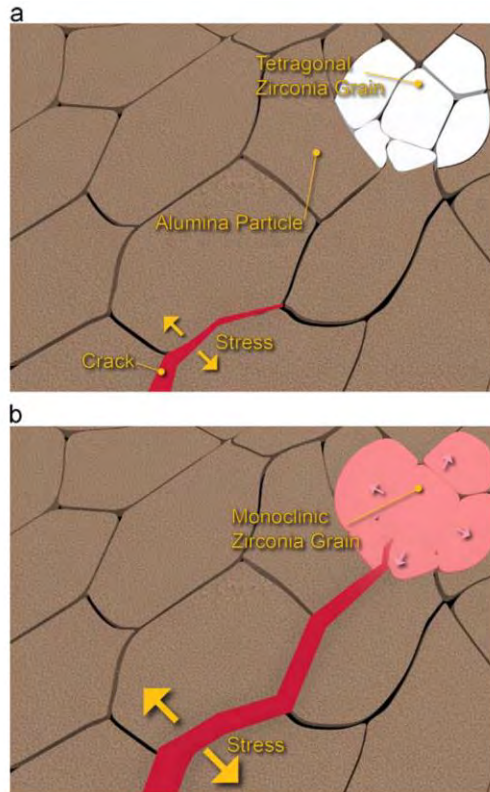


Figure 16: Crack propagation in a ZTA ceramic progressing at the alumina grain boundaries (a) and halting at the zirconia region (white – tetragonal phase) due to stress induced phase transformation and increased zirconia grain volume (red – monoclinic) (b).

Surface roughness for ZTA ceramics has also been scrutinized by researchers to ensure the hydrothermal effects that affect monolithic zirconia also did not affect ZTA. Inspection of the in vitro stability of commercially available zirconia and ZTA femoral heads after exposure to hydrothermal effects revealed superior performance of ZTA components. It was observed that the tetragonal-to-monoclinic transformation of the zirconia grains in the composite microstructure does not produce significant alterations to the surface topography larger than machining effects. The superiority was attributed to the overall architecture of the composite material, not to the individual property of the zirconia contained within the material [198]. A retrieval study of 15 ZTA heads obtained

from revised COP bearings analyzed surface roughness using white light interferometry and microstructural changes using Raman spectroscopy. These analyses revealed significant changes in the zirconia microstructure of the ZTA femoral heads, but no significant increase in roughness. These components also showed no regional variation in roughness with the equator, dome, worn and partially worn regions having the same average roughness value [142].

An additional toughening mechanism in ZTAs consists of using platelet-like crystals to block or deflect crack growth. These crystals are depicted in both the KYOCERA Medical AZ209 and the CeramTec BioloX Delta technical documentation. The CeramTec and KYOCERA Medical formula utilizes strontium oxide crystals to enhance toughness and diffuse crack energy [102]. Addition of strontium oxide creates strontium aluminate composites, which form rod structures with higher crack propagation energy. These rods possess a maximum length of 3 μ m and account for about 3% of the volume. Figure 17 illustrates the platelet toughening mechanism with the depiction of the Delta strontium aluminate rod. The frames in Figure 17 depict crack propagation through alumina grains until the crack is deflected by the strontium aluminate rod. Incorporating multiple reinforcing mechanisms throughout the structure of the material makes the component more reliable because it becomes more effective in deflecting cracks closer to the surface and in avoiding fracture [142].

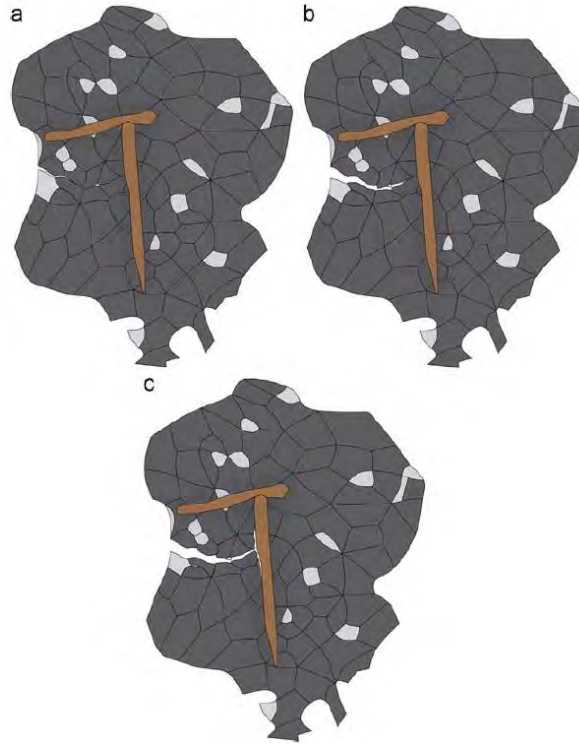


Figure 17: Crack propagation and halting in a ZTA ceramic with strontium aluminate (gold) and tetragonal zirconia (white) reinforcing particles present among the dark grey alumina grains.

ZTA components potentially offer reducing or eliminating current limitations in the performance of COP and COC bearings due to their higher fracture toughness and higher resistance to wear. The higher fracture toughness of ZTA enables the manufacture of thinner liners and larger femoral heads, components that provide greater range of motion in the joint but may be challenging for alumina due to its lower toughness and mechanical strength. Additionally, as described in the review of retrieval studies in Chapter 1, there is a need to understand the performance of ceramic femoral heads and their use to mitigate taper corrosion *in vivo*. At the time of the publication of the data presented in this section [143], there were not any matched cohort studies comparing the

in vivo taper corrosion of THA with ceramic and CoCrMo femoral heads and the studies still remain limited as will be detailed in the discussion section. Due to the multifactorial nature of the fretting-corrosion processes at the head-stem taper, matched cohort studies enable isolating the effect of individual device factors on fretting-corrosion when matching is possible.

2.3 Experimental Methods

2.3.1 Study Design and Matched Cohort Selection

Revision THA with ceramic heads are more difficult to collect when compared to THA with CoCrMo femoral heads due to the longer survivability of hips with ceramic femoral heads and because the number of implantation of ceramic components have increased relatively recently compared to CoCrMo femoral heads. Thus, from our retrieval collection, we first selected THA with ceramic heads and then found suitable matches of THA with CoCrMo femoral heads. In selecting components for this study, we accessed the combined retrieval collections of two academic engineering-based programs working in collaboration with 12 clinical revision centers from the northeast, midwestern, south, and western regions of the United States (Figure 18). Retrievals were collected at these revision centers since 2000 as part of an on-going institutional review board approved revision and retrieval program. An a priori power analysis was conducted and revealed that a sample size of 100 was more than sufficient to detect a difference in corrosion score of 1 between the metal and ceramic cohorts (power = 99.9%). Thus, a total sample size of 100 retrieval cases was judged to be adequate based on this analysis and previous research involving taper corrosion in MOM retrievals [109], in which

researchers detected significant differences in taper corrosion between study groups using a sample size of approximately 100 retrievals. The matching process and the device and clinical information for each cohort is described in detail in this section. These same matched cohorts of ceramic-metal and metal-metal head-stem pairs were later used and evaluated in the studies in Chapters 3 and 4 with quantitative methods.

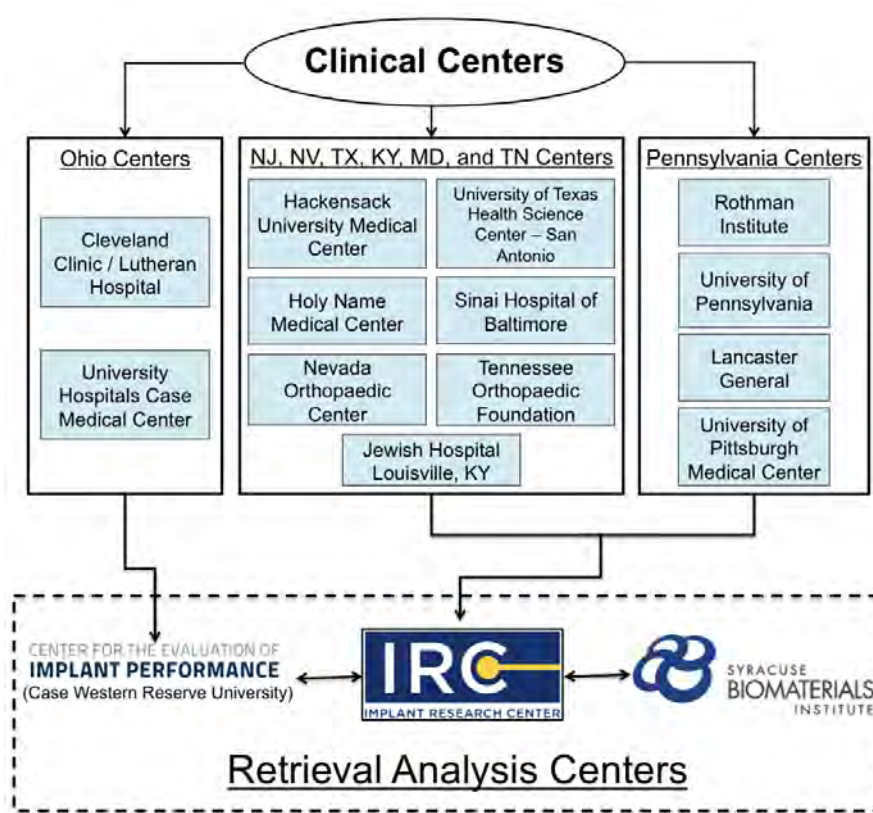


Figure 18: The flow of retrieved implants and deidentified patient data in the Repository.

From our combined interinstitutional database of over 2000 THAs, 96 sets of matched ceramic head/femoral stem taper pairs were identified as possibly suitable for this study. The identified sets were restricted to ceramic heads that were produced by the same supplier (Ceramtec GmbH, Plochingen, Germany). This study allowed the inclusion

of different grades of alumina released by the same supplier due to evolution of material over the years. The materials in the 96 sets included two grades of alumina (Biolox and Biolox forte; Ceramtec GmbH, Plochingen, Germany) and zirconia-toughened alumina (Biolox delta) ceramic heads. Since previous studies have shown implantation time to be one of the most important variables related to taper corrosion [55, 87, 94], we selected the ceramic-metal taper cohort to consist of the 50 ceramic-stem sets with the longest implantation time and which could be matched with a metal-metal taper cohort (described subsequently). The resulting sets had the following femoral head material distribution Biolox [n = 5], Biolox forte [n = 30], and Biolox delta [n = 15]. The ceramic-metal taper cohort included both CoC and/or CoP bearings (see Table XIII in the Appendix for the detailed device and clinical information about the ceramic cohort). Most of the components for this study were uncemented (94 of 100) with the cemented components having CoC (n = 1), CoP (n = 2), and MoP (n = 3) bearing couples. Given that cement was present in three samples for both study groups, cement is not considered to be a confounding factor for this study. Stems with dual-modularity (additional modularity at the stem-neck) were excluded from this study (11 out of 96 sets with ceramic heads) because of previous research suggesting that modular tapers were associated with increased risk of fretting-corrosion of the head taper in MOM bearings [109].

We identified the matched cohort of 50 metal-metal head-stem components from MoP bearings also with single modularity only at the head-stem interface (see Table XIV in the Appendix for the detailed device and clinical information about the metal cohort). The metal femoral head in the metal-metal taper cohort was always composed of CoCrMo alloy. The metallic head and stem material compositions of all samples were

confirmed using an x-ray fluorescence detector (Niton XL3t GOLDD+; Thermo Scientific, Waltham, MA, USA). Devices in the ceramic-metal taper cohort were matched to create the metal-metal taper cohort based on the following three criteria (in order of importance) based on significant variables published in previous retrieval studies of taper corrosion as detailed in the Chapter 1 literature review: (1) implantation time (most important); (2) stem neck flexural rigidity; and (3) lateral offset (least important). Although not specifically matched for, the resulting cohorts had similar head diameters (median = 32 mm and mean = 33 mm for both cohorts). In this study, the CoCr heads had the same manufacturer as the stems they were implanted with, eliminating manufacturer mixing as a confounding factor.

Stem flexural rigidity was calculated using the equation used by Goldberg et al. [94]. As mentioned in Chapter 1, the flexural rigidity of the stems was calculated using the Young's modulus (E) of the alloy multiplied by the second moment of area ($I = \pi[ND]^4/64$, where ND = diameter of stem at the distal contact point of the head taper). The diameters of the necks were measured by two independent observers and were assumed to be circular. The combined lateral offset of the stem and head was obtained by tracing component markings, patient records, and component dimensional measurements or directly from the manufacturer-supplied design tables. When possible, we matched stem flexural rigidity and offset in the two cohorts using the identical stem design and size (see Tables XIII and XIV in the Appendix for details). The stems were fabricated from one of the following three materials: 1) a proprietary titanium alloy (54%; TMZF; Stryker Orthopedics, Mahwah, NJ, USA) having an elastic modulus (E) of approximately 80 GPa, 2) Ti-6Al-4V alloy (29%; $E = 110$ GPa) or 3) from a CoCr alloy (17%; $E = 200$

GPa). Once again, the inclusion criteria of the study for stem design was for only monolithic femoral stems with a single taper interface for the head. Additionally, to eliminate any confounding factors, we excluded four ceramic heads with metal sleeves from the study. Likewise, none of the CoCr heads in the matched metal head cohort included an inner modular taper adapter or sleeve. In addition to the retrieved components, clinical data (implantation time, age, sex, body mass index [BMI], UCLA activity score, and reason for implant revision) were collected for all patients in the ceramic-metal and metal-metal taper cohorts (Tables XIII and XIV respectively). For the ceramic head cohort, the average implantation time was 3.3 ± 3.7 years (range, 0.5–18 years), the mean patient age at implantation was 52 ± 10 years, 17 of 50 (34%) were female, the mean BMI was 30 ± 7 kg/m², and the mean UCLA activity score was 6 ± 2 . For the metal head cohort, the average implantation time was 3.2 ± 3.8 years (range, 0.5–17 years), the mean patient age at implantation was 57 ± 14 years, 25 of 50 (50%) were female, the mean BMI was 30 ± 7 kg/m², and the mean UCLA activity score was 5 ± 2 . There was no significant difference in the implantation time ($p = 0.71$), sex ($p = 0.11$), BMI ($p = 0.91$), or UCLA activity levels ($p = 0.65$) between the ceramic and metal head cohorts. However, there was a significantly ($p = 0.03$) greater age in patients with a metal head as compared with the ceramic head cohort. The most frequently reported reasons for revision in both the ceramic and metal head cohorts were infection and loosening (Tables XIII and XIV in Appendix). According to the medical records, none of the heads or stems in either the ceramic-metal or metal-metal taper cohorts was revised because of an adverse local tissue reaction (ALTR).

2.3.2 Evaluation of Fretting-Corrosion Damage

Visual Fretting-Corrosion Scoring

Devices were cleaned in accordance with institutional procedures. The CoCr head and neck tapers were inspected visually for composite fretting and corrosion damage at the modular

CoCr head and metal stem interfaces using a previously published 4-point scoring technique (see Table II) [110]. Score of 1 indicates minimal fretting or corrosion (fretting on < 10% of the surface and no corrosion damage); 2 indicates mild damage (fretting on > 10% surface and/or corrosion attack confined to one or more small areas); 3 indicates moderate damage (fretting > 30% and/or aggressive local corrosion attack with corrosion debris); and 4 indicates severe damage (fretting over majority (>50%) of mating surface with severe corrosion attack and abundant corrosion debris). We analyzed metal transfer to the inner taper of the ceramic heads using a similar 4-point scoring technique with a score of 1 indicating minimal metal transfer (< 10% of the taper surface), 2 indicating metal transfer over 10%, 3 indicating metal transfer over 30%, and 4 indicating metal transfer over more than 50% of the inner head taper.

Steps were taken to minimize observer bias during the visual scoring of components. Before scoring, components were randomized using a random number generator in Microsoft Excel (Microsoft Inc, Redmond, WA, USA; components were scored from the lowest to highest random number generated) and scored independently by the same three investigators. In the event of disagreement between the scores, the three investigators convened to adjudicate the discrepancy and arrive at a consensus score for the taper. Additionally, the investigators were blinded to the cohort status of the stems

during scoring, but it was not possible to visually score the two head cohorts in a blinded fashion.

Scanning Electron Microscopy of Stems Implanted with Ceramic Heads

Representative TMZF, Ti6Al4V, and CoCrMo alloy stems, each with a visual score of 2 corresponding to the median value for the ceramic cohort, were selected for evaluation using scanning electron microscopy (SEM; JEOL 5600, Peabody, MA, USA) and energy dispersive analysis of x-rays (EDS; Princeton Gamma-Tech, Princeton, NJ, USA). Implants were either placed directly into the SEM with no additional preparation or, if too large, were sectioned distal to the taper in the neck region using a slow-speed diamond sectioning saw with water as the lubricant and then rinsed in distilled water and dried. Imaging was performed in both the backscattered and secondary electron mode and, when appropriate, EDS (Princeton Gamma-Tech) was used for elemental analysis for identification of corrosion and biological debris. The primary focus of this analysis was to characterize the surface topography of the stem taper surfaces and identify the damage modes due to fretting-corrosion if present.

Statistical Analysis

Preliminary evaluation of the visual corrosion damage scoring data demonstrated a non-normal distribution. Hence, nonparametric statistical analyses were performed using statistical software (JMP 10.0; SAS Institute, Cary, NC, USA). Mann-Whitney U, Kruskal-Wallis (with post hoc Dunn tests when necessary), and Wilcoxon tests were used to assess differences in taper damage grouped by categorical parameters (femoral head material, bearing type (for the ceramic cohort only), and ceramic material formulation (alumina versus zirconia-toughened alumina)). Spearman's rank order correlation was

used to identify correlations between continuous variables (implantation time, stem flexural rigidity, lateral offset, and head size). The level of significance chosen for all statistical analyses was $p < 0.05$.

2.4 Results

Fretting and corrosion scores were lower for the stems in the ceramic-metal cohort compared to the metal-metal cohort ($p = 0.03$; Figure 19). Evidence of fretting and corrosion, a combined fretting-corrosion score ≥ 2 , was observed in 42 of 50 (84%) stems in the ceramic head cohort and 42 of 50 (84%) stems in the metal head cohort. The median damage score for the stems in the ceramic-metal cohort was 2 (Figures 19 and 20), whereas for stems in the metal-metal taper cohort, the median score was 3 (Figures 19 and 20). We observed dark corrosion deposits outside the head-neck taper junctions in three of 50 (6%) of the metal-metal taper cohort and zero of 50 (0%) of the ceramic-metal taper cohort. Both stem alloy ($p = 0.004$; Kruskal Wallis test with post hoc Dunn Test; Figure 21) and decreased stem flexural rigidity (Spearman's $\rho = -0.35$, $p = 0.01$) were predictors of stem fretting and corrosion damage for the ceramic-metal taper cohort however, these variables did not have an effect for the metal-metal taper cohort (Figure 21). Stem corrosion for the ceramic-metal taper cohort was not significantly affected by implantation time ($p = 0.46$), lateral offset ($p = 0.35$), head size ($p = 0.26$), type of ceramic bearing ($p = 0.82$), or the ceramic material formulation ($p = 0.93$). However, these tests were generally underpowered (power $\leq 25\%$). The only variable in this study that was a significant predictor of the metal transfer score inside the ceramic heads was decreased flexural rigidity (Spearman's $\rho = -0.35$, $p = 0.01$). For the metal-metal taper cohort, none of the patient or device variables in this study was a significant predictor of

the stem corrosion for the metal-metal taper cohort. Patient weight was positively correlated with stem fretting and corrosion scores in the ceramic head cohort (Spearman's $\rho = 0.46$; $p = 0.002$), whereas only a trend was observed in the metal head cohort (Spearman's $\rho = 0.26$; $p = 0.08$). In the metal head cohort, patient age was negatively correlated with stem fretting and corrosion scores (Spearman's $\rho = -0.36$; $p = 0.01$); however, no correlation was observed in the ceramic cohort (Spearman's $\rho = 0.08$; $p = 0.59$). Patient sex, implantation time, and activity scores were not associated with higher or lower stem fretting and corrosion scores in either cohort ($p > 0.05$).

The mechanism of mechanically assisted crevice corrosion was similar in the metal and ceramic head cohorts, although in the case of ceramic femoral heads, only one of the two surfaces (the male metal taper) engaged in the oxide abrasion and repassivation process. SEM analysis showed damage on each implant that was reflective of the type of metallic surface topography present (also termed in the literature as imprinting). Interestingly, the surface topography for tapers was highly variable based on alloy (Co-based or Ti-based) and manufacturer. The taper surfaces were either finely machined (TMZF; Figure 22A) or with machined grooves present (both Ti-6Al-4V, Figure 22B–C, and CoCr, Figure 22D–E). The geometry of the grooves varied with design in terms of grooves per length and groove depth. For example, in Figures 22D and 22E, both implants are Co-Cr-Mo based, but Figure 22E shows tightly spaced grooves approximately 150 μm apart and roughly 60 to 100 μm deep, whereas in Figure 22D, the grooves are approximately 500 μm apart and 50 μm deep. The fretting corrosion damage seen in these tapers is intermittently distributed over the tapers and where grooves are present occur only at the top of the groove. With deep grooves, debris can accumulate

(Figure 22E) adjacent to the fretting damage. For the device in Figure 22A, the majority of fretting corrosion damage is seen in the proximal taper region (lower right of micrograph) indicating rim loading. Evidence of fretting damage and corrosion debris (dark regions) was observed on titanium alloy surfaces (Figure 23A–B). Different types of machining grooves on cobalt alloy surfaces (Figure 23C–D) exhibited different appearances. In one case (Figure 23C), the damage seen has a distinct (solely) corrosion-based appearance, whereas another case (Figure 23D) showed evidence of both fretting and corrosion damage.

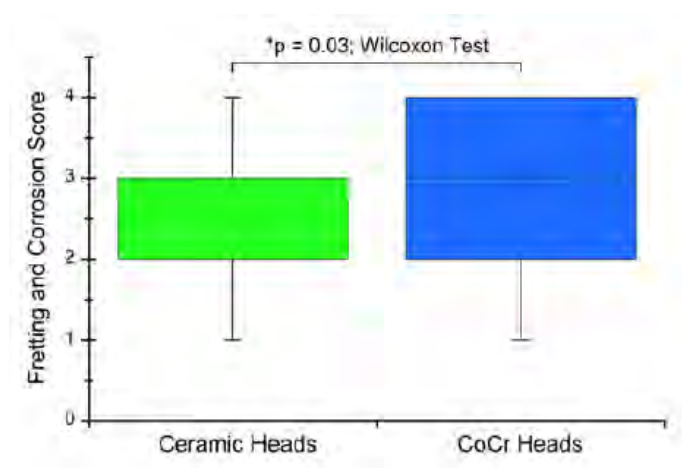


Figure 19: The femoral stem taper fretting and corrosion damage scores for the matched ceramic and CoCr head cohorts are shown. The damage scores were significantly lower for the ceramic cohort ($p = 0.03$).

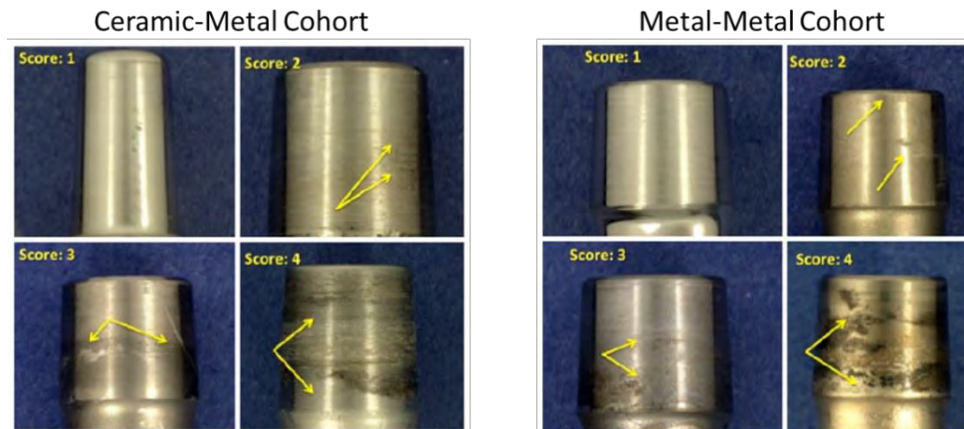


Figure 20: Some examples of stem taper fretting and corrosion scores for the ceramic-metal cohort (median score 2) and metal-metal cohort (median score 3).

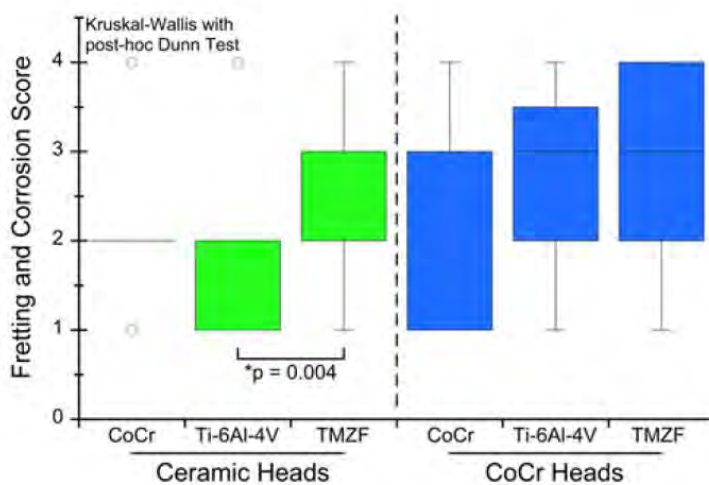


Figure 21: A boxplot illustrating femoral stem taper fretting and corrosion score versus stem alloy for the ceramic and metal head cohorts is presented.

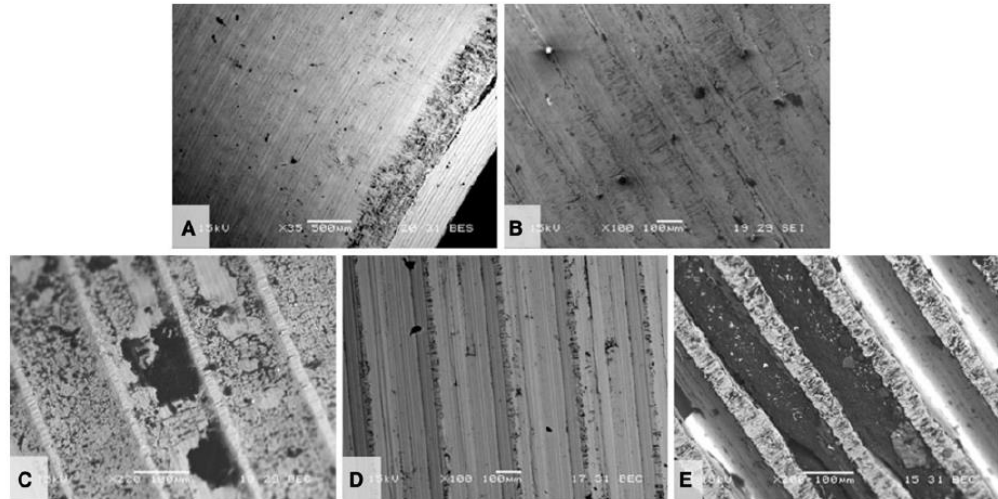


Figure 22: SEM images of five different design and materials for the stem tapers implanted with ceramic heads (A) TMZF (Stryker Orthopedics, Mahwah, NJ, USA) 9 35 BEC, (B) Ti-6Al-4V (Zimmer, Inc, Warsaw, IN, USA) 9 100 SEI, (C) Ti-6Al-4V (Wright Medical Technology, Inc, Arlington, TN, USA) 9 220 BEC, (D) Co-Cr-Mo (DePuy Orthopedics, Inc, Warsaw, IN, USA) 9 100 BEC, (E) Co-Ni-Cr-Mo (Zimmer) 9 100 BEC. SEI = secondary electron imaging; BEC = backscattered electron contrast image. A is a ground surface, whereas B–E have machining grooves present. Also shown are fretting scars and corrosion and biological debris present. For grooved implants, only the groove tips show evidence of fretting corrosion damage.

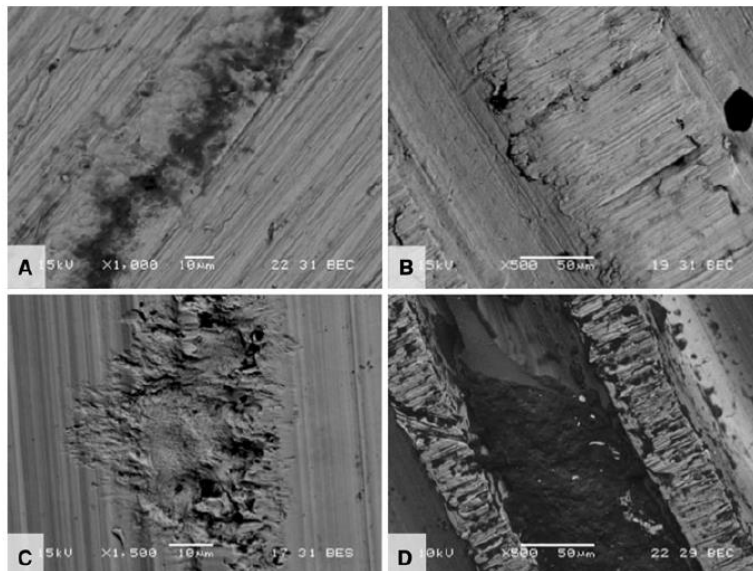


Figure 23: Backscattered electron micrographs of (A) TMZF, (B) Ti-6Al-4V, (C) Co-Cr-Mo, and (D) CoNiCrMo alloy tapers used in conjunction with ceramic femoral heads. Backscattered evaluation makes corrosion deposits appear black and help identify fretting damage and some corrosion debris present. In C, the damage has a distinctly corrosion-like appearance emanating from a machining ridge.

2.5 Discussion

This matched cohort retrieval study was undertaken to analyze stem taper corrosion with ceramic heads as compared with CoCr heads. The matched study design allowed for controlling the variability of fretting-corrosion severity due to stem design and isolate the effect of femoral head material. Fretting initiated crevice corrosion in modular head-stem connections is complex and multifactorial. Matched cohort retrieval studies are valuable to help to understand the clinical significance of a single factor. We hypothesized that ceramic femoral heads, which are electrical insulators, would lead to lower stem taper corrosion than previously reported with CoCr femoral heads. The results of this study show that this hypothesis holds true. Some findings that were consistent

with other retrieval studies in the literature review in Chapter 1 was that decreased stem flexural rigidity and stem alloy (which have significantly different stiffness based on their elastic modulus) predicted stem corrosion with modular ceramic femoral heads; but, interestingly not with CoCr heads. There was no difference in the mechanism of fretting corrosion between the ceramic and metal cohorts besides the fact that only the stem taper surface plays a role in the corrosion damage that occurs in the ceramic cohort.

This study had limitations. We used a matched cohort study design that was adequately powered to detect differences between the ceramic-metal and metal-metal taper cohorts, but the sample size was not sufficient to pick up correlations between taper design and secondary effects such as implantation time, which were not apparent in either cohort. The study was primarily designed to detect a difference of 1 in corrosion scores between junctions with ceramic-metal and metal-metal interfaces. The results pertaining to this comparison are sufficiently powered. As it was discussed in Chapter 1, there are still some unknowns about the patient and device factors, and since our study cohorts contained detailed information for each head-stem pair we wanted to investigate the secondary effects as well in relation to the fretting and corrosion scores. However, the mean differences of fretting and corrosion scores when analyzing the device and patient factors were approximately one-fourth of what the study was designed to detect. While these relationships were also of interest, a retrospective power analysis showed that to test the number of samples needed shows this study would require an unrealistically large sample size to be sufficiently powered to answer this secondary study question. Hence, we acknowledge that any correlations about patient and device factors would be underpowered. This study also shares the same limitation of all retrieval studies, namely

that they are based on analysis of clinical failures that do not necessarily reflect the population of well-functioning implants in the unrevised patient population. However, the presence of taper corrosion in this series was not associated with the reasons for revision for any of the components (no ALTR were reported).

Another limitation of this study is since this study focused on ceramic femoral heads by a single supplier with a consistent design, the findings in this study may not apply to other ceramic head suppliers and stem designs outside of this study. We also accounted for differences in stem surface finish and alloy composition between the cohorts by the matching protocol. Furthermore, we examined retrievals in which the only source of modularity with a metallic component was the head-stem interface. Therefore, the results of this study likewise do not apply to THA systems with multiple sources of modularity. Our results were also limited in that our methodology to assess the extent of corrosion was categorical and subjective. However, our methodology was consistent with the approach of other investigations in which corrosion and fretting of modular metallic interfaces were assessed [94, 110]. Taper analyses to quantify material loss will be discussed in Chapter 4.

These limitations pertaining to the study design using specific type of ceramic heads and stems made it difficult to compare results directly with the literature. We demonstrate that mechanically assisted crevice corrosion can also occur in ceramic head-metal neck devices, although to a lesser extent than in CoCr head-metal neck devices. There are few other studies that looked at the relationship of ceramic femoral heads and taper corrosion (as of time of publication). One study compared stem taper corrosion scores in a matched cohort study between monolithic zirconia and CoCrMo femoral

heads and did not find a significant difference between stem scores [107]. As mentioned earlier in this chapter, zirconia is no longer widely implanted due to concerns about fracture. Other studies looked at oxidized zirconium [41, 103, 228] using visual scoring and with one using profilometry additionally for the most severely scored parts [41]. All of these studies found a significant difference between OxZr and CoCrMo head-stem pair corrosion scores and material loss depth profiles. Cartner et al. [41] also found a positive correlation with fretting corrosion with greater head offsets, concluding that reducing the moment arm at the head-neck junction may reduce fretting corrosion damage. They did not find any effect of head size or implantation time with fretting-corrosion in this retrieval study with 210 femoral head tapers. OxZr components have a ceramized surface above a zirconium metal substrate and is also not as widely implanted as alumina or ZTA. Huot Carlson et al. and Di Laura et al. looked at that looked at the comparison between ceramic and CoCr heads and their stem tapers used stem designs with dual modularity where the stem neck or body had an additional modular junction [73, 120]. Not only have these stem designs been attributed with higher risk of corrosion [109]; but, also, Di Laura et al. report that the stem design they used was in fact recalled (Stryker Rejuvenate, V40) and they did not report any information about the corrosion at this additional junction nor the relationship of the corrosion severity of the stem body modular junction with the head-stem taper junction [73]. Huot Carlson et al. look at a different dual modular stem design (S-ROM, DePuy Orthopedics) [120] observed less proximal femoral stem taper corrosion for cases with a ceramic-metal taper interface as opposed to cases with metal-metal taper interfaces. However, details about the design or manufacture of the ceramic heads in the S-ROM series were not reported, making direct

comparisons to this study difficult. Finally, a study worth mentioning even though it is an in vitro study is a ceramic and metal femoral head comparison by Hallab et al. [100]. They examined fretting corrosion in CoCr-CoCr and CoCr-zirconia ceramic stem-head tapers in vitro to test the hypothesis that the harder ceramic surface would result in greater fretting corrosion debris from a CoCr stem as compared with a CoCr head and stem. Contrary to their hypothesis (and similar to the results of this retrieval study), the CoCr-CoCr head-stem taper generated 3 to 11-fold greater metal release than the CoCr-zirconia taper combination, but the authors cautioned against overgeneralization of their results to other head-stem designs. As mentioned previously in this chapter, the manufacturer of the zirconia heads in Hallab et al.'s study, St Gobain Desmarquest (Evreux Cedex, France), ultimately withdrew their product from the orthopedic market after a worldwide recall in 2001 and they are no longer in clinical use in orthopedics [50].

The damage modes observed on the SEM were consistent with those reported in the literature for fretting scars, corrosion debris and corrosion damage on the surface. The clinical impact of the associated corrosion debris from these interfaces for implants with femoral heads less than 36mm remains unclear at this point. Tissue samples were unavailable to determine the effects of these corrosion products locally and systemically. However, this study only looked at the femoral stems [85, 98]. In later studies, we looked at the CoCrMo femoral heads and their damage modes in more depth and I present this information in Chapters 3 and 4. The most important design and patient factors predicting increased fretting and corrosion scores of the ceramic head cohort in this study were stem material, flexural rigidity, and body weight. Previously, both in vitro and in vivo studies have found similar results as discussed in Chapter 1. We did not find lateral offset or sex

to be a predictor of corrosion, which is comparable to what Huot Carlson et al. recently found [120]. Cartner et al. [41] also found a positive correlation with fretting corrosion with greater head offsets, concluding that reducing the moment arm at the head-neck junction may reduce fretting corrosion damage. Goldberg et al. [94] found that lateral offset was a predictor of corrosion; however, this factor did not have an effect when the confounding factors of flexural rigidity and implantation were considered. Head size was not a predictor for corrosion in the current study and by Huot Carlson et al. [120] nor for Cartner et al. [41] which is not surprising as the results in Chapter 1 showed that the retrieval studies had very mixed results about the effect of head size on taper corrosion. Head size most likely is a factor that has a weak effect on taper corrosion and depends on the compounded effect of other device factors. Also, it should be noted that a post hoc power analysis revealed that this study was underpowered to detect the differences observed between head sizes (power = 21%).

This study provides new insight on the mechanisms of taper fretting corrosion using ceramic as an alternative to CoCr alloy femoral heads. The basic mechanism of mechanically assisted crevice corrosion was the same with the exception being that, in the case of a ceramic femoral head, only one of the two surfaces (i.e., the male metal taper) engaged in the oxide abrasion and repassivation process. This, in and of itself, will lower the overall extent of corrosion. Other potential differences between taper fretting corrosion behavior could be the result of how the male taper surface was prepared. The machining topography of the metal taper appears to localize damage to the peaks of the machining grooves where contact is made with the ceramic head. However, we accounted for differences in surface topography in the two study cohorts by matching not only alloy,

but stem manufacturer, where possible. Thus, the lower corrosion scores we observed between the ceramic-metal and metal-metal taper cohorts cannot be attributed to differences in surface topography. Recent studies that looked at the effect of taper topography on taper corrosion found none [4].

Previously, ceramic femoral heads have been discussed in the clinical literature solely in the context of an alternative bearing surface to reduce wear [11, 211]. This study has potentially important implications for modular component selection by surgeons who are concerned with Co and Cr debris release from the head-neck interface and the risk of adverse local tissue reactions [42, 91, 178, 179]. Recent reports have shown that ceramic heads have become the default choice in revision surgeries especially for revisions due to ALTR [31, 205]. Our results suggest that by using a ceramic femoral head, Co and Cr fretting and corrosion from the modular head-neck taper may be mitigated, although not eliminated. However, implant component selection is but one factor contributing to taper corrosion and metal debris production from modular interfaces in vivo. Taper impaction technique, engagement of the modular taper interface in a clean and dry environment, and the use of matching components are all technical factors that influence taper fretting and corrosion regardless of whether the femoral head is fabricated from CoCr or ceramic. The study here was an important primer for us to investigate the total material loss from the head-stem junction in this matched cohort study.

References

4. Arnholt C, Underwood R, MacDonald D, Higgs G, Chen A, Klein G, Hamlin B, Lee G, Mont M, Cates H, Malkani A, Kraay M, Rimnac C, Kurtz S. Microgrooved Surface Topography Does Not Influence Fretting Corrosion of Tapers in THA: Classification and Retrieval Analysis. *Modularity and Tapers in Total Joint Replacement Devices*. Conshohocken PA: American Society of Testing Materials (ASTM); 2015.
11. Bal BS, Garino J, Ries M, Rahaman MN. A review of ceramic bearing materials in total joint arthroplasty. *Hip international : the journal of clinical and experimental research on hip pathology and therapy*. 2007;17:21-30.
31. Bonner B, Arauz P, Klemm C, Kwon YM. Outcome of Re-Revision Surgery for Adverse Local Tissue Reaction in Metal-on-Polyethylene and Metal-on-Metal Total Hip Arthroplasty. *The Journal of arthroplasty*. 2020.
33. Boutin P. [Total arthroplasty of the hip by fritted aluminum prosthesis. Experimental study and 1st clinical applications]. *Revue de chirurgie orthopedique et reparatrice de l'appareil moteur*. 1972;58:229-246.
34. Boutin P, Blanquaert D. [A study of the mechanical properties of alumina-on-alumina total hip prosthesis (author's transl)]. *Revue de chirurgie orthopedique et reparatrice de l'appareil moteur*. 1981;67:279-287.
35. Boutin P, Christel P, Dorlot JM, Meunier A, de Roquancourt A, Blanquaert D, Herman S, Sedel L, Witvoet J. The use of dense alumina-alumina ceramic combination in total hip replacement. *Journal of biomedical materials research*. 1988;22:1203-1232.
41. Cartner J, Aldinger P, Li C, Collins D. Characterization of Femoral Head Taper Corrosion Features Using a 22-Year Retrieval Database. *HSS Journal*. 2017;13:35-41.
42. Chana R, Esposito C, Campbell PA, Walter WK, Walter WL. Mixing and matching causing taper wear: corrosion associated with pseudotumour formation. *The Journal of bone and joint surgery. British volume*. 2012;94:281-286.
45. Chevalier J. What future for zirconia as a biomaterial? *Biomaterials*. 2006;27:535-543.
47. Clarke IC. Metastable Nature of Zirconia Femoral Heads From a 20-Year Perspective of Clinical and Simulator Wear Studies. *Seminars in Arthroplasty*. 2006:165-178.
49. Clarke IC, Green DD, Williams PA, Kuboc K, Pezzotti G, Lombardi AV. Hip-simulator wear studies of an alumina-matrix composite (AMC) ceramic compared to retrieval studies of AMC balls with 1–7 years follow-up. *Wear*. 2009;267:702-709.
50. Clarke IC, Manaka M, Green DD, Williams P, Pezzotti G, Kim YH, Ries M, Sugano N, Sedel L, Delauney C, Nissan BB, Donaldson T, Gustafson GA. Current status of zirconia used in total hip implants. *The Journal of bone and joint surgery. American volume*. 2003;85-A Suppl 4:73-84.
55. Collier JP, Surprenant VA, Jensen RE, Mayor MB, Surprenant HP. Corrosion between the components of modular femoral hip prostheses. *The Journal of bone and joint surgery. British volume*. 1992;74:511-517.
65. Cuckler JM, Bearcroft J, Asgian CM. Femoral head technologies to reduce polyethylene wear in total hip arthroplasty. *Clinical orthopaedics and related research*. 1995:57-63.
68. De Aza AH, Chevalier J, Fantozzi G, Schehl M, Torrecillas R. Crack growth resistance of alumina, zirconia and zirconia toughened alumina ceramics for joint prostheses. *Biomaterials*. 2002;23:937-945.

73. Di Laura A, Hothi H, Henckel J, Swiatkowska I, Liow MHL, Kwon YM, Skinner JA, Hart AJ. Retrieval analysis of metal and ceramic femoral heads on a single CoCr stem design. *Bone & joint research*. 2017;6:345-350.
83. Fukui K, Kaneuji A, Sugimori T, Ichiseki T, Matsumoto T. Retrieval analysis of new-generation yttria-stabilized zirconia femoral heads after total hip arthroplasty. *European journal of orthopaedic surgery & traumatology : orthopedie traumatologie*. 2014;24:1197-1202.
85. Gilbert JL, Buckley CA, Jacobs JJ. In vivo corrosion of modular hip prosthesis components in mixed and similar metal combinations. The effect of crevice, stress, motion, and alloy coupling. *Journal of biomedical materials research*. 1993;27:1533-1544.
87. Gilbert JL, Jacobs JJ. The Mechanical and Electrochemical Processes Associated with Taper Fretting and Crevice Corrosion: A Review. In: Marlowe DE, Parr JE, Mayor MB, ed. *STP1301: Modularity of Orthopedic Implants*. West Conshohocken, PA: American Society for Testing and Materials; 1997.
91. Gill IP, Webb J, Sloan K, Beaver RJ. Corrosion at the neck-stem junction as a cause of metal ion release and pseudotumour formation. *The Journal of bone and joint surgery. British volume*. 2012;94:895-900.
94. Goldberg JR, Gilbert JL, Jacobs JJ, Bauer TW, Paprosky W, Leurgans S. A multicenter retrieval study of the taper interfaces of modular hip prostheses. *Clinical orthopaedics and related research*. 2002:149-161.
98. Hall DJ, Pourzal R, Lundberg HJ, Mathew MT, Jacobs JJ, Urban RM. Mechanical, chemical and biological damage modes within head-neck tapers of CoCrMo and Ti6Al4V contemporary hip replacements. *Journal of Biomedical Materials Research. Part B, Applied Biomaterials*. 2018;106:1672-1685.
100. Hallab NJ, Messina C, Skipor A, Jacobs JJ. Differences in the fretting corrosion of metal-metal and ceramic-metal modular junctions of total hip replacements. *Journal of orthopaedic research : official publication of the Orthopaedic Research Society*. 2004;22:250-259.
102. Hamilton WG, McAuley JP, Dennis DA, Murphy JA, Blumenfeld TJ, Politi J. THA with Delta ceramic on ceramic: results of a multicenter investigational device exemption trial. *Clinical orthopaedics and related research*. 2010;468:358-366.
103. Hampton C, Weitzler L, Baral E, Wright TM, Bostrom MPG. Do oxidized zirconium heads decrease tribocorrosion in total hip arthroplasty? A study of retrieved components. *Bone and Joint Journal*. 2019;101 B:386-389.
109. Higgs GB, Hanzlik JA, MacDonald DW, Gilbert JL, Rimnac CM, Kurtz SM. Is increased modularity associated with increased fretting and corrosion damage in metal-on-metal total hip arthroplasty devices?: a retrieval study. *The Journal of arthroplasty*. 2013;28:2-6.
110. Higgs GB, Hanzlik JA, MacDonald DW, Kane WM, Day JS, Klein GR, Parvizi J, Mont MA, Kraay MJ, Martell JM, Gilbert JL, Rimnac CM, Kurtz SM. Method of characterizing fretting and corrosion at the various taper connections of retrieved modular components from metal-on-metal total hip arthroplasty. In: *ASTM Symposium on Metal-on-Metal Total Hip Replacement Devices, May 8, 2012 - May 8, 2012*. Phoenix, AZ, United states: ASTM International: 2013:146-156.
116. Huet R, Sakona A, Kurtz SM. Strength and reliability of alumina ceramic femoral heads: Review of design, testing, and retrieval analysis. *Journal of the mechanical behavior of biomedical materials*. 2011;4:476-483.

119. Huo MH, Martin RP, Zatorski LE, Keggi KJ. Total hip replacements using the ceramic Mittelmeier prosthesis. *Clinical orthopaedics and related research*. 1996;143-150.
120. Huot Carlson JC, Van Citters DW, Currier JH, Bryant AM, Mayor MB, Collier JP. Femoral stem fracture and in vivo corrosion of retrieved modular femoral hips. *The Journal of arthroplasty*. 2012;27:1389-1396.e1381.
128. Knahr K, Bohler M, Frank P, Plenck H, Salzer M. Survival analysis of an uncemented ceramic acetabular component in total hip replacement. *Archives of orthopaedic and trauma surgery*. 1987;106:297-300.
135. Kurtz SM, ed. *UHMWPE Biomaterials Handbook: Ultra-High Molecular Weight Polyethylene in Total Joint Replacement and Medical Devices*: Elsevier; 2009.
142. Kurtz SM, Kocagoz S, Arnholt C, Huet R, Ueno M, Walter WL. Advances in zirconia toughened alumina biomaterials for total joint replacement. *Journal of the mechanical behavior of biomedical materials*. 2014;31:107-116.
143. Kurtz SM, Kocagoz SB, Hanzlik JA, Underwood RJ, Gilbert JL, MacDonald DW, Lee GC, Mont MA, Kraay MJ, Klein GR, Parvizi J, Rimnac CM. Do ceramic femoral heads reduce taper fretting corrosion in hip arthroplasty? A retrieval study. *Clinical orthopaedics and related research*. 2013;471:3270-3282.
148. Lancaster JG, Dowson D, Isaac GH, Fisher J. The wear of ultra-high molecular weight polyethylene sliding on metallic and ceramic counterfaces representative of current femoral surfaces in joint replacement. *Proceedings of the Institution of Mechanical Engineers. Part H, Journal of engineering in medicine*. 1997;211:17-24.
149. Langlois J, El Hage S, Madi F, Courpied JP, Kerboull M, Hamadouche M. Charnley-Kerboull total hip arthroplasty combining zirconia on polyethylene. A minimum eight-year follow-up prospective study. *International orthopaedics*. 2013;37:355-360.
158. Liang B, Kawanabe K, Ise K, Iida H, Nakamura T. Polyethylene wear against alumina and zirconia heads in cemented total hip arthroplasty. *The Journal of arthroplasty*. 2007;22:251-257.
168. Masonis JL, Bourne RB, Ries MD, McCalden RW, Salehi A, Kelman DC. Zirconia femoral head fractures: a clinical and retrieval analysis. *The Journal of arthroplasty*. 2004;19:898-905.
178. Meneghini RM, Hallab NJ, Jacobs JJ. Evaluation and treatment of painful total hip arthroplasties with modular metal taper junctions. *Orthopedics*. 2012;35:386-391.
179. Meyer H, Mueller T, Goldau G, Chamaon K, Ruetschi M, Lohmann CH. Corrosion at the cone/taper interface leads to failure of large-diameter metal-on-metal total hip arthroplasties. *Clinical orthopaedics and related research*. 2012;470:3101-3108.
188. Oonishi H, Kim SC, Kyomoto M, Iwamoto M, Ueno M. PE wear in ceramic/PE bearing surface in total knee arthroplasty: Clinical experiences of more than 24 years. In: Francesco Benazzo FF, Martin Dietrich, ed. *Bioceramics and Alternative Bearings in Joint Arthroplasty: 11th BIOLOX Symposium Proceedings*: Springer Science and Business Media; 2006:101-110.
198. Pezzotti G, Saito T, Padeletti G, Cossari P, Yamamoto K. Nano-scale topography of bearing surface in advanced alumina/zirconia hip joint before and after severe exposure in water vapor environment. *Journal of orthopaedic research : official publication of the Orthopaedic Research Society*. 2010;28:762-766.
199. Piconi C, Maccauro G. Zirconia as a ceramic biomaterial. *Biomaterials*. 1999;20:1-25.
205. Pourzal R, Lundberg HJ, Hall DJ, Jacobs JJ. What Factors Drive Taper Corrosion? *Journal of Arthroplasty*. 2018;33:2707-2711.

210. Roualdes O, Duclos ME, Gutknecht D, Frappart L, Chevalier J, Hartmann DJ. In vitro and in vivo evaluation of an alumina-zirconia composite for arthroplasty applications. *Biomaterials*. 2010;31:2043-2054.
211. Santavirta S, Bohler M, Harris WH, Konttinen YT, Lappalainen R, Muratoglu O, Rieker C, Salzer M. Alternative materials to improve total hip replacement tribology. *Acta orthopaedica Scandinavica*. 2003;74:380-388.
212. Santos EM, Vohra S, Catledge SA, McClenny MD, Lemons J, Moore KD. Examination of surface and material properties of explanted zirconia femoral heads. *The Journal of arthroplasty*. 2004;19:30-34.
214. Sheth NP, Lementowski P, Hunter G, Garino JP. Clinical applications of oxidized zirconium. *J Surg Orthop Adv*. 2008;17:17-26.
215. Shikata T, Oonishi H, Hashimoto Y. Wear Resistance of irradiated UHMW polyethylenes to Al₂O₃ ceramics in total hip prostheses. In: *Third Annual Meeting of the Society for Biomaterials*. 1977.
220. Sommer F, Landfried R, Kern F, Gadow R. Mechanical properties of zirconia toughened alumina with 10–24 vol% 1Y-TZP reinforcement. *Journal of the European Ceramic Society*. 2012;32:4177-4184.
228. Tan SC, Lau ACL, Del Balso C, Howard JL, Lanting BA, Teeter MG. Tribocorrosion: Ceramic and Oxidized Zirconium vs Cobalt-Chromium Heads in Total Hip Arthroplasty. *Journal of Arthroplasty*. 2016;31:2064-2071.
230. Tateiwa T, Clarke IC, Williams PA, Garino J, Manaka M, Shishido T, Yamamoto K, Imakiire A. Ceramic total hip arthroplasty in the United States: safety and risk issues revisited. *American journal of orthopedics (Belle Mead, N.J.)*. 2008;37:E26-31.

3 Taper Angle Clearance Measurement

3.1 Introduction

The biomechanical forces being applied to a THA in vivo are variable with gait motion and other everyday activities. The regions of the femoral stem are under combined tension, compression, and torsion depending on the position of joint in relation to the applied loads [206]. These dynamic movements create numerous opportunities for micromotions and other damage modes at the modular femoral head and stem taper junction (Figure 24) by potential proximal-distal slipping of the femoral head and/or bending of the stem neck/head cone [206]. It has been documented that micromotions initiate fretting and the cyclical nature of the forces applied lead to mechanically assisted crevice corrosion when fretting begins. Modular junction design, including angular mismatch and conicity [94], has been hypothesized as a factor that may affect the severity of taper mechanical damage and corrosion [37, 238]. However, the potential effect of head bore and stem cone taper angles on taper damage is unclear [23, 152, 184]. The contact mechanics of the taper-trunnion junction may be influenced in part by the angular mismatch between the head and the trunnion, as well as other variables of the head-neck interface. Two previous explant studies, neither of which measured taper angle clearance in their retrieved components, have speculated that angular clearance may contribute to material loss at the taper-trunnion junction through taper surface damage analysis [22, 56]. Bishop et al. [22] observed that in LHMOM asymmetric wear patterns in the female taper most likely indicated toggling motion (as illustrated in Figure 24). Similarly, the failure analysis by Cook et al. [56] observed material loss from the distal end of the head taper/stem trunnion interface and they postulate that the use of a proximal contacting

taper design had provided insufficient mechanical locking between the head and the stem, enabling the head to toggle on the trunnion.

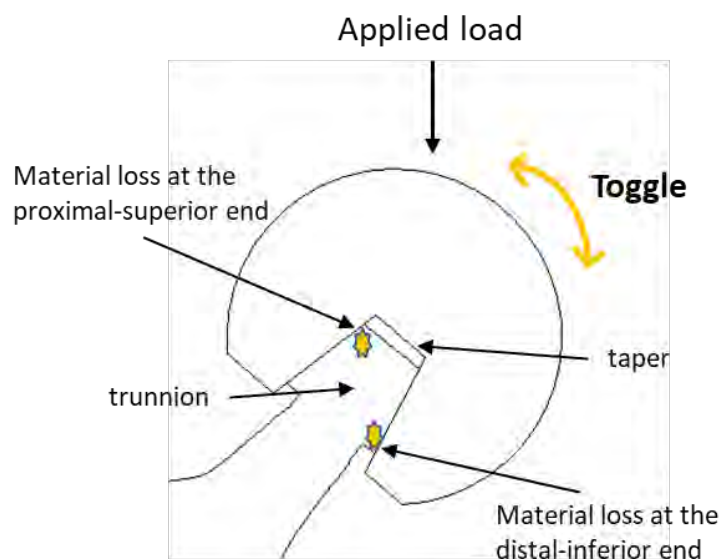


Figure 24: Illustration of hypothesized toggling mechanism of the femoral head due to applied cyclic loading and mismatched stem taper. Asymmetric damage mode may be seen in proximal-superior and distal-inferior regions.

The variation in observed taper material loss patterns in prior retrieval studies have prompted other studies of retrieval analyses, in vitro tests, and FEA simulations to systematically measure and investigate the potential effect of taper angle and design on fretting-corrosion damage and have found evidence that design variation appears to play a role in taper-trunnion junction failure. Brock et al. [36] looked at 104 explanted LHMOM female tapers all revised due to adverse reactions to metal debris and found a significant difference between the volumetric material loss from female tapers mated

with a shorter 12/14, threaded trunnion ($0.403\text{mm}^3/\text{year}$) and those mated with a longer, smooth 11/13 stem trunnion ($0.123\text{mm}^3/\text{year}$). Nassif et al. [185] also looked at 40 LHMOM explant tapers material loss using high-resolution confocal measurements and unlike Brock et al. found there was no significant difference in volumetric material loss based on taper type (11/13, 12/14 and Type 1). In fact, contrary to other retrieval studies, their study showed thicker tapers with longer contact lengths were associated with greater fretting scores, whereas no relationship was found among the three designs for corrosion scores or volumetric material loss. Kao et al. [125] visually graded the head tapers and stem trunnions for fretting and corrosion obtained from a total of 77 metal-on-polyethylene total hip arthroplasties. In this study, stem fretting was inversely related to rigidity and taper angle, while positively correlated to contact length while head fretting, and head and stem corrosion were not associated with any of these parameters. While not conclusive about the effect of taper angle mismatch, retrieval studies demonstrate the wide variation of the taper angles among the commercially available taper types. Design specifications are manufacturer specific; thus, mixing head and stem components from different systems, even when the mating trunnions are described as the same design (such as 12/14) may affect the subsequent fretting and corrosion at the connection. There is also variation in the interference fit between components of the same type by the same manufacturer due to machining tolerances [125, 152]. The effect of these tolerances is not clear and variable between manufacturers. For example, the manufacturing process of ceramic heads have a much tighter tolerance compared to CoCrMo femoral heads as demonstrated in manufacturer specifications and in the results in section 3.3. Retrieval studies show limitations to study these effects, yet, it has been shown that FEA studies

can be designed to detect the significant magnitude for manufacturing tolerances [152]. Retrieval studies also demonstrate the difficulty in isolating and studying the effect of taper angle clearance alone due to additional variations seen in taper designs including alloy material, flexural rigidity, surface finish, taper length and impaction force during implantation [111]. Through a combination of FEA and in vitro studies, the effect of the factors on fretting-corrosion in isolation has been studied by researchers.

A test to quantitatively assess the differences in fretting corrosion of head-neck modular tapers was developed by Mali et al [165]. This test setup was designed to better relate motion measurements to fretting currents, hence, linking the mechanical and electrochemical processes present during testing certain material or taper designs. This type of test enables observing the changes occurring progressively in the interference fit and brings together simultaneous measurement of subsidence and micromotion of the head on the neck with fretting current response. The setup is an incremental cyclic fretting corrosion test method [165] that is a versatile means of assessing potential new taper designs in the future. This test setup was used to evaluate the short-term corrosion and micromechanical behavior of 32 unique head-neck taper design/material/assembly conditions [191] which concluded that head-neck offset and seating load magnitude were the primary factors that influenced the acute fretting corrosion response and angular mismatch was not a significant factor. These findings are consistent with Danoff et al. [67] who investigated the influence of femoral head impaction force, number of head strikes, the energy sequence of head strikes, and head offset using 30 titanium-alloy trunnions mated with 36-mm zero-offset cobalt-chromium femoral heads of corresponding taper angle. By controlling taper angle and implant type, they found that

femoral head impaction force influenced femoral head-trunnion taper stability, whereas offset did not affect pull-off force. Multiple head strikes did not add additional stability, if a single strike achieved 14 kN force at the mallet-head impactor interface. The study by Panagiotidou et al. [193] also concluded that surgeons could minimize mechanically assisted crevice corrosion by using higher impact loads when assembling the head to the stem in total hip arthroplasty, although the range of acceptable impaction force was lower (4-8 kN). Other in vitro studies [78, 105] including those that have investigated the stem-neck taper fretting-corrosion damage [18] also have consistent findings that depending on the contact geometry and loads, fretting damage can be minimized if sufficient contact pressures are achieved in the interference fit.

Some FEA studies found a relationship between taper angle mismatch and taper damage [1, 9, 17, 80]. Ashkanfar et al. [9] has compared their analysis with taper angle and material loss measurements of 54 Articuleze femoral heads (all 36mm diameter) collected using a CMM. While the simulation results agree with the retrieval depth of material loss and mechanical damage patterns, the actual load history and changes in rate of material loss over time is unknown for retrievals and the model only includes fretting, not corrosion. Bitter et al. [24] cautions that simulating a single load cycle is a simplification often made in finite element studies. The modelling of a single cycle of loading gives insight into the initial conditions and may not be representative for the changes in contact mechanics that occur during the fretting process. The contact pressures and micromotions may change over time due to mechanical fretting and plastic deformation, which in turn can affect the progression of fretting. An example of the change in rate of material loss overtime is shown in the progressively increasing taper

damage and eventual catastrophic gross trunnion failure of “Accolade I” type stems [167, 183]. Additionally, there is currently no consensus among FE studies that demonstrate a relationship between taper angle mismatch and taper damage as to which conditions are favorable for mitigating taper material loss. Fallahnezhad et al. [80] found that contact stress, amplitude of sliding and contact length are the key parameters that influence the amount of material loss and fretting damage and concluded that ‘base fit’ mismatches are more resistant to fretting, while Ashkanfar et al. [9] found the opposite, with ‘base fit’ tapers having significantly higher mechanical wear rates, reportedly caused by the larger moment arm in the case of a ‘base fit’ taper. Another limitation for the Ashkanfar et al. study is that the measured validation explant samples were only the femoral heads and the actual taper angle mismatch between the head and the stem was not measured and theoretically calculated. These taper parameters vary over the fretting wear cycles and are highly dependent on the type and magnitude of the taper angle mismatch.

Retrieval studies analyses of taper damage modes and limitations of FE analysis methods have demonstrated the need to develop an FEA routine in which adaptations to the implant geometry are made during the computation to account for material removal during the fretting process. Bitter et al. [24] present a finite element wear prediction using adaptive meshing at the modular taper interface of hip implants. In their study, the maximum experimental depth of material loss was $30.5 \pm 17 \mu\text{m}$, while the FE predicted a maximum depth of material loss of $27 \mu\text{m}$. They show that adaptive meshing method delivered results that are closer to the experimental test data compared to the results from modeling a single cycle without adaptive meshing. They use this adaptive modeling method to next evaluate the effect manufacturer tolerances on taper mechanical wear. As

mentioned previously, design specifications are manufacturer specific and show large variability in design parameters. Taper designs for the femoral modular junctions are defined by the taper angle, length and distal or proximal diameter, roundness, straightness, surface finish and material (Figure 4). General manufacturing tolerance requirements as described in ISO 2768-1:1989 have not changed since 1989, while manufacturing processes have considerably improved. In the study by Bitter et al. [23] the effects of manufacturing tolerances on the volumetric material loss of taper surfaces are studied by varying the parameter of the stem taper tolerance in their computational model in accordance with the ISO 2768-1:1989 guidelines. This resulted in the following combination scenarios that were investigated: 1) 'Perfect fit': no angular mismatch between the stem taper and the taper adaptor, 2) 'Tip fit': angular mismatch causes the taper adaptor to seat proximally, 3) 'Base fit': angular mismatch causes the taper adaptor to seat distally, 4) 'Oval frontal': a perfect fit in the superior-inferior (SI) direction and an angular mismatch in the anterior-posterior (AP) direction, 5) 'Oval coronal': a perfect fit in the AP direction and a mismatch in the SI direction. The effect of each of these fit scenarios were studied in combination with assembly force on the volumetric material loss. The study showed that higher assembly forces and smaller mismatches result in the least volumetric material loss [25].

The primary goal of our study was to compare the severity of taper corrosion between total hip implants with ceramic vs. metal femoral heads. The literature review shows the need to conduct a controlled investigation of the effect of taper angle clearance on material loss and corrosion in non-LHMoM retrievals. The manufacturing practices between metal and ceramic show differences and the tolerances for each material and

manufacturer show variability even if they are nominally designed to have the same cone angle. Profilometers and other surface inspection devices such as coordinate measurement machines (CMM) have been used to evaluate the surface damage on modular tapers in various studies. These tools have been used to map entire taper regions [152] or used trace inspection to identify changes in taper surface by inspecting surface roughness [194]. The goal of the present study was to investigate the hypothesized relationship between taper angle clearance and fretting-corrosion damage in stems mated with ceramic and metal heads. Building on our previously assembled cohorts of ceramic head and metal head retrievals [143], we asked (1) whether a novel methodology for characterizing the taper angle clearance in retrieved heads and stem pairs would be sufficiently repeatable and reproducible to accurately measure the explanted components; (2) if there was a difference in clearance angle and contact location between the ceramic and metal cohorts; (3) did taper angle clearance help explain the variability in the extent and severity of taper damage in the ceramic and metal cohorts; and (4) was there evidence of mechanical wear/corrosion in taper regions identified with material loss?

3.1.2 Surface Profilometry

There are several inspection methods available in the biomedical, aerospace and automotive industry for evaluating manufactured parts. Most of the techniques used for large sections and parts include contact methods, optical interference, diffuse or specular reflection and surface replication methods. For localized inspection microscopic techniques such as scanning tunneling microscopy, atomic force microscopy but are limited in being able to analyze only small areas at a time and in the case of the scanning

tunneling microscopy conducting surfaces. For our inspection purposes, we needed a technique suitable to evaluate large sections for a lot of parts.

In contact methods a stylus physically contacts the surface and takes traces to measure the surface. Optical instruments use incident application of electromagnetic radiation and analyses the local physical properties of a surface based on the specular or diffuse distribution of the reflected energy [232]. Optical interference, white light interferometry, is another technique used for surface roughness measurements. Replication techniques use a soft replica material that is designed to replicate surface roughness and needs to be removed before measurement. Each have their advantages and disadvantages and should be selected based on the specific needs of the application. For manufacturing, these inspection methods are used to evaluate the quality of production by ensuring predefined metrics such as surface roughness, tolerances and other dimensions meet specifications. In the work described here, we have used the contact surface profilometry technique to measure retrieval taper surfaces.

Using a stylus to contact and trace the surface is the most accurate method to measure surfaces, and a roundness machine is specifically suitable to measure the femoral head and stem tapers because it is designed to measure cylinders. Specular reflection and diffuse reflection methods are semi-quantitative and do not always correlate with stylus readings. Also, these methods may not work on highly reflective surfaces such as metals and give inaccurate results. I refer to the use of an optical microscope with surface profiling capability in section 5 of this dissertation (KH-8700, HIROX) however, for the work completed in sections 3 and 4 we have chosen to use a roundness machine (Talyrond 585, Taylor Hobson UK) as it provides the greatest ease

and accuracy for measuring roundness or axial traces in conical taper bores and stem trunnions. A roundness machine measures the deviations from a perfect circle, which is defined by a precision spindle on which the specimen component is rotated. A stylus contacts the surface of the component as it is rotated and measures the deviation from an assumed perfect circle. It is also possible to take linear, also known as axial, traces. Some roundness machines also measure absolute dimensional values and allow traces to be stitched together to make three-dimensional (3D) surface maps. The use of a surface map software TalyMap was available for use with the Talyrond 585. The Talyrond 585 also had two types of stylus tips available for measurements, a 4mm diameter ruby ball and a 5 μ m diameter diamond tip (Figure 25). The Talyrond can provide higher resolution with the use of the diamond stylus which is not available on a CMM while very small diameter ruby styli (<1mm) are available. Figure 26 shows the difference in resolution between the surface map using the diamond stylus and the ruby stylus.

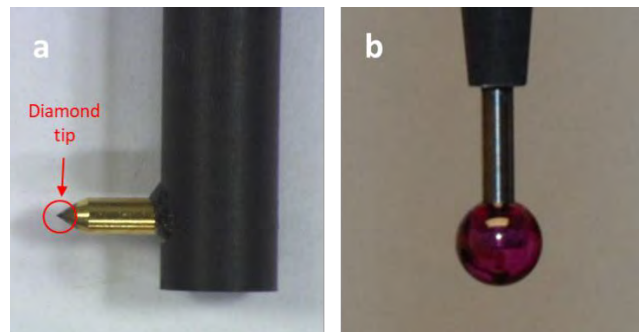


Figure 25: Stylus types available on the Talyrond 585 a) 5 μ m diameter tip diamond stylus, b) 4mm diameter ruby sphere.

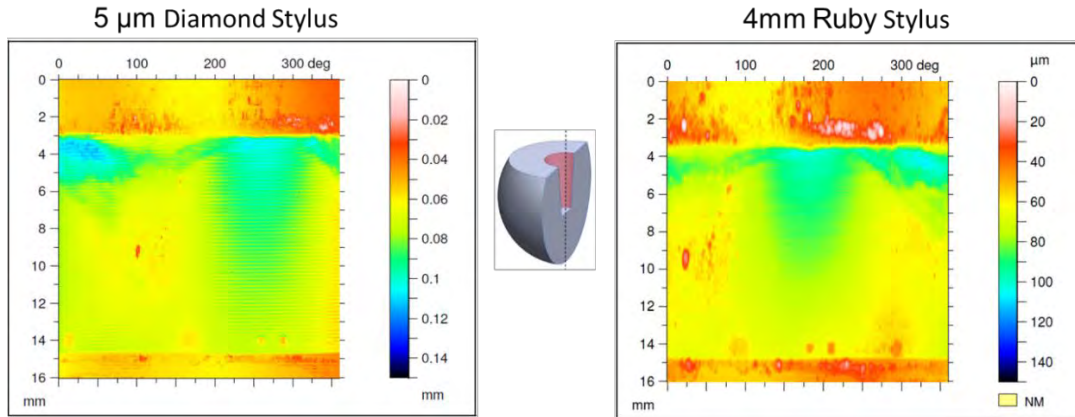


Figure 26: Measurement of the internal taper of a femoral head using a diamond stylus and a ruby stylus. There are clear resolution differences between the two measurements even though measurements with both styli collected the same number of data points. Each surface map is comprised of 720 profiles, 160001 points per profile and 11.5 million data points. Axial profiles

Sources of Uncertainty

As it can be seen from figures 26 and 27 the difference in stylus size may lead to a source of measurement uncertainty. Figure 27 shows a representation of a surface with peaks and valleys with sharp angles, which is the original profile if we could measure it accurately. In the figure we are shown the stylus tip (not to scale) and the profile it traces on the original surface. The traced profile recorded by the stylus is the locus of the center of the stylus. Compared to the original profile in Figure 27, the radius of curvature of a peak may be exaggerated and a valley may be represented as a cusp. It becomes clear that as the size of the stylus tip becomes smaller it can trace the surface with closer approximation to the original profile. Hence the difference in resolution shown in Figure 26 between a 5 μ m tip diamond stylus and the 4mm ruby stylus. However, due to the finite dimensions of the stylus tip, there will always be some level of uncertainty present in the measurements. Studies have shown that in measurements of real surfaces, the

slopes are significantly more gentler at the scale on which the diamond stylus measures them and the uncertainty becomes negligible [232].

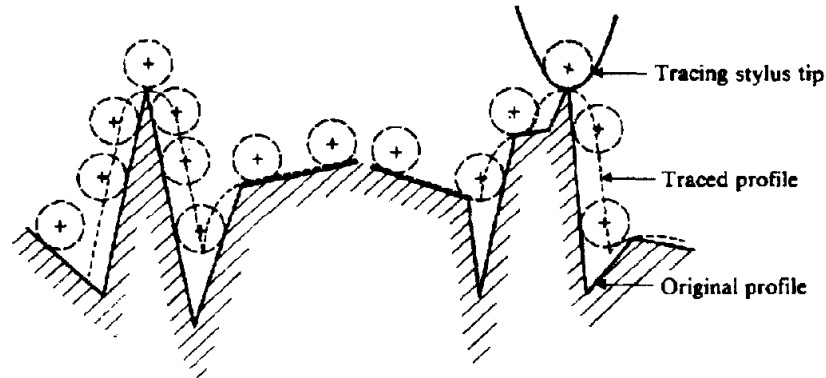


Figure 27: Distortion of a measured profile due to finite dimensions of stylus tip [232].

Another factor that is related to stylus size and potentially a source of uncertainty during contact profilometry is the stylus load. The concern about stylus load is that it may lead to elastic and even plastic deformation on the surface. The ceramic materials being measured in our studies are not of concern about being deformed elastically or plastically under the applied loads due to their high hardness. Studies have looked at the measurement of metals under various contact loads and have shown that with low and high loads (0.06mN to 0.8mN) repeatable measurements with identical profiles. Nearly identical profiles were achieved even when traces with low load, followed by high load and then a low load again was taken. So, it has been established that even if there is deformation taking place, the surface is everywhere deformed by the same amount [232].

Roughness

In nature, entropy drives surfaces to roughness and disorder. For manufactured surfaces, there are different roughness values depending on material and manufacturing method but there is a defining quality and uniformity that is achieved as a result of applying work to a surface. Manufactured surfaces are recognizable by this achieved pattern and distinguishable from fretting-corrosion damage based on defined average properties of the surface. One defining parameter for profiles is the root mean square (RMS) roughness:

$$R_q = \sqrt{\frac{1}{L} \int_0^L z^2(x) dx}$$

Where L is the evaluation length. Another parameter that is more commonly used today is the center-line average (CLA) roughness:

$$R_a = \frac{1}{L} \int_0^L |z(x)| dx$$

By this calculation, the area under the profile above the mean line is equal to the total area under the profile below the mean line (Figure 28) [232].

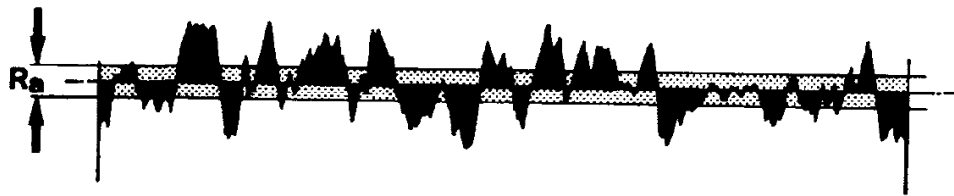


Figure 28: Distortion of a measured profile due to finite dimensions of stylus tip [232].

Quantitative definitions such as R_q and R_a help determine any changes that may occur locally or on a large scale to the surface. The average roughness values have limitations; however, they are helpful to compare surface profiles and roughness values between materials and parts. For example, a retrieval analysis of ceramic heads used R_a values to quantify the changes of the roughness on the bearing surfaces in vivo [175]. Figure 29 shows an example of a ceramic taper axial trace using the roundness machine. Ceramic materials are very smooth, and yet the visual appearance of the profile visually looks very rough. During the evaluation of profiles, the scale of inspection and quantitative values such as R_a are helpful to determine objective differences between profiles and any changes from as-machined surfaces. As-machined surfaces have profiles with repeating features within expected limits. Figure 29 is showing examples of as machined surfaces of a ceramic head taper and a CoCrMo head taper. Mechanical wear, corrosion and form deviations due to implantation will cause deviations from these profiles. This will become important as we look at circumferential profiles and other axial traces and exclude regions with debris or material loss. The exclusion selection is discussed in more detail in section 3.2 and 3.3 when discussing damage modes and imprinting.

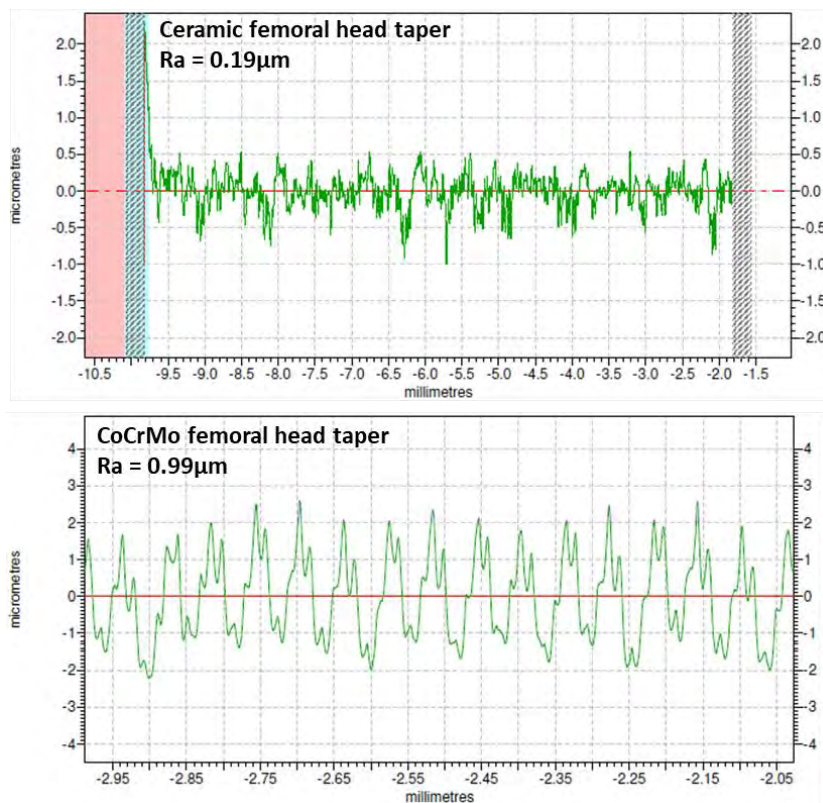


Figure 29: Example axial trace from a ceramic (Biolog Delta) head taper.

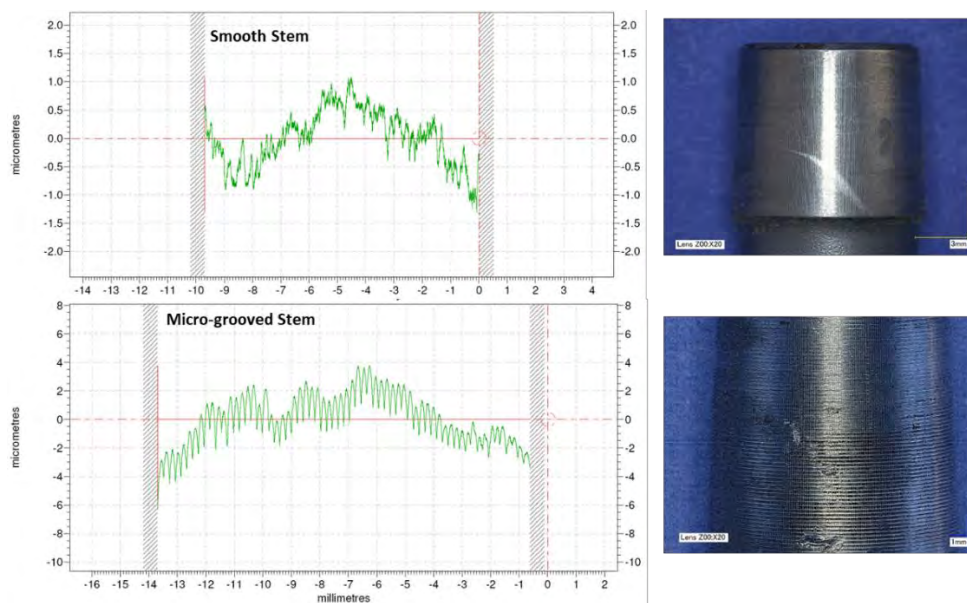


Figure 30: Axial profiles showing differences in surface topography for a smooth and micro-grooved stem taper. The bell-shaped curve of the profile is due to manufacturing form.

3.2 Experimental Methods

3.2.1 Study Design, Cohort Selection, and Clinical Information

The same components used in the matched cohort study mentioned in Chapter 2 were used for a comparative study of taper angle mismatch and corrosion as a function of femoral head material. As mentioned previously, components were selected from the retrieval collections of two academic engineering-based programs working in collaboration with 12 clinical revision centers around the United States as part of an ongoing institutional review board approved revision and retrieval program started in 2000. In our previous study [143], an *a priori* power analysis revealed that a total sample size of 100 would be adequate to detect a difference in visual fretting-corrosion score of 1 on a scale of 1-4 between the ceramic and metal cohorts. For the current study, we continued our previous study by measuring the taper angle clearance in the same matched cohorts of 50 ceramic and 50 metal head-stem pairs because it allowed us to isolate and investigate taper angle clearance for the present study (Table III more details in Table XIII and XIV in the Appendix).

Table V: Patient and device information for ceramic and CoCr cohorts. Cohorts were matched previously [143].

Information from Operation Notes	Ceramic Cohort	CoCr Cohort	p-value
Patient Information (mean \pm SD)			(Mann-Whitney U)
Implantation Time (years)	3 \pm 3	3 \pm 2	0.7
Age at implantation (years)	52 \pm 10	57 \pm 14	0.03
Gender (F:M) (number (%))	17 (34%)	25 (50%)	0.11
BMI (kg/m ²)	30 \pm 7	30 \pm 7	0.91
UCLA Activity Score	6 \pm 2	5 \pm 2	0.65
Reason for revision (# of components)			0.065 (Pearson)
Loosening	28	22	
Infection	13	20	
Fracture	1	4	
Pain	2	1	
Other	6	3	
Stem Design (# of components)			0.34 (Pearson)
Accolade (Stryker, Mahwah, NJ)	28	27	
M/L Taper (Zimmer, Warsaw, IN)	3	4	
Versys (Zimmer, Warsaw, IN)	2	4	
Tri-Lock (Depuy/Synthes, West Chester, PA)	2	2	
Corail (Depuy/Synthes, West Chester, PA)	3	3	
Other	12	10	

3.2.2 Taper Angle Measurement Method Development

Retrieval Measurements

The head and trunnion taper angles were measured using a roundness machine (Talyrond 585, Taylor Hobson, UK), equipped with a diamond or ruby stylus. The component was mounted in a custom fixture on the Talyrond rotating stage and the angular position was referenced against a landmark (e.g. laser etched markings) on the

component to identify a starting position at 0 degrees around the 360 degree rotation about the Z axis of the cone geometry. The component was centered and leveled using regions visually identified with little or no corrosion debris to align the axis of symmetry of the machine with the axis of rotation of the component. The as-manufactured surfaces were identified by visual inspection of the taper surface and 4 axial profiles, measured at 90° intervals around the taper. The as-manufactured regions have a distinctly different profile in linear traces and can be identified by the periodicity of the manufacturing process. Each manufacturing process will produce different surface roughness parts depending femoral head material, CoCrMo vs. ceramic (Figure 29), or surface finish of stem trunnion based on manufacturer design, smooth vs. micro-grooved (Figure 30).

The presence of unworn surfaces which will be used as the reference surface is a requirement for accurate taper angle measurements. The reliable identification and fitting of as-manufactured surfaces are usually dependent on a skilled operator for accurate least squares fitting. In order to calculate the material loss from the measured data points from the roundness machine or CMM, the as-manufactured surfaces must be identified using an initial inspection to confirm the absence of mechanical damage and corrosion in the regions being intended to be used for data fitting. This initial inspection can be completed visually, by using a microscope, taking preliminary traces to compare surface roughness of regions, or all three methods. Figure 31 is showing examples of axial and circumferential traces used to preliminarily inspecting tapers and the regions that are not as-manufactured and will be excluded.

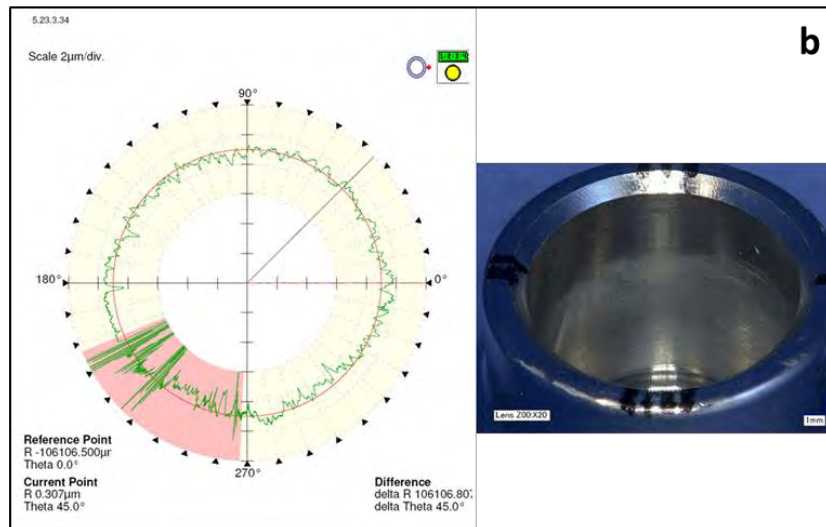
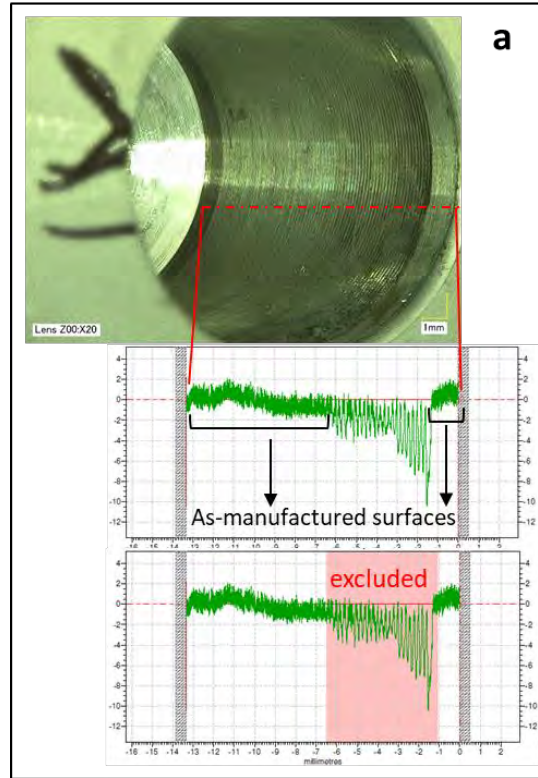


Figure 31: Process showing the preliminary axial (a) and circumferential (b) traces measured for inspection and determination of regions with material loss and corrosion. The Talyrd 585 software allows the manual exclusion of user defined regions and does least squares fitting only on the as-manufactured sections of the profile. The axial profile shows exclusion of material loss and the circumferential profile shows the exclusion of debris.

When manufactured, the components are usually nominally conical, but there are variations resulting from manufacturing tolerances or deformation during implantation, use or revision. These are called form variations and are different than mechanical wear through abrasive or corrosion processes. As much as possible, form deviations must be separated from the mechanical damage by the analysis and measurement protocol to reduce uncertainties in the calculated material loss. Figure 32 is showing an example of a possible change in the profile due to form variation at the proximal end of the stem taper microgrooves. As mentioned previously, all profile analyses are most accurate when verified visually and/or with microscopy. Regions with form deviations if caused during implantation or revision, including iatrogenic damage, are also excluded from least squares fitting of as-manufactured surfaces.

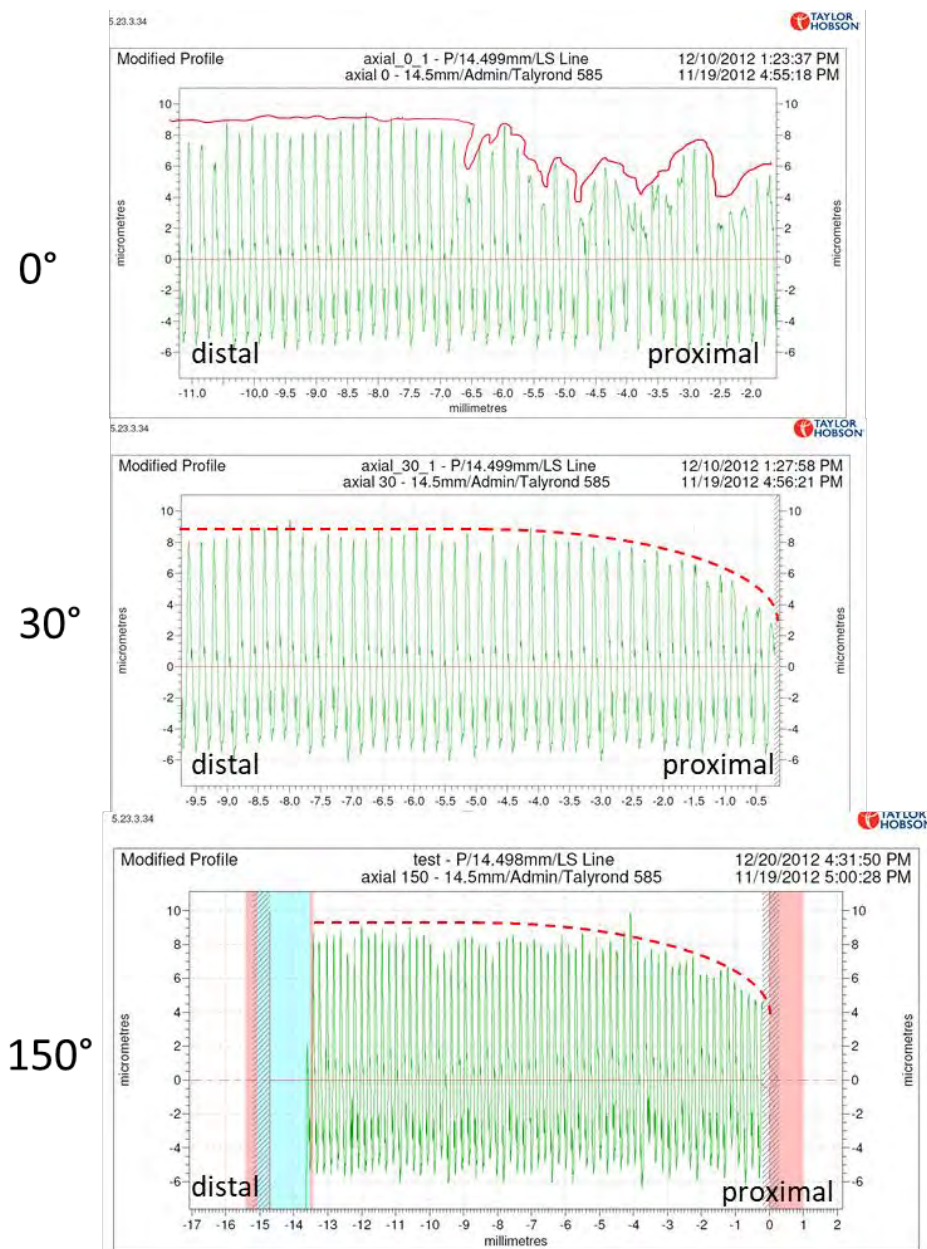


Figure 32: Stem taper axial profiles taken from the same stem at different locations 360° around the circular axis. The profile taken at 0° shows irregular changes in the profile which has been determined to be material loss due. For the profiles taken at 30° and 150°, the change in the profile seen in the proximal end is an example of change of form during implantation due to stem taper proximal end getting fitted into the head taper and getting compressed in the proximal region.

Taper and Trunnion Angle Measurements

The taper angle is defined as twice the measured half angle of the geometric cone forming the head taper or stem trunnion. Taper angle clearance is the difference between the head taper angle and trunnion angle:

$$\text{Taper angle clearance} = \text{Taper angle of head} - \text{trunnion angle of stem} \quad (2)$$

Positive clearance, which will result in proximal contact between the head and trunnion, occurs when the taper angle is greater than the trunnion angle. Negative clearance, on the other hand, will result in distal contact (Figure 33).

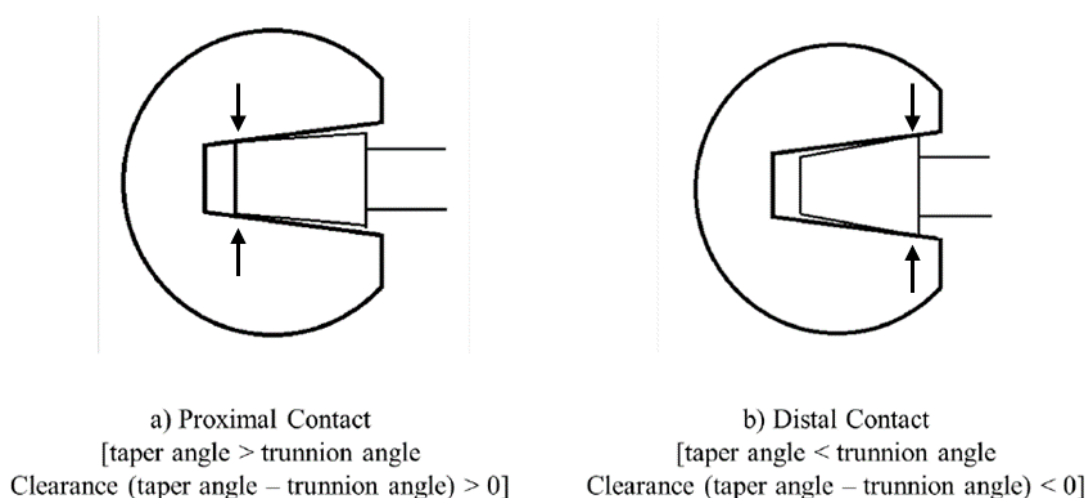


Figure 33: Schematic diagram showing the taper angle clearance, a) shows positive taper angle clearance and proximal head/stem contact, b) shows negative taper angle clearance and distal head/stem contact. These figures are only representatives of the theoretical contact at the taper-trunnion junction. In vivo, while the overall contact area will be located proximally or distally, the contact surfaces may not be axisymmetric and may have a contact area larger on the superior or inferior side with only a point contact on the other side.

The component was centered and leveled once again using measurements in the confirmed as-manufactured regions to align the axis of symmetry of the machine with the axis of rotation of the component. After this final centering and leveling, an axial profile was measured over the top edge of the taper to establish a height datum. A series of 5 to 7 circumferential profiles were measured in the identified as-manufactured region(s) of the taper surface, typically spaced at a vertical distance of 1 – 3 mm. The number and spacing of the profiles depended on the length of the taper and the location and size of the as-manufactured regions. The head tapers were measured using a diamond stylus with a tip radius of 5 μ m. Due to the presence of microgrooves and sometimes extensive iatrogenic damage, a 4mm diameter ruby stylus was used to measure the surface of all trunnions to prevent damage to the diamond tip and provide mechanical filtering of the microgrooves. Each roundness profile was analyzed using Ultra software [Taylor Hobson, UK] and a least-squares (LS) circle was fitted. The LS fit was improved by excluding regions of asymmetric material loss or point defects. For consistency, it was required that after exclusions, at least 55% of the profile was used in the fit and the deviation of the points in each remaining profile was less than 10 μ m. A second skilled operator identified the as-manufactured regions for each component and cross-checked for agreement of the selected vertical height location and exclusions applied on each roundness profile. The radius and height of each LS circle was compiled in a spreadsheet and the linear slope of the radius of the 5-7 profiles was used to calculate the taper angle (Figure 34). Repeatability measurements for taper angle were performed using both the diamond and ruby styli on a reference taper ring gauge. The diamond stylus is used for taper angle measurements because of higher resolution and the 4mm ruby stylus is used

for trunnion angle measurements to prevent damage to the diamond stylus from the as-manufacture grooves on some of the trunnions.

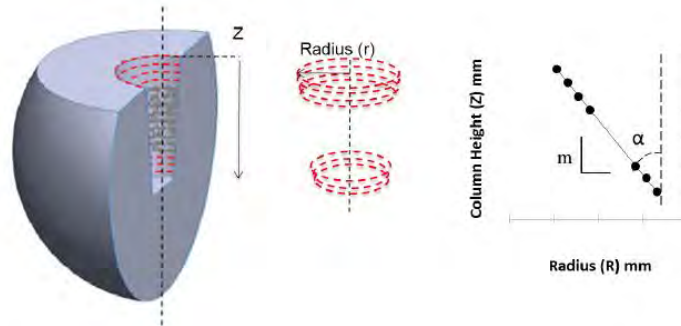


Figure 34: The radius and relative height of each LS circle was compiled in a spreadsheet and the linear slope of the 5-7 profiles were used to calculate the angle. Areas with corrosion debris were excluded from the measurements. Measurements were only taken in as-manufactured surfaces.

$$\text{Taper Angle} = 2\alpha = 2 \cdot \tan^{-1} \left(-\frac{1}{m} \right) \quad (3)$$

Surface Topography Characterization

The regions with material loss were identified by the axial Talyrond profiles and visual inspection. Twenty-four female metal taper surfaces showed evidence of material loss and thirteen were inspected using scanning electron microscopy (SEM, JEOL JSM-5600) and an optical microscope (KH-8700, HIROX) for evidence of fretting-corrosion mechanisms (up to 320x). The thirteen representative components selected for imaging had the most severe cases of corrosion. Representative Talyrond profiles showing material removal can be seen in Figure 35. Backscatter electron composition (BEC) images are used to inspect surfaces during SEM imaging because the intensity of the

backscattered electron signal is related to the atomic number of the entities being imaged. Using BEC allowed differentiation between the accumulated biological and corrosion deposits and the electrochemical/mechanical topography changes on the metal surfaces being imaged.

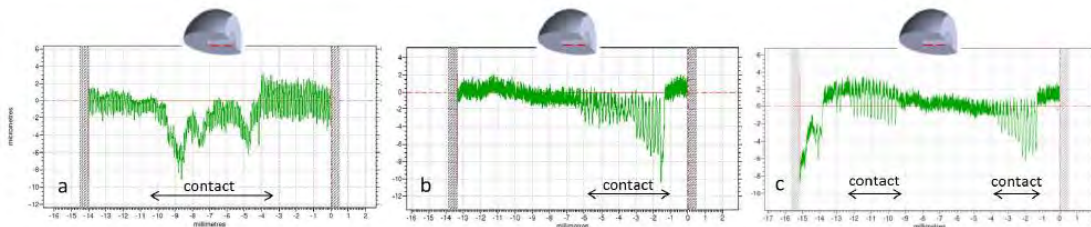


Figure 35: Examples of Talyrond traces for components with observable regions of material loss proximally (a), distally (b) and in both proximal and distal locations (c). The red lines on the schematic of the femoral heads represent the orientation of the profiles being measured. These profiles provide information about the taper-trunnion junction in addition to the clearance values observed for the metal cohort.

3.2.3 Repeatability Study

A repeatability study was conducted to characterize the uncertainty in the taper and trunnion angle measurements. Repeatability of angle measurements using the Talyrond for as-manufactured surfaces was validated with a study conducted using a precision machined part and ceramic femoral head exemplars that were never implanted (Figure 36). Twenty-five angle measurements were performed on different days and using both the diamond and ruby stylus.

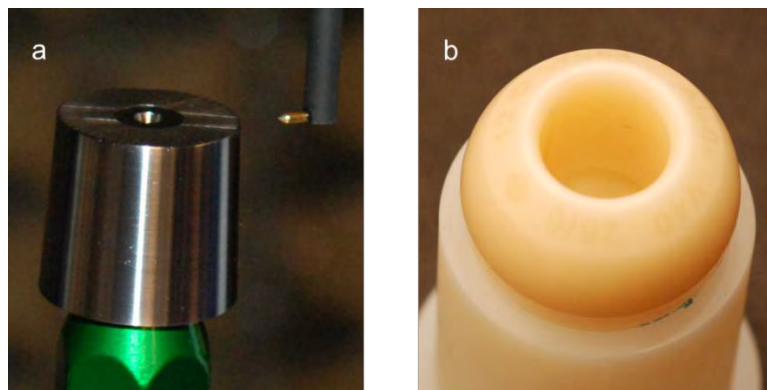


Figure 36: Examples of Talyrond traces for components with observable regions of material loss proximally (a), distally (b) and in both proximal and distal locations (c). The red lines on the schematic of the femoral heads represent the orientation of the profiles being measured. These profiles provide information about the taper-trunnion junction in addition to the clearance values observed for the metal cohort.

3.3 Results

The standard deviation of the repeatability study was 13.3 seconds. By contrast, a previous explant study [152] has measured the range of head taper angles in retrieved implants and reported a variation of 0.23 degrees (13.8 minutes). Two stems had extensive iatrogenic damage, preventing accurate trunnion angle measurements and thus, 2 head-stem pairs had to be removed from the study. Taper angle measurements for ceramic and metal heads resulted in no overlap between the taper and trunnion angles in the ceramic cohort, while there was overlap in the metal cohort (Figure 37). Hence, calculation of taper angle clearance revealed a difference between the ceramic and metal cohorts. The ceramic cohort had exclusively positive taper angle clearance, geometrically indicating proximal contact (Figure 39). The metal taper cohort had both positive (n=35) (proximal) and negative (n=15) (distal) taper angle clearance (Figure 38). Proximal contact in the ceramic cohort was further verified visually by evidence of metal transfer at the proximal end of the head taper (Figure 39). Profile traces taken in regions with and

without metal transfer did not show any differences, metal transfer was not quantifiable. For metal head-stem pairs, it was possible to confirm proximal or distal contact by inspecting the surface topography of measured profiles when there was observable material loss, as determined by a skilled operator who could identify deviations in topography in profiles. Profiles of metal heads showed one of the following conditions: a pristine surface with no detectable material loss (n= 32), region with material loss indicating proximal contact (n = 3), distal contact (n = 9), or proximal and distal contact simultaneously (n = 6) (Figure 35).

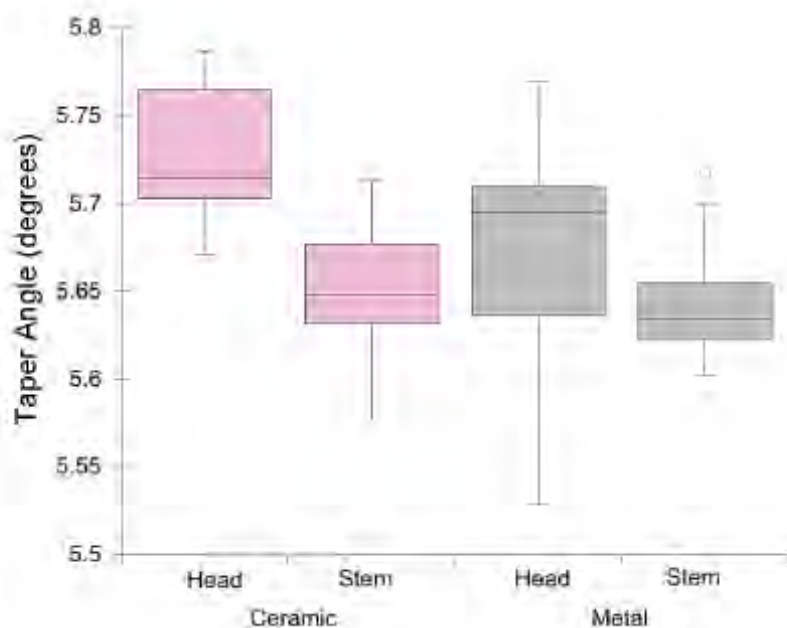


Figure 37: Taper angle measurements for the ceramic and metal head-stem pairs. There is no overlap in the taper and trunnion angle measurements for the ceramic cohort, while there is overlap in the metal cohort.

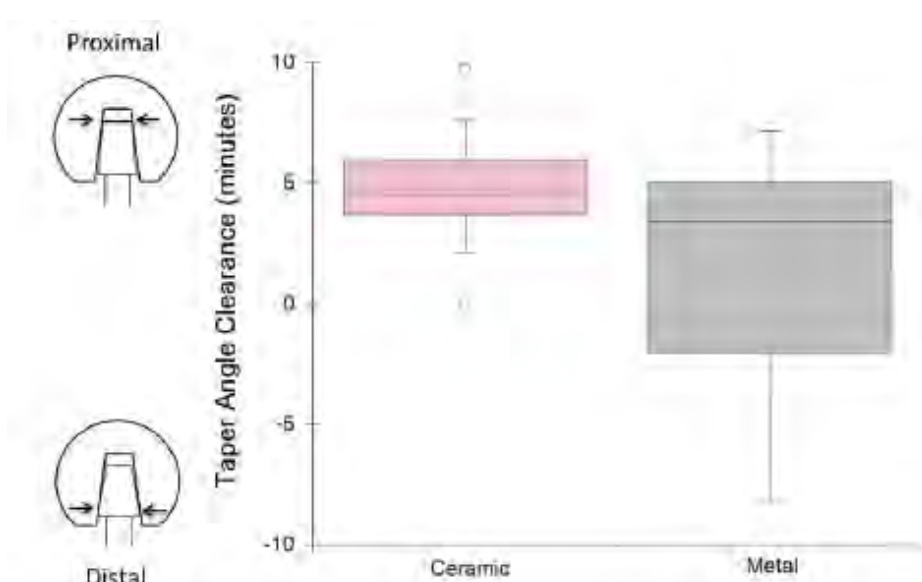


Figure 38: Taper angle clearance distribution for the ceramic and metal cohorts. The taper angle clearance for the ceramic cohort is always greater than zero (indicating proximal contact), while the metal cohort has clearance values that are greater and smaller than zero (indicating a mixture of proximal and distal contact).

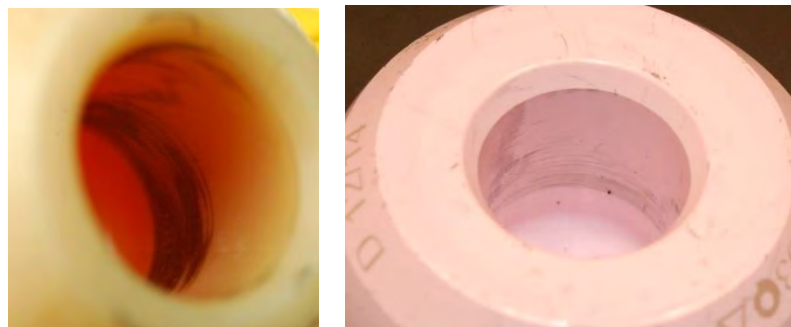


Figure 39: Metal transfer was observed on the proximal ends of the internal tapers of ceramic heads, providing visual confirmation for clearance values greater than zero for the ceramic cohort.

There was no significant correlation observed between taper angle clearance and visual fretting-corrosion scores for trunnions in the ceramic cohort ($\rho = -0.17$), trunnions in the metal cohort ($\rho = 0.24$) nor the femoral head tapers in the metal cohort ($\rho = -0.05$) (Figure 40). Additionally, visual fretting-corrosion scores in the metal cohort were

similar between components with distal contact (negative taper angle clearance) and components with proximal contact (positive taper angle clearance) ($p = 0.43$ and 0.56 for taper and trunnion scores, respectively; Wilcoxon Test).

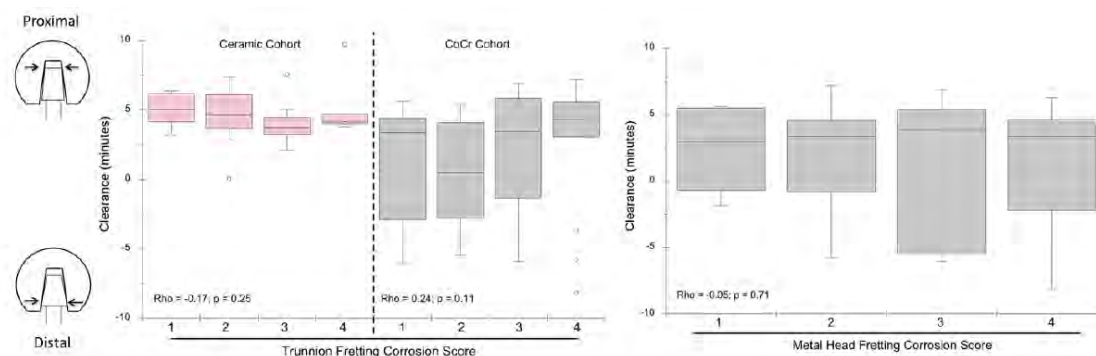


Figure 40: Distribution of measured ceramic and metal cohorts according to a) trunnion fretting corrosion score, and metal cohort according to b) metal head fretting corrosion score.

SEM imaging for metal female tapers with evidence of material loss proximally, distally, or both on measured profiles showed features which are consistent with the findings reported in other studies which identified mechanically assisted corrosion (Figures 41 and 42) [85, 94, 98]. SEM also evidenced that electrochemical material loss (pitting) preferentially evolved in regions that showed evidence of fretting (scratches in the scale $5\text{-}40\mu\text{m}$) or had larger scratches ($50\text{-}500\mu\text{m}$) (Figure 42). We hypothesize that these larger scratches may have been caused when the head was impacted onto the trunnion during the primary surgery or during removal. Local changes in the surface topography were observed in heads mated with both “microgrooved” and “smooth” trunnions (Figure 43 and 44). The measured profiles and SEM images of the head taper (Figure 45) both showed changes in surface topography (the amplitude and wavelength of

circumferential grooves) consistent with the microgrooves found on the trunnions – suggesting that “imprinting” had occurred (Figures 46 and 47).

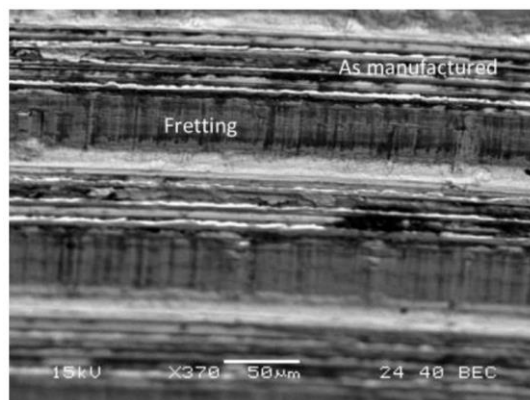


Figure 41: SEM image taken in distal portion of metal head taper showing fretting in regions with horizontal bands of material loss. Bands of material loss most likely corresponded to regions in contact with trunnion as-manufactured grooves (370x, BEC).

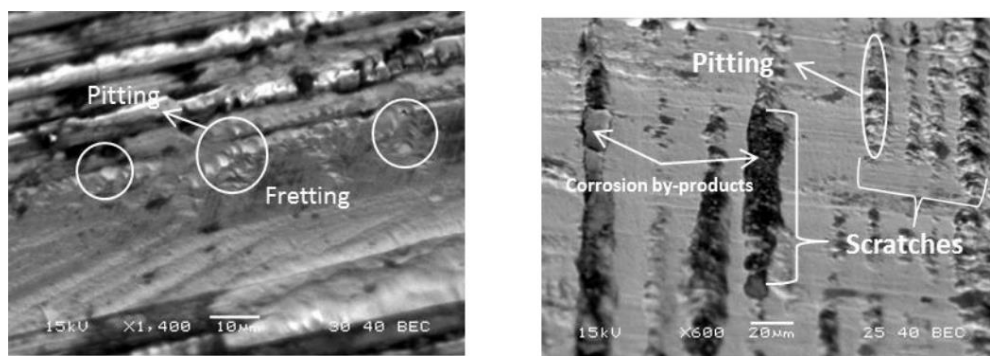


Figure 42: A component showing pitting corrosion (marked in white circles) initiated preferentially in a crevice formed due to fretting abrasion (5-40µm scratches), imaged midway between proximal and distal ends on the taper (left, BEC, 1400x). A different component showing scratches (50-500µm) throughout head taper, with preferential pitting inside the scratches, imaged midway between proximal and distal ends on the taper (right, BEC, 600x). Corrosion by-products (biological and electrochemical deposits) have accumulated inside the scratches.

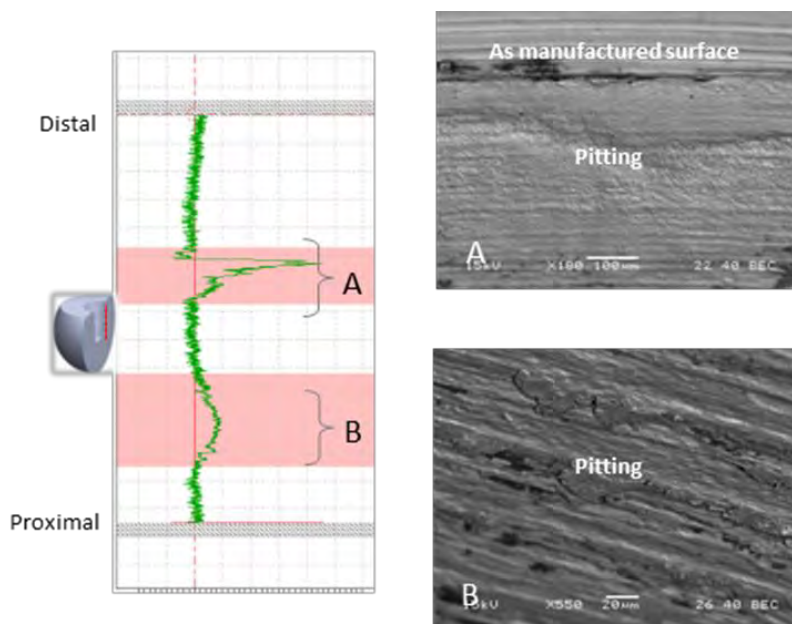


Figure 43: Axial profile of a metal head implanted with a trunnion with a “smooth” finish (left). Regions corresponding to the material loss, marked A and B were imaged using the SEM (right). Both regions of material loss on the Talyrond profile showed evidence of change to the as-manufactured surface.

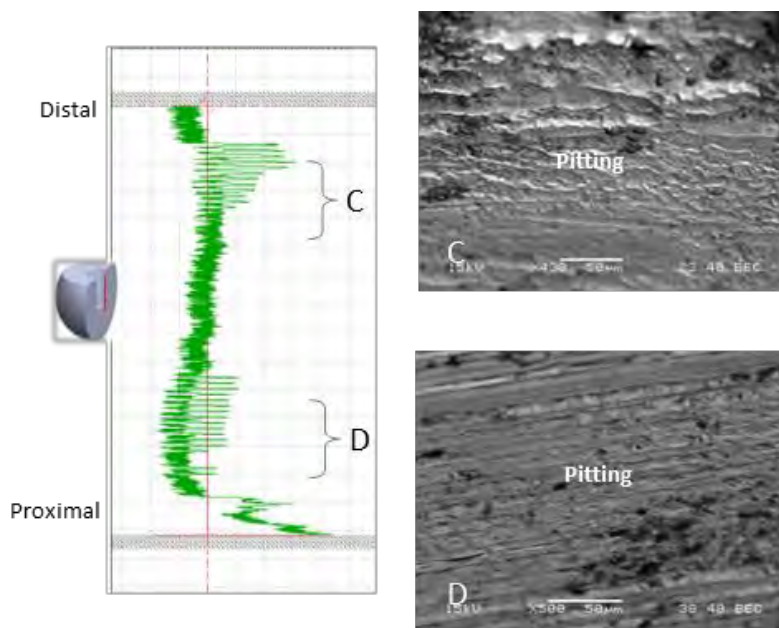


Figure 44: Axial profile of a metal head implanted with a “microgrooved” trunnion finish (left). Regions corresponding to the material loss, marked C and D were imaged using the SEM (right). Both regions of material loss on the Talyrond profile showed evidence of change to the as-manufactured surface.

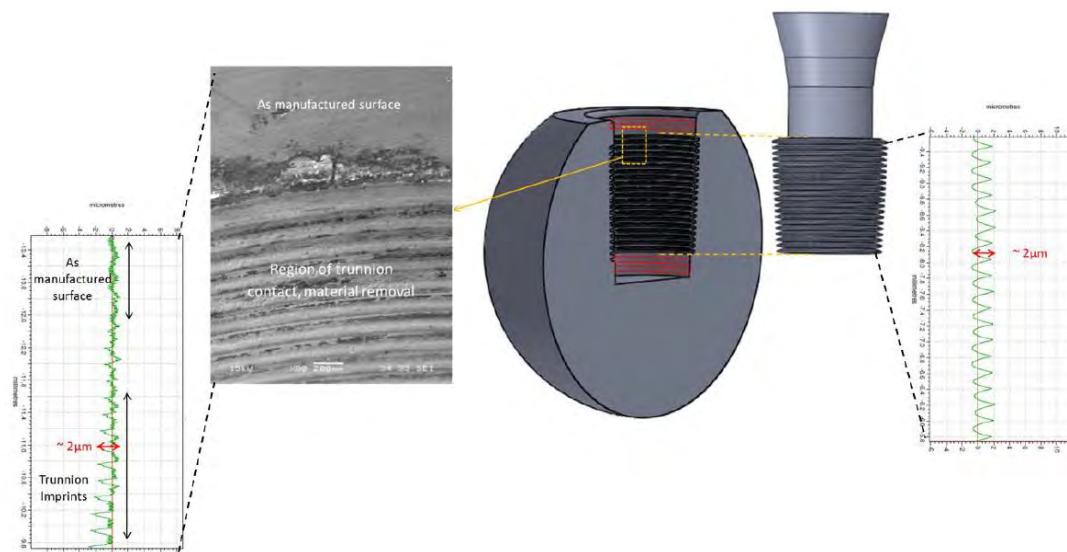


Figure 45: Schematic diagram showing the taper-trunnion interface and typical SEM image and measured profiles from head taper mated with microgrooved trunnion. The red dotted lines represent locations used for roundness profile measurements.

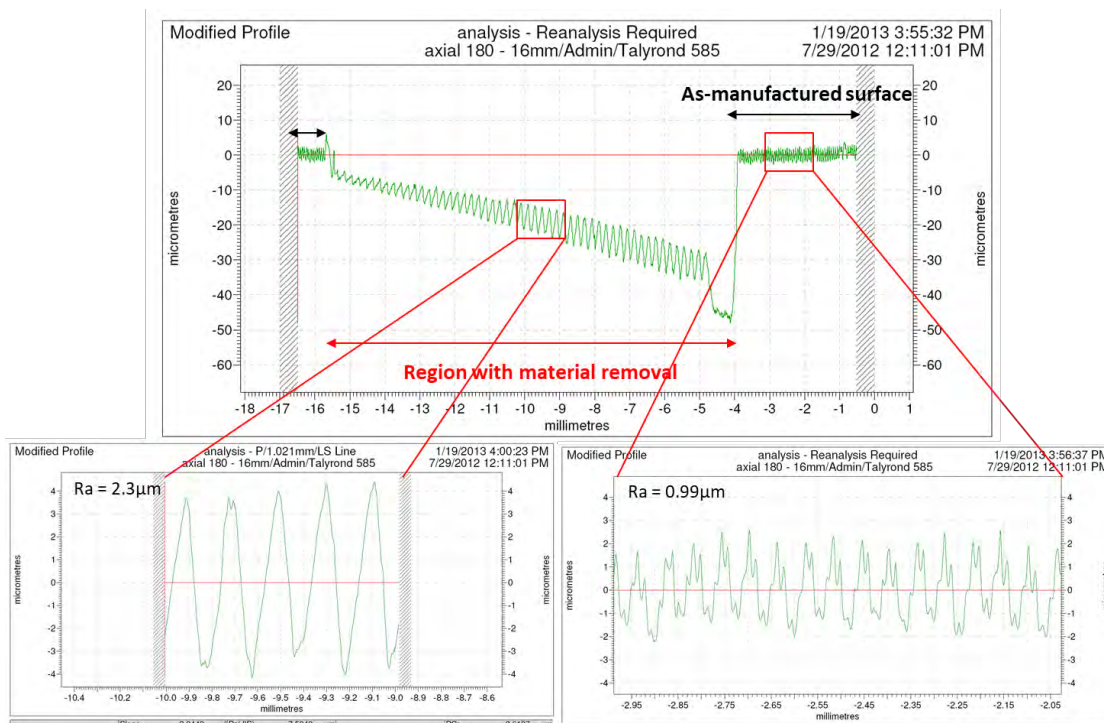


Figure 46: An example femoral head axial profile inspected using the Talyrd software. The regions with material removal and in this case appear like imprinting on the femoral head had a significantly higher surface roughness. The Ra value of the as-manufactured surface was $0.99\mu\text{m}$, and the region with material removal had an Ra value of $2.3\mu\text{m}$.

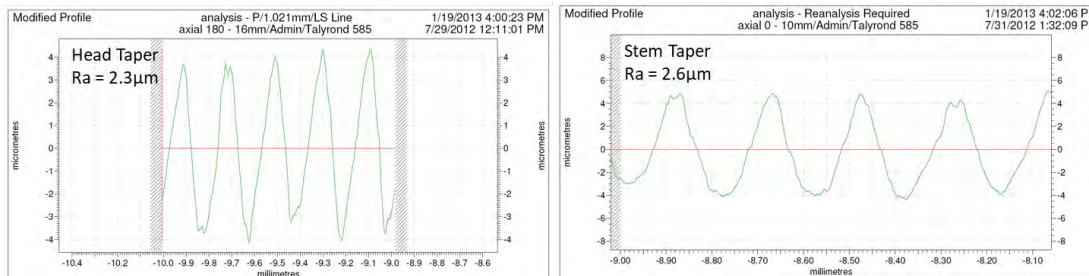


Figure 47: The profile of the regions that appear like imprinting on the femoral head was compared with the stem axial profile. They had very similar profiles, both with a topography amplitude of $\pm 4\mu\text{m}$ and similar surface roughness. The region with material removal on the femoral head (same from Figure 46) had an Ra value of $2.3\mu\text{m}$ and the stem profile had an Ra value of $2.3\mu\text{m}$.

3.4 Discussion

In this study we investigated the effect of the taper angle clearance (defined as the difference in angle between the head taper and stem trunnion) on the visual fretting and corrosion score of a cohort of ceramic and metal head tapers. For both the ceramic and the metal head cohorts, the results of this study did not support the hypothesis that taper angle clearance is associated with fretting and corrosion damage of the head or the taper. Factors other than taper angle clearance, the flexural rigidity of the stem, explained the variation in fretting and corrosion scores between ceramic and CoCr alloy femoral heads. Since there are a number of factors that affect MACC in modular tapers, there was not a strong enough effect of taper angle clearance on taper material loss and corrosion compared to the other factors present in the hip system designs investigated in this study. This is consistent with findings from other studies where there is a consensus that stable and well fitted tapers minimize movement at the head-stem taper [37, 56, 98, 159]; however, there is no clear consensus on the specific taper design parameters such as taper

type (11/13, 12/14, Type 1...etc.) or size that prevents fretting-corrosion damage modes. There are reports that thinner and smaller tapers lead to more fretting-corrosion [43, 111, 125, 217, 229]; however, this may be confounded by stem material and flexural rigidity. The conclusion about this factor was not entirely clear and since there are studies that report the opposite finding [185] further investigation is needed. There are consistent reports of higher stem flexural rigidity [94, 111, 120, 183, 202] and higher impaction forces [67, 78, 105] reducing fretting-corrosion. Each type of study that has studied the effect of taper angle clearance, whether a retrieval, in vitro or FEA study, have faced limitations due to these mentioned confounding factors related to other taper design and material factors, including manufacturing tolerances [25, 125, 152]. The FEA study that investigated the effect of manufacturing tolerances showed that higher assembly forces and smaller mismatches result in the least volumetric material loss [25].

This study had some limitations. First, the taper angles and tolerances reflect matched heads and stems that were designed for compatibility by their respective manufacturer. The study did not include “mixed and matched” heads and stems in which the head of one manufacturer is placed on the stem of another, such as may occur during a revision surgery with limited availability of implant inventory. Second, the stems in this study were single modular in design, such that the only source of modularity was at the femoral head-stem interface. The results of this study, therefore, should not be generalized to head stem designs with additional modular taper connections at the stem. A third limitation of the study was the semi-quantitative, 4-point visual scoring method for assessing the severity of fretting and corrosion. The scoring method was modified from the Goldberg method [94], which is widely used in the literature. This visual

assessment does not provide an objective measure of the volume of material lost from the taper surface. Our previous study has shown that there was a correlation between the visual corrosion score and volume of material loss, but it was also shown that there was a large range in the volume of material lost from tapers with the same corrosion score (Table VI in the next section). These results indicated that the visual corrosion scoring method is suitable for preliminary categorization of taper damage; but does have some limitations. There is a need to quantitatively measure material loss for improved correlation of fretting-corrosion damage with other device and clinical factors. The method to estimate material loss using surface profilometry from femoral head and stem tapers is discussed in Chapter 4.

Another limitation was the small remaining band of as-manufactured taper surface in some femoral head tapers, typically found at the distal end of the head taper. For the current study, the minimum height of this band was 3mm. The uncertainty in the calculated taper angle will increase as the total distance between the circumferential profiles used to calculate the angle decreases. The uncertainty of using a narrow band of as-manufactured surface compared to using a wider band to calculate the taper angle can be estimated. The positional uncertainty of the radial arm and Z-column of the Talyston is $\pm 0.25 \mu\text{m}$. If the taper angle were to be calculated from two measurements, with a radial and height uncertainty of $\pm 0.25 \mu\text{m}$, the uncertainty for taper angle is $\pm 0.01^\circ$ (± 36 seconds) for profiles spaced 3mm apart and $\pm 0.0019^\circ$ (± 6.8 seconds) for profiles spaced 16mm apart. This uncertainty is decreased by taking a minimum of 5 circumferential profiles in the as-manufactured surfaces. The R-squared value of the data points used to calculate the head angle (Figure 34) was at least 0.9999 or better for all tapers.

This study presented an accurate and repeatable method to measure taper angle and calculated taper angle clearance from retrieved femoral heads and stem trunnions. To our knowledge, this is the first study to report the measurement of the taper and trunnion angles of retrieved femoral head and stem pairs using a roundness machine [131]. Roundness machines are widely used in other industries, such as automotive and bearing, to measure the geometry of precision tapered components. The accuracy and repeatability of our method was validated with a study conducted using a precision tapered ring gauge for angle measurements on an as-manufactured surface using the Talyrond on different days. For the retrieved implants in our study, repeated measurement and analysis of components identified as outliers, showed reproducibility within the machine uncertainty range.

The results of our study showed that the ceramic cohort had exclusively proximal contact. This is consistent with the design rationale for ceramic femoral heads, in which the angles of the head taper and stem trunnion are specified so that contact occurs at the center of the head where the material cross-section is largest to resist tensile hoop stresses [116]. The metal cohort showed contact at both the distal and proximal end, however, the different contact patterns did not appear to affect the visual fretting-corrosion scores at the head or the trunnion. This suggests that other factors may have a greater effect on the mechanical and electrochemical processes of material loss. The simultaneous presence of proximal and distal material loss observed on some metal tapers may indicate toggling motion [22], however, the identification of the mechanism leading to material loss was beyond the scope of this study.

Components with visible distal, proximal and dual contact were examined using SEM to investigate evidence of corrosion in regions of material loss. The investigated components suggest that the imaged mechanical and electrochemical alterations to surface topography correspond to locations of material loss observed in measured profiles. However, further study is needed to understand the mechanism of material loss. For this study, only head taper surfaces were imaged under the SEM and trunnions will be investigated in future work. However, previous investigators have observed significant material loss at the head taper and not at the trunnion [22, 173] or that head tapers tended to be corroded more severely than trunnions [94]. Analysis of the measured profiles and SEM images for some metal femoral head tapers, showed a change in surface topography that was consistent with the topography of the microgrooves on the trunnion (Figure 46 and 47). This apparent “imprinting” may suggest preferential material loss from the female taper, also reported in previous studies [22, 98, 152, 173].

In summary, taper angle clearance was not correlated with the visual fretting-corrosion scores in the ceramic or metal cohort in the present study. The effects of taper angle clearance may not be significant compared to other factors leading to material loss or the lack of correlation may be due to the limitations in the visual scoring method. Research is underway to better characterize the volume of material release from explants to better understand the reasons for reduced fretting and corrosion previously observed in the ceramic femoral head cohort.

References

1. Abdullah KA. Finite element modelling of the neck-stem interface of a modular hip implant for micro-motion study. In: *19th IASTED International Conference on Modelling and Simulation, MS 2008, May 26, 2008 - May 28, 2008*. Quebec City, QC, Canada: Acta Press: 2008:364-369.
9. Ashkanfar A, Langton DJ, Joyce TJ. A large taper mismatch is one of the key factors behind high wear rates and failure at the taper junction of total hip replacements: A finite element wear analysis. *Journal of the mechanical behavior of biomedical materials*. 2017;69:257-266.
17. Baumann AP, Vesnovsky O, Topoleski LDT, Donaldson F, McMinn NLL, Vignola A, Di Prima MA. Specimen Specific Finite Element Models for Predicting Fretting Wear in Total Hip Arthroplasty Tapers. *J Biomech Eng*. 2020.
18. Baxmann M, Jauch SY, Schilling C, Blomer W, Grupp TM, Morlock MM. The influence of contact conditions and micromotions on the fretting behavior of modular titanium alloy taper connections. *Medical Engineering and Physics*. 2013;35:676-683.
22. Bishop N, Witt F, Pourzal R, Fischer A, Rutschi M, Michel M, Morlock M. Wear patterns of taper connections in retrieved large diameter metal-on-metal bearings. *Journal of orthopaedic research : official publication of the Orthopaedic Research Society*. 2013;31:1116-1122.
23. Bitter T, Khan I, Marriott T, Lovelady E, Verdonschoff N, Janssen D. The effects of manufacturing tolerances and assembly force on the volumetric wear at the taper junction in modular total hip arthroplasty. *Computer Methods in Biomechanics and Biomedical Engineering*. 2019;22:1061-1072.
24. Bitter T, Khan I, Marriott T, Lovelady E, Verdonschot N, Janssen D. Finite element wear prediction using adaptive meshing at the modular taper interface of hip implants. *Journal of the mechanical behavior of biomedical materials*. 2018;77:616-623.
25. Bitter T, Khan I, Marriott T, Lovelady E, Verdonschot N, Janssen D. The effects of manufacturing tolerances and assembly force on the volumetric wear at the taper junction in modular total hip arthroplasty. *Computer Methods in Biomechanics and Biomedical Engineering*. 2019;22:1061-1072.
36. Brock TM, Sidaginamale R, Rushton S, Nargol AV, Bowsher JG, Savisaar C, Joyce TJ, Deehan DJ, Lord JK, Langton DJ. Shorter, rough trunnion surfaces are associated with higher taper wear rates than longer, smooth trunnion surfaces in a contemporary large head metal-on-metal total hip arthroplasty system. *Journal of orthopaedic research : official publication of the Orthopaedic Research Society*. 2015;33:1868-1874.
37. Brown SA, Flemming CA, Kawalec JS, Placko HE, Vassaux C, Merritt K, Payer JH, Kraay MJ. Fretting corrosion accelerates crevice corrosion of modular hip tapers. *Journal of Applied Biomaterials (New York)*. 1995;6:19-26.
43. Chaplin RPS, Lee AJC, Hooper RM. Assessment of wear on the cones of modular stainless steel Exeter hip stems. *Journal of Materials Science: Materials in Medicine*. 2004;15:977-990.
56. Cook RB, Bolland BJ, Wharton JA, Tilley S, Latham JM, Wood RJ. Pseudotumour formation due to tribocorrosion at the taper interface of large diameter metal on polymer modular total hip replacements. *The Journal of arthroplasty*. 2013;28:1430-1436.

67. Danoff JR, Longaray J, Rajaravivarma R, Gopalakrishnan A, Chen AF, Hozack WJ. Impaction Force Influences Taper-Trunnion Stability in Total Hip Arthroplasty. *Journal of Arthroplasty*. 2018;33:S270-S274.
78. Falkenberg A, Biller S, Morlock MM, Huber G. Micromotion at the head-stem taper junction of total hip prostheses is influenced by prosthesis design-, patient- and surgeon-related factors. *Journal of Biomechanics*. 2020;98.
80. Fallahnezhad K, Oskouei RH, Badnava H, Taylor M. An adaptive finite element simulation of fretting wear damage at the head neck taper junction of total hip replacement: The role of taper angle mismatch. *Journal of the mechanical behavior of biomedical materials*. 2017;75:58-67.
85. Gilbert JL, Buckley CA, Jacobs JJ. In vivo corrosion of modular hip prosthesis components in mixed and similar metal combinations. The effect of crevice, stress, motion, and alloy coupling. *Journal of biomedical materials research*. 1993;27:1533-1544.
94. Goldberg JR, Gilbert JL, Jacobs JJ, Bauer TW, Paprosky W, Leurgans S. A multicenter retrieval study of the taper interfaces of modular hip prostheses. *Clinical orthopaedics and related research*. 2002:149-161.
98. Hall DJ, Pourzal R, Lundberg HJ, Mathew MT, Jacobs JJ, Urban RM. Mechanical, chemical and biological damage modes within head-neck tapers of CoCrMo and Ti6Al4V contemporary hip replacements. *Journal of Biomedical Materials Research. Part B, Applied Biomaterials*. 2018;106:1672-1685.
105. Haschke H, Jauch-Matt SY, Sellenschloh K, Huber G, Morlock MM. Assembly force and taper angle difference influence the relative motion at the stem-neck interface of bi-modular hip prostheses. *Proceedings of the Institution of Mechanical Engineers, Part H: Journal of Engineering in Medicine*. 2016;230:690-699.
111. Higgs GB, MacDonald DW, Gilbert JL, Rimnac CM, Kurtz SM, Implant Research Center Writing C. Does Taper Size Have an Effect on Taper Damage in Retrieved Metal-on-Polyethylene Total Hip Devices? *The Journal of arthroplasty*. 2016;31:277-281.
116. Huet R, Sakona A, Kurtz SM. Strength and reliability of alumina ceramic femoral heads: Review of design, testing, and retrieval analysis. *Journal of the mechanical behavior of biomedical materials*. 2011;4:476-483.
120. Huot Carlson JC, Van Citters DW, Currier JH, Bryant AM, Mayor MB, Collier JP. Femoral stem fracture and in vivo corrosion of retrieved modular femoral hips. *The Journal of arthroplasty*. 2012;27:1389-1396.e1381.
125. Kao YYJ, Koch CN, Wright TM, Padgett DE. Flexural Rigidity, Taper Angle, and Contact Length Affect Fretting of the Femoral Stem Trunnion in Total Hip Arthroplasty. *Journal of Arthroplasty*. 2016;31:254-258.
131. Kocagoz SB, Underwood RJ, Sivan S, Gilbert JL, Macdonald DW, Day JS, Kurtz SM. Does Taper Angle Clearance Influence Fretting and Corrosion Damage at the Head-Stem Interface? A Matched Cohort Retrieval Study. *Semin Arthroplasty*. 2013;24:246-254.
143. Kurtz SM, Kocagoz SB, Hanzlik JA, Underwood RJ, Gilbert JL, MacDonald DW, Lee GC, Mont MA, Kraay MJ, Klein GR, Parvizi J, Rimnac CM. Do ceramic femoral heads reduce taper fretting corrosion in hip arthroplasty? A retrieval study. *Clinical orthopaedics and related research*. 2013;471:3270-3282.
152. Langton DJ, Sidaginamale R, Lord JK, Nargol AV, Joyce TJ. Taper junction failure in large-diameter metal-on-metal bearings. *Bone & joint research*. 2012;1:56-63.
159. Lieberman JR, Rimnac CM, Garvin KL, Klein RW, Salvati EA. An analysis of the head-neck taper interface in retrieved hip prostheses. *Clinical orthopaedics and related research*. 1994:162-167.


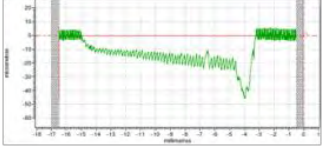

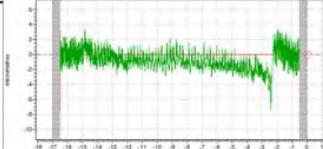

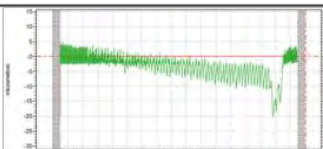

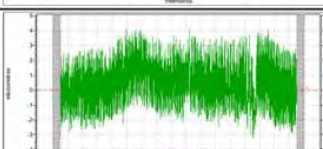
165. Mali SA, Gilbert JL. Correlating fretting corrosion and micromotions in modular tapers: Test method development and assessment. In: *ASTM Special Technical Publication*. 2015:259-282.
167. Martin AJ, McGrory BJ, Edidin AA, Van Citters DW. Using coordinate measuring machine validated with white light interferometry to identify contributors to material loss due to corrosion of total hip replacement modular junctions. In: *ASTM Special Technical Publication*. 2018:118-130.
173. Matthies AK, Racasan R, Bills P, Blunt L, Cro S, Panagiotidou A, Blunn G, Skinner J, Hart AJ. Material loss at the taper junction of retrieved large head metal-on-metal total hip replacements. *Journal of orthopaedic research : official publication of the Orthopaedic Research Society*. 2013;31:1677-1685.
175. Medel FJ, Shah P, Kurtz SM. Retrieval Analysis of Contemporary Alternative Femoral Head Materials: Oxinium and Biolox Delta. In: *Orthopedic Research Society*. 2009.
183. Morlock MM, Dickinson EC, Günther KP, Bünte D, Polster V. Head Taper Corrosion Causing Head Bottoming Out and Consecutive Gross Stem Taper Failure in Total Hip Arthroplasty. *Journal of Arthroplasty*. 2018;33:3581-3590.
184. Nassif NA, Nawabi DH, Stoner K, Elpers M, Wright T, Padgett DE. Taper Design Affects Failure of Large-head Metal-on-metal Total Hip Replacements. *Clinical orthopaedics and related research*. 2013.
185. Nassif NA, Nawabi DH, Stoner K, Elpers M, Wright T, Padgett DE. Taper design affects failure of large-head metal-on-metal total hip replacements. *Clinical orthopaedics and related research*. 2014;472:564-571.
191. Ouellette ES, Mali SA, Kim J, Grostefon J, Gilbert JL. Design, Material, and Seating Load Effects on In Vitro Fretting Corrosion Performance of Modular Head-Neck Tapers. *The Journal of arthroplasty*. 2019;34:991-1002.
193. Panagiotidou A, Cobb T, Meswania J, Skinner J, Hart A, Haddad F, Blunn G. Effect of impact assembly on the interface deformation and fretting corrosion of modular hip tapers: An in vitro study. *Journal of Orthopaedic Research*. 2018;36:405-416.
194. Panagiotidou A, Meswania J, Hua J, Muirhead-Allwood S, Hart A, Blunn G. Enhanced wear and corrosion in modular tapers in total hip replacement is associated with the contact area and surface topography. *Journal of orthopaedic research : official publication of the Orthopaedic Research Society*. 2013;31:2032-2039.
202. Porter DA, Urban RM, Jacobs JJ, Gilbert JL, Rodriguez JA, Cooper HJ. Modern trunnions are more flexible: a mechanical analysis of THA taper designs. *Clinical orthopaedics and related research*. 2014;472:3963-3970.
206. Pruitt LA, Chakravartula AM. *Mechanics of Biomaterials: Fundamental Principles for Implant Design*. Cambridge University Press; 2011.
217. Siljander MP, Gehrke CK, Wheeler SD, Sobh AH, Moore DD, Flierl MA, Baker EA. Does Taper Design Affect Taper Fretting Corrosion in Ceramic-on-Polyethylene Total Hip Arthroplasty? A Retrieval Analysis. *Journal of Arthroplasty*. 2019;34:S366-S372.e362.
229. Tan SC, Teeter MG, Del Balso C, Howard JL, Lanting BA. Effect of Taper Design on Trunnionosis in Metal on Polyethylene Total Hip Arthroplasty. *The Journal of arthroplasty*. 2015;30:1269-1272.
232. Thomas TR. *Rough Surfaces*: Imperial College Press; 1999.
238. Urban RM, Gilbert JL, Jacobs JJ. Corrosion of modular titanium alloy stems in cementless hip replacement. *Journal of ASTM International*. 2005;2:357-366.

4 Volumetric Material Loss

4.1 Background and Significance

Visual damage scoring has been established as a useful method to rank the severity of fretting corrosion in an available group of retrievals [94] and we have, along with the rest of the scientific community, used a modified method (Table VI) to evaluate retrievals [131, 143]. However, this method is not always sufficient to assess fretting-corrosion damage, particularly in components that have severe corrosion, and the volume of material loss shows high variability (Figure 48). In our studies, we have shown that there is a correlation between visual fretting-corrosion scores and volumetric material loss; however, accumulated debris may be misleading in representing the severity of corrosion in components with moderate (3) and severe (4) visual fretting corrosion scores [129]. Using surface profilometry (Talyrond 585, Taylor Hobson, UK) to take measurements inside tapers we have shown that there is a significant difference between the depth and volume of material loss between components with the same visual fretting-corrosion score (Table VI and Figure 48). Therefore, it is necessary in some cases, especially those with moderate and severe visual scores, to quantify material loss by direct measurements.

Table VI: Comparison of visual appearance and score of femoral heads with a single selected axial trace measured from the inside of that femoral head taper and the estimated wear parameters calculated using the axial traces.

Score	Visual Appearance	Example Axial Trace	Estimated wear parameter
4			Max Depth: 52.2 μ m Ave. Depth: 17.2 μ m Volume: 8.1mm ³
4			Max Depth: 12.2 μ m Ave. Depth: 0.3 μ m Volume: 0.1mm ³
3			Max Depth: 51.2 μ m Ave. Depth: 5.9 μ m Volume: 3.3mm ³
3			Max Depth: 0 μ m Ave. Depth: 0 μ m Volume: 0 mm ³

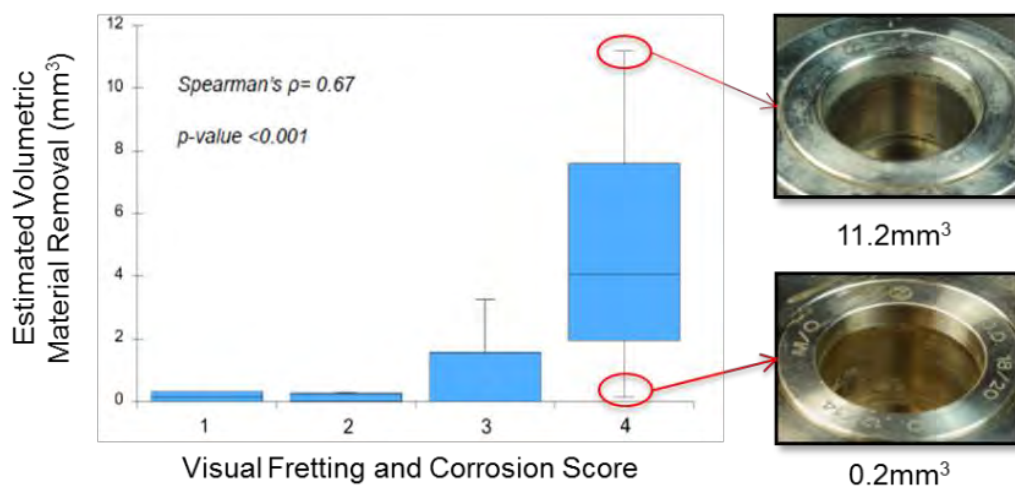


Figure 48: There is a large variability in the range of estimated volumetric material loss in components with severe (4) visual fretting-corrosion scores.

There are numerous retrieval studies that have investigated corrosion at modular connections over the past decades using the established visual fretting scoring qualitative techniques or quantitative methods to evaluate the severity of MACC. Other researchers have also demonstrated the correlation between visual fretting corrosion scoring and quantitative methods by measuring from vertical straightness profiles using a profilometer [41]. The material loss resulting from taper corrosion has been estimated in large head MoM hip bearings [152, 173] due to their higher clinical risk of revision as established; however, there are significantly fewer studies that estimate the volume of material loss from ceramic-on-polyethylene (CoP), ceramic-on-ceramic (CoC), or MoP bearings. The relevant studies are discussed in detail in the systematic review in section 1.4.3 of this document. The visual or quantitative evaluation techniques have been used to investigate the material and design factors of femoral heads and stems that affect the severity of corrosion show that there are no metallic biomaterials or modular interface designs by any manufacturer that are currently immune to fretting corrosion in the modular junctions. MACC is prevalent in MoM and non-LHMoM systems as well as in single or dual modularity systems and may lead to revision even in MoP hip replacements.

The effect of the device factors that were evaluated in the articles that met the selection criteria relevant to our study are summarized in Table III of section 1.4.3. Table III shows that there is consensus on the effect of some device factors such as flexural rigidity, implantation time, taper fit and taper type on the severity of MACC, the effect of other device factors such as head material are not clear. Most of these articles in the review used visual methods of examining fretting corrosion and used the semi-qualitative

visual scoring method in correlating the device factors and severity of corrosion. There is still a need to evaluate device factors in non-LHMoM systems using quantitative methods. In the literature, there are only 5 other articles that looked at quantitative material loss from the head-stem interface of retrievals from non-LHMoM bearing systems. One of them only measured stems and the other used a non-contact replicator method and used roundness machine measurements as verification [30, 242]. The third study used a CMM and looked at the material loss from a single design and calculated material loss up to 20.8mm^3 [183]. Two studies used a roundness machine to take vertical axial traces around the taper surfaces; however, one of the studies only measured the most severe components [41] and the other study looked at THA with a dual modular stem, but, only quantified the material loss from the head-stem surface even though they reported severe corrosion also at the stem-neck modular interface [73]. There is a need for practical quantitative method for the evaluation of material loss from taper surfaces and a study that quantitatively evaluates the effect of head material while controlling for other confounding factors.

We previously studied a matched cohort of 50 ceramic and 50 metal head-stem pairs, also mentioned in Chapters 2 and 3, using visual fretting and corrosion damage scores [143]. The cohorts were matched according to (1) implantation time; (2) stem flexural rigidity; and (3) lateral offset. We sought to use the quantitative volumetric material loss method in the same 50-50 cohort and address the following research questions: (1) Do ceramic heads result in less volume of material loss at the head-stem junction compared with CoCr heads; (2) do stem cone tapers have less volumetric material loss compared to CoCr head bore tapers; (3) do visual fretting-corrosion scores

correlate with volumetric material loss; and (4) are device, patient, or intraoperative factors associated with volumetric material loss?

4.2 Experimental Methods

4.2.1 Study Design

The 50 ceramic and 50 CoCr cohorts were matched according to (1) implantation time; (2) stem flexural rigidity; and (3) lateral offset. The flexural rigidity of each stem is calculated by multiplying the elastic modulus (E) of the stem material and second moment of area (I). The moment of area $I = \frac{\pi}{4} r^2$ was determined using the radius of the stem cone taper (r) at the distal end where the trunnion exits the bore. The stem materials for the ceramic cohort are: CoCr alloy (n = 6, E = 220 GPa); Ti-6Al-4V alloy (n = 16, E = 110 GPa); and TMZF alloy (n = 28, E = 79.5 GPa). The stem materials for the CoCr cohort are: CoCr alloy (n = 8, E = 220 GPa); Ti-6Al-4V alloy (n = 17, E = 110 GPa); and TMZF alloy (n = 25, E = 79.5 GPa). The ceramic and CoCr cohorts had similar head diameters (median = 32 mm, mean = 33 mm for both cohorts, p = 0.65, Mann-Whitney U. Ceramic cohort range = 28-36 mm, CoCr cohort range = 22-40 mm). On average, the patients in the ceramic cohort were 5 years younger than the CoCr cohort. The ceramic cohort included both CoP (n = 41) and CoC bearings (n = 9), while the CoCr cohort included only MoP (n = 50) bearings. This study did not include components with large head MoM bearings or modular femoral stems or necks. The reasons for revision included loosening (ceramic cohort, n = 28; CoCr cohort, n = 22), infection (ceramic cohort, n = 13; CoCr cohort, n = 20), periprosthetic fracture (ceramic cohort, n = 1; CoCr cohort, n = 3), component fracture (CoCr cohort, n = 1) and pain (ceramic cohort, n = 2; CoCr

cohort, n= 1). No components were reported to have a revision reason involving pseudotumor formation or metallosis (Table XIII and XIV in the Appendix details all device and clinical information for the cohorts).

4.2.2 Estimation of Material Loss From Head Bore Tapers

The taper surface was measured using a roundness machine (Talyrond 585, Taylor Hobson, UK) equipped with a diamond stylus. The axis of the taper was aligned with the axis of rotation of the Talyrond rotation using the automatic centering and leveling routine. A total of 24 equally spaced axial profiles were measured on the surface of each head taper. The profiles were analyzed, and the volume of material loss was estimated using a customized Matlab script (see Appendix for full script). The volumetric material loss was estimated from the following steps: (1) the user identified regions of “as-manufactured” surface on each profile (detailed methodology of identifying as-manufactured surfaces has been described in Chapter 3); (2) a least squares line was fitted through “as-manufactured” regions to establish the presumed as-manufactured surface profile in the areas of material loss; (3) integrated areas of material loss are calculated using the spacing between each measured data point and the distance between the measured surface and the estimated as-manufactured surface (4) area of material loss is used to calculate the volume of a partial annulus based on the taper local radius and spacing to the next axial profile; and (5) all partial annuli were summed to estimate the volume of material loss in the taper (Figure 49) (also shown in Table VII).

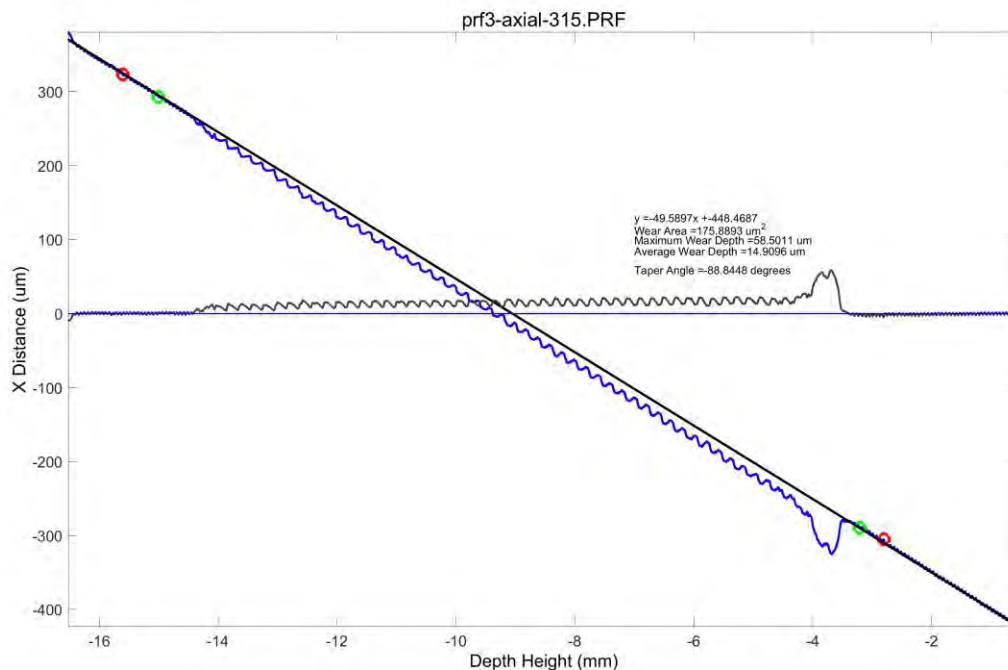


Figure 49: Example of an imported axial trace and analysis in custom MATLAB R2016a. The user is prompted to select limits on the proximal and distal ends to select region to exclude during least squares fitting to identified as-manufactured surfaces.

Table VII: Method to quantify volumetric material loss from retrieval female taper surfaces with fretting-corrosion damage using in-vitro simulated surfaces for method validation.

Step	Method	Figures
Visual Fretting-Corrosion Scoring	Visual scoring method developed by Goldberg et al. [94] or modified methods [109] are used in the literature to evaluate fretting-corrosion severity on taper surfaces using a scale of 1 to 4, with 1 being the least severe and 4 being the most severe.	

Table VII (continued):

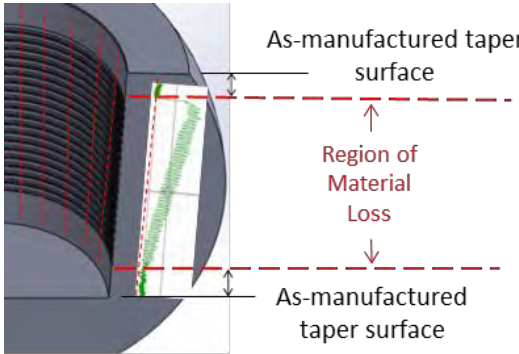
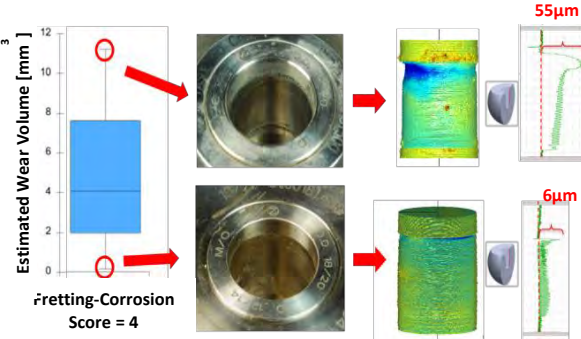

<p>Identifying Patterns of Material Loss</p>	<p>Surface profile measurements (red dotted lines) of retrieval taper surfaces are a quantitative representation of surface damage. They also show that as-manufactured surfaces are present in retrievals which can be used to estimate the entire as-manufactured surface through mathematical fitting.</p>	
<p>Comparing visual scores and surface profiles</p>	<p>Retrievals with a visual score of 4 have wide range of volumetric loss and depth of material loss in their surface profiles. Visual scoring is semi-quantitative and has limitations in estimating the severity of fretting-corrosion damage. Surface profiles are quantitative representations of fretting-corrosion damage and material loss.</p>	
<p>Method Development – Simulating Material Loss in Vitro</p>	<p>A quantitative method to estimate the severity of material loss in vitro was developed using surface profiles. Never implanted taper adapter sleeves and CoCr femoral heads were machined to simulate the same patterns and depth of material loss seen in retrievals.</p>	

Table VII (continued):

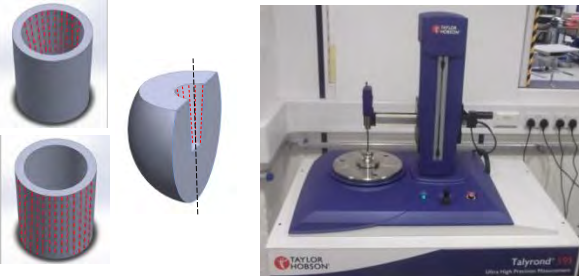
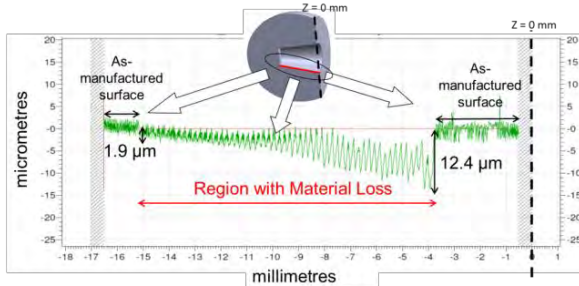
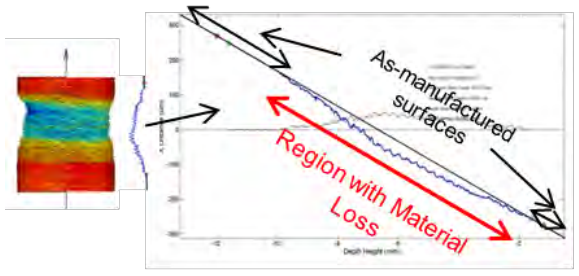
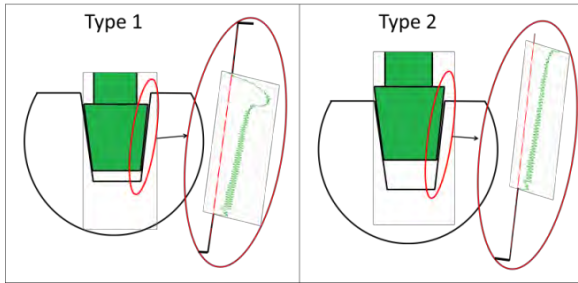
<p>Measuring Simulated Surfaces</p>	<p>Taper surfaces with simulated material loss were measured using a roundness machine (Talyrond 585, Taylor Hobson, UK) equipped with a diamond stylus. 24 equally spaced axial profiles (red dotted lines) were measured around each taper surface.</p>	
<p>Identifying regions of as-manufactured surfaces</p>	<p>A trained user identified regions of “as-manufactured” surface on each profile.</p>	
<p>Estimating as-manufactured surfaces with LS linear fitting</p>	<p>Measured profiles were imported into Matlab. A custom script was used with the in-built <i>polyfit</i> function for least squares (LS) linear fitting. Only user specified regions of as-manufactured surfaces were used for fitting. The fitted line is the reference, estimated as-manufactured surface for volumetric material loss calculation.</p>	

Table VII (continued):

<p>Estimating Volumetric Material Loss</p>	<p>The LS fit was established as the estimated as-manufactured surface (1). Integral rectangular areas of material loss were calculated using the spacing between each data point and the distance between the measured surface and the estimated as-manufactured surface (2). Each rectangle is used to calculate the volume of a partial annulus based on the taper local radius, known from axis alignment before profile measurements (3). All partial annuli were summed to estimate the volume of material loss in the taper (4).</p>	
<p>Validating Method</p>	<p>There was a high correlation between estimated volumetric material loss calculated using the Matlab script and the gravimetric measurements of volumetric material removal ($R^2 > 99.5\%$, Slope = 1.0149).</p>	

Table VII (continued):

<p>Comparing Type 1 and Type 2 patterns</p>	<p>Volumetric material loss values calculated for Type 2 heads had higher uncertainty using this method because as-manufactured surfaces were available on only one side of taper for Type 2. The correlation between gravimetric measurements and Type 2 analyses is lower compared to Type 1 ($R^2 = 94.3\%$, Slope = 0.94).</p>	 <p>The diagram illustrates two types of taper adapter sleeves. Type 1 shows a sleeve with a green stem and a red dashed line indicating a full 360-degree scan path. Type 2 shows a sleeve with a green stem and a red dashed line indicating a scan path limited to one side of the taper.</p>
---	---	--

4.2.3 Gravimetric validation of volumetric material loss method

We validated the estimation of material loss method using a gravimetric technique. We acquired 10 exemplar taper adapter sleeves (made of Ti alloy) with microgrooved outer surfaces to simulate stem surfaces and smooth female taper surfaces. We also acquired 3 V40 femoral heads to represent CoCr material for this validation study (Figure 50).

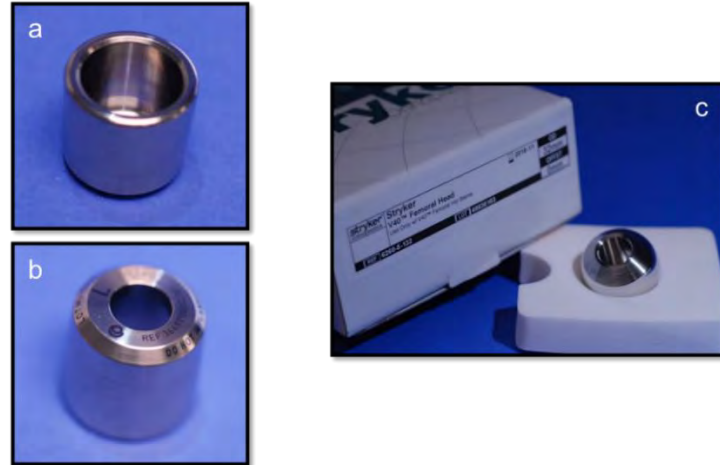


Figure 50: Exemplar taper adapter sleeves and femoral heads used for gravimetric validation.

We inspected the results from the measured metal retrieval cohort and found the range of depth of material loss and commonly observed patterns in retrieval tapers. Figure 51 shows a representative cylinder map of one of the retrieval tapers with the most severe material loss. Based on retrieval results, the target for simulating material loss was to create samples with a material loss depth in the range of 15-65 μm . Also, we decided to simulate axisymmetric material loss as well as asymmetrical material loss. None of the retrieval material loss patterns in this study showed asymmetrical material loss; however, this pattern has been reported in the literature [22] where they also report maximum depths of material loss of 65 μm . Even though we did not observe asymmetrical material loss, it is relevant to this study because it is believed to be caused due to toggling.

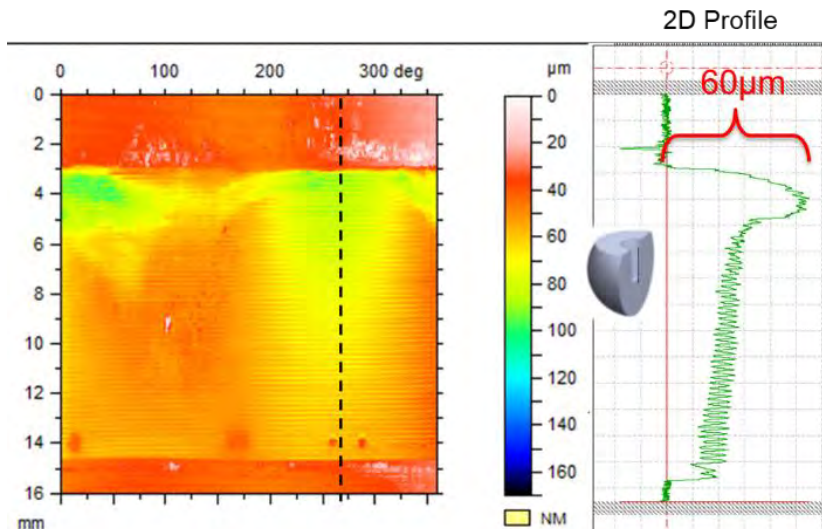


Figure 51: Example cylinder map of one of the most severe cases of material loss among the retrieval tapers.

The exemplars were weighed, then placed in a protective fixture on the lathe to rotate samples at a controlled speed to achieve the axisymmetric material removal pattern using a Dremel bit as shown in Figure 52. Example surface maps of the induced material removal for the low and high quantities are shown in Figure 53. The desired range of depth of material loss consistent with retrievals (Figure 51) was achieved using the lathe and Dremel setup shown. Material loss was induced on the both the internal and external surfaces to ensure there was not a bias created due to measurement direction on the Talyrond. Asymmetric material loss was induced in some taper adapter sleeves to represent possible toggling damage reported in retrieval studies[152]. The taper adapter sleeves and exemplar heads with induced material loss were weighed a second time to determine the gravimetric material loss. They were also measured and analyzed for volumetric material loss using the previously described method in section 4.2.2 and Table VII, except instead of 24 traces, 144 traces were measured on each sample (one profile

every 2.5°). Analytical calculated volumetric material removal is plotted against gravimetric material removal and the linear fit is $R^2=0.9965$. There is very good agreement between the analytical method and the gravimetric validation for the values of volumetric material loss (Figure 55). There are some limitations about the analytical calculation of volumetric material loss which are described in depth in the discussion section of this chapter.

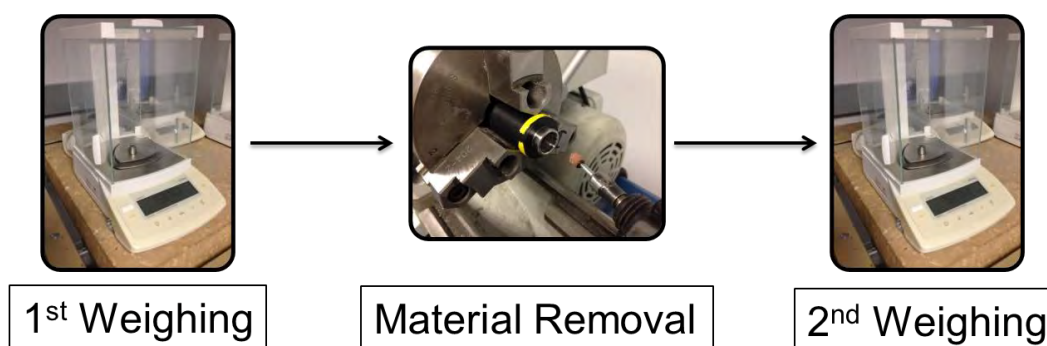


Figure 52: Summary of gravimetric material removal using a lathe and Dremel.

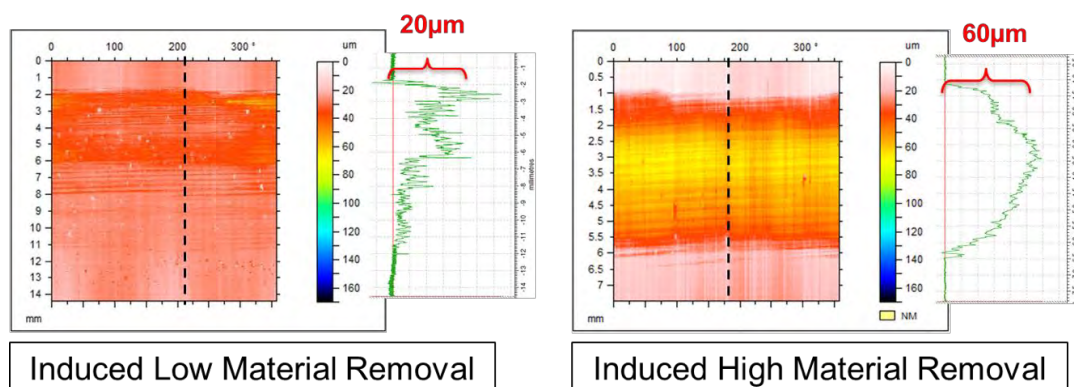


Figure 53: In vitro material removal using lathe and Dremel setup to simulate axisymmetric material loss. The low amount of depth of material loss (20 μm) and the high amount of depth of material loss (60 μm) are within the range of in vivo material loss observed in the retrieval cohorts also evaluated earlier in Chapter 4.

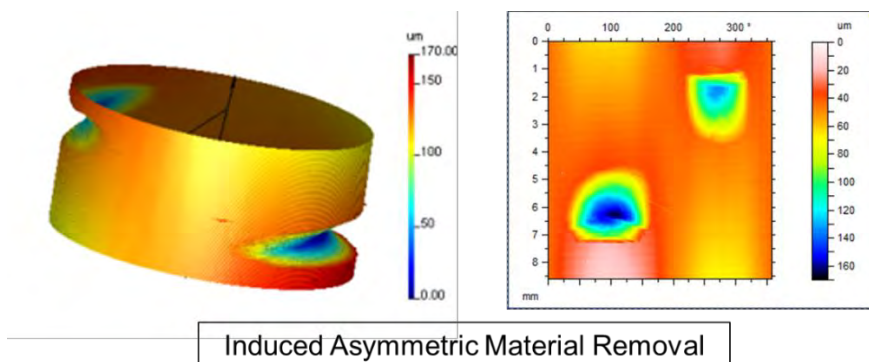


Figure 54: In vitro material removal using lathe and Dremel setup simulating asymmetric material loss. Asymmetric material loss is speculated to occur due to toggling.

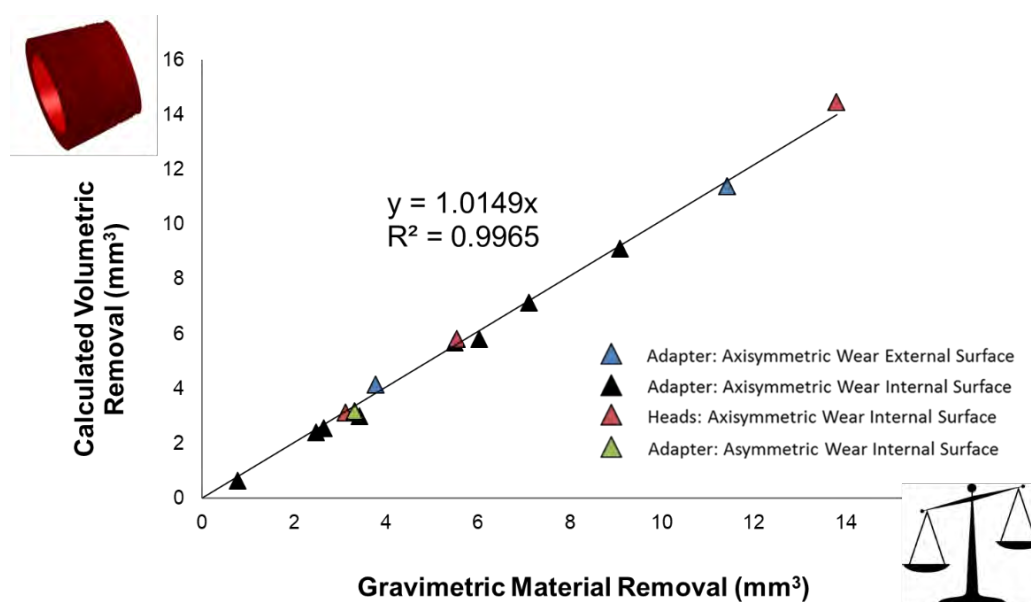


Figure 55: Linear fitting calculated volumetric removal data using our previously described method with a customized Matlab script and the gravimetric material removal measurement. There is very good fit (>95%) between the two sets of data showing >99% reliability of the volumetric removal estimation method.

Finally, we conducted a sensitivity analysis using the 144 measured traces for each taper surface with induced material removal. We used a subset of the number of traces to understand the minimum number of traces that needed to be measured for an accurate measurement of volumetric material loss. We calculated material loss using 2, 8, 12, 20, 24, 36, 48, 72 and 144 axial profiles around the taper. This sensitivity analysis showed that 24 profiles are within 1% error of 144 profiles. 24 profiles are an acceptable number of profiles for tapers showing axisymmetric material loss with as-manufactured surfaces on either side available for fitting. 24 profiles also save a significant amount of time and takes less than $\frac{1}{2}$ hour compared to 144 traces taking $2\frac{1}{2}$ hours to measure (Figure 56).

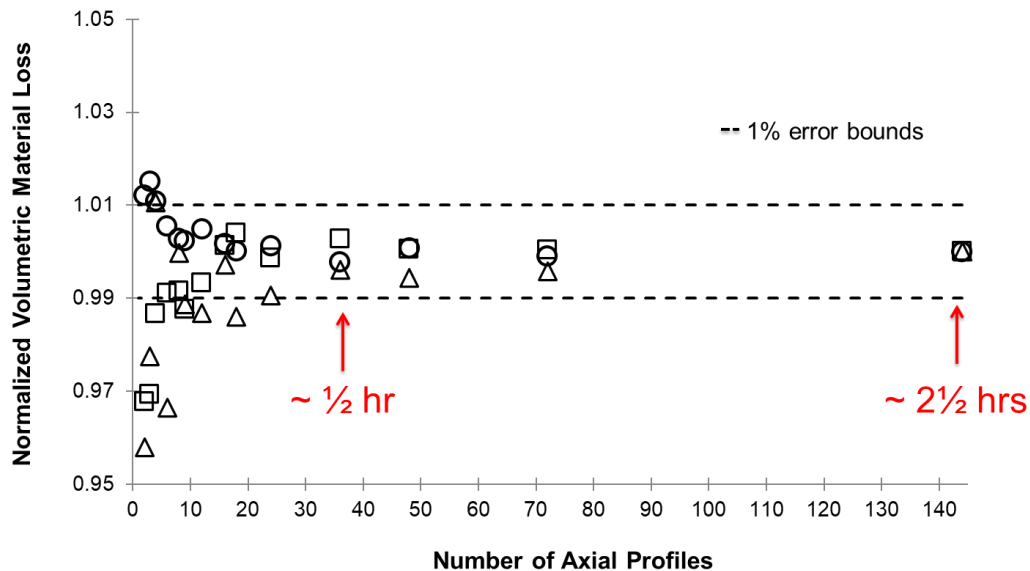


Figure 56: Sensitivity analysis comparing number of axial profiles and normalized volumetric material loss. With this analysis we were looking for the minimum number of profiles needed to stay within 1% accuracy of 144 profile measurements and 24 profiles meets this requirement and saves >2 hrs in measurement time.

4.2.3 Estimation of Material Loss from Stem Cone Tapers

To estimate the volume of material loss from the stem cone taper, the method used to estimate the material loss from head bore tapers was modified due to the presence of “microgrooves.” In this study, stem cone tapers that had a surface topography with a periodic pattern, a wavelength $>100\ \mu\text{m}$, and an amplitude $>4\ \mu\text{m}$ were considered “microgrooved,” as described in another study [4, 90]. For stem cone tapers that did not meet these criteria, they were considered “smooth” or “non-microgrooved.” For microgrooved surface topography, it is not possible for a least squares straight line to represent the as-manufactured surface because the uncertainties introduced by this approximation may be larger than the volume of material loss. Furthermore, our experience has shown that some regions of microgrooves on stem cone tapers may have plastic deformation but no material loss or regions of iatrogenic damage, which need to be excluded from the estimation of material loss. Preliminary observations of stem cone tapers under optical microscopy also showed that in vivo material loss was seen in isolated regions (Table VIII), unlike head bore tapers in which material loss may be seen in larger regions in contact with the stem. As a result of the difference observed in the patterns of material loss between head bore tapers and stem cone tapers, our previously described method for estimation of material loss method was modified for stem cone tapers.

A roundness machine (Talyrond 585, Taylor Hobson, UK) equipped with a diamond stylus, was used to measure 360 equally spaced axial profiles on each stem cone taper to capture damage in each isolated region. Initially, the surface of the five stem cone tapers with highest damage was inspected using a scanning electron microscope (SEM; Zeiss Supra 50VP; Oberkochen, Germany) and optical microscopy (Keyence;

Osaka, Japan) in conjunction with the inspection of the measured profiles and surface maps (TalyMap, Taylor Hobson, Leicester, UK). This allowed the differentiation between fretting-corrosion damage and material loss, iatrogenic damage and material loss, and as-manufactured regions. Material loss resulting from iatrogenic damage was excluded during estimation of volumetric material loss (Table VIII).

Table VIII: Method to quantify volumetric material loss from retrieval male taper surfaces with fretting-corrosion damage.


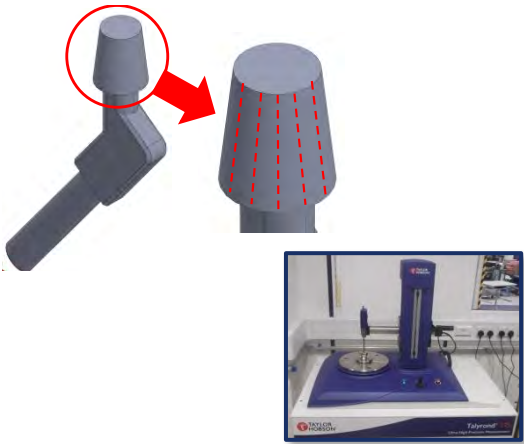
Step	Method	Figures
Identifying regions with iatrogenic damage	Male tapers have risk of getting iatrogenic damage during removal surgery (regions in white boxes). Iatrogenic damage needs to be identified and eliminated from material loss calculation.	
Measuring retrieval tapers	Tapers were measured using a roundness machine (Talyrond 585, Taylor Hobson, UK) equipped with a diamond stylus. 360 equally spaced axial profiles (red dotted lines) were measured around each taper surface to form a surface map and capture isolated regions of in vivo material loss.	

Table VIII (continued):

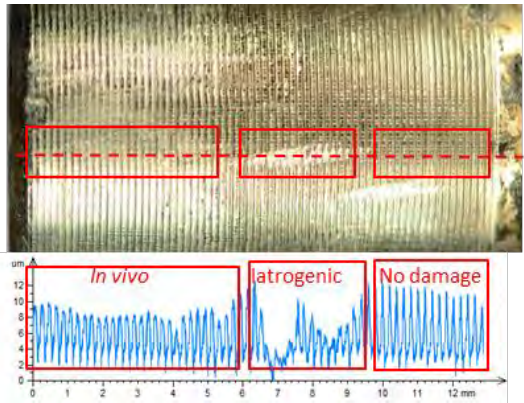
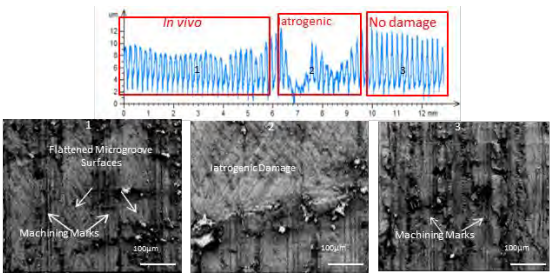
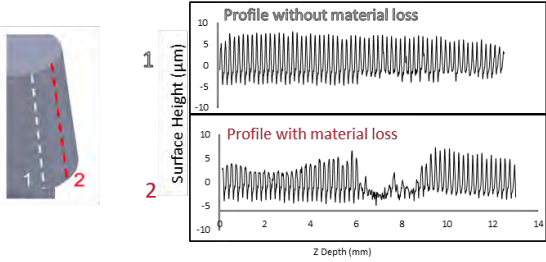
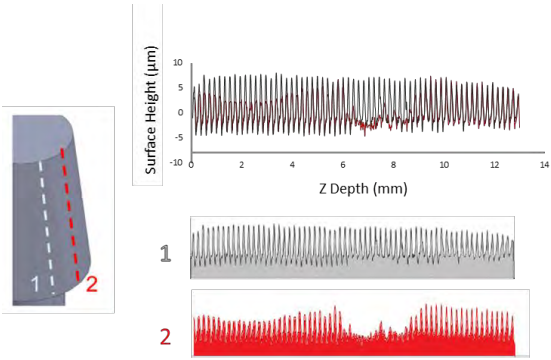
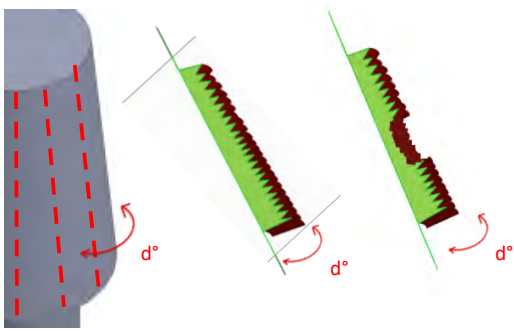
<p>Matching observations with optical microscopy with regions on measured profiles</p>	<p>Surface mapping using 360 profiles detected the changes in the surface morphology in isolated regions for material loss estimation. Each profile is inspected for regions of material loss. Optical microscopy is used to eliminate regions that have iatrogenic damage from the material loss analysis.</p>	
<p>SEM imaging identified regions with damage</p>	<p>SEM imaging was used to cross-check the mode of damage identified using optical microscopy and measured profiles. The location and appearances of features for in vivo and iatrogenic damage seen in the SEM were matched with features seen in the optical microscope, the latter which was used for subsequent inspections.</p>	
<p>Identify regions without material loss</p>	<p>Profiles without material loss on the same stem taper, or regions without loss, is the most accurate way to calculate volumetric material loss on male tapers. The circumferential overlay allows for alignment of peaks and valleys for identification of regions with material loss.</p>	

Table VIII (continued):

<p>Calculation of area of material loss</p>	<p>The area under the curve of each radial profile depends on the smooth or grooved topography of the stem cone. Equal depth of surface height <math> < 100 \mu\text{m}</math> is used to capture changes in surface topography and material loss between profiles with damage and no damage. Material loss resulting from iatrogenic damage was excluded during estimation of volumetric material loss.</p>	 <p>The figure illustrates the method for calculating the area of material loss. On the left, a 3D diagram shows a stem cone with two radial profiles, labeled 1 and 2, indicated by dashed red lines. Profile 1 is smooth, while profile 2 shows surface damage. To the right, a graph plots Surface Height (μm) on the y-axis (ranging from -10 to 10) against Z Depth (mm) on the x-axis (ranging from 0 to 14). The main graph shows a noisy signal with a red dashed line representing the mean surface height. Below it, two smaller graphs, labeled 1 and 2, show the surface height profiles for the smooth and damaged areas, respectively, with profile 2 showing significantly lower surface heights.</p>
<p>Calculation of volumetric material loss</p>	<p>The difference between the volume enclosed by the profiles projected over a 1° partial annulus with no material loss and profiles with fretting-corrosion spanning equal radial slices was used to calculate total volumetric material loss from stem cone tapers. This difference is multiplied by the number of degrees (d) the type of deformation is observed in profiles and optical microscopy.</p>	 <p>The figure shows a 3D diagram of a stem cone taper. On the left, a dashed red line indicates a radial slice. To the right, two green 3D models of the taper are shown, each with a red dashed line representing a radial slice. The angle of the taper is labeled as d° with a red arrow.</p>

4.3 Results

In this study, the cumulative volumetric materials loss from ceramic taper junctions was significantly less than CoCr taper junctions (mean difference = 0.3mm^3 ; $p < 0.001$; Figure 57). Specifically, the cumulative volumetric material loss estimated for the ceramic cohort had a median of $0.0\text{mm}^3/\text{year}$ (range $0.0 - 0.4\text{mm}^3$) and the CoCr cohort had a median of $0.1\text{mm}^3/\text{year}$ (range $0.0-9\text{mm}^3$). This result was similar when Type 1 and Type 2 patterns were analyzed separately. For the CoCr cohort, 44/50 (88%) femoral heads had Type 1 pattern of material loss and the remaining 6/50 CoCr heads had a Type 2 pattern. Head-stem pairs with Type 1 pattern had median material loss 0.07mm^3 (range 0.0 to $0.91\text{mm}^3/\text{year}$). We did not observe evidence of fretting-corrosion or material loss for the ceramic head bore tapers, but we did observe metallic material transfer or oxide corrosion debris on the head bore taper surface (Figure 58). There was no detectable material gain in measured profiles of ceramic head bore tapers even in those that had visual evidence of metal transfer.

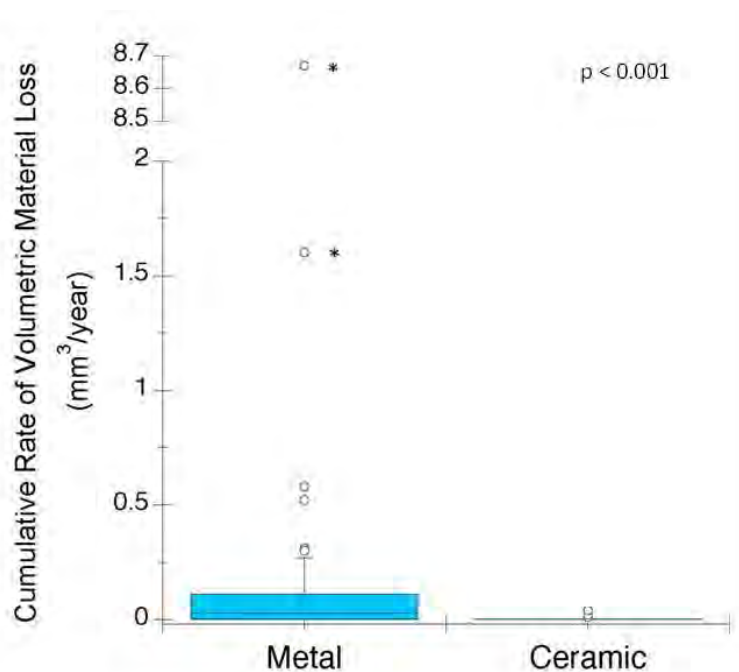


Figure 57: Box plots showing the rate of material loss from the metal and ceramic cohorts. The median and the maximum value seen for the CoCr cohort (median = 0.1 mm³, maximum = 9 mm³) are an order of magnitude greater compared to the ceramic cohort (median = 0.0 mm³, maximum = 0.4 mm³). Outliers with asterisks indicate a value taken from a Type 2 pattern of material loss.

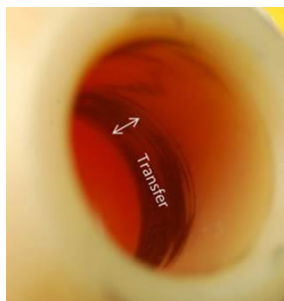


Figure 58: A region of metal transfer was observed on the proximal end of 42/50 of the ceramic tapers. For ceramic heads, the head bore taper and matching stem cone taper geometry is designed to have highest contact pressure at the proximal end.

For the CoCr cohort, most of the cumulative material loss at the taper junction occurred on the head bore taper (Figure 59, $p < 0.0001$). Specifically, the femoral head bore tapers had a median material loss of 0.02mm³ (range 0.0-8.7mm³/year) and the stem

cone tapers had a median material loss of 0.0mm^3 (range $0.0 - 0.32\text{mm}^3/\text{year}$). Most of the material loss in CoCr cohorts is from the femoral heads (over 90%) as opposed to the stem tapers ($p < 0.001$; Table IX). Moreover, the estimated volumetric material loss rate was higher in CoCr head bore tapers compared with the stem cone tapers (mean difference = 0.26mm^3). Inspection of the linear traces of the stem cone tapers revealed depths of material loss (range = $0 - 20 \mu\text{m}$) similar to the head bore tapers (range = $0 - 35 \mu\text{m}$). However, the fretting-corrosion damage was restricted to small, isolated areas on the stem cone tapers, resulting in less material loss. The outlier stem value in Table IX with 2.5mm^3 of material loss had extensive intergranular corrosion and grain pullout. The depth of material loss for that stem from the Talyrond profiles was greater compared to other stems ($> 100 \mu\text{m}$). The implantation time for this component was 9 years and the rate of volumetric material loss was approximately $0.27 \text{mm}^3/\text{year}$.

Table IX: Estimated total volumetric material loss and rate of volumetric material loss for CoCr and ceramic cohorts.

Metric for Material Loss	CoCr Cohort Heads (n=50)		CoCr Cohort Stems (n=50)		Ceramic Cohort Heads (n=50)		Ceramic Cohort Stems (n = 50)	
	Volume (mm^3)	Rate (mm^3/year)	Volume (mm^3)	Rate (mm^3/year)	Volume (mm^3)	Rate (mm^3/year)	Volume (mm^3)	Rate (mm^3/year)
Median	0.04	0.02	0.00	0.00	0.00	0.00	0.00	0.00
Range	0 - 4.34	0 - 8.67	0 - 2.5	0 - 0.32	0 - 0.03	0 - 0.04	0 - 0.74	0 - 0.37

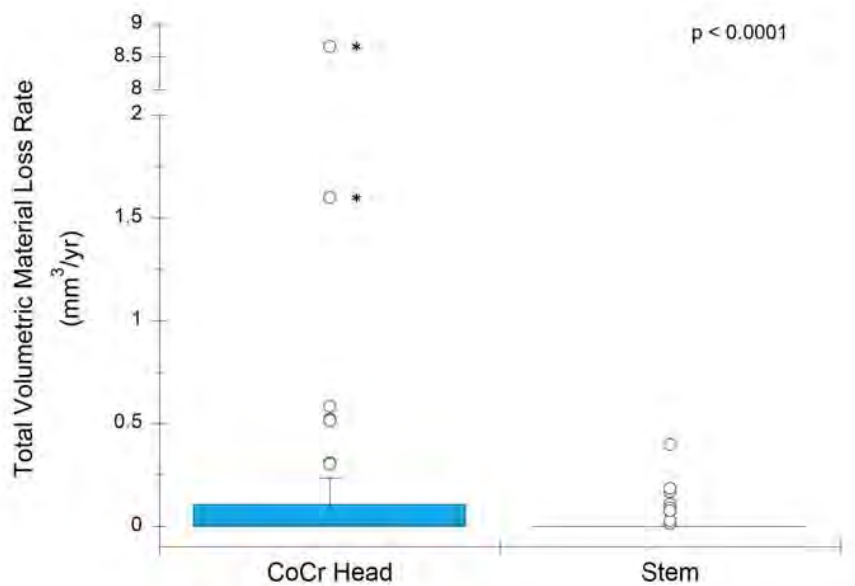


Figure 59: The box plots for rate of material loss at CoCr head bore and stem cone tapers show a difference between head and stem surfaces. Outliers with asterisks indicate a value taken from a Type 2 pattern of material loss.

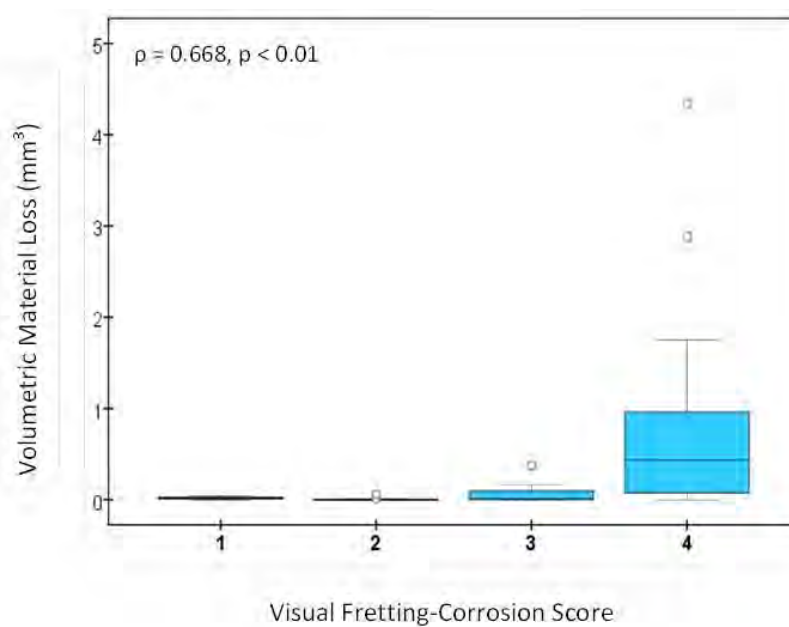


Figure 60: Correlation between visual fretting corrosion score and estimated volumetric material loss in the CoCr cohort.

There was a positive correlation between visual scoring and volumetric material loss (Spearman's $\rho = 0.668$, $p < 0.01$; Figure 60). CoCr head bore tapers that were scored with a 4 had the highest range of volumetric material loss (0–4.34 mm³, $n = 21$) followed by head bore tapers with a score of 3 (0–0.37 mm³, $n = 12$). CoCr head bore tapers scored 1 and 2 had the lower volumetric loss with a range of 0 to 0.04 mm³ ($n = 4$) and 0 to 0.06 mm³ ($n = 13$), respectively. We did not observe any correlations between cumulative volumetric material loss and the available device factors including taper angle clearance ($\rho = 0.06$, $p = 0.70$), head size ($\rho = 0.05$, $p = 0.72$), head offset ($\rho = 0.15$, $p = 0.29$), lateral offset ($\rho = 0.15$, $p = 0.29$), stem taper material (Ti6Al4V, TMZF, CoCrMo Alloys) ($p = 0.71$), and stem surface finish ($p = 0.2$). With the numbers available, we did not observe any correlations between the rate of cumulative material loss and patient factors including implantation time ($\rho = 0.19$, $p = 0.18$), patient age at implantation ($\rho = -0.06$, $p = 0.35$), activity levels ($\rho = 0.15$, $p = 0.16$), and BMI ($\rho = 0.23$, $p = 0.07$) (Table X).

Table X: List of correlation between cumulative rate of volumetric material loss from head-stem CoCr cohort and device and patient factors.

Device Factors	Spearman's Correlation (ρ)	p-value (significant if <0.05)
Taper Angle Clearance* [131]	0.06	0.70
Absolute Taper Angle Clearance* [131]	0.20	0.16
Head Size	0.05	0.72
Head Offset	0.15	0.29
Lateral Offset	0.26	0.07
Stem Taper Material	Kruskal-Wallis	0.71
Stem Taper Surface Finish	Mann Whitney U	0.20
Patient Factors	Spearman's Correlation (ρ)	p-value (significant if <0.05)
Implantation Time	0.19	0.18
Patient Age at Implantation	-0.06	0.35
BMI	0.23	0.07
UCLA Activity Score	0.15	0.16
Gender	Mann Whitney U	0.06

*the absolute value of previously estimated taper angle clearance for head-stem junctions, looking at the effect of the net gap on material loss [131]

4.4 Discussion

Fretting-corrosion has been observed in retrieval femoral head-stem junctions since the introduction of modularity in hip joint arthroplasty; however, with the introduction of large head MoM implants there has been more interest in this phenomenon [22, 152, 173, 179, 235] and implants with dual modularity. MoP bearings remain the historical gold standard in THA due to these clinical concerns with large head MoM and dual-modular designs. Additionally, increased fracture resistance of latest generation ceramic bearings (CoP and CoC) has led to recent wide-spread adoption, with over 40% use in THAs in the United States [177] and over 50% in the United Kingdom and Australia [231]. Fretting-corrosion is still seen in retrieved head-stem tapers of modern MoP and ceramic bearings. There is no standardized method to measure volumetric material loss in tapers and no quantitative loss information available for designs other than large head MoM. In this study, we estimated the volume of material loss from 100 paired explanted male stem cones and female head bore tapers subdivided into matched cohorts of 50 ceramic heads and 50 CoCr heads. This study is the first to quantify volumetric material loss from tapers other than large head MoM designs. In the present study, total volumetric material loss in the CoCr cohort was an order of magnitude higher from the loss in the ceramic cohort. Femoral head material was the only factor that correlated with volumetric material loss, among the device and patient factors investigated in this study. These findings support the hypothesis that the use of ceramic heads may mitigate metallic material loss from taper junctions. Visual fretting-corrosion scores were correlated with volumetric material loss.

This study had several limitations. In the present study we used a method that was originally developed to estimate material loss from Type 1 tapers and this method has greater uncertainty for the Type 2 tapers (Table VII). In the CoCr cohort, 6 of 50 (12%) head cone tapers are Type 2, presenting with regions of an as-manufactured surface at only one end of the taper. For Type 2 tapers, the as-manufactured surface is estimated by extrapolating over the length of the taper from the as-manufactured region at one end of the taper, compared to the Type 1 taper where the as-manufactured surface is estimated from interpolating between the two as-manufactured regions at each end of the taper. The extrapolation process, where the as-manufactured surface is estimated from the as-manufacture region at one end of the paper may lead to significant uncertainties, particularly in the cases where there is a unworn region of a few millimeters in length used to extrapolate over a taper that may be between 10 and 20 mm in length. Extrapolation from one end may lead to significant uncertainty compared to having as-manufactured surfaces on either end. An uncertainty analysis for Type 2 tapers was beyond the scope of this study; however, measurements from the previously mentioned cohort of never implanted femoral heads and taper adapter sleeves were re-analyzed as Type 2 tapers, excluding the available as-manufactured surfaces on the distal end (Figure 61). Estimation of material loss as Type 2 tapers, for the same samples, had a lower correlation with gravimetric measurements ($R^2 = 94.3\%$, Table VII).

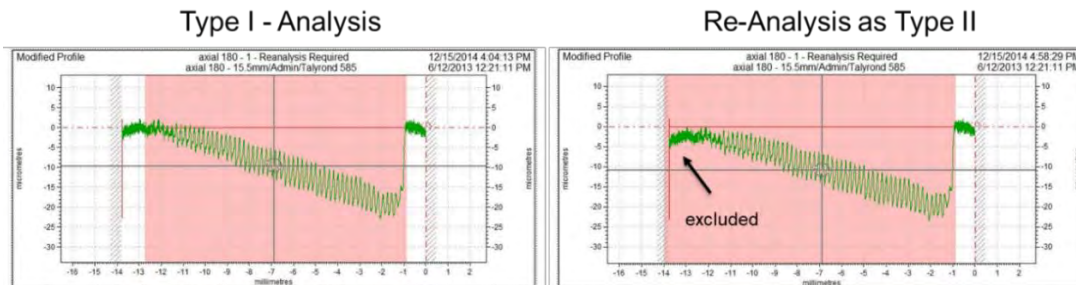


Figure 61: Correlation between visual fretting corrosion score and estimated volumetric material loss in the CoCr cohort.

Another limitation of this study, like all retrieval studies, is that it is a sample of clinical failures, and it does not necessarily reflect the performance for the population of well-functioning implants. The described validation method developed for head cone tapers in this study used new components. The present study selected ceramic implants with the longest implantation time available in our retrieval collection at the time of selection; however, it was limited to revised implants and the matching criteria [143]. The final limitation in this study is a phenomenon seen in all surface profilometry studies using a diamond stylus. At times, the contact measurement method induced submicron, visible scratches during measurement (Figure 62). This concern was also addressed in Chapter 3, Section 3.1.2 Surface Profilometry under sources of error. The surface is deformed by the same amount everywhere and was shown to be in the 20- to 40-nm range, resulting in a true displaced resultant profile. The stylus tip displaced some debris attached to the surface during measurement. Debris is a mixture of oxide and biological products that has reattached to the surface after the reactions. Debris displacement from the surface did not affect the measurements of net material loss from the taper surfaces [232].

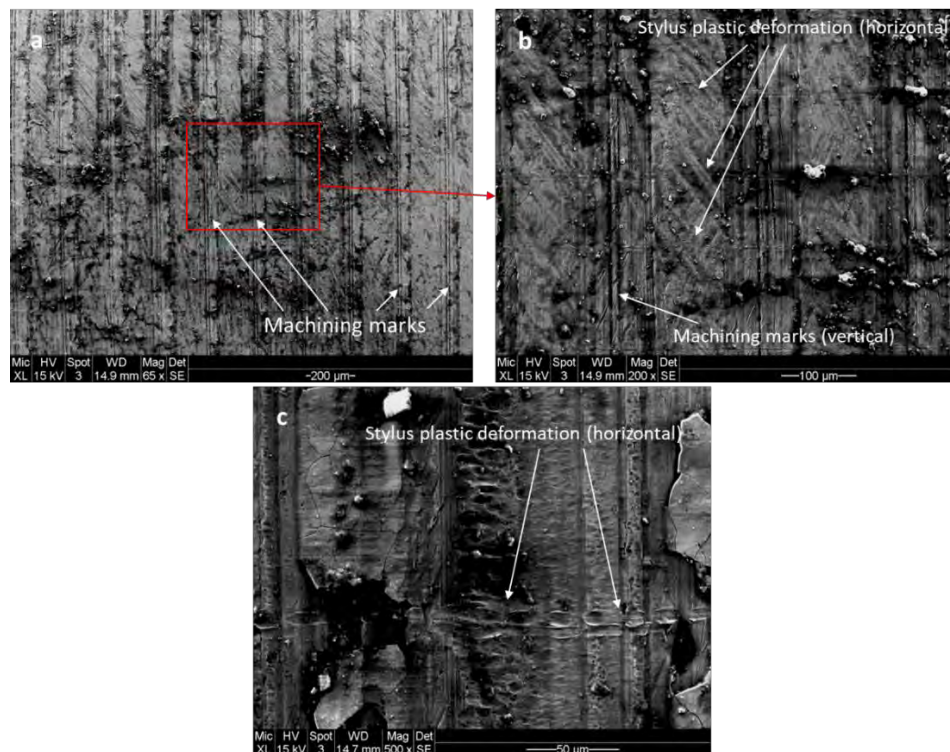


Figure 62: Stylus tip evidence of plastic deformation on the taper surface of one of our measured CoCrMo femoral heads. This deformation does not affect the results and the effects are negligible. The same area is shown with different magnifications to give an idea of the plastic deformation relative to the size of other features, a) mag 65x, showing machining marks, b) mag 200x, showing machining marks and stylus tip plastic deformation, c) mag 500x showing plastic deformation up close.

As discussed in the systematic review in section 1.4.3 of this thesis, the severity of fretting-corrosion in tapers is multifactorial and can vary significantly based on device design. The significance of using matched cohorts in the retrieval study is in eliminating any confounding factors of femoral stem material and design. Since the completion of this study, there have been other studies that looked at material loss from tapers of MoP bearings [41, 73, 153, 183], including one that compared the material loss from head-

stem tapers of MoP and LHMOM bearings in the same study [153]. The material loss from the tapers in our study is one order of magnitude lower compared with those reported in LHMOM tapers and the same with material loss from liner backside (Table XI, [2, 22, 115, 152, 153, 173]). This is consistent with other studies that measured material loss from non-LHMOM female tapers as reported in Table XI. Langton et al. [151] reported the median volumetric loss from the MoM cohort was over four times larger than the MoP cohort (1.01 mm^3 vs 0.23 mm^3 , $p < 0.001$) despite a significantly shorter median period *in vivo* for the MoM group compared to the MoP group (48 months vs 90 months respectively, $p < 0.001$). In the study by Whittaker et al. on the effect of using components from different manufacturers on the rate of material loss and corrosion of the head-stem taper junction of MoM hip arthroplasties, the size of the head was the only factor significantly associated with the rate of taper damage. They reported a 5 mm increase in the size of the head was associated with a 26% increase in the rate of material loss [248].

This matched cohort study found that the rate of material loss from head-stem tapers in MoP bearings is an order of magnitude higher when compared to head-stem tapers in CoP and CoC bearings. Most of the material lost from modular taper interfaces is from the female tapers of CoCrMo femoral heads and significantly less material loss is measured from the male tapers they are implanted together. This fact supports using ceramic femoral heads as a means of eliminating material loss from the modular head-stem taper interface (Table XI). Other researchers have also observed a higher material loss from female tapers compared to the male tapers [73, 153, 183]. Di Laura et al. calculate material loss from the head-stem junctions with median taper material loss rates

of 0.210 mm³/year (0.030 to 0.448) for the metal head group and 0.084 mm³/year (0.059 to 0.108) for the ceramic group. The dual-modularity is a confounding factor, and they mention in the discussion that severe corrosion was observed at the stem-neck interface at the time of revision and retrieval examination.

Di Laura et al. [73] and Morlock et al. [183] have studied stem designs that are now recalled due to the clinical reports of these models leading to high rates of revision. The factors leading to higher material loss are discussed in each study. It is important to note that in both studies, the stem designs are different yet from the same manufacturer. The stem designs investigated in these studies were made from a proprietary titanium alloy, TMZF with a lower flexural rigidity. As discussed in Table III in section 1.4.3, there is consensus that both lower flexural rigidity and smaller taper sizes, typically used in TMZF stems, lead to higher material loss [94, 120, 183, 202]. Additionally, numerous studies {Banerjee, 2015 #237; Bansal, 2020 #702; Urish, 2017 #1370} including Morlock et al. referenced in the table [183] describe, gross trunnion failure (GTF), a progressive damage mechanism that leads to the severe abrasion of the stem taper and catastrophic failure of the implant system in vivo. These studies investigate some of the most extreme cases of taper material loss, which explains the significantly higher mean volume of material loss seen in both the “wear only” and “gross trunnion failure” cases in the table for the Morlock et al. study. Finally, our cohorts did not include explants that were revised due to adverse reactions to metal particles; however, some studies such as Martin et al. have investigated components with a revision reason due to “metal wear/reaction” which could account for the higher mean volume seen in their study [167]. Interestingly, they also report a negative material loss value for some components and attribute it to

errors due to the presence of adhered material and suggest that more emphasis should be placed on the analysis of maximum linear depth.

The studies in Table XI all used profilometry to measure surfaces and identify as-manufactured surfaces. Consistent to our findings, other researchers have also observed that regions with corrosion and material loss show changes in surface roughness compared to as-manufactured surfaces [150]. All the studies below have observed distinct regions of contact and non-contact on CoCrMo head tapers in cases with measurable material loss [41, 73, 153, 167, 183]. Similar to our observations (Figures 45, 46), other studies have also seen evidence of imprinting in head taper surfaces [150, 173] [41, 167]. The stylus tip acts as a morphological filter when measuring material loss and may lead to measurement error, especially in regions with imprinting (Figure 27, [236]). Some of the studies have higher risk of error due to profilometer and stylus type compared to the Talyrond 585 roundness machine used in our studies. In some cases, researchers using other types of surface measurement techniques have attempted to correct for the error in their methods [150, 167]. In our explant cohorts, inspection of the linear traces of the stem cone tapers revealed depths of material loss (range = 0 – 20 μ m) similar to the head bore tapers (range = 0 – 35 μ m). However, the fretting-corrosion damage was restricted to small, isolated areas on the stem cone tapers, resulting in less material loss. The maximum linear material loss depths measured in our study was on the same order of magnitude as other studies. For example, from female taper bores Martin et al. [167] measured a median maximum linear material loss depth of 27.94 μ m (range 1.85 – 74.93 μ m) from 18 components, Cartner et al. [41] a range of 1 – 103 μ m from 17 components and Langton et al. [153] a range of 1.0 – 42.9 μ m from 70 components.

Table XI: Reported values of quantified material loss from head-stem tapers in previous studies.

Measured Surface	Bearing Type	Study	Number of implants	Mean Volume (\pm SD)* (Range) mm ³	Mean Rate (\pm SD)* (Range) mm ³ /year
Female Taper	CoCr heads on PE	Current Study	50	0.39 (\pm0.83) (0 - 4.34)	0.29 (\pm1.24) (0 - 8.67)
		Morlock [183]	30	Wear only (n = 18): 5.1 (\pm4) Gross trunnion failure (n=12): 20.8 (\pm3.6)	N/A
		Di Laura [73]	21	N/A	0.112 (0.032 - 0.326)
		Martin [167]	18	1.63 (-2.56 - 12.49)	N/A
		Langton** [153]	95	0.23 (0.0 to 3.93)	0.05 (0.0 to 3.84)
	LHMOM (dia \geq 36mm)	Whittaker [247]	50	N/A	0.27 (0.0 to 3.45)
		Hothi [115]	150	1.52 (0.13 - 25.89)	N/A
		Whittaker [248]	151	N/A	Same manufacturer ("SM") (n = 211): 0.25 (0.01 to 8.34) Mixed Manufacturer ("MM") (n = 38): 0.29 (0.0 to 3.15)

Table XI (continued):

Female Taper	LHMoM (dia \geq 36mm)	Langton [152]	111	N/A	Design I: 0.13 (0.01-3.15) Design II: 0.44 (0.02 – 8.34)
		Langton** [153]	249	With Ti stem (“mixed”) (n = 211): 0.98 (0.02 to 26.8) With non-Ti stem (“similar”) (n = 38): 1.1 (0.0 to 34)	With Ti stem (“mixed”) (n = 211): 0.25 (0.01 to 8.34) With non-Ti stem (“similar”) (n = 38): 0.29 (0.0 to 3.15)
		Brock [36]	104	N/A	12/14 (n = 72): 0.403 11/13 (n = 32): 0.123
		Bishop [22]	5	8.4 (2.6-20.2)	2.02 (0.6-4.9)
Male Taper	CoCr heads on PE	Current Study	50	0.10 (\pm0.37) (0 – 2.5)	0.04 (\pm0.08) (0 – 0.32)
		Di Laura [73]	21	N/A	0.045 (0.005 – 0.077)
	Ceramic on PE	Current Study	50	0.04 (\pm0.14) (0 – 0.74)	0.02 (\pm0.08) (0 – 0.37)
		Di Laura [73]	27	N/A	0.053 (0.017 – 0.079)
	LHMOM (dia \geq 36mm)	Matthies [173]	36	0.29 (0 – 0.83)	0.08 (0 – 0.36)
		Bishop [22]	2	0.03 (0.02 – 0.035)	0.01 (0.005 – 0.006)
Liner Backside	LHMOM (dia \geq 36mm)	Agne [2]	21	0.4 (0 -1.7)	0.2 (0 – 1.2)

*added when available. Standard deviation information was only available for the current study.
CoCr = cobalt chromium; LHMoM = large head metal on metal; N/A = information not available in the referenced manuscript.

**head-stem combined data reported

To our knowledge, the present study investigated the largest number of male tapers in a single study complete with mating femoral heads. We found that in the CoCr cohort, the stem cone tapers had one magnitude lower mean rate of material loss compared with head taper bores. Previous studies also reported higher volumetric material loss from head bore tapers compared with stem cone tapers [22, 173]. Previous researchers have also observed differences in patterns of material loss between components where stem cone tapers had damage in isolated regions unlike head bore tapers with bands of material loss around the taper [22, 152, 173]. These same researchers have offered possible electrochemical and biomechanical explanations as to why the pattern of material loss is prominently axisymmetric in head bore tapers and, if seen at all, is in localized areas on stem cone tapers; but the exact mechanism of the differences in the patterns of material loss between head bores and stem cones is unknown. The variability in the patterns of material loss and the different surface topographies (grooved or smooth) do not affect the sensitivity of measurement.

We found a positive correlation between the visual fretting-corrosion scores and the volumetric material loss for MoP bearings. A correlation between visual fretting-corrosion scores and volumetric material loss has been reported for large head MoM bearings [115]; however, visual fretting-corrosion scoring is semiquantitative and does not provide a quantitative measure of the amount of material lost from the surface. Similar to large head MoM bearing results [115], our visual fretting-corrosion scores for the present study were unable to differentiate within the high range of material loss in CoCr heads with moderate and severe visual fretting-corrosion scores (scores of 3 and 4) (Fig. 4). In cases of severe fretting-corrosion damage, the severity of the discoloration seems to be

unrelated to the actual material loss. Thus, although useful, visual fretting-corrosion scoring methods have limitations and fully quantifying the amount of material loss at these interfaces may be more useful when analyzing fretting corrosion in the context of patient and device factors.

In our study, the only factor that we found that was associated with decreasing cumulative material loss from taper junctions was femoral head material. We found no correlation between cumulative rate of material loss from the taper junctions in the CoCr cohort and the stem material Ti6Al4V alloy, CoCr alloy, or TMZF alloy. There was no correlation between taper angle clearance and the volumetric material loss for the presently investigated cohorts. Taper angle clearance is positive or negative with proximal or distal engagement respectively [131]. To account for the effect of net clearance, in the present study, we looked at the effect of absolute clearance on material loss and found no correlation. To our knowledge, one other study has investigated the effect of device factors and rate of volumetric material loss from LHMOM bearings. In their study, they investigated two types of commercially available designs of LHMOM bearings and found statistically significant ($p < 0.05$) correlations between rate of volumetric material loss and taper angle, head offset, distance (taper engagement level to center of rotation) and horizontal lever arm distance (lateral offset) [152]. Other studies which have quantified the volumetric material loss have not investigated the relationship between material loss and device design factors [115, 173]. Some previous studies which have looked at the effect of device factors have not quantified the rate of material loss [94]. Moreover, with the numbers available, we did not observe any correlations between material lost and patient or device factors.

The use of ceramic heads with CoCrMo alloy stems reduced exposure to Co and Cr products from the taper junctions in this small matched-pair series. The use of a ceramic head with a titanium alloy stem will completely eliminate Co and Cr exposure. The results from this study show that ceramic head combinations decreased overall metal release caused by taper fretting and corrosion compared to MoP bearings. The majority of cumulative metal released from the taper junctions was from the CoCr femoral head bore taper. This is the first study that quantifies material loss from taper junctions with MoP and CoC, CoP bearings. Quantitative data provides comparable material loss information for future studies looking at different device and material factors. It may also be used for correlations between systemic cytotoxicity with volumetric material loss. Provided a titanium alloy stem is used, the corrosion products are considered to be less cytotoxic than Co and Cr [66, 101]; however, more information is still needed to determine the long term clinical effects. The reduction of corrosion products makes ceramics a potentially attractive bearing for ALTR revisions [60, 61]. The decision of which bearing to use in clinical practice for primary THA (and for other revision diagnoses) is complex and based on a host of factors including risk of fracture, bearing noise, and cost (for ceramics) and polymer wear and corrosion issues (for metal). The most recent Australian Joint Registry reports that the risk of ceramic fracture using new generation ceramic composite heads is known to be extremely low, 0.17 per 10,000 (0.0017%) [10]. The present study contributes to this conversation by confirming that ceramic indeed does not have the same trunnion issues that metal heads do and can be factored into the surgeon's choice on that basis.

References

2. Agne MT, Underwood RJ, Kocagoz SB, MacDonald DW, Day JS, Parvizi J, Kraay MJ, Mont MA, Klein GR, Cates HE, Kurtz SM. Is there material loss at the backside taper in modular CoCr acetabular liners? *Clinical orthopaedics and related research*. 2015;473:275-285.
4. Arnholt C, Underwood R, MacDonald D, Higgs G, Chen A, Klein G, Hamlin B, Lee G, Mont M, Cates H, Malkani A, Kraay M, Rimnac C, Kurtz S. Microgrooved Surface Topography Does Not Influence Fretting Corrosion of Tapers in THA: Classification and Retrieval Analysis. *Modularity and Tapers in Total Joint Replacement Devices*. Conshohocken PA: American Society of Testing Materials (ASTM); 2015.
10. Australian Orthopaedic Association. *Australian Orthopaedic Association National Joint Replacement Registry. Annual Report. Adelaide:AOA; 2019*.
22. Bishop N, Witt F, Pourzal R, Fischer A, Rutschi M, Michel M, Morlock M. Wear patterns of taper connections in retrieved large diameter metal-on-metal bearings. *Journal of orthopaedic research : official publication of the Orthopaedic Research Society*. 2013;31:1116-1122.
30. Bone MC, Sidaginamale RP, Lord JK, Scholes SC, Joyce TJ, Nargol AVF, Langton DJ. Determining material loss from the femoral stem trunnion in hip arthroplasty using a coordinate measuring machine. *Proceedings of the Institution of Mechanical Engineers Part H-Journal of Engineering in Medicine*. 2015;229:69-76.
36. Brock TM, Sidaginamale R, Rushton S, Nargol AV, Bowsher JG, Savisaar C, Joyce TJ, Deehan DJ, Lord JK, Langton DJ. Shorter, rough trunnion surfaces are associated with higher taper wear rates than longer, smooth trunnion surfaces in a contemporary large head metal-on-metal total hip arthroplasty system. *Journal of orthopaedic research : official publication of the Orthopaedic Research Society*. 2015;33:1868-1874.
41. Cartner J, Aldinger P, Li C, Collins D. Characterization of Femoral Head Taper Corrosion Features Using a 22-Year Retrieval Database. *HSS Journal*. 2017;13:35-41.
60. Cooper HJ. The local effects of metal corrosion in total hip arthroplasty. *The Orthopedic clinics of North America*. 2014;45:9-18.
61. Cooper HJ, Della Valle CJ, Berger RA, Tetreault M, Paprosky WG, Sporer SM, Jacobs JJ. Corrosion at the head-neck taper as a cause for adverse local tissue reactions after total hip arthroplasty. *The Journal of bone and joint surgery. American volume*. 2012;94:1655-1661.
66. Dalal A, Pawar V, McAllister K, Weaver C, Hallab NJ. Orthopedic implant cobalt-alloy particles produce greater toxicity and inflammatory cytokines than titanium alloy and zirconium alloy-based particles in vitro, in human osteoblasts, fibroblasts, and macrophages. *Journal of biomedical materials research. Part A*. 2012;100:2147-2158.
73. Di Laura A, Hothi H, Henckel J, Swiatkowska I, Liow MHL, Kwon YM, Skinner JA, Hart AJ. Retrieval analysis of metal and ceramic femoral heads on a single CoCr stem design. *Bone & joint research*. 2017;6:345-350.
90. Gilbert JL, Sivan S, Liu Y, Kocagoz SB, Arnholt CM, Kurtz SM. Direct in vivo inflammatory cell-induced corrosion of CoCrMo alloy orthopedic implant surfaces. *Journal of Biomedical Materials Research - Part A*. 2015;103:211-223.

94. Goldberg JR, Gilbert JL, Jacobs JJ, Bauer TW, Paprosky W, Leurgans S. A multicenter retrieval study of the taper interfaces of modular hip prostheses. *Clinical orthopaedics and related research*. 2002;149-161.
101. Hallab NJ, Mikecz K, Vermes C, Skipor A, Jacobs JJ. Orthopaedic implant related metal toxicity in terms of human lymphocyte reactivity to metal-protein complexes produced from cobalt-base and titanium-base implant alloy degradation. *Molecular and cellular biochemistry*. 2001;222:127-136.
109. Higgs GB, Hanzlik JA, MacDonald DW, Gilbert JL, Rimnac CM, Kurtz SM. Is increased modularity associated with increased fretting and corrosion damage in metal-on-metal total hip arthroplasty devices?: a retrieval study. *The Journal of arthroplasty*. 2013;28:2-6.
115. Hothi HS, Matthies AK, Berber R, Whittaker RK, Skinner JA, Hart AJ. The reliability of a scoring system for corrosion and fretting, and its relationship to material loss of tapered, modular junctions of retrieved hip implants. *The Journal of arthroplasty*. 2014;29:1313-1317.
120. Huot Carlson JC, Van Citters DW, Currier JH, Bryant AM, Mayor MB, Collier JP. Femoral stem fracture and in vivo corrosion of retrieved modular femoral hips. *The Journal of arthroplasty*. 2012;27:1389-1396.e1381.
129. Kocagöz S, Underwood R, MacDonald D, Day J, Kurtz S. What Is the Clinical Relevance of Visual Inspection of the Head/Stem Taper Junctions in Large Head Metal-on-Metal Hips? In: *American Academy of Orthopedic Surgeons*. New Orleans, LA, USA: 2014.
131. Kocagoz SB, Underwood RJ, Sivan S, Gilbert JL, Macdonald DW, Day JS, Kurtz SM. Does Taper Angle Clearance Influence Fretting and Corrosion Damage at the Head-Stem Interface? A Matched Cohort Retrieval Study. *Semin Arthroplasty*. 2013;24:246-254.
143. Kurtz SM, Kocagoz SB, Hanzlik JA, Underwood RJ, Gilbert JL, MacDonald DW, Lee GC, Mont MA, Kraay MJ, Klein GR, Parvizi J, Rimnac CM. Do ceramic femoral heads reduce taper fretting corrosion in hip arthroplasty? A retrieval study. *Clinical orthopaedics and related research*. 2013;471:3270-3282.
150. Langton D, Ahmed I, Avery P, Bone M, Cooke N, Deehan D, Duffy P, Foguet P, Green S, Holland J, Jafri A, Longstaff L, Lord J, Loughhead J, Meek RMD, Murray H, Nanu A, Nargol AVF, Scholes SC, Sidaginamale RP, Waller S, Joyce T. Investigation of Taper Failure in a Contemporary Metal-on-Metal Hip Arthroplasty System Through Examination of Unused and Explanted Prostheses. *Journal of Bone and Joint Surgery-American Volume*. 2017;99:427-436.
152. Langton DJ, Sidaginamale R, Lord JK, Nargol AV, Joyce TJ. Taper junction failure in large-diameter metal-on-metal bearings. *Bone & joint research*. 2012;1:56-63.
153. Langton DJ, Wells SR, Joyce TJ, Bowsher JG, Deehan D, Green S, Nargol AVF, Holland JP. Material loss at the femoral head taper: a comparison study of the Exeter metal-on-polyethylene and contemporary metal-on-metal total hip arthroplasty. *The bone & joint journal*. 2018;100-B:1310-1319.
167. Martin AJ, McGrory BJ, Eddin AA, Van Citters DW. Using coordinate measuring machine validated with white light interferometry to identify contributors to material loss due to corrosion of total hip replacement modular junctions. In: *ASTM Special Technical Publication*. 2018:118-130.
173. Matthies AK, Racasan R, Bills P, Blunt L, Cro S, Panagiotidou A, Blunn G, Skinner J, Hart AJ. Material loss at the taper junction of retrieved large head metal-on-metal total hip replacements. *Journal of orthopaedic research : official publication of the Orthopaedic Research Society*. 2013;31:1677-1685.

177. Mendenhall S. Hospital resources and implant cost management—a 2013 update. *Orthopedic Network News*. 2014;25:9-15.
179. Meyer H, Mueller T, Goldau G, Chamaon K, Ruetschi M, Lohmann CH. Corrosion at the cone/taper interface leads to failure of large-diameter metal-on-metal total hip arthroplasties. *Clinical orthopaedics and related research*. 2012;470:3101-3108.
183. Morlock MM, Dickinson EC, Günther KP, Bunte D, Polster V. Head Taper Corrosion Causing Head Bottoming Out and Consecutive Gross Stem Taper Failure in Total Hip Arthroplasty. *Journal of Arthroplasty*. 2018;33:3581-3590.
202. Porter DA, Urban RM, Jacobs JJ, Gilbert JL, Rodriguez JA, Cooper HJ. Modern trunnions are more flexible: a mechanical analysis of THA taper designs. *Clinical orthopaedics and related research*. 2014;472:3963-3970.
231. The National Joint Registry [NJR] for England W, Northern Ireland and the Isle of Man. *National Joint Registry 15th Annual Report 2018*.
232. Thomas TR. *Rough Surfaces*: Imperial College Press; 1999.
235. Underwood RJ, Fowell M, Sayles RS, Kurtz SM, PM C. *The Development of a Standard Method for Assessing Wear of Explanted Metal-on-Metal Hip Joints*. West Conshohoken, PA: American Society for Testing and Materials,; 2013.
236. Underwood RJ, Kocagoz SB, Smith R, Sayles RS, Siskey R, Kurtz SM, Cann PM. A Protocol to Assess the Wear of Head/Neck Taper Junctions in Large Head Metal-on-Metal (LHMoM) Hips. In: Kurtz SM, Greenwald AS, Mihalko WM, Lemons JE, ed. *Metal-on-Metal Total Hip Replacement Devices*; 2013:209-234.
242. Walton K, Petrucci M, Racasan R, Blunt L, Hart A, Bills P. Focus variation measurement and advanced analysis of volumetric loss at the femoral head taper interface of retrieved modular replacement hips in replica. In: *Journal of Physics: Conference Series*. 2019.
247. Whittaker RK, Hothi HS, Eskelinen A, Blunn GW, Skinner JA, Hart AJ. Variation in taper surface roughness for a single design effects the wear rate in total hip arthroplasty. *Journal of Orthopaedic Research*. 2017;35:1784-1792.
248. Whittaker RK, Hothi HS, Meswania JM, Berber R, Blunn GW, Skinner JA, Hart AJ. The effect of using components from different manufacturers on the rate of wear and corrosion of the head–stem taper junction of metal-on-metal hip arthroplasties. *Bone and Joint Journal*. 2016;98B:917-924.

5 In vitro comparison of PEEK/metal and metal/metal fretting-corrosion

5.1 Introduction

In previous studies, it was shown that the use of ceramic femoral heads, an alternative to CoCr alloy heads, may mitigate corrosion at the modular head-neck interface in hip joint arthroplasties. Using biochemically inert materials may mitigate or eliminate mechanically assisted crevice corrosion (MACC) [130, 205], the mechanism of material release at the modular junctions [85, 94, 98, 209, 238]. Poly(Ether Ketone) (PEEK) is a high-performance semi-crystalline thermoplastic that was first synthesized in the late 1970s, and has become increasingly popular in the orthopedics communities due its biocompatibility, strength to weight ratio, chemical stability and wear properties [137, 189]. PEEK is a versatile material and has provided opportunity for its exploration and use in a diversity of different types of implant applications. In the clinic, numerous studies have reported the successful performance of PEEK spinal fusion cages and has been shown to possess advantageous properties for this application because of its mechanical strength, biocompatibility and radiolucency for inspecting bone integration [136, 137]. Investigation of wear properties of unfilled and composite (fiber-reinforced or filled) PEEK are also of interest of bearing applications. In vitro tests of sliding wear of PEEK and its composites date back to the early 90s due to interest for its use in high temperature applications [82]. Early studies and later studies of linear reciprocating and multi-directional sliding pin-on-plate tests helped determine the factors related to composition, surface finish, temperature, self-lubricating film formation that affect wear properties of PEEK [154]. Siskey et al. have tested the wear performance of PEEK-on-ceramic as an alternative bearing combination for orthopedic implants and have found the

wear rates to be comparable to other polymer-on-hard bearing couples [218]. Boudeau et al. tested the performance of injection molded, carbon fiber reinforced-PEEK femoral stems, which eliminates the metal taper surface from the stem as well, and reported good results under walking load and compared stress shielding, stress deficiency, debonding and global deformation to bone and bone-metal implant systems [32].

Recently, PEEK materials and its processing methods have been investigated for use in modular tapers to mitigate taper corrosion. Ouellette et al. have developed a custom method to produce self-reinforced composites (SRC) with PEEK fibers [189] and later used the SRC-PEEK samples in a pin-on-disk metal-on-metal interface test to evaluate its ability to inhibit fretting corrosion [190]. The method of producing SRC-PEEK was shown to result in samples with higher crystallinity and crystalline orientation and improved monotonic tensile properties compared to bulk PEEK available commercially and successfully showed the ability to insulate two metal surfaces from fretting-corrosion damage. The pin-on-disk (POD) testing used during this study [190] has been shown to be a good means of understanding the fundamental electrochemical behavior of materials when undergoing small-scale cyclic motions and will be described in detail in the next section. For the study described in this chapter we have used the same POD testing setup and compared the tribochemical properties of PEEK/metal and metal/metal interfaces. PEEK manufacturing processes are still widely explored, and the optimal method will depend on the final application. Injection molding is one of the most commonly methods for unfilled and fiber-reinforced PEEK composites [32, 104]. To our knowledge, no other studies have reported the tribochemical properties of injection molded PEEK/metal interfaces.

5.1.1 Modified Pin-on-Disk Tribocorrosion Testing

Prior use of pin-on-disk use and value for biomaterials research has been summarized in Chapter 1. Instrumented pin-on-disk tests are the current methods used to study the mechanics and electrochemistry of fretting-corrosion in vitro. Measurements from these tests include direct instantaneous determination of COF, fretting energy dissipated per cycle of motion, and actual fretting current density. Pin-on-disk tests are an ideal way to assess specific material combinations, the role of different solutions, and the effect of stress compliance on fretting processes [4]. This study used a previously developed triboelectrochemical POD test set-up designed to simulate MACC in vitro designed by Swaminathan et al. [226]. Their test setup and MACC corrosion model, also detailed in Chapter 1, accounts for all the mechanical and electrochemical parameters involved in fretting-corrosion and allows for testing any material combination. The test system consists of a combination of subsystems for precision loading, motion control and electrochemical parameter controls (voltage, current, impedance). The purpose of this study was to use the electrochemical set-up presented [226] to test the tribochemical properties of PEEK-CoCr alloy and PEEK-Ti alloy interfaces and compare with CoCr-CoCr and CoCr-Ti combination test results.

In vivo fretting-corrosion is dependent on the rate of disruption of the protective oxide film. When the oxide film is mechanically disrupted, fretting-currents are generated during the biometallic implant materials instantaneously reform aqueous environments formation of a new layer of oxide film (repassivation) and dissolution of ions on the surface of the metal. Using this relationship, in the previously developed test setup [226], the current density generated was used to measure the effect of nominal load and material couple on the rate of disruption of oxide films. Previous studies have shown that contact

conditions in fretting change with increasing displacement amplitude and is dependent on the applied load normal to the interface, perpendicular to the fretting direction. Vingsbo and Soderberg have characterized three different regimes of fretting 1) *stick regime*: very limited surface damage by oxidation and wear, 2) *mixed stick-slip regime*: mechanical wear and oxidation effects are small, fretting fatigue is observed, 3) *gross slip regime*: severe surface damage by wear assisted by oxidation, fretting wear[241]. It is hypothesized that stick conditions will not disrupt the oxide layer and fretting currents will not be generated.

In the present study, we compared the fretting-corrosion behavior of metal/metal interfaces with PEEK/metal interfaces and asked 1) what the values are for maximum fretting-currents, work done per cycle of fretting and CoF values for each material couple and whether they are significantly different 2) whether the applied normal load has an effect on measured fretting-current density and coefficient of friction and 3) whether the observed fretting-wear scars are representative of the scars observed in retrievals and the literature and if there is any difference between material couples. During the study, we also expect to observe all the fretting regimes depending on loading: slip at low loads, stick-slip at low and medium loads and eventual full stick at a high load.

5.2 Experimental Methods

The previously described fretting corrosion test system [226] induces sliding contact between a flat circular disk (diameter 35mm) and a cone shaped flat bottom cylindrical pin (cylinder top diameter 8mm, cone shaped flat bottom diameter 0.5-1mm). The pins and disks used for this study were made from PEEK (Invibio Ltd., Lancashire,

UK), Ti6Al4V alloy (ASTM-F1472) and CoCrMo alloy (ASTM- F1537) with the following test combinations: CoCrMo pin-CoCrMo disk, PEEK pin-CoCrMo disk, PEEK pin-Ti6Al4V disk, Ti6Al4V pin –CoCrMo disk (Figure 63).



	CoCrMo	Ti6Al4V	PEEK	PEEK
	CoCrMo	CoCrMo	CoCrMo	Ti6Al4V

Figure 63: Flat circular disk and cone-shaped flat bottom pin (tip diameter ranging from 0.35 to 0.8 mm) combinations tested in triplicate.

Additionally, a fifth test combination was conducted using small diameter and thin additional disks that were machined out of PEEK. These disks were 1.5mm in diameter and 0.35mm thick. This test was designed to simulate a PEEK sleeve or membrane inserted on top of a CoCrMo stem before a CoCrMo femoral head was fitted on top of the stem/sleeve combination (Figure 64).

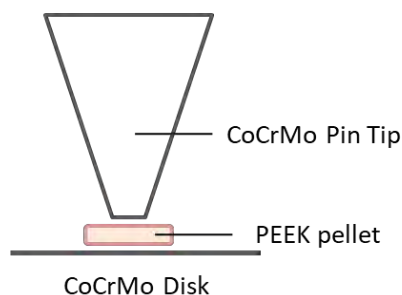


Figure 64: “PEEK pellet sandwich” testing setup where a thin and small PEEK disk is placed between a CoCrMo pin and disk and variable load pin-on-disk testing was carried out in this configuration.

Prior to testing, the pin tips and disks are polished to 600 grit and covered with acrylic coating material for a controlled test area. The polishing is Only the pin tip and a small area surrounding the contact region of the pin tip on the disk (approx. diameter 2.5mm) were exposed. The pin tip and disks were inspected after being polished and prior to testing using an optical microscope to ensure an even surface and to take photos and surface profiles for comparison before and after testing (KH-8700, HIROX) (Figure 65).

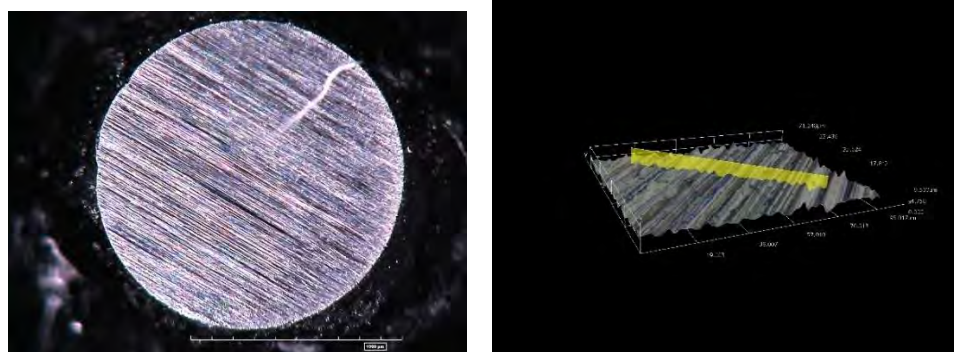


Figure 65: Microscopic examination and optical profiling of surfaces of each sample using the KH-8700, HIROX optical microscope.

Experiments were performed at room temperature in phosphate buffered saline (PBS) solution (pH 7.4). This is a solution that is commonly used for POD testing for simulating the biological milieu. Disks are placed horizontally in a chamber attached to a high-load piezoelectric actuator (Piezo-Jenna Systems, Germany), which is used to simulate fretting motion displacement of 50 μ m at 3Hz frequency by moving the XY stage shown in Figure 66. The piezoelectric actuator is controlled by an amplifier and function

generator which controls the frequency and motion amplitude. The pins were attached beneath the multi-axial load cell in the vertical orientation. The loading assembly is a six-axis load cell (MINI 45 F/T, ATI Industrial Measurement Inc., USA) coupled to the vertical motion system, comprising of a linear adjustable Z-stage (Newport Inc., USA) with a micrometer screw actuator to control the vertical position of the pin. The incremental increase in vertical applied load is enabled by using dead weights and micrometer adjustment. The load cell measures vertical and axial loads and three axis moments. During testing, the pin is fixed, and fretting is simulated by the relative XY movement of the stage and disk to the pin. A differential variable reluctance transducer (DVRT, Microstrain Inc., USA) is used to record the motion of the pin relative to the disk.

As shown in Figure 66, the pin and disk were electrically coupled to act as a working electrode with a Ag/AgCl reference electrode and carbon counter electrode connected to the potentiostat (Solartron 1280C Potentiostat/Frequency Response Analyzer, Solartron Analytical Inc., USA). The potentiostat controls the potential of the sample and measures currents that arise during fretting. Electrical data was acquired using CorrWare software (Scribner Associates). The electrochemical data was fed into the same data acquisition card and analyzed together with the load data. This allowed simultaneous, real-time acquisition of fretting parameters including normal and tangential loads and moments, pin displacement using the DVRT, current, voltage and other relevant data.

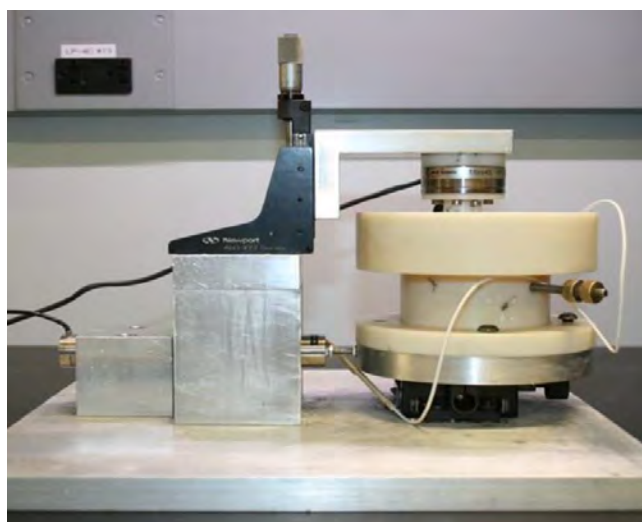
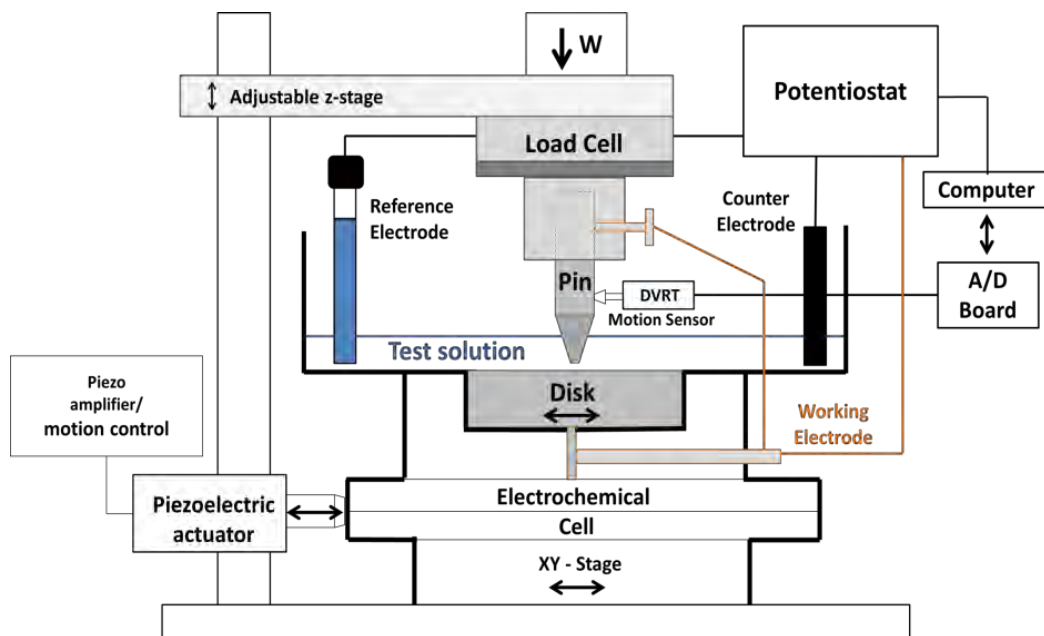


Figure 66: Previously published tribocorrosion test set-up schematic and photo [226]. Test solution PBS (pH 7.4). Fretting is simulated by the piezoelectric actuator. Motion of pin relative to disk is captured with the DVRT.

Variable-load, fretting corrosion tests were performed on all material combinations and each combination was tested in triplicate. Normal loads were varied from 0.5N to 50N or until a load is reached where there is no longer any translational motion of the pin but only pivoting due to “sticking” to the surface of the disk. Sticking is confirmed by a customized LabView software (National Instruments, Austin, TX) used to

display multi-axial loads and coefficient of friction. Potential is kept fixed at 0V vs Ag/AgCl which is representative of the open circuit potential of these metals in PBS. At the beginning of the test, the pin and the disk are allowed to equilibrate in solution at the test potential for 10 minutes. The desired load is set by adjusting the z-axis micrometer. At each load, fretting motion is induced for 120 seconds with a 300 second break in between to allow baseline current to restabilize before the next higher loading condition is tested. All tests were conducted at a fixed fretting amplitude (50 μ m) and fixed fretting frequency (3Hz). CoreView (CoreView Systems Private Limited, Maharashtra, India) is used to record and monitor electrochemical data and confirm stability of baseline current. During testing, the pin tip and disk contact were not separated between different applied normal loads. At the end of the entire test, the pin and disk were carefully removed, and the contact surfaces were separated only at this time.

Post testing, pin tips and contact locations on disks were inspected using scanning electron microscopy (SEM, JEOL JSM-5600) and an optical microscope (KH-8700, HIROX) for quantification of contact area (Figure 67). Average current density is calculated by taking the difference between the fretting current at each applied normal load and subsequent baseline current. Nominal stresses are calculated by dividing the applied normal load by the contact area identified by microscopy. Work done per fretting cycle at each load is calculated by multiplying the applied normal load with the DVRT displacement data at the given cycle. Fretting COF was calculated by identifying sliding portion from the force curve and averaging the ratio of tangential force to normal force at each load.



Figure 67: Pin tips and disks inspected using scanning electron microscopy (JEOL JSM-5600) and optical microscopy (KH-8700, HIROX) for quantification of contact area. Area calculation feature is available on the KH-8700 by selecting the worn area.

5.3 Results

Figures 68 and 69 show the summary of the measured fretting currents vs. time for all the material couples tested. The scales on these graphs are the same to show the difference in fretting magnitude between the metal/metal interfaces and those that contain PEEK in the interface. Figure 70 has the plots for Ti/CoCr couple and the Ti/PEEK couple plotted together to show the significant difference in fretting current density. In the fretting-current density plots, there was an immediate increase in the currents in response to the initiated fretting motion (Figure 70). The fretting current density is consistent for the duration of fretting (120s) for a certain load. During the subsequent resting phase, the fretting-current density rapidly drops back to the baseline current value.

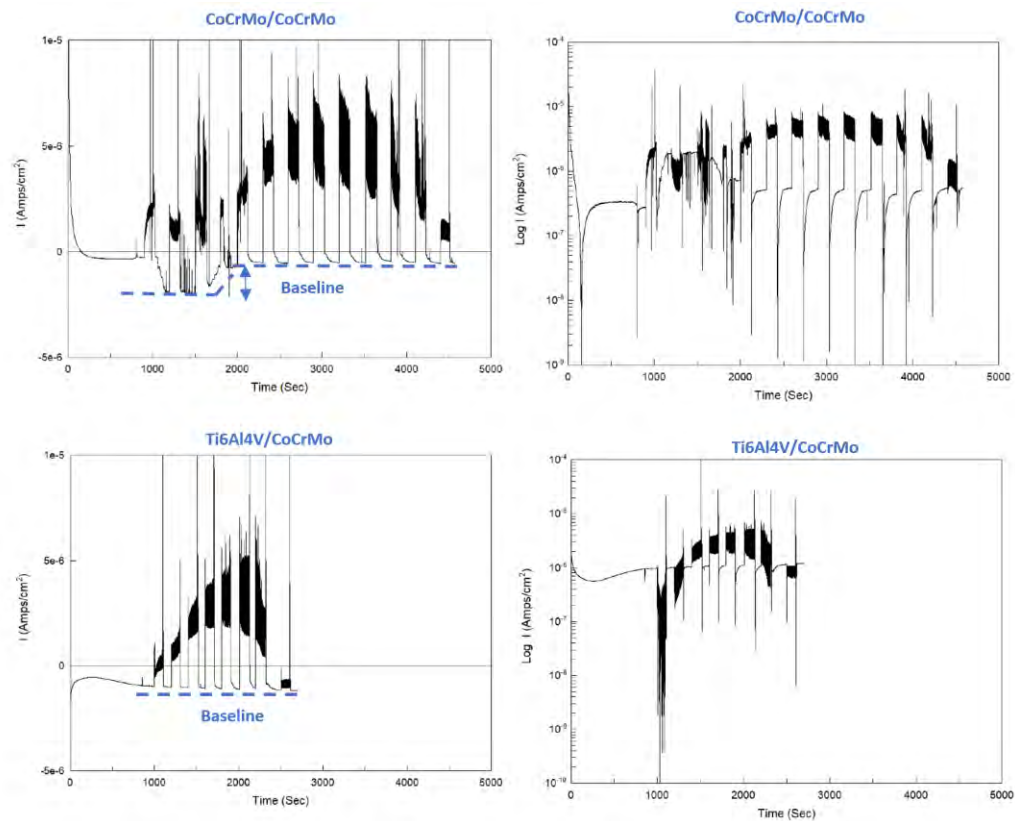


Figure 68: Pin tips and disks inspected using scanning electron microscopy (JEOL JSM-5600) and optical microscopy (KH-8700, HIROX) for quantification of contact area. Area calculation feature is available on the KH-8700 by selecting the worn area.

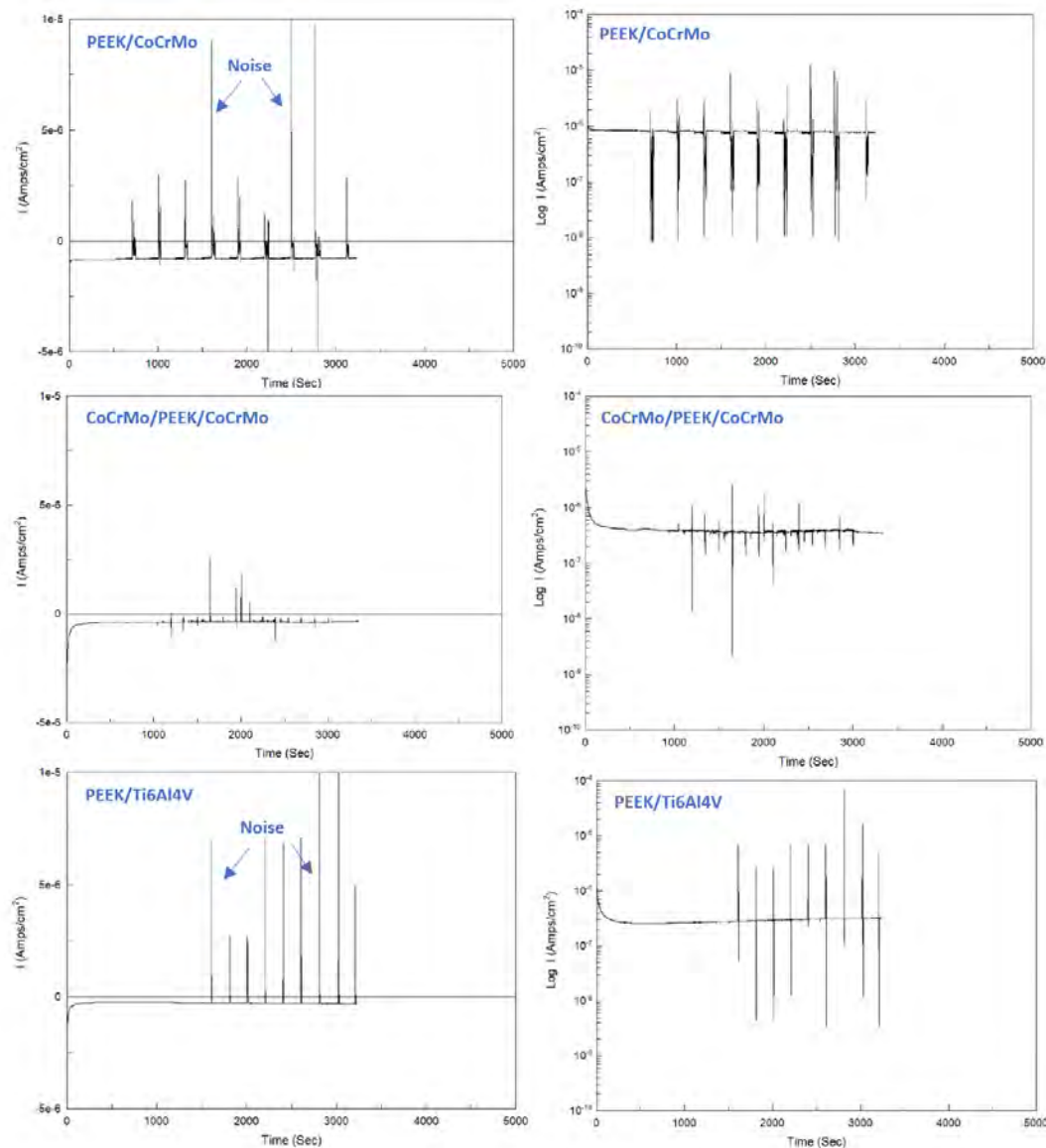


Figure 69: Pin tips and disks inspected using scanning electron microscopy (JEOL JSM-5600) and optical microscopy (KH-8700, HIROX) for quantification of contact area. Area calculation feature is available on the KH-8700 by selecting the worn area.

The difference in current density response between the PEEK material couples and the metal-metal material couples were statistically significant ($p < 0.05$). Average fretting current densities for the CoCr pin on disk tests and the Ti pin on CoCr disks were 1.01mA and 1.03mA respectively. The average fretting current densities for the PEEK pin on CoCr

disk and PEEK pin on Ti disks were $4.2\mu\text{A}$ and $3.2\mu\text{A}$ respectively. The average fretting current density is always higher for the former metal-metal couples compared to the latter PEEK-metal couples for all normal loads applied during the tests (Figure 71). During the tests, the normal load applied during each fretting period is incrementally increased. It is observed that the fretting-currents generated during each 120s period increases with increasing load and after a critical normal load starts to decrease and continues to decrease. The increase and then decrease of the fretting currents are related to the mechanical contact fretting regimes: sliding, slip-stick and sticking at the highest loads.

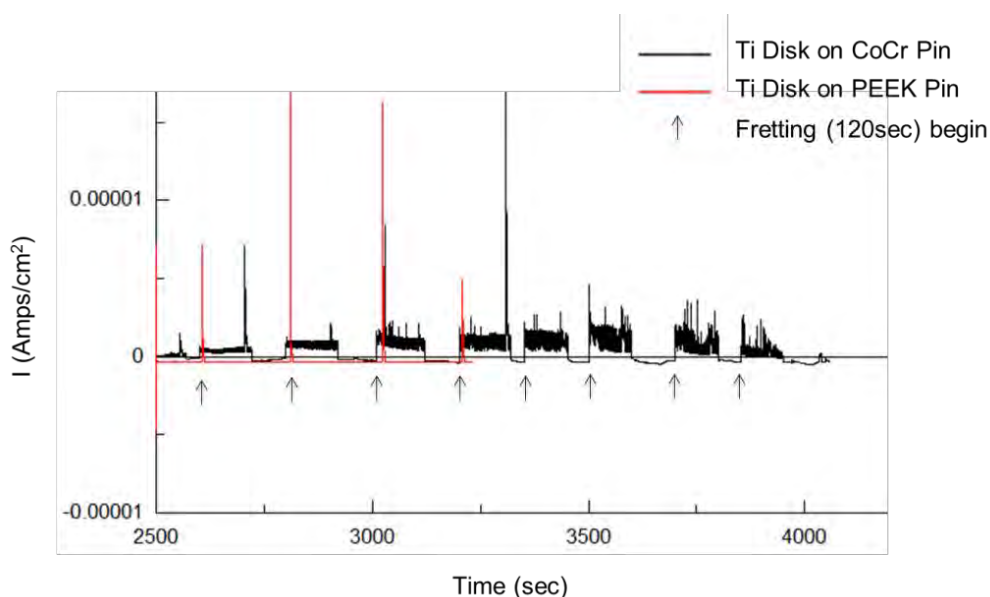


Figure 70: Fretting-current density ($I(\text{Amps}/\text{cm}^2)$) vs. time depicts the orders of magnitude difference in currents generated between the Ti/CoCr material couple (in black) and the Ti/PEEK couple. Arrows show fretting initiation. The spikes in fretting-current at the initiation of fretting (where the arrows are) and sometimes at the end of fretting are noise and were excluded from analysis.

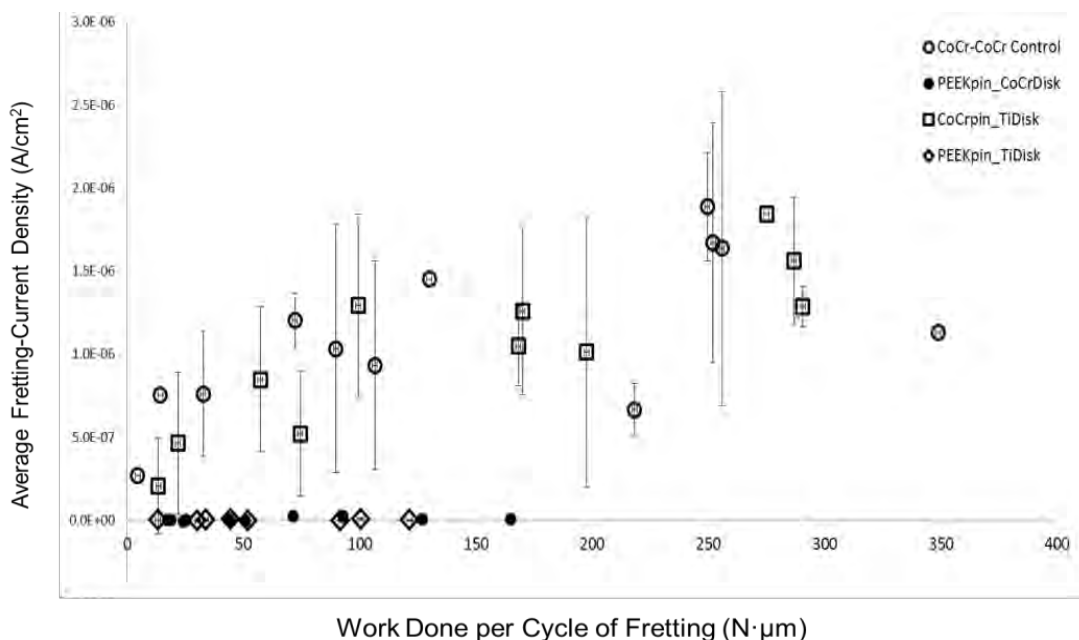


Figure 71: Average fretting current density vs. work done per cycle of fretting for all four material couples. Work done and average fretting current density is significantly higher for metal-metal couples compared to PEEK-metal. Average values obtained from triplicate tests for each material couple is compiled.

There was slight elevation in the baseline current for CoCrMo/CoCrMo couple after the first few fretting cycles were completed and remained at a new baseline for the rest of the test. Ti6Al4V/CoCrMo did not exhibit any change in baseline, nor did any of the PEEK coupled interfaces. The baseline current is a representation of the solution conditions and the potential at equilibrium, and changes to the baseline may indicate changes in the chemical changes in the surrounding environment, in this case the solution during the CoCrMo/CoCrMo test.

Fretting currents and coefficient of friction (COF) vary with load. The COF data gives information about the sliding motion of the pin on the disk, or if it has ceased to slide due to high loading and sticking has occurred. Figure 72 shows the difference in the COF graphs when sliding is occurring and when sticking has been achieved. In Figure 72, the

graph on the left shows a constant COF value once fretting has begun, and it remains constant until fretting is stopped after 120s as the pin is sliding or slipping across the disk. The graph on the right in Figure 72 does not show this plateau region of constant COF, instead there is the upside down V shape as the pin is rocking back and forth in place because it is unable to slip due to the high normal force making it stick.

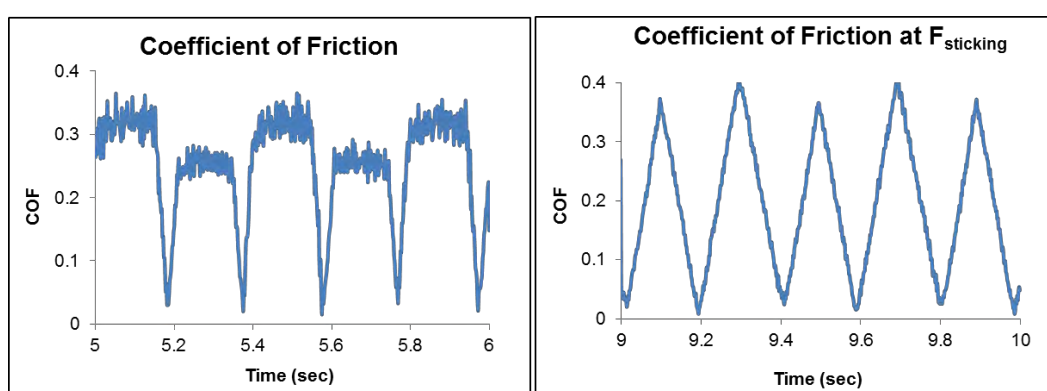


Figure 72: Coefficient of friction during sliding motion (left) vs. sticking (right).

Sticking at the end of the test is confirmed looking at the tangential force (F_t) vs. displacement hysteresis loop behavior throughout the fretting motion. Figure 73 shows that at each applied load, fretting motion exhibits a hysteresis loop behavior. The maximum tangential force increases, and displacement decreases during fretting with increasing applied normal load F_N . At the maximum normal load of 30N in this case, there is no displacement, sticking is achieved. The F_t seen is elastic behavior and for that fretting loop, the work is equal to zero. At lower forces (0.5N), full slip can be observed, where there are no tangential forces and the pin only exhibits displacement. As the force is increased, a mixture of stick-slip is observed in the rising tangential force vertically in a slope (due to

the slight tilt or rocking forwards or backwards of the pin) and the eventual plateau where slipping is seen.

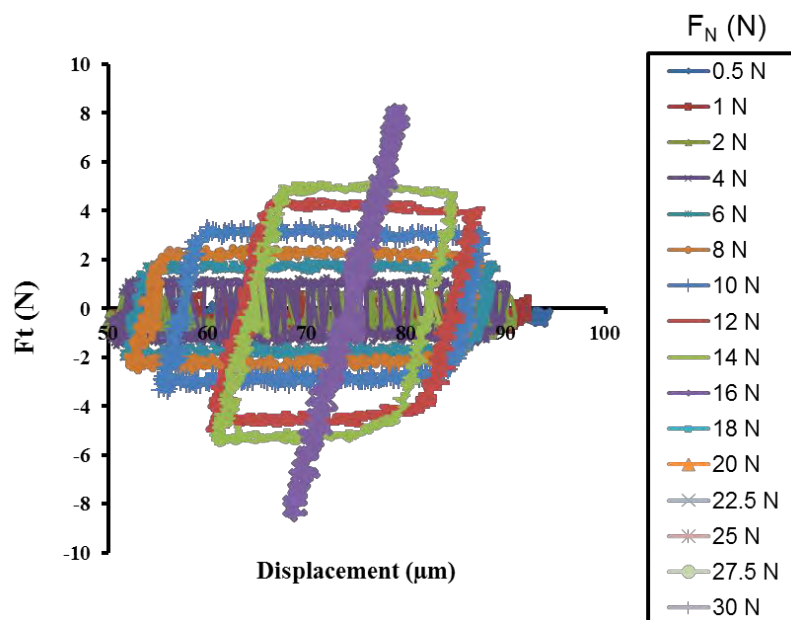


Figure 73: Representative tangential force vs. displacement graph for CoCrMo/Ti6Al4V. At each applied load, fretting motion exhibits a hysteresis loop behavior. The maximum tangential force increases, and displacement decreases during fretting with increasing applied normal load F_N . At the maximum normal load of 30N in this case, there is no displacement, sticking is achieved. The F_t seen is elastic behavior and for that fretting loop, the work is equal to zero.

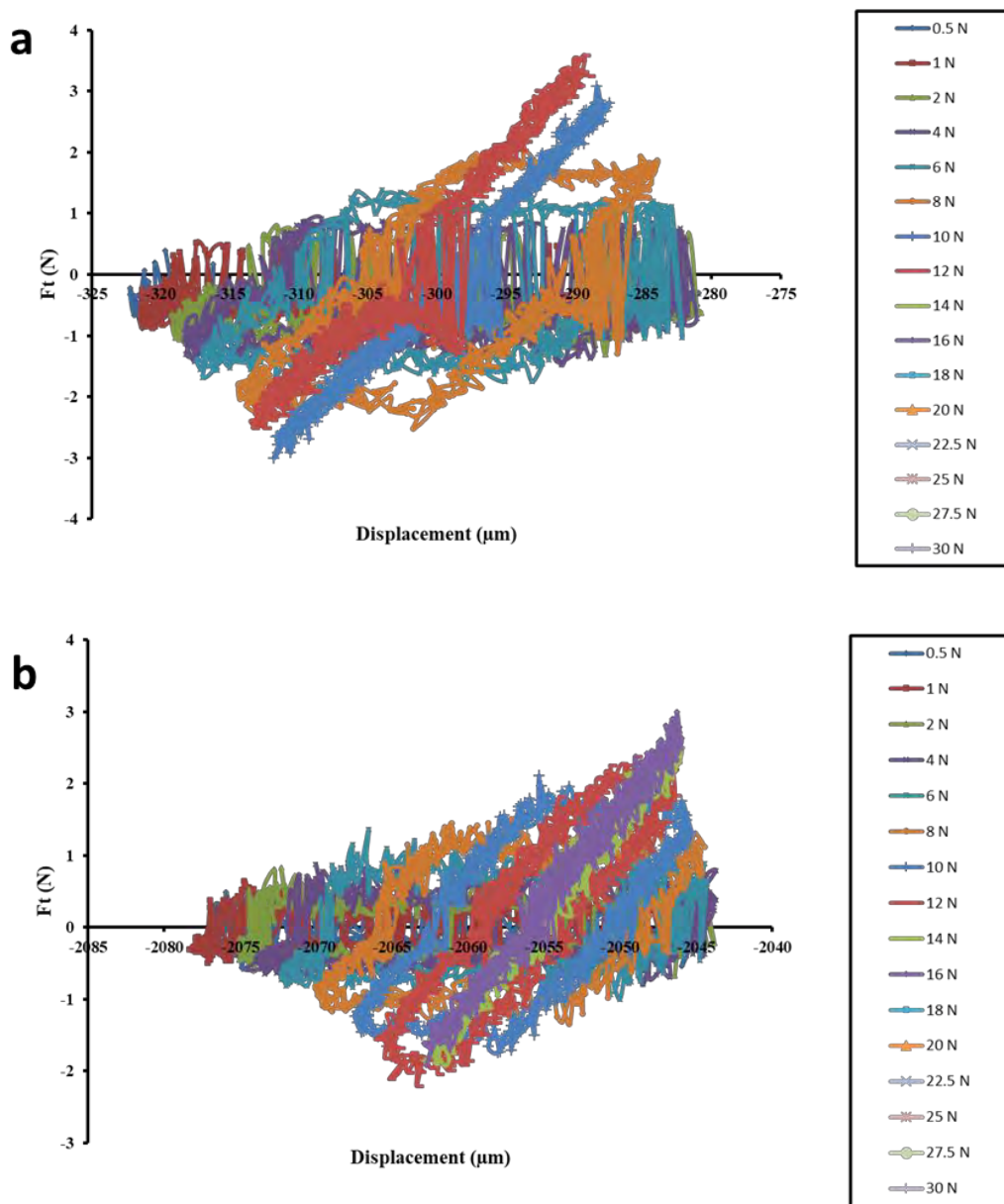


Figure 74: Representative tangential force vs. displacement graph for a) PEEK/Ti6Al4V and b) PEEK/CoCrMo. At each applied load, fretting motion exhibits a hysteresis loop behavior. The maximum tangential force increases, and displacement decreases during fretting with increasing applied normal load F_N . The maximum normal load where stick happens is reached at 12N for (a) and 16N for (b) which is lower than the maximum load for metal/metal couples.

Figure 74 shows the tangential force vs. displacement for the PEEK/metal couplings. Compared to metal/metal, the transition from slip to stick is quicker and happens at lower loads. As seen in Figure 75, the peak work for PEEK/metal combinations are reached at significantly lower real normal stresses compared to metal/metal combinations. Since the mechanical energy of a single cycle of fretting is directly proportional to the normal load, the magnitude of the maximum work per cycle of fretting is about 1/3 or 1/2 of the work per cycle of fretting compared to the metal/metal couples. Since metal/metal couples continue fretting at higher loads without sticking behavior starting, larger stresses are applied at the pin and disk during the test and we would expect greater damage to the surface before the stability of sticking is reached. The bell-shaped behavior of increase then decrease in work with increasing stress (also increasing load) is seen in all couples (Figure 75). This is due to slip-stick mixed mode beginning at the peak work value. In the first half of the curve, during the rise of the magnitude of work is the slip region. Then the work starts to decrease as displacement of the pin is limited due to mixed slip and stick and the stress keeps rising as the applied normal load is increased. When displacement reaches zero, or when stick happens, there is very little work done per cycle of fretting only because of the pin rocking back and forth. Real normal stress calculation is completed using the real contact area calculated. Figure 76 shows the method of visual inspection and selection of the actual damaged area.

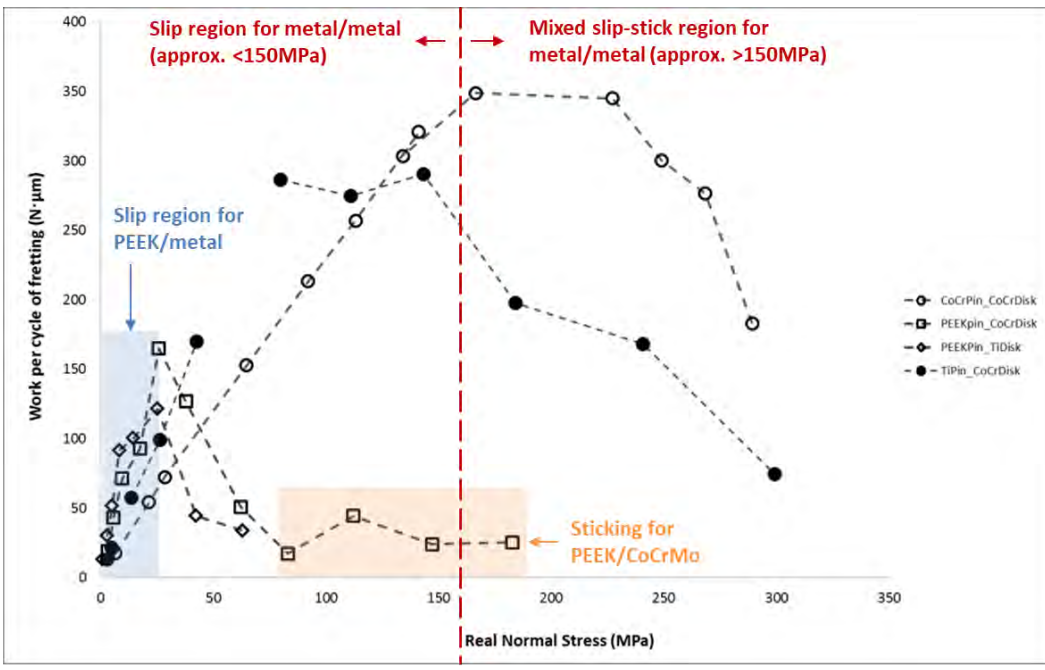


Figure 75: Work per cycle of fretting vs. real normal stress is reported for all material couples. Sticking of the pin on the disk begins at the peak work value. Average values obtained from triplicate tests for each material couple is compiled.

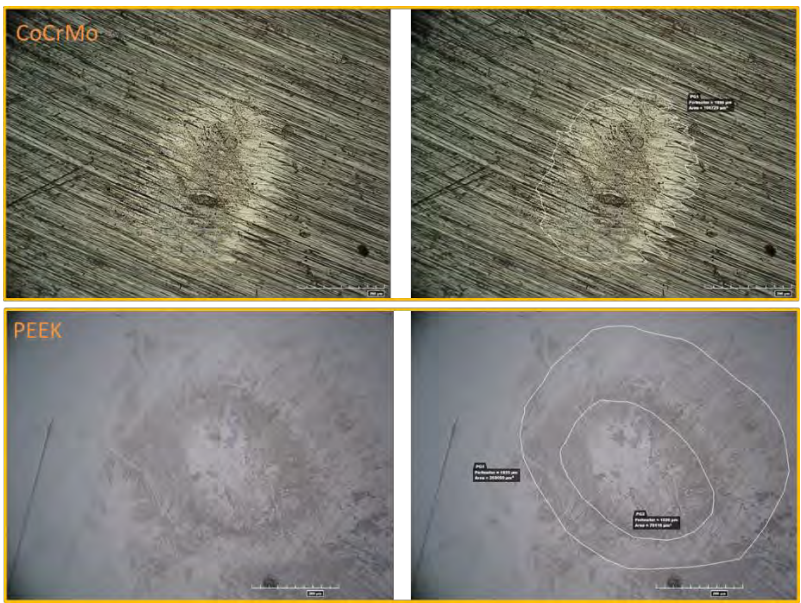


Figure 76: Example damage zones identified on the optical microscope (KH-8700, HIROX) for CoCrMo and PEEK post testing. Damage zones identified based on scratches in different appearance than machining marks. The surface area calculation feature on the microscope is used to find real contact area.

There was no significant difference between the resulting coefficient of friction values for the various couples, which was approximately 0.2 (Figure 77). For all material combinations, COF value were higher at low stresses (between 0.7- 1.3) and then dropped to lower values as applied stress increased. Individual material coefficients of frictions are significantly different, yet this did not seem to affect the interface coefficient of frictions. It is interesting that all coefficients of friction for these pin-on-disk tests resulted in approximately the same value. This would suggest that there is a similar dominating mechanical interaction for sliding between all of these combinations.

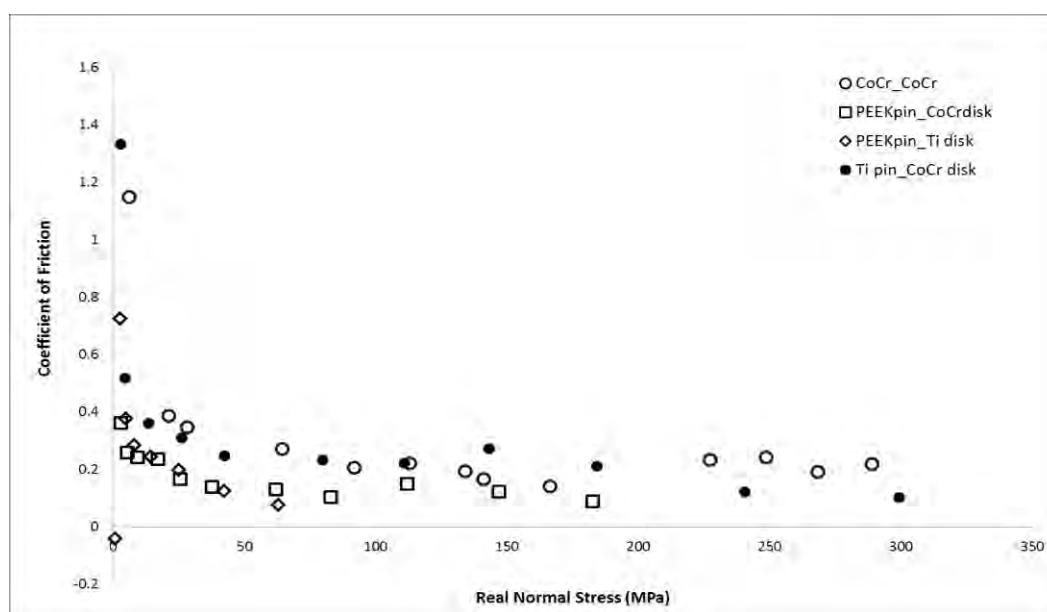


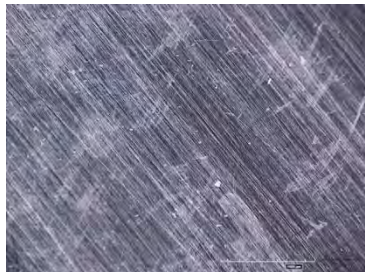

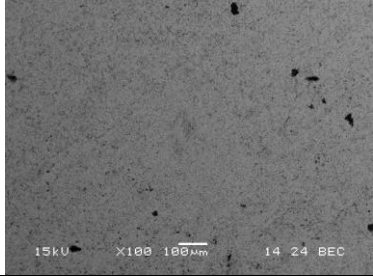

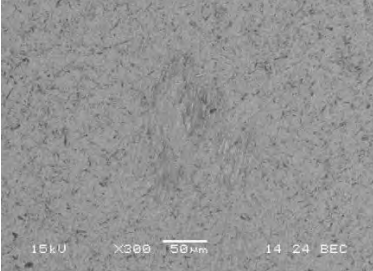
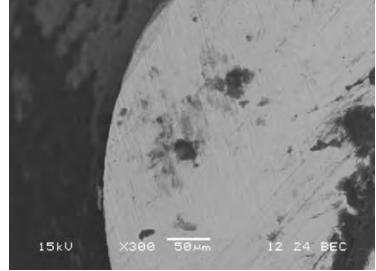
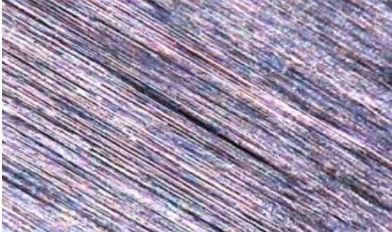
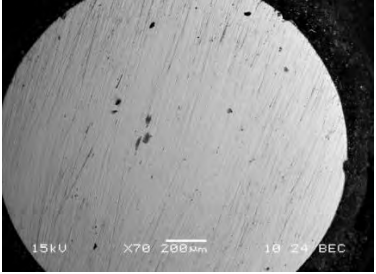


Figure 77: Coefficient of friction (COF) values vs. real normal stress for all material couples. Irrespective of material couple, COF values start higher and decreases quickly in a small range of applied stress and reaches a plateau value. Average values obtained from triplicate tests for each material couple is compiled.

The visual and optical inspection of the disks and pins post-testing showed that there were identifiable fretting-scars for all samples except for the CoCrMo disks tested with PEEK pins (Table XII). Titanium surfaces had galling type damage with potentially greater material loss compared to the scratched surfaces of CoCrMo alloy surfaces. All PEEK pins had some type of tribofilm formation on the surface post-testing. Highly scratched surfaces were inspected in SEM in both SEI as well as the back-scatter electron mode (BEC). BEC mode inspection usually makes corrosion debris look black. When black debris was detected, EDS spectra analysis was run on the identified debris to get composition information. The dark regions in the micrographs represent the corrosion debris composed mostly of oxide particles that are continuously formed and removed from the surface. Figure 78 is showing a typical SEM inspection and representative damage modes seen for PEEK pellets used during the CoCrMo/PEEKpellet/CoCrMo “PEEK pellet sandwich” testing. Figure 79 is showing representative scratching damage for CoCrMo and close-up inspection of debris and the galling type damage seen for Ti6Al4V.

Table XII: Fretting-scars and other surface changes on the disks and pins post-testing.

Material Couple (Disk/Pin)	Disk	Pin
CoCrMo/ CoCrMo		
CoCrMo/ PEEK		
Ti6Al4V/ PEEK		
CoCrMo/ Ti6Al4V		
CoCrMo/PEEK/ CoCrMo		

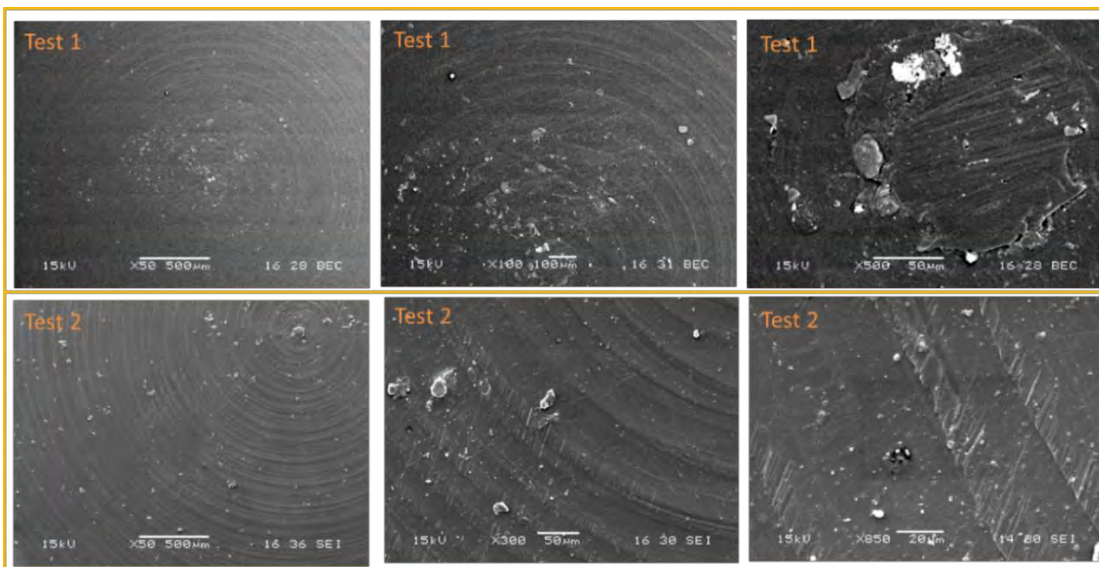


Figure 78: PEEK pellet SEM scratching seen after test 1 and test 2. Different pellets were used for each test. The images above are the same region with different magnification, focusing on the most damaged area.

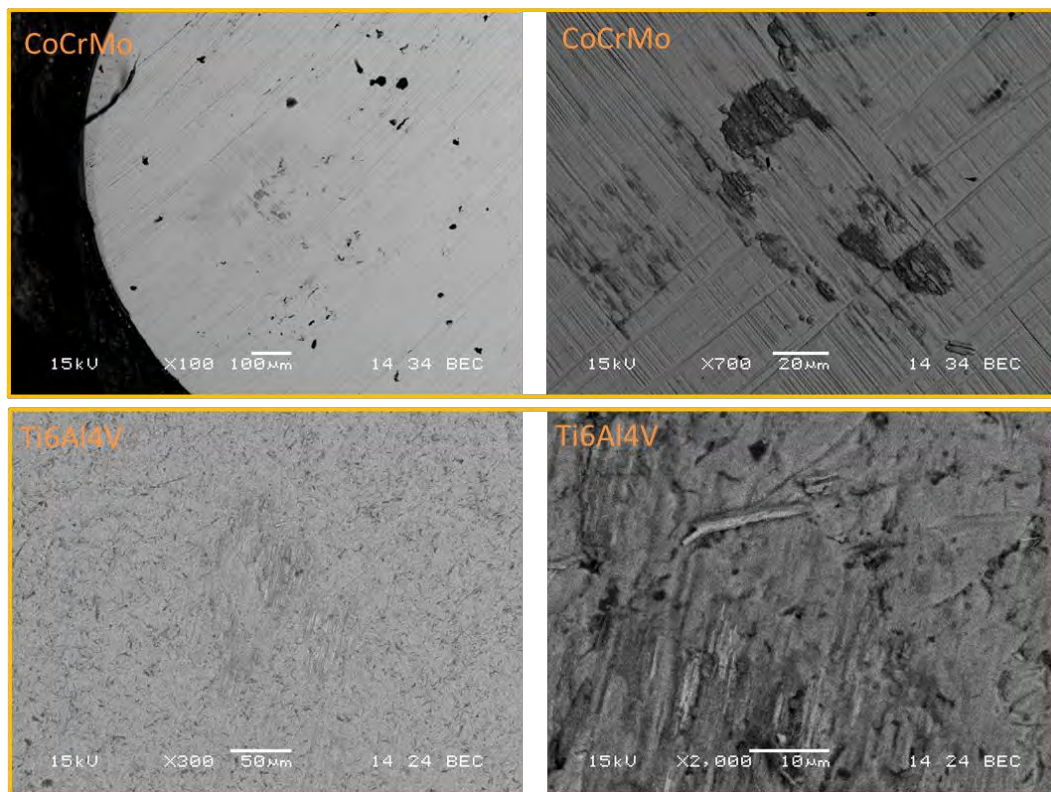


Figure 79: Representative surface scratching for CoCrMo post-test. Representative galling damage for Ti6Al4V post-test.

5.4 Discussion

This study tested and compared the fretting-current responses of different material couples using metal alloy/metal alloy (Ti6Al4V/CoCrMo and CoCrMo/CoCrMo) and PEEK/metal alloy (PEEK/ Ti6Al4V and PEEK/CoCrMo) combinations. A pin-on-disk tester was used to induce clinically relevant mechanical disruption of passive oxide films of titanium alloy and measure the subsequent currents during the repassivation and redevelopment of a new layer of oxide film. The design of total joint replacements uses modular interfaces at various locations in the acetabular and femoral components. The electrochemical POD tester used in this study is ideal for testing the interaction of different material couples that are currently being used in implant modular tapers today and for testing potential implant material combinations for the future. For this testing, only variable load testing of the mentioned material combinations was performed; however, this test setup also allows for testing variable potential and frequencies. The variable loading is intended to simulate the tightness of fit and amount of micromotion under tight vs. loosely fitted femoral head-stem modular taper conditions. The potential variation may occur in crevice conditions due to the change of the pH of the fluids in a crevice environment. It has been shown that

These modular interfaces contain any of the possible metal/metal, metal/polymer and metal/ceramic biomaterial couples. It has been shown that micromotions at these interfaces may lead to disruption of the protective oxide layer on the metal surfaces and subsequently lead to corrosion at these modular connections. The fretting-current behavior of metal/metal interfaces has been extensively studied; yet this is the first study to investigate the fretting-current response of PEEK/metal interfaces which may be an

alternative in future designs. Here, we have shown that using a PEEK/metal interface generates negligible fretting-currents, three orders of magnitude smaller than those generated for metal/metal interface, indicating that the protective oxide layer disruption and subsequent corrosion processes may be significantly lower or even non-existent. This assumption is based on the surface observation of the stick regime at higher normal loads.

This study had some limitations. The fretting-area used to calculate normal stress is not the actual area of the asperity-asperity contact during each test. During the test, the asperity contact areas plowed and scratched the surface of the pin and disk during sliding motion. Also, the estimated nominal area is not measured after each load. It would be expected that the true area of contact and sliding is increasing, and the inter-asperity distance is decreasing with increasing load, peak at a maximum area at a critical load and then decrease until sticking is achieved. The true contact area is smaller than estimated and real stresses would be greater than estimated values. It may be possible to improve the accuracy of these calculations of area by gaining more information about the density and approximate shape of asperities on the surface each material according to the surface finish (Figures 80 and 81).

Another limitation of this study is that it is an *in vitro* study, and an estimation of *in vivo* conditions is created during this test. The pin-on disk setup is not designed to simulate the exact geometry of the materials that will be in operation and a hip simulator needs to be used in the next validation. The solution used during this test was at room temperature and did not contain any proteins. Researchers have shown that representative of body conditions, possible effect of adding proteins [250].

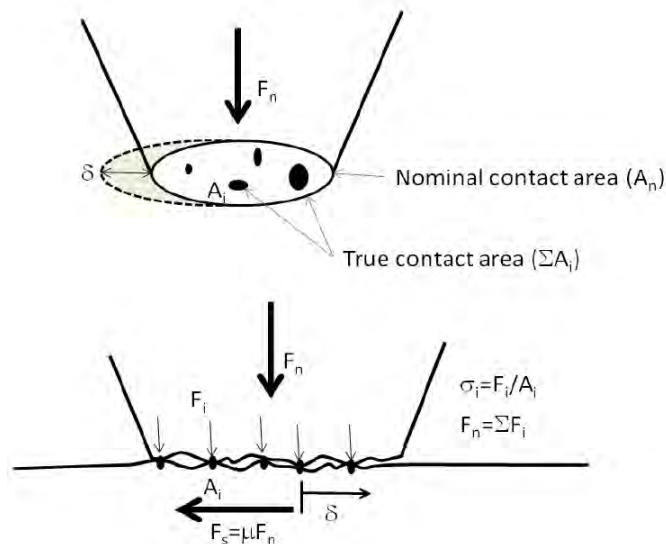


Figure 80: Discrepancy between the true asperity-asperity contact area and the nominal contact area. The nominal contact area is equal to the area of the observed fretting-wear scar post-testing [225].

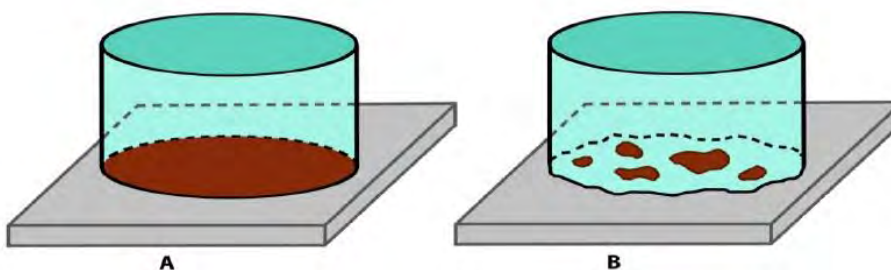


Figure 81: Schematic representation of the pin on disk contact of the pin tip and disk. A) ideal smooth, nominal contact is in brown. B) real asperity-asperity contact area in brown.

Average fretting current densities for the CoCr pin on CoCr disk tests and the Ti pin on CoCr disks (1.01mA/cm^2 and 1.03mA/cm^2 respectively) is consistent with a previous study that used the same test system and same metallic material couples. Swaminathan et al. recorded that when Ti6Al4V is coupled with CoCrMo, currents (0.6mA/cm^2) and COF (0.3), and the fretting corrosion behavior was comparable to

CoCrMo/CoCrMo couple (1.2 mA/cm^2 and COF 0.3) [225]. This study is also consistent with the load dependent COF values that are observed in previous literature [19, 222, 226].

Fretting-displacement is load dependent and decreases with increasing load until stick regime is observed. Under stick regime, surface damage by oxidation and mechanical wear is very limited, no fatigue crack formation is observed and there is low damage fretting [241]. Therefore it is important to understand under what type of conditions interfaces are in stick regime or slip regime. Mixed stick-slip regime and gross slip regime interactions between surfaces lead to fretting and oxidation. The minimum load needed to achieve full stick varied between material couples and was higher for metal/metal couples compared to PEEK/metal; but, eventually, sticking was achieved for all. The tangential force and displacement curves show a clean map of the mode of the elastic sliding response for all loads up to sticking (Figure 82) [170]. Another element of this analysis is the onset load needed to disrupt the oxide layer. Oxide disruption will occur when the local contact stresses reach a critical level for oxide fracture. If the contact stresses do not reach this, then even if there is abrasion, no fretting currents will arise. It is likely that the local asperity contact stresses will always be high enough to induce local oxide film disruption, since even at low loads, the area of contact is likely to be low and the local contact stresses will therefore be high.

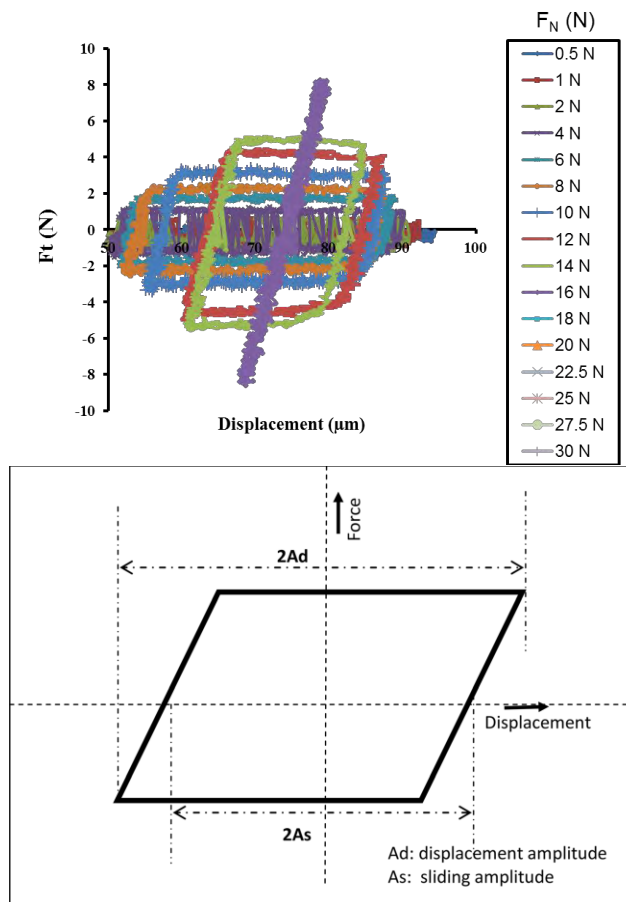


Figure 82: Characteristic elastic-sliding response hysteresis loop (right image, [170]) was observed in the current study (left image). The sliding amplitude at a given normal load can be directly measured from the F_t vs. displacement graph.

The resultant fretting scars were consistent in appearance of fretting scars in the literature [170, 223, 226]. Fretting scars were not observed on pins and disks used in tests with PEEK/metal couples. However, the lubricating film formation seen on PEEK/metal couples were consistent with the self-lubricating property of PEEK and resulting lower material loss is consistent with previous observations [154]. This tribofilm formation is worth exploring in the future and the lack of fretting damage on PEEK/metal couples is consistent with the negligible fretting current density measured during PEEK/metal fretting-corrosion tests. The average fretting current densities for the PEEK pin on CoCr

disk and PEEK pin on Ti disks were $4.2\mu\text{A}$ and $3.2\mu\text{A}$ respectively, three orders of magnitude lower than the metal/metal couples. Currently there are no studies in the literature to compare these values; however, the calculated work done and the observed surface with little or no damages to the corresponding CoCrMo disks. Previous researchers have observed possible tribofilm formation (Figure 83), which has the ability to protect the surface from electrochemical and mechanical damage [170]. Similar patterns of film formation, which may be tribofilm, was only observed on PEEK pins post-testing during this study. While there is need for further investigation about the exact mechanism leading to lower currents at the PEEK/metal interfaces, film formation may be a contributing factor (Figure 84).

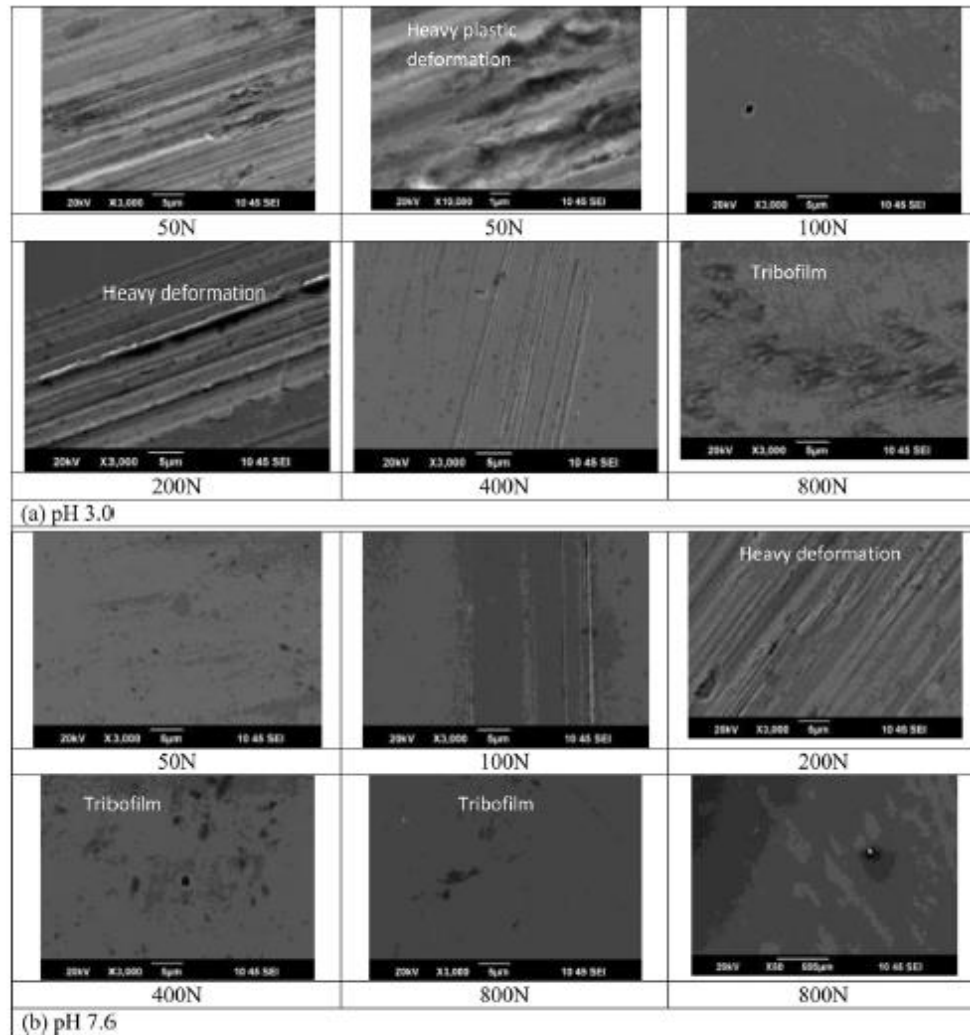


Figure 83: SEM images from a study investigating the effect of load and pH on fretting-corrosion [170]. They have observed tribofilm formation at high loads.

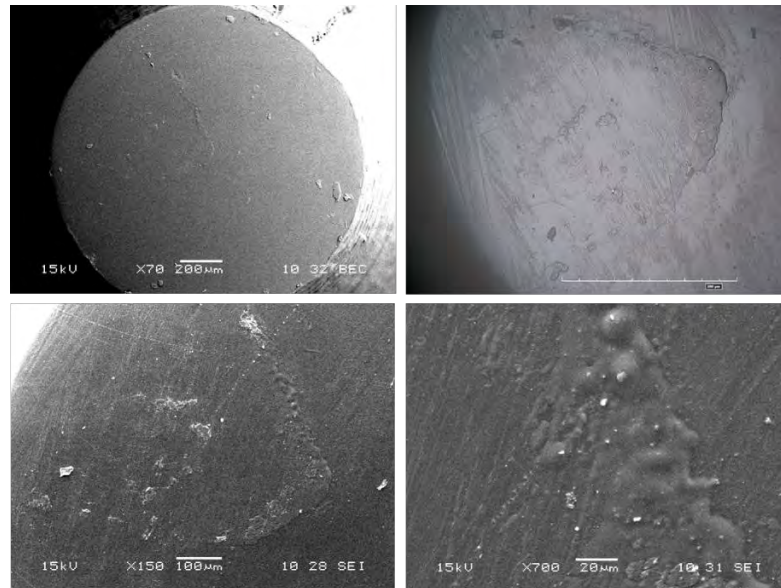


Figure 84: SEM and HIROX microscopy of PEEK pin surface after testing. There appears to be some type of film formation surrounding the surface that has evidence of mechanical wear. The exact composition and process of formation of this film is unknown, let alone the role it plays during the fretting-corrosion tests. We would like to note; however, that we observed this film on all three PEEK pins post testing and on none of the metal surfaces.

There is significant difference between the fretting-current response between the material couples that use a PEEK interface and those that do not. Measurements of current during fretting and subsequent microscopic surface inspection indicates that there was little to no disruption of the passivation film on the surface of the metal disks when they are coupled with a PEEK pin. Subsequent SEM and optical microscopy also did not reveal any visible disruption to the metal surface in the tests using PEEK pins. These visual observations are consistent with the lower fretting current density generated during PEEK/metal couple tests. These preliminary results indicate that PEEK may be a promising biomaterial for use in orthopedic applications to mitigate fretting-corrosion and may be used to design interfaces that are more forgiving to micromotions and vibrations.

References

4. Arnholt C, Underwood R, MacDonald D, Higgs G, Chen A, Klein G, Hamlin B, Lee G, Mont M, Cates H, Malkani A, Kraay M, Rimnac C, Kurtz S. Microgrooved Surface Topography Does Not Influence Fretting Corrosion of Tapers in THA: Classification and Retrieval Analysis. *Modularity and Tapers in Total Joint Replacement Devices*. Conshohocken PA: American Society of Testing Materials (ASTM); 2015.
19. Baykal D. Tribological Assessment of Hydrogels for Replacing Damaged Articular Cartilage. *Biomedical Engineering, Science and Health Systems*: Drexel University; 2013.
32. Boudeau N, Liksonov D, Barriere T, Maslov L, Gelin J-C. Composite based on polyetheretherketone reinforced with carbon fibres, an alternative to conventional materials for femoral implant: Manufacturing process and resulting structural behaviour. *Materials and Design*. 2012;40:148-156.
82. Friedrich K, Kargerkocsis J, Lu Z. Effects of Steel Counterface Roughness and Temperature on the Friction and Wear of Pe(E)K Composites under Dry Sliding Conditions. *Wear*. 1991;148:235-247.
85. Gilbert JL, Buckley CA, Jacobs JJ. In vivo corrosion of modular hip prosthesis components in mixed and similar metal combinations. The effect of crevice, stress, motion, and alloy coupling. *Journal of biomedical materials research*. 1993;27:1533-1544.
94. Goldberg JR, Gilbert JL, Jacobs JJ, Bauer TW, Paprosky W, Leurgans S. A multicenter retrieval study of the taper interfaces of modular hip prostheses. *Clinical orthopaedics and related research*. 2002:149-161.
98. Hall DJ, Pourzal R, Lundberg HJ, Mathew MT, Jacobs JJ, Urban RM. Mechanical, chemical and biological damage modes within head-neck tapers of CoCrMo and Ti6Al4V contemporary hip replacements. *Journal of Biomedical Materials Research. Part B, Applied Biomaterials*. 2018;106:1672-1685.
104. Harper CA, Petrie EM. *Plastics Materials and Processes: A Concise Encyclopedia*: Wiley; 2003.
130. Kocagoz SB, Underwood RJ, MacDonald DW, Gilbert JL, Kurtz SM. Ceramic Heads Decrease Metal Release Caused by Head-taper Fretting and Corrosion. *Clinical orthopaedics and related research*. 2016;474:985-994.
136. Kurtz SM, ed. *PEEK Biomaterials Handbook*: William Andrew - Elsevier; 2012.
137. Kurtz SM, Devine JN. PEEK biomaterials in trauma, orthopedic, and spinal implants. *Biomaterials*. 2007;28:4845-4869.
154. Laux KA, Schwartz CJ. Influence of linear reciprocating and multi-directional sliding on PEEK wear performance and transfer film formation. *Wear*. 2013;301:727-734.
170. Mathew MT, Patel M, Royhman D, Runa MJ, Jacobs JJ, Wimmer MA, Hallab NJ. Tribocorrosion in Hip Modular Taper Junctions: Load-Triggered Transitions in Electrochemical and Mechanical Behavior. In: Greenwald S, Kurtz SM, ed. *STP1591: Modularity and Tapers in Total Joint Replacement Devices*. West Conshohocken, PA: ASTM International; 2015.
189. Ouellette ES, Gilbert JL. Production and characterization of melt-spun Poly(Ether Ether Ketone) fibers for biomedical applications. *Polymer*. 2015;63:10-18.

190. Ouellette ES, Gilbert JL. Properties and Corrosion Performance of Self-reinforced Composite PEEK for Proposed Use as a Modular Taper Gasket. *Clinical Orthopaedics and Related Research*. 2016;474:2414-2427.
205. Pourzal R, Lundberg HJ, Hall DJ, Jacobs JJ. What Factors Drive Taper Corrosion? *Journal of Arthroplasty*. 2018;33:2707-2711.
209. Rodrigues DC, Urban RM, Jacobs JJ, Gilbert JL. In vivo severe corrosion and hydrogen embrittlement of retrieved modular body titanium alloy hip-implants. *Journal of biomedical materials research. Part B, Applied biomaterials*. 2009;88:206-219.
218. Siskey R, Ciccarelli L, Lui MK, Kurtz SM. Are PEEK-on-Ceramic Bearings an Option for Total Disc Arthroplasty? An In Vitro Tribology Study. *Clinical orthopaedics and related research*. 2016;474:2428-2440.
222. Stachowiak GW. 10. Fundamentals of Contact Between Solids. *Engineering Tribology*; 2014.
223. Stachowiak GW, Batchelor AW. 15. Fretting and Minor Wear Mechanisms. *Engineering Tribology*; 2014.
225. Swaminathan V. FRETTING CREVICE CORROSION OF METALLIC BIOMATERIALS: INSTRUMENT DEVELOPMENT AND MATERIALS ANALYSIS. *Biomedical and Chemical Engineering*. Syracuse, NY, USA: Syracuse University; 2012:224.
226. Swaminathan V, Gilbert JL. Fretting corrosion of CoCrMo and Ti6Al4V interfaces. *Biomaterials*. 2012;33:5487-5503.
238. Urban RM, Gilbert JL, Jacobs JJ. Corrosion of modular titanium alloy stems in cementless hip replacement. *Journal of ASTM International*. 2005;2:357-366.
241. Vingsbo O, Soderberg S. On Fretting Maps. *Wear*. 1988;126:131-147.
250. Williams RL, Brown SA, Merritt K. Electrochemical studies on the influence of proteins on the corrosion of implant alloys. *Biomaterials*. 1988;9:181-186.

6 Synthesis and Future Directions

6.1 Summary of work

The aim of this dissertation was to identify the clinical and device risk factors associated with modular taper corrosion and adverse local tissue reactions (ALTR) and to study the taper materials and designs through retrieval studies and in vitro testing.

Historically, the challenges of designing total joint replacements have been related to the mechanical wear in articulating interfaces. It has been shown here that the challenges for the next generation of total hip implants are in resolving the material loss and corrosion in modular interfaces. The mechanisms by which these various products of tribocorrosion lead to ALTR are still a matter of considerable research. ALTRs were first associated with patients with failed metal-on-metal (MoM) surface replacements and large head metal-on-metal LHMOM THA. However, an increasing number of cases of ALTR in metal-on-polyethylene (MoP) THA patients is being reported [97]. It has been shown through studies here and in the literature that tribocorrosion of modular junctions are the cause of ALTR even in modern MoP patients and loosening is still the most prevalent reason for revision in modern designs [10, 231].

After advancements in polyethylene cross-linking led to significantly lower wear debris in MoP [135], modular designs and LHMOM bearings were the next step of advancement in total hip replacements. Modularity allows the surgeon to adjust for excess femoral anteversion, offset and leg length when necessary and to restore the biomechanics of the hip joint independent of femoral fixation [243]. In total knee replacement surgeries, modularity allows for adjustment of polyethylene thickness and degree of constraint, use of the femoral and tibial stems of different lengths, addition of

different inserts such as blocks, wedges, and other devices to restore the level of the joint line and customize the revision associated with lost bone stock.

Adverse reactions due to corrosion and corrosion products released from modular tapers are a relatively new clinical problem compared to bearing wear debris. As stated by the registry for England and Wales, the reported numbers are likely to be underestimated because ALTR was not an option on the revision forms until 2008 [231]. Corrosion and corrosion products have been observed in retrievals and histological samples a few decades prior to 2008, ever since the introduction of modular designs in the 1980s, yet it did not become a clinical concern until the increased popularity of LHMOM and hip resurfacing arthroplasty (HRA) led to reports of poor survival, ALTRs and elevated cobalt and chromium metal ion levels in the blood of patients receiving certain MoM implants [147, 151, 237]. Specifically, the articular surface replacement (ASR) HRA had a higher-than-expected revision rate at 5 years and inferior survival compared to other HRAs or MoM THAs [147]. The ASR HRA and ASR XL THA by DePuy Orthopedics was recalled in 2010. Adverse reactions due to corrosion products may pose the risk of being more severe in adverse tissue reactions compared to wear debris for certain designs of implants [42, 91, 179]. Aseptic loosening and adverse reactions due to fretting-corrosion may not be entirely unrelated phenomena, and corrosion products from tapers may be a contributing factor in loosening in addition to wear debris. Metal hypersensitivity-induced osteolysis and aseptic loosening represent underappreciated and incompletely understood mechanisms of implant failure [123]. The mechanism of taper corrosion is a complex interplay of material, crevice conditions and taper design that results in mechanically assisted crevice corrosion (MACC).

Additionally, inflammatory cell induced corrosion and other biological interactions with taper corrosion are newly being investigated as contributors and are not yet fully understood. Retrievals have at times exhibited more severe and types of corrosion attacks that have been irreproducible in vitro. This suggests the interaction with the biological environment adds more complexity [4, 90].

We started with the thorough examination of the literature for reported design and clinical risk factors causing material loss and corrosion at the femoral head-stem modular taper. There is consensus in the literature that it has become common practice to abandon CoCrMo alloy femoral heads in favor of ceramic heads to minimize the risk of ALTRs due to MACC, especially if a revision is needed due to ALTR [31]. Clinical studies following up on blood metal levels found that patients undergoing revision surgery for ALTR due to MACC show a fast decline of blood metal levels and resolution of symptoms related to ALTR when a ceramic head/titanium sleeve is exchanged with the CoCrMo femoral head. The use of ceramic heads increased from 37% to 53% between 2012 and 2016 among the medical centers participating in the American Joint Replacement Registry. During the same time, the use of metal heads decreased from 60% to 43%. The long-term clinical performance of ceramic heads with modern titanium alloy stems must be followed closely in the coming years [205].

In Chapter 2, I have shared information about the improvement of the fracture resistance of ceramics in the new generation of materials which is the main concern when it comes to ceramic components. Chapter 2 also contains information about the performance of ceramic femoral heads compared with a matched cohort with CoCrMo femoral heads in a retrieval analysis. Retrieval analyses are very valuable and provide the

most direct information about the clinical outcome of a certain design and material, especially when there are statistically significant number of samples to use in a study and the retrievals have carefully documented patient information. Significantly more insights can be gained from a matched cohort multi-institutional retrieval study spanning two decades compared to a case report.

The studies in chapter 3 were designed to address the concerns related to taper angle clearance and toggling leading to movement and initiating fretting-corrosion at the modular taper. This is also one of the first studies to compare ceramic femoral heads and CoCrMo femoral heads in a matched cohort study. Chapter 3 has looked at the location of contact compared to expected location of contact based on taper angle clearance. The damage modes observed in the contact areas such as pitting corrosion attack, fretting and imprinting were consistent with observations by previous researchers [85, 98]. The fact that corrosion damage was seen in taper contact areas and overlapping with mechanical damage confirms mechanically assisted crevice corrosion as a damage mode in the modular tapers; however, there was no correlation between taper angle clearance and corrosion scores for the cohorts in the study.

Chapters 3 and 4 have provided internationally accepted quantitative methods of measuring taper angle clearance and volumetric material loss from taper surfaces. This research is the first to measure taper angle and volumetric material loss from taper junctions with MoP and CoP bearings. This research has also investigated another possible non-corrosive surface as an alternative to metal components, PEEK. Metallic materials and modularity will continue to be used for various applications in vivo. The techniques developed here will help understand materials and design interventions that

can be used to mitigate corrosion at the taper surfaces and to further optimize performance of total hip arthroplasties in vivo. Interfacing metallic surfaces with bioinert ceramic or PEEK surfaces and focusing future design efforts in improving the integration between interfaces to minimize vibrations and movement at the interfaces may significantly help mitigate taper corrosion.

There are some limitations for the taper angle and volumetric material loss measurement techniques presented. Inspection of retrieval surfaces are still highly dependent on a skilled operator for the identification of as-manufactured regions and exclusion of debris from calculations. It is possible to develop an automated technique in the future and improve existing mapping software to exclude these regions if desired by using the surface roughness and specific periodicity of as machined surfaces. Also, for quantification of material loss from any retrieval, enough retained as-manufactured surface is needed for a good estimation of the original shape of the surface prior to use in vivo. If there is significant iatrogenic damage, then the parts need to be excluded from the study. If there is significant level of fretting-corrosion damage over the entire surface, such as intergranular corrosion throughout the entire taper region, then we recommend a different type of inspection [86].

Based on the literature search presented in Chapter 1, in vivo fretting corrosion encompasses a series of processes that are varied and complex [89, 98]. There are common mechanical damage and corrosion types and patterns on retrieval surfaces which enable using the taper angle and material loss calculation methods presented in this body of work; however, every retrieval may not be suitable for this type of inspection. For certain highly severe cases, the entire surface of the taper is damaged with corrosion and

mechanical wear or there is a metallic stem fracture due to the loss of structural integrity. In these cases, the exact value of metallic material loss in vivo is not possible to estimate as accurately due to the loss of all or most as-manufactured surfaces. However, for highly severe cases, accurate estimation of material loss is not as important as determining the cascade of parameters and events that caused the severe damage mechanisms. For highly damaged parts, a closer inspection through sectioning and using SEM and EDS will be more suitable and provide more answers [5, 7, 86]. These detailed inspections and simulations for long term use of the components with various materials and designs will enable the development of improved predictive models for taper designs and materials. The damage modes observed are discussed in further detail in the next section.

6.2 Observed damage modes and proposed mechanisms of fretting-corrosion

Damage modes observed on the male and female taper surfaces of femoral heads and stems can be described as mechanical, electrochemical or composite fretting-corrosion damage. The mechanical damage modes observed in retrievals are a) those that occur during assembly, which are the intended plastic deformation of machining mark peaks during assembly, and b) those that occur during in vivo use, such as fretting marks associated with micro-motions and material transfer. The electrochemical damage modes observed are intergranular corrosion, phase boundary corrosion, pitting corrosion and etching that occur due to changes in the crevice environment during in vivo use. The mechanical and electrochemical damage modes have been observed by themselves or as the synergistic interaction of mechanical and electrochemical damage modes overlapping in the taper, also referred to as fretting-corrosion. These mechanical and electrochemical

damage modes have been reported for the past 25 years in a large number of different types of head and stem taper designs and materials from various manufacturers [85, 94] in retrieval studies in the literature mentioned in section 1.4.3 and the studies in my research. In this section, I will summarize the damage modes we have seen in our studies and compare it with other publications and talk about the potential mechanisms that led to these damage modes in the tapers.

Fretting damage has been reported early on [85] and in recent studies [89] including our own studies in Chapters 3 and 4. It can be difficult to distinguish between actual fretting damage, damage caused by assembly and impaction of the head onto the neck, and damage during revision and disassembly of the head and neck. Fretting is identified as damaged areas with small scars, perpendicular to and interrupting machine lines. Additionally, irregularly shaped, flattened areas containing fretting scars were considered to be indications of fretting [94]. Fretting is a mechanical process during which two surfaces in contact and under some normal cyclic load rub relative to one another in a small-amplitude cyclic fashion (less than 100 μm) [89]. Fretting takes place due to the movement of the head taper surface on the stem taper. There are numerous forces acting on the hip joint that may lead to movement and fretting motion at the head-stem taper interface. During normal daily activity, the ball and socket articulation of the hip and the heel-strike gait leads to variable, repetitive loading at the self-locking head-stem taper [206]. The forces across this taper interface consist of cyclic axial (compressive) loads, torsional moments about the axis of the taper and bending moments perpendicular to the taper axis [89].

Many retrieval studies, including studies in our lab, have observed axially oriented fretting scars and not circumferential fretting (Figure 85). The axial orientation of fretting scars indicate that cyclic axial (compressive) loads have a more significant effect on the loading conditions compared to moments about the axis of the taper (torsional moment) which would lead to circumferential fretting scars [89]. Taper seating and engagement mechanics during assembly and use help to understand fretting motion and the cumulative effects of repeated cyclic loading. The compressive cyclic force arises from the component of the hip joint reaction force in the neck axial direction and acts to continue to seat the head on the neck. These compressive loads can induce fretting motion when the loads approach disengagement conditions and the asperity-asperity contacts in the taper “slip” by overcoming the frictional and normal forces acting on the surfaces. The joint reaction force, leading to compressive loads, changes during daily activities; however, during single leg stance, the largest component of the load is axial to and compressive on the neck. The moments that give rise to these forces are affected by factors like patient weight, activity, and motion, and they potentially may be influenced by design parameters like head offset, coefficient of friction (COF), and possibly head size [89]. These factors will be discussed further in the next section 6.3.

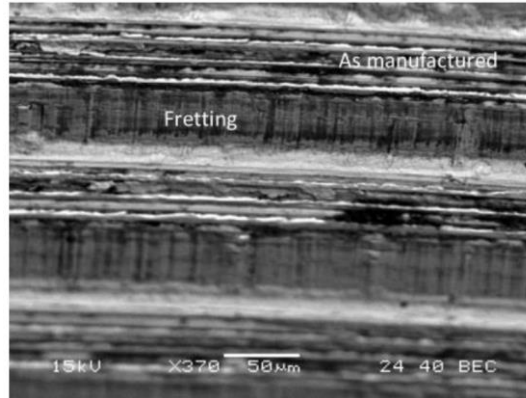


Figure 85: Also Figure 41 from Chapter 3, SEM image taken in distal portion of metal head taper showing fretting in regions with horizontal bands of material loss. Bands of material loss most likely corresponded to regions in contact with trunnion as-manufactured grooves (370x, BEC).

In an aqueous environment, fretting of a metal surface is soon followed by corrosion [84, 89, 94]. If the protective oxide layer is fractured because of fretting, the base alloy is exposed to water and is re-oxidized. The mechanically assisted crevice corrosion model predicts that continuous fretting and oxidation in a crevice environment will lead to a decrease in the open circuit potential as well as a decrease in pH. These changes in turn accelerate the crevice corrosion which may lead to etching and pitting corrosion of the surfaces. There is evidence that fretting, while not the only factor, leads to changes in the solution conditions that may progressively become severe enough to lead to pitting, etching and intergranular corrosion seen in retrievals. These corrosion processes will remove fretting damage from the surfaces. It has been reported that the probability of observing fretting decreases over time which may be explained by the dissolution of fretting damage due to the acidic environment created in the crevice [94]. Pitting damage has been observed in the presence of fretting and inside scratches (Figure 86). We saw pitting in femoral heads implanted with stems with a smooth or

microgrooved trunnion finish and in both the proximal and distal regions (Figures 87 and 88). The simultaneous presence of proximal and distal material loss observed on some metal tapers may indicate toggling motion [22], however, the identification of the mechanism leading to material loss was beyond the scope of this study. In addition to cyclic axial fretting and toggling, cyclic strains on the taper surfaces in the crevice may be large enough to fracture the protective oxide layers. Similar to fretting damage, when continued, this would increase the acidity of the crevice solution due to depletion of oxygen [85] and lead to corrosion. The proximal and distal extremes of the taper contact regions are where bending stresses are likely to be highest. The exact chain of events that led to corrosion in a retrieval taper surface may not be possible to learn through retrospective analysis due to lack of information. Additionally, there are no standardized in vitro tests of modular junctions that have fully reproduced the severity and type of fretting and corrosion processes documented in retrieval studies yet, showing the complexity of these processes [89, 95].

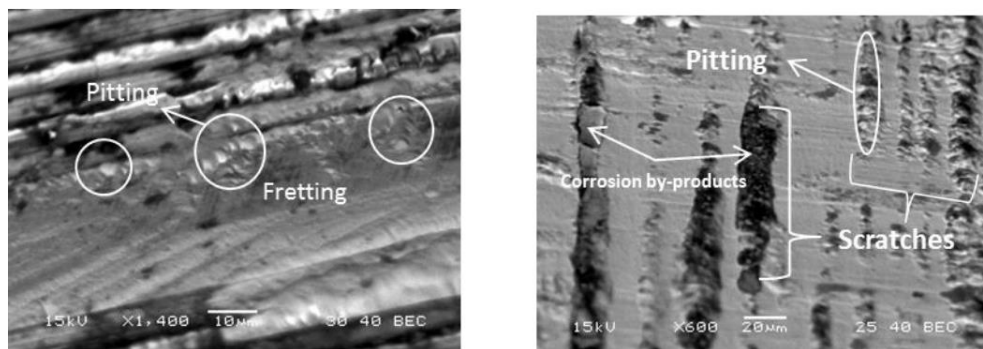


Figure 86: Also Figure 42 from Chapter 3, a component showing pitting corrosion (marked in white circles) initiated preferentially in a crevice formed due to fretting abrasion (5-40µm scratches), imaged midway between proximal and distal ends on the

taper (left, BEC, 1400x). A different component showing scratches (50-500 μ m) throughout head taper, with preferential pitting inside the scratches, imaged midway between proximal and distal ends on the taper (right, BEC, 600x). Corrosion by-products (biological and electrochemical deposits) have accumulated inside the scratches.

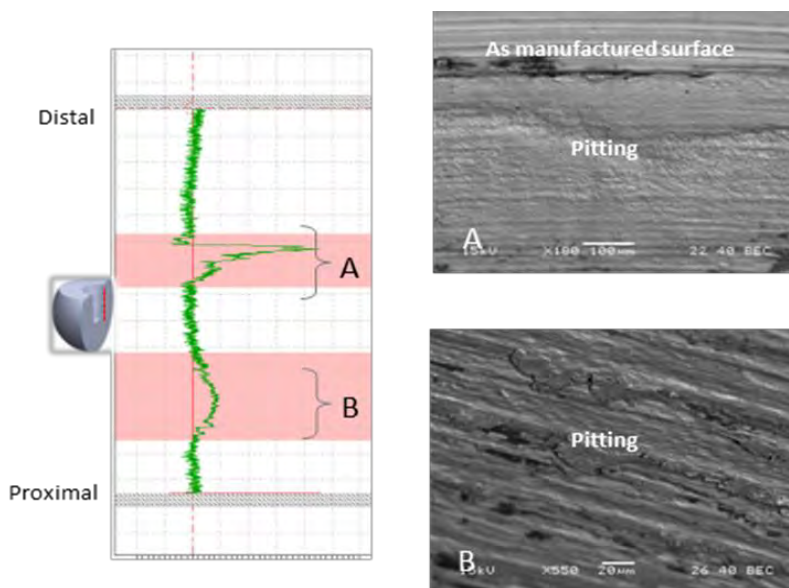


Figure 87: Also Figure 43 from Chapter 3, axial profile of a metal head implanted with a trunnion with a “smooth” finish (left). Regions corresponding to the material loss, marked A and B were imaged using the SEM (right). Both regions of material loss on the Talyrond profile showed evidence of change to the as-manufactured surface.

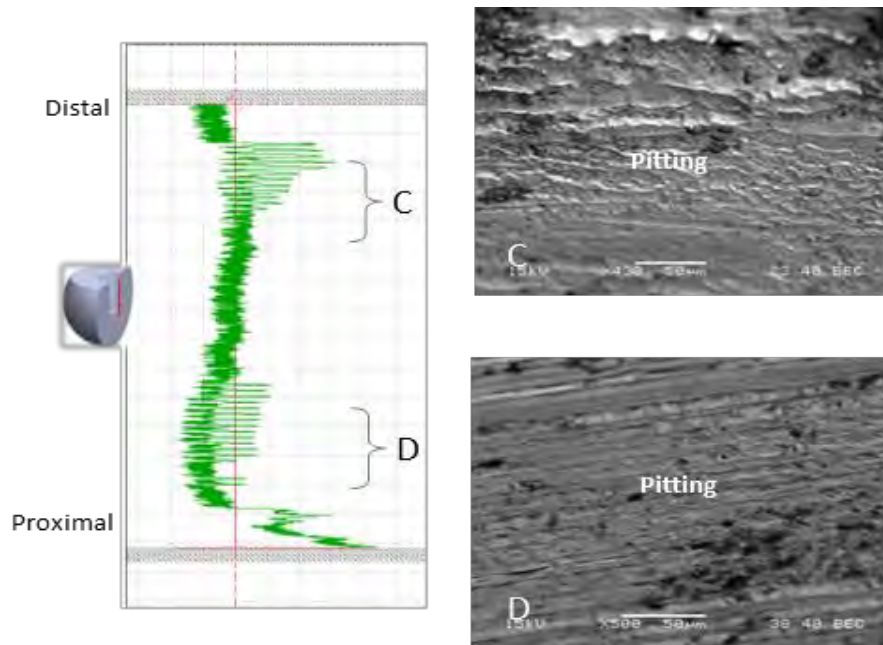


Figure 88: Also Figure 44 from Chapter 3, axial profile of a metal head implanted with a “microgrooved” trunnion finish (left). Regions corresponding to the material loss, marked C and D were imaged using the SEM (right). Both regions of material loss on the Talyrond profile showed evidence of change to the as-manufactured surface.

In addition to the mentioned damage modes above, imprinting and column damage modes are relatively new damage types [194]. These are both concerning and have been investigated by researchers because they can cover large areas of the femoral head taper surface. Column damage has been shown to be highly dependent on the microstructure of wrought CoCrMo alloys. Imprinting on the other hand is a damage mode only seen in femoral heads implanted with stems characterized with a microgrooved surface topography (Figure 89), unlike other modes such as pitting corrosion damage, which has been seen in both smooth and microgrooved head tapers as shown in figures 87 and 88. Other researchers have confirmed that imprinting is independent of stem material and highly dependent on its topography [98]. Historically, relatively smooth finishes were applied to both the male and female tapers, and most previous work has focused on metallurgical, geometrical, and mechanical challenges to

these interfaces; however, smooth taper junctions pose potential problems for unlined ceramic heads and, during impaction, can lead to high local hoop stresses. To decrease the risk of burst fracture of ceramic heads, microgrooving or threading has been applied to the male stem tapers.

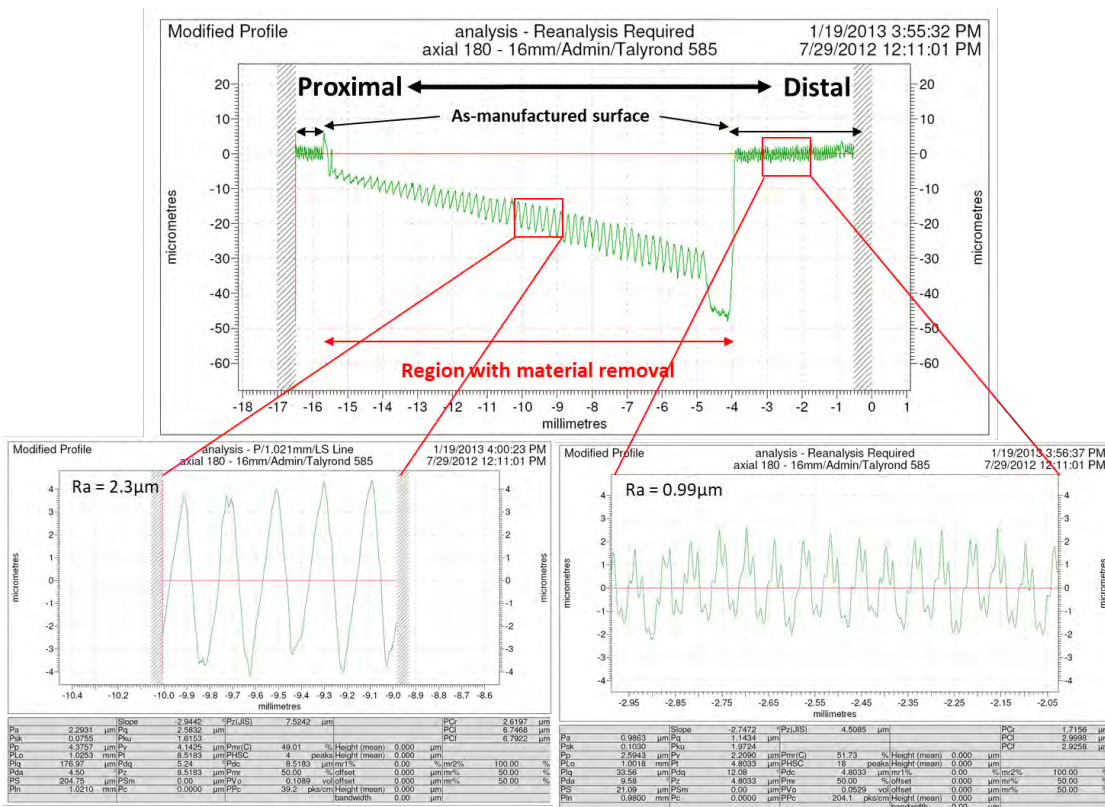


Figure 89: Also figure 46 from Chapter 3, an example femoral head axial profile inspected using the Talyrd software. The regions with material removal and in this case appear like imprinting on the femoral head had a significantly higher surface roughness. The Ra value of the as-manufactured surface was $0.99\mu\text{m}$, and the region with material removal had an Ra value of $2.3\mu\text{m}$.

Imprinting is easily identified as a topographical transition of the smoother as-manufactured surface of the femoral head to a surface with a regular topography of circumferential microgrooves that matches the topography of the stem. As it can be seen in figure 89, the axial profile of a femoral head with imprinting damage shows a change

in the as-manufactured surface with the Ra value of $0.99\mu\text{m}$, to a region with material removal that had an Ra value of $2.3\mu\text{m}$. The topological transition can also be seen visually and with imaging using the SEM as shown in figure 90. Figure 90 also shows the axial profile from a matched head and stem couple. When the two profiles are compared, it is seen that the region with material loss on the femoral head has the same Ra value as the stem profile. Other studies have also observed that that the topography of the imprinted surface matched the machining mark topography of the stem taper. They have also observed that the penetration depth was higher in the distal area and gradually decreased in the proximal direction (Figure 91, [98]). The gradual decrease in penetration depth from distal to proximal was consistent with the imprinting damage modes observed in our study as seen in Figure 89. Aldinger et al. have attempted to simulate imprinting damage and compare the test specimens, which did exhibit simulated imprinting at the end of their test, with retrievals. They also report that maximum material loss occurred on the distal inferior side of the head taper for all samples [3] as have studies that looked at axial profiles from retrievals of LHMOM femoral head surfaces [237]. Greater severity of corrosion damage in the distal region has been observed prior to the observation of imprinting damage and been reported. They have attributed the higher severity in the distal end to being the location where fluid ingress, mechanical loading and the effects of crevice geometry combine to produce the most aggressive corrosive environment [94].

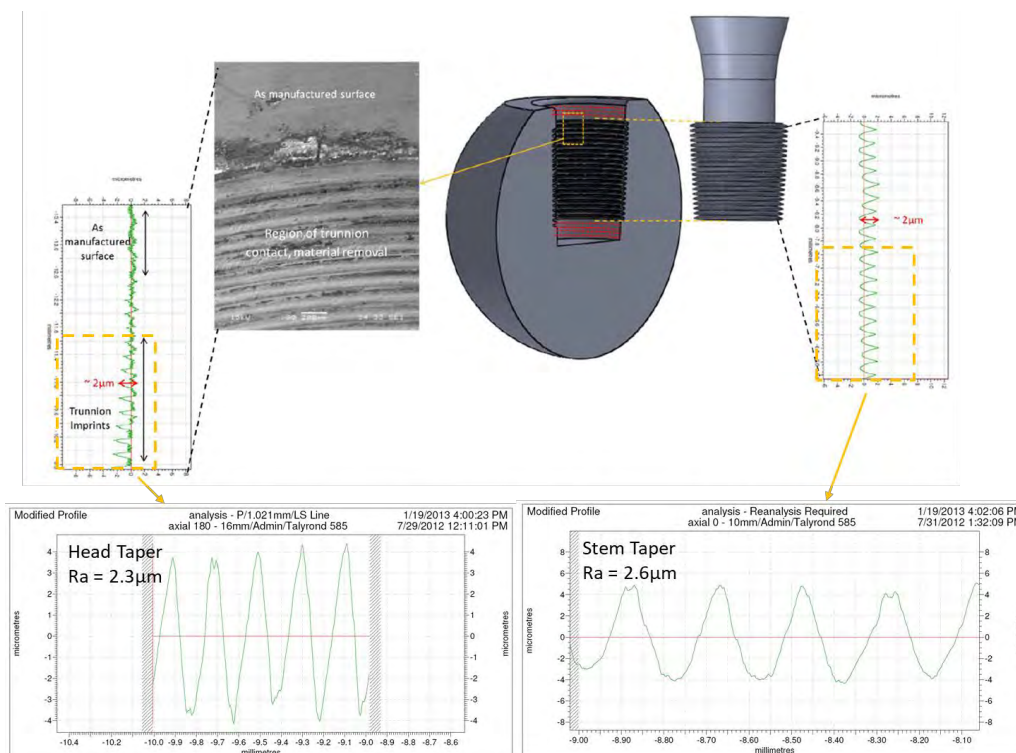


Figure 90: Schematic diagram showing the taper-trunnion interface and typical SEM image and measured profiles from head taper mated with microgrooved trunnion. The red dotted lines represent locations used for roundness profile measurements. The profile of the regions that appear like imprinting on the femoral head was compared with the stem axial profile. They had very similar profiles, both with a topography amplitude of $\pm 4\mu\text{m}$ and similar surface roughness. The region with material removal on the femoral head (same from Figure 46) had an Ra value of $2.3\mu\text{m}$ and the stem profile had an Ra value of $2.3\mu\text{m}$.

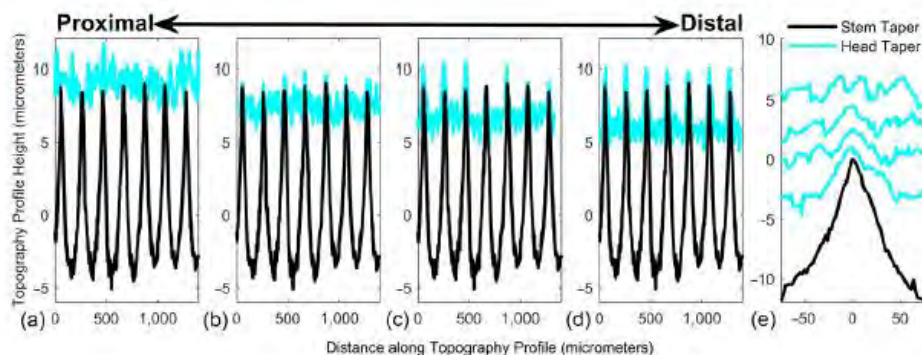


Figure 91: Published by Hall et al. 2018 [98], comparison of the initial stem taper topography (black) with the head taper topography (blue) showing imprinting has shown matching of the imprinting pattern with the stem taper topography. They also observed higher imprinting damage in the distal end of the taper and gradual decrease along the axis towards the proximal end.

Imprinting has been observed in both Co/Co and Co/Ti material couples in our study as well as other literature. The occurrence of imprinting of the softer Ti-alloy onto the hard CoCrMo has been unexpected and widely discussed in the literature. There have been different theories proposed about the mechanism that leads to imprinting damage including chemically dominated corrosion [240], mechanically dominated fretting process [95] and the mechanism also linked to local hardening of the titanium alloy due to oxide formation [182]. In the study by Van Citters et al., they studied LHMOM THA retrievals implanted with taper adapter sleeves between the femoral head and stem. The adapter sleeves had a smooth finish on both the female and male surfaces of the sleeve. They only observed imprinting on the female adapter sleeve surface that was in contact with a microgrooved stem surface and no imprinting between the sleeve-head interface which both had smooth finishes. They propose the imprinting observed is an electrochemical reaction driven by the presence of stagnant, high-chloride fluid in roots of the thread form of the stem taper and crevice corrosion that takes place in the fluid filled gaps of the microgrooves. This proposed mechanism is a theoretical explanation based on observation and they mention this mechanism does not preclude micromotion [240]. As mentioned previously in this chapter, fretting damage may get removed as other corrosion damage mechanisms progress. In many cases several damage modes occur simultaneously or consecutively and therefore results in overlapping damage features. The in vitro and retrievals study conducted by Moharrami et al. [182] looked at the differences in hardness of oxide films formed by CoCrMo and Ti alloys under physiological conditions and report a higher hardness for Ti-oxide films. They conclude

that due to this higher hardness, the stem microgrooved surface must have the ability to abrade and penetrate the femoral head surface leading to imprinting damage. However, this study only looked at CoCrMo and Ti alloy couples and the Ti-oxide hardening mechanism does not explain why imprinting damage is also seen on CoCrMo/CoCrMo couples.

Hall et al. [95, 98] looked at CoCrMo heads implanted with CoCrMo stems and show that an actual imprinting process took place, where the hills of the deeper stem topography appeared to dig into the head taper surface, thus approaching a negative copy of the stem surface on the head. Their SEM investigation of the taper couple that exhibited early localized imprinting further confirmed that the initial damage process of imprinting was purely driven by fretting. Most of the fretting damage they observed occurred on the head surface where contact with the stem taper surface peaks took place. In our retrievals from the CoCrMo vs. ceramic heads study, CoCrMo femoral heads with imprinting show evidence that suggests the fretting-initiated mechanism of imprinting described by Hall et al. took place, as shown in figure 85. Areas that are regressed and have material loss show fretting damage and in between these areas the as-manufactured surface of the head taper is preserved. Additionally, our group observed fretting on the top of the grooves of stem tapers and debris accumulation between the grooves ([143], Figure 95). Another retrieval study by Arnholt et al. [5, 7], with a different set of cohorts also saw evidence of fretting for components exhibiting imprinting damage. They used SEM and focused ion beam (FIB) analysis and revealed a more apparent fretting mechanism in the femoral head bores paired with micro-grooved stems, compared with

the smearing mechanism observed in smooth stems. However, in this study there was no difference in the amount of pitting or fretting within the femoral head bores [7].

From these observations, it can be concluded that fretting damage due to partial slip in the contact between ridges of the stem microgroove peaks led to material loss through fretting-corrosion and imprinting on the femoral head taper surface (Figure 85) [131]. The factors that initiate micromotions and fretting damage is due to a combination of material surface and bulk properties, as well as, taper design and surgical factors, discussed in the next section. The head and stem alloys used have different bulk rigidity and surface hardness and alloy material plays a role in the rate of the tribocorrosion process [5, 130]; however, when it comes to imprinting damage, stem topography is the common factor reported among all the studies for either CoCr/CoCr alloy or CoCr/Ti alloy pairs [4, 7, 95, 98, 131, 182, 240]. The effect of surface topography on the severity of taper corrosion and cumulative material loss is summarized in section 6.31.6.

Column damage, characterized by long troughs running parallel to the taper axis and thus perpendicular to the initial machining mark topography, has been shown to be the result of an etching process and strongly linked to the microstructure of wrought CoCrMo alloys. Hall et al. [93] report column damage was a common occurrence that affected large areas and resulted in surface penetration of several tens of micrometers and did not see evidence of any mechanical process linked to the damage pattern (Figure 92). This damage mode has been linked with the microstructure of wrought CoCrMo alloys because of the banding exhibited in the distal-proximal direction resulting from alloy segregations that were characterized by molybdenum depletion attributed to the processing method of the alloy. As this is a relatively recently described damage type, we

did not specifically investigate for column damage in our retrieval studies; however, the description and images of column damage patterns matches the orientation, dimension and spacing of the scratches we reported on a femoral head surface in figure 86 (right image). It is unclear if these scratches in our study are also column damage and needs further investigation. A study by Pourzal et al. [203] investigated the alloy microstructures from retrievals and found that the banding in wrought alloys unfavorably influenced corrosion behavior, independent of manufacturer, compared to a homogenous alloy microstructure. Future retrieval studies need to document and investigate column damage further.

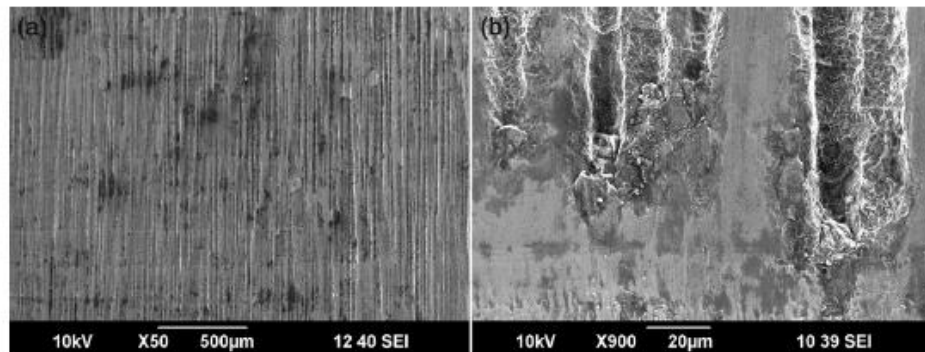


Figure 92: Published by Hall et al. 2018 [95], a) SEM micrograph of column damage on a femoral head taper that is characterized by deep grooves or troughs in proximal distal direction. (b) Close up image on column damage showing the etched appearance within the troughs of the damage pattern. Locally, organic residue has accumulated within the troughs.

6.3 Factors that influence fretting crevice corrosion and recommendations for surgeons and designers

6.3.1 Factors that influence MACC

Mechanically assisted crevice corrosion (MACC) has been well documented and described in the previous sections of this dissertation document. The most common inciting event to MACC is fretting at the head-stem modular interface. The initialization of micromotion and fretting depends on factors that can be separated into implant design, surgical assembly process and patient related factors. These factors act synergistically to determine the seating and asperity-asperity conditions and fretting-corrosion damage mechanisms that take place during in vivo use (Figure 93). Researchers have investigated several implant design related factors and how they affect modular taper corrosion in retrieval, in vitro and finite element analysis studies. Table III in Chapter 1 of this document reviews some of the key factors identified that affects taper corrosion for non-LHMoM THA systems. There is consensus among researchers about some of these while others still need further investigation. The studies conducted and described in this body of work have aimed to analyze the connection between some of these factors that still needed further investigation (such as femoral head material and taper angle clearance/mismatch) and severity of fretting-corrosion damage observed in retrievals. The aim was also to help explain the corrosion mechanisms taking place and make decisions about future design modifications, as shown in Figure 93. Some of the most important factors related to taper fretting-corrosion will be highlighted here with some of the key information gathered from studies. A summary of recommendations to surgeons

and designers based on the observed damage modes discussed in the previous sections and the important implant factors identified are at the end of this section.

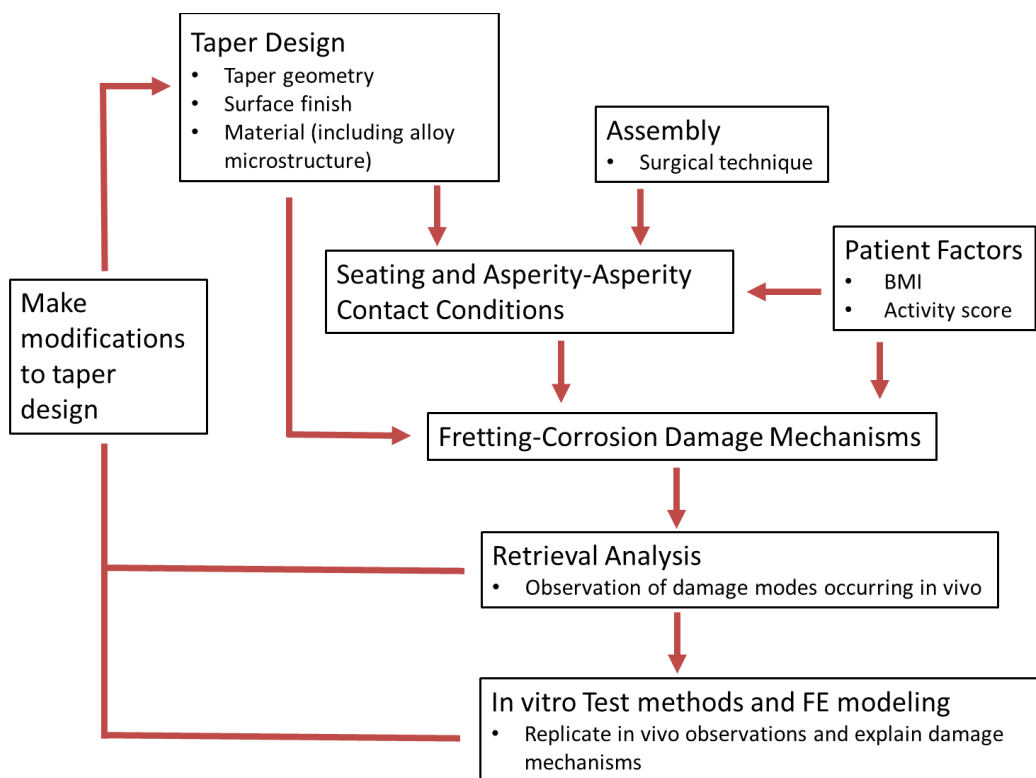


Figure 93: The occurrence of fretting-corrosion damage is multifactorial, dependent on taper design (implant), assembly (surgical technique) and patient factors. The current workflow includes observing these damage mechanisms using retrieval analysis, replicating damage modes and verifying mechanisms using in vitro testing and making modifications to taper designs based on results from retrieval analyses and in vitro tests.

6.3.1.1 Head Material

In our matched cohort retrieval studies comparing ceramic vs. CoCrMo femoral head use, the most effective means to reduce the amount of material loss due to taper corrosion has been shown to be to use ceramic femoral heads. This is the most impactful implant related factor in reducing or preventing cumulative material loss from taper

junctions. This matched cohort study found that the rate of material loss from head-stem tapers in MoP bearings is an order of magnitude higher when compared to head-stem tapers in CoP and CoC bearings. Most of the material lost from modular taper interfaces is from the female tapers of CoCrMo femoral heads and significantly less material loss is measured from the male tapers they are implanted together. This fact supports using ceramic femoral heads as a means of eliminating material loss from the modular head-stem taper interface (Table XI). The higher material loss from the CoCrMo femoral head taper surfaces is consistent with the damage modes observed and discussed in the previous section.

There is mostly agreement from other retrieval studies that ceramic heads are likely to protect from corrosion [31, 120, 228] and that CoCrMo femoral head tapers corrode more than stem tapers [43, 94]. The studies that did not find a significant difference between the taper corrosion severity of THA with ceramic and CoCrMo femoral heads had other confounding factors that were not accounted for in their studies and this was discussed in Chapter 1. Clinical success is reported with the use of ceramic heads whether it serves to reducing overall metallic material loss [130] or exchanging CoCrMo head with a ceramic head/titanium sleeve leading to a decline of blood metal levels and resolutions of ALTR symptoms [201]. Reports show that CoP has surpassed use of MoP [107] and surgeons performing revision for ALTR and corrosion at the head-stem taper prefer replacing the CoCrMo with a ceramic head at revision and place a titanium adapter sleeve on the stem taper [132]. The use of ceramic heads increased from 38% to 68% between 2012 and 2019 among the medical centers participating in the American Joint Replacement Registry. During the same time, the use of metal heads

decreased from 56% to 24% [224]. Ceramic heads with titanium adapter sleeves show good survivability [160, 163] but the long term survivability of ceramic heads with titanium stems needs to be investigated [205].

6.3.1.2 Head Size

Larger femoral heads were an attractive option to reduce dislocation rates and offer increased range of motion without impingement. Theoretically, larger heads (defined as $\geq 36\text{mm}$) lead to increased frictional torque at the modular taper interface and it was suggested that this may lead to higher incident of taper corrosion, especially since the prevalence of ALTR has been linked to the higher revision rate of LHMOM THA systems [121, 236]. It has been reported that LHMOM THAs exhibit a failure rate of 48% after just 6 years with a percentage of failed implants having little or no femoral head-acetabular cup surface bearing wear [152, 162]. However, there are mixed reports about the effect of head size on taper corrosion [41, 69, 70, 74, 144] and ALTR related to MACC has been reported in head sizes of 28 and 32mm as well [130, 201]. The factor of head size alone is not enough to predict the extent of MACC at the head-stem taper and the findings depend on study design and other confounding factors such as increased modularity [109], design [186] and offset. Larger offsets in both negative and positive direction which potentially leads to higher bending was shown to be positively correlated with fretting corrosion. Neutral head offsets showed the least fretting-corrosion damage [41]. This evidence demonstrates that MACC and ALTRs related to MACC are not strictly a large head phenomenon and validates the level of concern surrounding the investigation of MACC in MoP systems [98, 205].

6.3.1.3 Flexural Rigidity

Taper designs have been changing over the years which may influence the damage mode and severity of fretting-corrosion. Porter et al. have shown a shift in the preferred taper size and flexural rigidity being used over time to smaller and more flexible tapers [202]. This is a concern because flexural rigidity has been statistically correlated with higher fretting-corrosion damage in retrieval studies [5, 94]. There is a wide variability in the elastic modulus of the base alloys used as femoral stem material; however, as discussed in Chapter 1, even when controlling for elastic modulus, changes in taper geometry still accounted for a large variability in the flexural rigidity of the trunnion and ranged from 89 to 676 10^9 Nm^2 (Appendix, Table XIII and XIV). Flexural rigidity is the product of the Young's modulus, E (GPa), the stiffness of the alloy material and the second moment of area (I). The second moment of area is a measure of the spread of the area of the cross-section about its bending axis (the center of the stem taper). The calculation of the second moment of area uses the neck diameter (ND) raised to the fourth power (as seen in figure 3, $I = (\pi (\text{ND})^4)/64$). Taper neck diameter was reduced to improve the range of motion of the hip joint [106, 202]; however, this design parameter greatly influences flexural rigidity. Taper geometry modifications need to take into consideration the flexural rigidity to ensure sufficient stiffness for optimal performance under the biomechanical demands in vivo. Our matched cohort study has controlled for flexural rigidity by matching the stem designs and manufacturers [130, 131, 143]. Other retrieval studies have also taken the care to control for this factor [204] as it is recognized as a confounding factor for MACC [121, 205].

6.3.1.4 Implantation Time

Studies looking at retrieval tapers and damage modes all agree that the fretting-corrosion damage taking place is progressive over time [5, 7, 94, 98, 109, 130, 144, 183]. The progressive nature has been explained by the processes related to the mechanical, electrochemical or the synergistic interaction of mechanical and chemical damage modes leading to mechanically assisted crevice corrosion [89, 95]. Each of these damage modes occur under certain contact and electrochemical conditions which may change during the service life of the implant in vivo. To fully understand the mechanism of fretting-corrosion damage for the commonly used taper designs and materials, we need to consider the changes occurring in the asperity-asperity contact conditions and electrochemistry of the aqueous environment in the crevices over time. As discussed in the previous section 6.2, in an aqueous environment, fretting of a metal surface is soon followed by corrosion [84, 89, 94]. If the protective oxide layer is fractured because of fretting, the base alloy is exposed to water and is re-oxidized. The mechanically assisted crevice corrosion model predicts that continuous fretting and oxidation in a crevice environment will lead to a decrease in the open circuit potential as well as a decrease in pH. These changes in turn accelerate the crevice corrosion which may lead to etching and pitting corrosion of the surfaces. These corrosion processes will remove fretting damage from the surfaces. It has been reported that the probability of observing fretting decreases over time which may be explained by the dissolution of fretting damage due to the acidic environment created in the crevice [94]. Retrieval studies are the most reliable source of information for quantification and analysis of damage modes happening in vivo; however, these explants have been removed from the patient due to various factors after

an uncontrolled duration of implantation and use. Valuable information can be gained from retrieval studies designed to isolate device factors by controlling patient and manufacturer information, especially when a large sample size with a wide distribution of implantation time is available. The multicenter retrieval analysis of 231 modular hip implants conducted by Goldberg et al. [94] was specifically designed to investigate the effects of material combination, metallurgic condition, flexural rigidity, head and neck moment arm, neck length and implantation time on corrosion and fretting of modular taper surfaces.

Each retrieved component represents a snapshot of events taking place at the time they were removed. Synthesis of multiple retrieval studies over the last 3 decades looking at the same female and male taper designs by the same manufacturers show different mechanisms of damage depending on the progressive stage of fretting-corrosion severity. Hall et al. refer to their detailed report of imprinting damage and make the distinction between “early” imprinting and later stages of imprinting because it is assumed that the early stages of this damage mode is different and the observable features are changing over time [98]. Pourzal et al. [204] also reported for damage scores 1 to 3, damage is more mechanically driven including cyclic creep, plastic deformation and mechanically dominated fretting. They also report the occurrence of severe damage to head tapers appears to be independent of counter alloy. As discussed previously, there are different mechanisms proposed for imprinting damage and researchers proposing chemically dominated damage mode [240] did not observe fretting damage during their retrieval analysis. The reason could be because the samples they were inspecting were in the later stages of imprinting. Additionally, at the very early stages of imprinting, fretting damage

from the stem taper machining marks may not be associated with imprinting until the damage becomes more severe.

In many cases, several damage modes occur simultaneously or consecutively and therefore one damage mode may enable others over time. For example, widening of the taper crevice due to fretting or imprinting may lead to further infiltration of joint fluid, and subsequently trigger changes in the local pH that initiate corrosive damage modes [95, 98]. One example of consecutive damage modes and changing mechanisms is described in the process that led to gross taper failure (GTF) in the Accolade I stems by Morlock et al. [183]. They describe evidence of imprinting in the female tapers, which also has been observed in other retrieval studies [41, 95, 98, 112, 173] including our matched cohort study detailed in Chapters 3, Figures 45 and 46 [130]. Figure 46 is replicated again in this chapter as Figure 89 and additionally marked to show the proximal and distal regions. As discussed previously, imprinting on a femoral head taper has been shown to be a mechanism for material loss and have the same Ra value as the stem taper grooves (Figures 45, 46). The damage mode observed in the study by Morlock et al. [183] does not fit this description of imprinting, especially since there is consensus that microgrooved stem taper topography leads to imprinting and the Accolade I stems have a smooth surface finish. There is evidence of damage and alteration of the femoral head and stem surfaces and it is proposed that GTF could be the result of gradual material loss due to MACC leading to a progressively loose junction and continued abrasive wear [239]. There were also cases of impending GTF reported [239] indicating the progressively worsening level of abrasion prior to failure and dissociation of the femoral head from the stem as shown in Figure 94. Other researchers have also observed the same

GTF in this specific TMZF (Accolade) stem design [166] and observed all cases of disassociation occurred at greater than 65 months with a minimum of 50 μm of loss at on the head bore which supports the progressively worsening severity of corrosion and material loss. Similarly, in the study by Morlock et al. the components with GTF have the longest implantation times relative to the other Accolade stems that did not exhibit bottoming out. However, other retrieval studies, including our own that have included this exact same stem design in the evaluation (Table XIII), GTF of the stem is not always present with the Accolade TMZF stem [239]. Additionally, GTF has been reported across manufacturers and stem designs and the exact etiology of GTF is unknown [12, 13, 239]. Urish et al. [239] has identified GTF and corrosion at the head-stem interface of THA implanted with the recalled LFIT CoCr femoral heads. The fact that GTF was not seen in an Accolade stem in a certain study may simply mean that the femoral heads used were not manufactured from a recalled lot and less prone to potential progressive loosening of the head-stem interface.

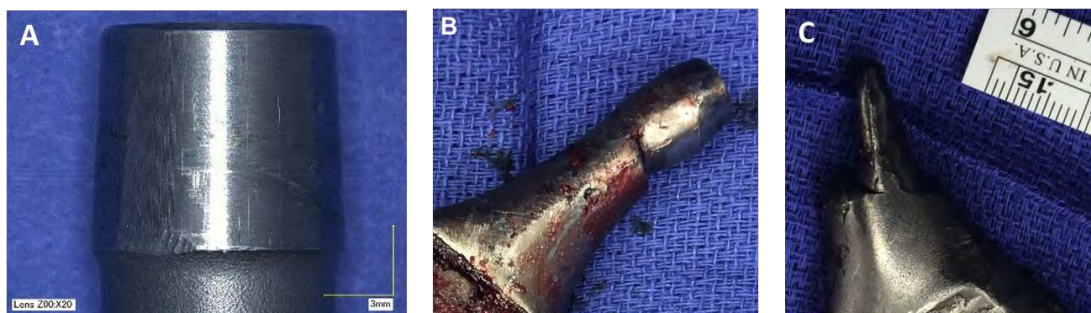


Figure 94: A) Accolade TMZF femoral stem retrieval taper without any signs of GTF, B) Accolade TMZF stem retrieval taper with impending GTF, C) Accolade TMZF stem retrieval taper with a severe case of GTF. Images B and C were published by Urish et al. [239] and image A is from our retrieval studies in chapters 3 and 4.

6.3.1.5 Taper Angle Clearance

There is a consensus that stable and well fitted tapers minimize movement at the head-stem taper [37, 56, 98, 159]; however, there is no clear consensus on the specific taper design parameters such as taper type (11/13, 12/14, Type 1...etc.) or size that prevents fretting-corrosion damage modes. There are reports that thinner and smaller tapers lead to more fretting-corrosion [43, 111, 125, 217, 229]; however, these studies do not control for stem material, flexural rigidity and surface finish. Additionally, the opposite finding is reported in a study that looked at the effect of different taper types on fretting-corrosion in LHMOMs and concluded that thicker tapers with longer contact lengths were associated with greater fretting scores [185]. Chapter 3 describes a quantitative method to measure taper angle using as-manufactured surfaces and we looked at the effect of taper angle clearance on visual corrosion damage scores in a matched cohort study [131]. The matched cohorts allowed controlling for implantation time, stem material, flexural rigidity and surface finish and evaluate the effect of head material and taper angle clearance on fretting corrosion damage scores and later volumetric material loss [130, 143].

Taper angle clearance is positive or negative with proximal or distal engagement respectively [131]. To account for the effect of net clearance we looked at the effect of absolute clearance on material loss and found no correlation. Taper angle clearance was also not correlated with the visual fretting-corrosion scores in the ceramic or metal cohort in our studies. Another study conducted within our research group used a different and larger set of retrievals to investigate the effect of taper type in a controlled study and did not find a correlation between fretting corrosion damage and taper type [111]. One other

study has investigated the effect of device factors and rate of volumetric material loss from LHMOM bearings. In their study, they investigated two types of commercially available designs of LHMOM bearings and found statistically significant ($p < 0.05$) correlations between rate of volumetric material loss and taper angle, head offset, distance (taper engagement level to center of rotation) and horizontal lever arm distance (lateral offset) [152]. The effects of taper angle clearance may not be significant compared to other factors leading to material loss such as head material in our study. Quantitative data provides comparable material loss information for future studies looking at different device and material factors. It may also be used for correlations between systemic cytotoxicity with volumetric material loss.

Some FEA studies found a relationship between taper angle mismatch and taper wear [1, 9, 17, 80] and one study has gone on to develop an FEA routine in which adaptations to the implant geometry are made during the computation to account for material loss during the fretting process. Bitter et al. [24] present a finite element mechanical wear prediction using adaptive meshing at the modular taper interface of hip implants. The study showed that higher assembly forces and smaller mismatches result in the least volumetric material loss [25]. Further studies using retrievals, in vitro testing and in silico investigations using the FE method are needed to understand the multifactorial parameters that lead to a good fit at the head stem taper. Taper angle clearance alone does not provide sufficient information to determine if the contact between two tapers is optimal. Other device, surgical and patient factors may have a more significant effect on fretting-corrosion and material loss.

6.3.1.6 Taper Surface Topography

Among the observed damage modes discussed in the previous section, I had summarized that taper topography played a role in imprinting damage; however, it is unclear if this localized damage mode leads to more severe fretting-corrosion and higher cumulative material loss from the taper surfaces. Currently, there are no ASTM standards that govern the characteristics of trunnion and head taper surface topography, and further work should be directed toward development of such standards. Researchers characterized stem taper surface topography based on wavelength and amplitude and found that the surface topography of stem tapers are highly variable depending on manufacturer and material alloy used [4, 7, 162]. This is consistent with the studies presented in my body of research and we had also reported variable machining on the stem taper surfaces based on alloy and manufacturer; however, this design factor was not a primary study question and underpowered to make statistical conclusions [143], Figure 95). Figure 95 shows a representative group of different design and materials based on manufacturer used in the ceramic head cohort in our study. Accumulation of corrosion debris was observed in black in the grooves adjacent to the fretting damage (Figure 95). Other retrieval studies looked at the effect of stem taper surface topography on MACC and have taken different approaches in the classification system of taper topography and study design. Arnholt et al. [4, 7] have designed a matched cohort study by categorizing taper topographies as smooth or microgrooved based on measurements using a profilometer. Other researchers have characterized surface topography by average roughness [36] or by considering machining mark height as a continuous variable [204]. Both Arnholt et al. and Pourzal et al. excluded the TMZF, Co-Ni-Cr-Mo (A and E in

figure 95, TMZF is also the material for the stems with GTF in the study by Morlock et al. [183] previously discussed under the Implantation Time section) and femoral stems with any other alloys except for CoCrMo and Ti6Al4V alloys. Both studies used the Higgs-Goldberg composite visual fretting-corrosion scoring and Arnholt additionally measured the maximum depth of material loss from the most cases.

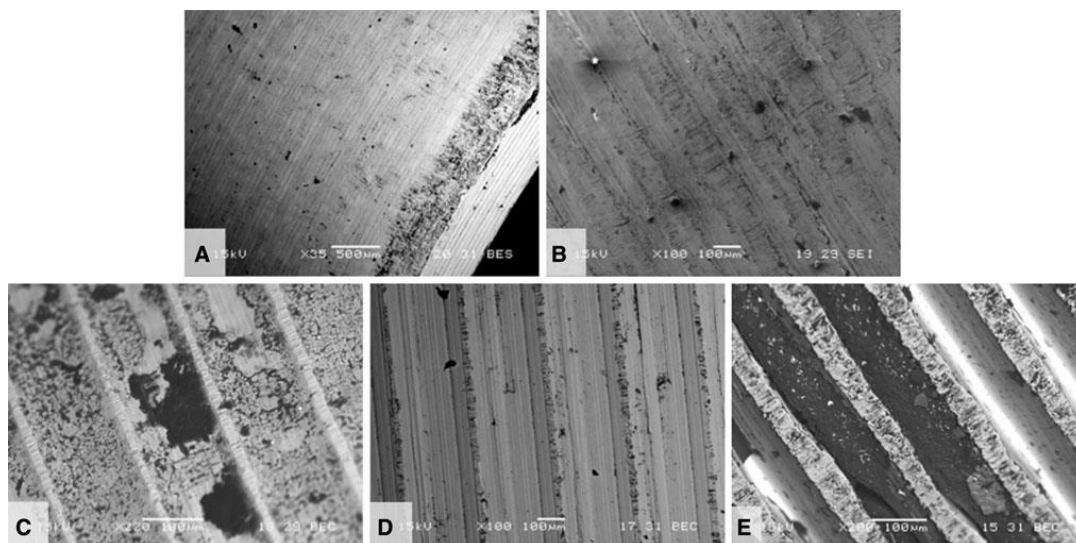


Figure 95: Also published in [143] SEMs of five different design and materials for the male taper of ceramic-metal trunnions. (A) TMZF (Stryker Orthopaedics, Mahwah, NJ, USA) \times 35 BEC, (B) Ti-6Al-4V (Zimmer, Inc, Warsaw, IN, USA) \times 100 SEI, (C) Ti-6Al-4V (Wright Medical Technology, Inc, Arlington, TN, USA) \times 220 BEC, (D) Co-Cr-Mo (DePuy Orthopaedics, Inc, Warsaw, IN, USA) \times 100 BEC, (E) Co-Ni-Cr-Mo (Zimmer) \times 100 BEC. SEI = secondary electron imaging; BEC = backscattered electron contrast image. (A) is a ground surface, whereas (B–E) have machining grooves present. Also shown are fretting scars and corrosion and biological debris present. For grooved implants, only the groove tips show evidence of fretting corrosion damage.

In the study by Arnholt et al. [7], a matched cohort of 120 retrieved head-stem pairs from metal-on-polyethylene bearings was created controlling for implantation time (most important factor), flexural rigidity, apparent length of engagement, and head size. There were two groups of 60 heads each, mated with either smooth or micro-grooved

stem tapers. A high precision roundness machine was used to measure and categorize the surface morphology. They classified stem tapers as micro-grooved if they exhibited a periodic surface profile with a wavelength $> 100 \mu\text{m}$ and an amplitude of $> 4\mu\text{m}$. This study focused exclusively on metal-on-polyethylene hip bearings incorporating a CoCr femoral head and a monolithic femoral stem of CoCr or Ti-6Al-4V alloy, with no other sources of modularity in the head or stem. In this study, the CoCr heads had the same manufacturer as the stems they were implanted with, eliminating manufacturer mixing as a confounding factor. Fretting corrosion damage at the head/neck junction was characterized using the Higgs-Goldberg scoring method. Fourteen of the most damaged heads, were analyzed for the maximum depth of material loss and focused ion beam (FIB) cross-sectioned to view oxide and base metal. The most severely damaged femoral heads ($n=7$ from each cohort, femoral head damage score = 4) did not show a statistically significant difference for maximum depth of material loss between the microgrooved and smooth groups. Their study saw differences in the damage mechanisms between micro-grooved and smooth stems. A more apparent fretting mechanism was observed in the femoral head bores paired with micro-grooved stems, compared with the smearing mechanism observed in smooth stems. However, there was no difference in the amount of pitting or fretting within the femoral head bores. Their study did not find any difference between femoral head fretting corrosion damage and surface morphology in metal-on-polyethylene THAs.

In the study by Pourzal et al. [204] a total number of 70 THAs were evaluated (37 CoCrMo/CoCrMo, 33 CoCrMo/Ti6Al4V). Their study was not exclusively comprised of metal-on-polyethylene bearings. The bearing surfaces of the retrievals were metal-on-

polyethylene (N = 59), metal-on-metal (N = 6), hemiarthroplasty (N = 5). Components with severely damaged stem tapers (score 4) were excluded from this study, because evaluation of the initial surface topography could not be ensured. While the Arnholt study was sufficiently powered, Pourzal report their study had a power of 80% to detect a true difference and further studies need to be conducted with a larger sample size to achieve higher power. They compared the differences in damage scores between the CoCr/CoCr and CoCr/Ti groups and did not find a significant difference in the average damage scores of stem and head tapers between the two material couples. Arnholt et al. did not include femoral stem alloy as a criteria for matching the cohort, because it was not statistically significant in the initial investigation of surface finish [15], or within this study cohort. They instead controlled for flexural rigidity which includes the elastic modulus of the stem material in the calculation. Pourzal et al. found that for CoCr/CoCr stem tapers, machining mark height and time in situ were associated with higher damage scores, but for CoCr/CoCr head tapers, only stem taper machining mark height was associated with higher damage scores. For CoCr/Ti couples, the only factors associated with stem taper damage were head taper roughness and the stem taper machining mark height, whereas only head taper roughness was associated with head taper damage. Unlike the Arnholt study, which did not find any effect of stem taper topography on fretting-corrosion damage, Pourzal et al. conclude that stem taper machining mark height plays a crucial role in modular junction performance, especially for CoCr/CoCr couples, where a higher stem taper machining mark height results in lower damage score over implantation time.

The study by Brock et al. [34] also make a connection between stem taper topography and MACC and found that shorter taper with microgrooves had a higher incidence of fretting-corrosion. This study had multiple confounding factors due to the taper designs being studied and they did not control for these factors other than taper surface topography. Additionally, unlike the studies by Arnholt and Pourzal, this study comprised of explanted tapers from LHMOM THAs (n=104) that were revised due to adverse reaction to metal debris. The heads were mated with either a shorter 12/14, threaded trunnion (n=72) or a longer, smooth 11/13 trunnion (n=32). The abductor moment arm was calculated from pre-revision radiographs. Independent predictors of linear and volumetric material loss included taper angle, stem type, and the horizontal moment arm. They also conclude that design variation appears to play an important role in taper-trunnion junction failure; however, due to the confounding factors, the role of taper topography is unclear.

6.3.2 Recommendations for Assisting Surgical Technique

Studies conducted over the years have demonstrated some key findings regarding the seating mechanics of tapers. High assembly loads and clean taper surfaces are more likely to enable optimum stability [133, 197, 205]. Mali et al. [165] found that poor seating engagement due to a low assembly force resulted in higher micromotion at the head-neck interface and higher measured fretting currents in an in vitro modular taper fretting corrosion test. Heiney et al. [108] showed that an increase in impaction force was associated with higher extraction forces during head pull-off. In a study by Lavernia et al. [155] it was shown that the presence of blood and fat at the taper interface significantly

reduced the extraction forces compared with clean taper interfaces and Pennock et al. [197] demonstrated that the presence of wet contaminants at the interface created unpredictable taper connections.

Surgeons vary widely in their assembly methods, which include the force of impaction, number of impact blows, use or not of other tools, the patient (osteoporotic bone) and other factors. Some advocate for hand tightening or an odd number of strikes with the impaction hammer, whereas others use a single blow.[89] Some studies have quantified the impaction requirements and aimed to provide guidelines to surgeons. Rehmer et al. [208] suggested that sufficient head-taper junction strength in all bearing conditions is achieved by impaction forces of at least 4 kN and a single impact is sufficient to achieve fixation. A fertile area for future research is the establishment of assembly parameters that minimize the propensity for fretting leading to MACC. Less invasive approaches have become widespread, and anterior approaches have become more popular. This makes it more difficult to avoid off-axis impaction, misalignment and maintain a dry and clean environment due to limited visibility [89, 121].

Surgeons can take some preventative steps to minimize or eliminate fretting-corrosion by selecting appropriate designs and optimizing material selection. Surgeons should be aware of implant recalls and be cognizant of ongoing litigation against implant manufacturers. Additionally, many surgeons are choosing to use a ceramic femoral head instead of CoCr heads as discussed previously. Clinical success is reported with the use of ceramic heads whether it serves to reduce overall metallic material loss [130] or exchanging CoCrMo head with a ceramic head/titanium sleeve leading to a decline of blood metal levels and resolutions of ALTR symptoms [201]. Reports show that CoP has

surpassed use of MoP [107] and surgeons performing revision for ALTR and corrosion at the head-stem taper prefer replacing the CoCrMo with a ceramic head at revision and place a titanium adapter sleeve on the stem taper [132]. The surgeon should strive to preoperatively identify the angle and type of taper in the well-fixed stem and request that the proper implants are available for the revision total hip arthroplasty [246].

6.3.3 Recommendations for Improving Modular Taper Design

Designers need to invest in improving the predictive capabilities to test and investigate the complex interactions that initiate and accelerate fretting corrosion at the modular interfaces. These predictive techniques include finite element test strategies; however, these also need to be improved to account for the variable damage modes taking place over time due to the progressive nature of mechanically assisted crevice corrosion. Some researchers have attempted to develop finite element routines that account for the changes taking place over time such as the work by Bitter et al. which adaptations to the implant geometry are made to account for material removal during the fretting process [24, 25]. Lundberg et al. have developed a multiscale FEA model that uses the Young's Modulus of various alloys and ceramic material used for implants to model the deformation and actual contact area of alloy/alloy or alloy/ceramic couples with the variable surface topographies consistent with those measured from retrievals [162]. Other researchers have also stated the importance for determining the actual contact area for the accurate prediction of the fretting regime (slip, partial slip or stick) and determining the ideal contact conditions achieving the best fit [89, 226]. These

improvements to the finite element analysis methods as well as their validation with in vitro techniques, as discussed further in section 6.4, will be crucial tools for designers.

Tests to understand seating mechanics and determination of the asperity-asperity contact area [191, 192] including worse-case loading and corrosive conditions which accelerate MACC and create damage modes and material loss at the level observed on retrieved devices will help optimize materials and designs resistant to in vivo conditions [3, 89]. Additionally, quantitative measurement techniques are critical for post-test evaluation of modular surfaces for the most accurate assessment of the effect of parameters on fretting-corrosion damage. For example, Hall et al. have observed that that in many cases imprinted heads appear entirely clean and shiny, and show little signs of surface damage, but the head taper topography has been almost entirely replaced by the stem taper topography. Such cases can easily be scored as minimally or mildly damaged, even though the amount of material loss due to imprinting may warrant a higher damage score [98]. This finding is consistent with the variability we observed in the visual fretting corrosion scores of the most severely damaged tapers in our studies and these tapers with the most severe damage had a weaker correlation with visual fretting corrosion scores (Figure 60).

6.4 Future Directions

Total hip arthroplasty research is an ongoing and actively clinical field of study. This fact provides the opportunity and the need to study past and present performance of total hip arthroplasty through retrieval studies of both revision and post-mortem surgeries. Retrieval studies are very insightful, especially with the development of quantitative evaluation methods; however, they represent information about failure because revision surgery and post-mortem analysis are most often performed when something went wrong. Statistical evaluation of clinical performance is also highly important for a wider understanding of factors that lead to successful outcomes along the failures in total hip arthroplasty. Scandinavia, the UK and Australia are some countries that have started total joint registries for every patient that has received a hip or knee replacement including information about resurfacing surgeries. They spend resources to maintain, update and publish the data containing patient and device information available through an annual report. Registries can monitor revision rates after total joint replacements using the collected information every year. There has been an initiative to start and grow the American Joint Replacement Registry [224] since 2010 and the number of participating hospitals have grown considerably since; however, there is no national registry in the U.S.A. as of yet [77]. In the future, registries around the globe will continue to provide vitally useful information for the field of orthopedics and initiatives to expand should continue.

While retrieval studies and registries can help us gain information about the implants that are on the market and being clinically used, we need to improve methods of in vitro testing and analytical modeling to evaluate potential new materials and designs.

As mentioned in the previous sections, there are various contributing factors synergistically interacting that may initiate MACC and lead to implant failure. Any new design and material introduced will need to perform under these defined mechanically and chemically demanding conditions. In the past decade, both research types, retrieval analysis and statistical analysis of registries, have been complemented by a significant number of in vitro analysis methods. During literature search for the review in Chapter 1, with the keywords mentioned about taper corrosion, I encountered more publications that used in vitro electrochemical testing and finite element modeling (FEM) compared to retrieval studies even though “in vivo” and “retrieval” keywords were included in the search terms. One reason for the difference in the number of the article types is that it is not easy or possible to setup a multi-institutional, long term, IRB approved implant retrieval program and conduct studies on a statistically significant number of samples for researchers that are new in this field. The interesting fact about the in vitro article type is not only the volume but the rate of increase over the years. This indicates that there is greater interest to try to understand the interaction of asperity-asperity contacts in a biological setting prior to implantation.

The factors that incite micromotion and fretting damage for a combination of design, surgical and patient factors need to be studied further. The current challenges that need to be explored to minimize the impact of MACC are 1) improving predictive capabilities of assessing surface contacts for new designs, 2) prevention of micromotion at the modular junctions and 3) understanding the role of alloy metallurgy in the short and long term survivability and the material interactions with inflammatory cell types.

6.4.1 Improving Predictive Capabilities of New Designs

Total joint arthroplasty (TJA) is a clinically active research field, yet there are continuous efforts that exist outside of the clinic to test material and design iterations. As the value of modularity has been understood for intra-operative success, there is an understanding among the orthopedics community that we need to improve the longevity of modular interfaces. There have been efforts to understand, standardize and improve the in vitro test methods over the past decade. One initiative has been spearheaded by the American Society for Testing and Materials (ASTM) in the Special Technical Papers publications on addressing modularity, LHMOMs, ALTR and implant analysis techniques. In order of release these have been STP 1301: Modularity of Orthopedic Implants (1997) [138], STP 1560: Metal-on-Metal Total Hip Replacement Devices (2013) [139], STP 1591: Modularity and Tapers in Total Joint Replacement Devices (2015) [140], STP 1606: Beyond the Implant – Retrieval Analysis Methods for Implant Surveillance (2018) [141]. The work presented in this dissertation are all relevant to this ongoing effort of improving taper modularity.

The current standard for validating new THA designs is insufficient at detecting the effect of all the factors for taper corrosion and needs to be updated for future generation implant validation [165]. As discussed briefly in section 6.3.3 recommendations for improving modular taper design, predictive capability of in vitro testing needs to be improved because they are valuable for conducting controlled studies for factors that are not possible to measure or control in a clinical setting. For example, the impaction force, controlled contamination and pull-off forces are some variables that in vitro testing provides useful insights pertaining to the effect of surgical technique [67,

133, 191, 213]. These insights, with further validation, may help develop surgical techniques and tools to assist intraoperative methods and device designs that are more forgiving to variation in surgical technique. Finite element modeling is useful for testing interaction of variables, yet, still needs to be improved [24, 25, 162], as discussed in section 6.3.3, and validated using in vitro tests [8, 9, 187].

The body of work in the previous chapters demonstrated the insights that can be gained from retrievals, especially through quantitative examination methods of taper surfaces, as well as the in vitro tribocorrosion testing using a pin on disk setup to understand the fretting and corrosion in modular tapers. In vitro tribochemical testing methodology is a very valuable resource that will continue to be a key part of new material and design development in the future. The tribocorrosion test setup with a pin on disk (POD) is the most basic setup to observe the electrochemical and mechanical interaction between two surfaces using normal loads and controlled solution and potential conditions. This setup is useful for initial screening material couples, or new materials or coatings for their performance in a simulated biological environment under fretting-corrosion conditions. The next level of testing in vitro is conducted with hip simulators [165, 191], which are better for estimating the assembly conditions and applied mechanical loads in vivo. Hip simulators enable testing materials and interfaces with their intended geometries and interacting in configurations as they would be in vivo.

To prevent future designs with vulnerabilities from being released, it will be important to investigate the progressive nature of MACC in vitro by monitoring the changes in contact micromotions and the solution electrochemistry. Understanding the interaction of seating mechanics with the design and materials of the taper surfaces

remains an important question for the improvement of THA as well as TKA modular tapers [169, 191-193, 200, 213]. Ceramic materials have been compared to CoCrMo femoral heads in hip simulators [100]. Hip simulators are actively being used for assessment of taper corrosion including the use of PEEK films [190-192]. Our results for PEEK/metal interfaces using the tribochemical POD tester establishes the basic viability of this material in a comparable setup for future tests. We only tested under variable loading conditions, but other insights can be gained with other variables such as variable potential and solution conditions.

6.4.2 Preventing Micromotion

In the review of damage modes and mechanisms, there was consensus that prevention of fretting will help reduce the severity of MACC and it is important that the implant design and machining tolerances promote seating conditions that minimize the risk of micromotion. Stable fixation in each modular surface [59, 109] as well as the entire implant fixation to bone will help in preventing micromotions and osteolysis in TJR. During the use of ceramic femoral heads for revision surgery, the use of titanium adapter sleeves have been shown to be necessary during revision [76, 79]. This provides an additional modular interface that has been shown to provide good survivability [163], yet, the alternatives with other materials such as PEEK have been proposed for future applications to eliminate additional metal crevices and used as an insulating material for any modular surfaces between metal/metal contacts [189, 190]. Introducing a gasket-like liner, from PEEK or similar chemically inert alternatives, between components can reduce or eliminate both fluid uptake and fretting abrasive processes that disrupt the

oxide layer. Other strategies proposed to prevent fretting include sticky-compliant interface design for which high friction, but compliant, interfaces achieve sticking condition and no micromotions occur [89]. Additionally, there are several strategies proposed to limit bending and frictional torques as discussed in Chapter 1 in detail. The overall fixation of the femoral stem to the bone interface is also an important factor to increase overall stability and minimize micromotions at the modular tapers. In the literature search, I have not encountered any publications that link the stem-bone fixation to head-stem modular taper corrosion in THA; however, material loss from device-bone interface and induced osteolysis [39, 48, 118] and the investigation of improved fixation with both cemented [180] and uncemented components [27, 28, 124] are an important research question with unknowns to reduce micromotions at the device-bone interface during the service life of the implant [181]. Uncemented fixation, which traditionally mostly uses tantalum, is an attractive option because of the elimination of need to use cement, which has risk of releasing particles and adds an intra-operative variable in the TJR procedure [156, 157].

One of the key features of uncemented fixation devices is the porous surface structure that enables osseointegration and fixation with the native bone. It is commonly known from tissue engineering studies that porous structure of biomaterials play a key role in regulating cell response and tissue integration; however, there are still some unknown variables that affect the rate of cell migration into a porous structure [46]. Porous metals can allow for bone ingrowth and avoid stress shielding by reducing stiffness without too high a loss in strength and thus are suitable to be used as bone substitute materials in load-bearing applications. Manufacturing of porous scaffolds with

complex shapes are challenging and the materials that are ideal for this application (tantalum, titanium alloys and PEEK) are expensive; however, some recent publications have manufacturing and tested the osseointegration of porous metallic and PEEK biomaterials for use in orthopedic implants. Wauthle et al. [245] used selective laser melting for the first time to manufacture highly porous pure tantalum implants with fully interconnected open pores. They evaluated the bone regeneration performance of the porous tantalum in vivo using an orthotopic load-bearing bone defect model in the rat femur. After 12 weeks, substantial bone ingrowth, good quality of the regenerated bone and a strong, functional implant–bone interface connection were observed. Compared to identical porous Ti–6Al–4V structures, laser-melted tantalum shows excellent osteoconductive properties, has a higher normalized fatigue strength and allows for more plastic deformation due to its high ductility. Later, the same additive manufacturing technique was used to show the capability of this technology to produce a variety of porous materials and optimized structures for use as orthopedic implants or bone-substituting biomaterials [26]. These techniques are a first step towards a new generation of open porous implants manufactured using selective laser melting.

The widespread use of PEEK in spinal applications has raised interest in improved manufacturing techniques and osseointegration. Additionally, the interest in PEEK is due to its versatility and synthesis of PEEK composites with improved antibiotic properties [71], and functionalization of surfaces and structural changes for improvements in osteoinduction [195]. The optimization of porous scaffold structure to enable cell migration and maintain the required load bearing strength for orthopedic

applications is underway [14-16] and is another possible avenue for a new generation of orthopedic implants that eliminates the use of metals.

6.4.3 Understanding the Role of Alloy Metallurgy

There is variability in the manufacturing of the taper surfaces and the microstructure of both cast and wrought CoCrMo alloy used for components, and it has been shown that implant alloy microstructure is not sufficiently standardized and may dictate specific corrosion modes and increased risk of subsequent metal ion release [95, 196, 203]. There is difference in hardness as well as basic corrosion properties, such as corrosion potential and stability of oxide film, between cast and wrought alloys [95]. There is evidence suggesting that the variation in microstructure is leading to certain types of corrosion damage on the implant surfaces. Column damage is highly dependent on the microstructure of wrought CoCrMo alloys, which can exhibit banding resulting from slight alloy segregations that were characterized by molybdenum depletion. Therefore, column damage may be prevented by avoiding banding of the alloy during the thermomechanical processing [98, 205]. Other microstructural features such as carbides and intermetallic phases were also associated with specific damage patterns such as intergranular corrosion, phase boundary corrosion, and pitting [203]. The volume fraction, type, and size of such hard phases can vary widely and are not specified in the material standards [121, 205]. One retrieval study has demonstrated intergranular corrosion may primarily be associated with cementless cobalt alloy stems with sintered beads. This could be another example of metallurgical changes leading to microstructural changes due to the specific processing required for adhesion of the porous surface [96].

Current studies suggest that a more homogeneous implant alloy microstructure may be a possible strategy to minimize material loss due to corrosion; however, further information is needed about the role of alloy microstructure.

Researchers that have studied corrosion of these CoCrMo and Ti alloys report that very severe chemical (acidic pH) or electrochemical (cyclic anodic potential) conditions were needed to simulate some of these corrosion damage features, such as column damage, *in vitro* [95]. It is unclear if crevice corrosion alone leads to these severe conditions or if reactive oxidative species, which would require the presence of cells, are also contributing to the corrosion in the crevice. The future challenges for all biomaterials research lies in understanding the fundamental interaction between the cell response to the artificially introduced biomaterial whether it is for cell integration as described above or for mitigating adverse inflammatory reactions and systemic manifestations. In the case of taper fretting and corrosion and other particle release from bearing wear in THA, researches have shown that the cell response is variable based on wear particles type, composition, shape [62, 99]. The origin of debris and the electrochemical conditions at the sites of material loss both play a role in determining the physicochemical characteristics of the particles, and thus influence their *in vivo* reactivity. In addition to wear debris the changes in cathodic potential due to fretting-corrosion has been shown to play a significant role in cell viability [117]. Conversely, it has been shown that inflammation within a joint can lead to severe conditions at the surface of the implant and may represent a driving force of corrosion which is not well understood. Leukocytes can produce an array of reactive oxidative species (ROS) which may alter the balance of oxidation and reduction reactions occurring at the surface of the implant and lead to

accelerated corrosion of the metallic implant. The specific inflammatory specie hypochlorous acid (HOCl) has been investigated and has been shown to affect the tribocorrosion behavior of orthopedic alloys [134]. This phenomenon of inflammatory cell-induced corrosion was documented in retrieval studies with evidence on the bearing surface as well as within the taper contact area of cell induced etching damage [90, 98]. Finally, it has been proposed that the process of corrosion cytotoxicity may be exploited in a controlled manner as a targeted therapy for targeting bacterial infection or cancerous cells [126]. Every new variable discovered further supports the fact that fretting corrosion is a complex and varied series of processes. Every variable also brings us closer to understanding the big picture and presents a new opportunity for learning and applying new principles.

References

1. Abdullah KA. Finite element modelling of the neck-stem interface of a modular hip implant for micro-motion study. In: *19th IASTED International Conference on Modelling and Simulation, MS 2008, May 26, 2008 - May 28, 2008*. Quebec City, QC, Canada: Acta Press; 2008:364-369.
3. Aldinger P, Cartner J, Jones B. Validating a Simplified Method for Assessing Total Hip Arthroplasty Taper Corrosion Susceptibility with a 15-Year Retrieval Database. In: Greenwald AS, Kurtz SM, Lemons JE, Mihalko WM, ed. *Modularity and Tapers in Total Joint Replacement Devices*; 2015:113-131.
4. Arnholt C, Underwood R, MacDonald D, Higgs G, Chen A, Klein G, Hamlin B, Lee G, Mont M, Cates H, Malkani A, Kraay M, Rimnac C, Kurtz S. Microgrooved Surface Topography Does Not Influence Fretting Corrosion of Tapers in THA: Classification and Retrieval Analysis. *Modularity and Tapers in Total Joint Replacement Devices*. Conshohocken PA: American Society of Testing Materials (ASTM); 2015.
5. Arnholt C, Underwood R, MacDonald DW, Higgs GB, Chen AF, Klein G, Hamlin B, Lee GC, Mont M, Cates H, Malkani A, Kraay M, Rimnac C, Kurtz SM. Microgrooved surface topography does not influence fretting corrosion of tapers in total hip arthroplasty: Classification and retrieval analysis. In: *ASTM Special Technical Publication*. 2015:99-112.
7. Arnholt CM, MacDonald DW, Underwood RJ, Guyer EP, Rimnac CM, Kurtz SM, Implant Research Center Writing C, Mont MA, Klein GR, Lee GC, Chen AF, Hamlin BR, Cates HE, Malkani AL, Kraay MJ. Do Stem Taper Microgrooves Influence Taper Corrosion in Total Hip Arthroplasty? A Matched Cohort Retrieval Study. *Journal of Arthroplasty*. 2017;32:1363-1373.
8. Ashkanfar A, Langton DJ, Joyce TJ. Does a micro-grooved trunnion stem surface finish improve fixation and reduce fretting wear at the taper junction of total hip replacements? A finite element evaluation. *Journal of Biomechanics*. 2017;63:47-54.
9. Ashkanfar A, Langton DJ, Joyce TJ. A large taper mismatch is one of the key factors behind high wear rates and failure at the taper junction of total hip replacements: A finite element wear analysis. *Journal of the mechanical behavior of biomedical materials*. 2017;69:257-266.
10. Australian Orthopaedic Association. *Australian Orthopaedic Association National Joint Replacement Registry. Annual Report. Adelaide:AOA; 2019*.
12. Banerjee S, Cherian JJ, Bono JV, Kurtz SM, Geesink R, Meneghini RM, Delanois RE, Mont MA. Gross trunnion failure after primary total hip arthroplasty. *The Journal of arthroplasty*. 2015;30:641-648.
13. Bansal T, Aggarwal S, Dhillon MS, Patel S. Gross trunnion failure in metal on polyethylene total hip arthroplasty—a systematic review of literature. *International orthopaedics*. 2020;44:609-621.
14. Basgul C, MacDonald DW, Siskey R, Kurtz SM. Thermal Localization Improves the Interlayer Adhesion and Structural Integrity of 3D printed PEEK Lumbar Spinal Cages. *Materialia (Oxf)*. 2020;10.
15. Basgul C, Yu T, MacDonald DW, Siskey R, Marcolongo M, Kurtz SM. Structure-Property Relationships for 3D printed PEEK Intervertebral Lumbar Cages Produced using Fused Filament Fabrication. *J Mater Res*. 2018;33:2040-2051.
16. Basgul C, Yu T, MacDonald DW, Siskey R, Marcolongo M, Kurtz SM. Does annealing improve the interlayer adhesion and structural integrity of FFF 3D printed PEEK lumbar

- spinal cages? *Journal of the mechanical behavior of biomedical materials*. 2019;102:103455.
17. Baumann AP, Vesnovsky O, Topoleski LDT, Donaldson F, McMinn NLL, Vignola A, Di Prima MA. Specimen Specific Finite Element Models for Predicting Fretting Wear in Total Hip Arthroplasty Tapers. *J Biomech Eng*. 2020.
 22. Bishop N, Witt F, Pourzal R, Fischer A, Rutschi M, Michel M, Morlock M. Wear patterns of taper connections in retrieved large diameter metal-on-metal bearings. *Journal of orthopaedic research : official publication of the Orthopaedic Research Society*. 2013;31:1116-1122.
 24. Bitter T, Khan I, Marriott T, Lovelady E, Verdonschot N, Janssen D. Finite element wear prediction using adaptive meshing at the modular taper interface of hip implants. *Journal of the mechanical behavior of biomedical materials*. 2018;77:616-623.
 25. Bitter T, Khan I, Marriott T, Lovelady E, Verdonschot N, Janssen D. The effects of manufacturing tolerances and assembly force on the volumetric wear at the taper junction in modular total hip arthroplasty. *Computer Methods in Biomechanics and Biomedical Engineering*. 2019;22:1061-1072.
 26. Bobbert FSL, Lietaert K, Eftekhari AA, Pouran B, Ahmadi SM, Weinans H, Zadpoor AA. Additively manufactured metallic porous biomaterials based on minimal surfaces: A unique combination of topological, mechanical, and mass transport properties. *Acta biomaterialia*. 2017;53:572-584.
 27. Bobynd JD, Poggie RA, Krygier JJ, Lewallen DG, Hanssen AD, Lewis RJ, Unger AS, O'Keefe TJ, Christie MJ, Nasser S, Wood JE, Stulberg SD, Tanzer M. Clinical validation of a structural porous tantalum biomaterial for adult reconstruction. *The Journal of bone and joint surgery. American volume*. 2004;86-A Suppl 2:123-129.
 28. Bobynd JD, Stackpool GJ, Hacking SA, Tanzer M, Krygier JJ. Characteristics of bone ingrowth and interface mechanics of a new porous tantalum biomaterial. *The Journal of bone and joint surgery. British volume*. 1999;81:907-914.
 31. Bonner B, Arauz P, Klemm C, Kwon YM. Outcome of Re-Revision Surgery for Adverse Local Tissue Reaction in Metal-on-Polyethylene and Metal-on-Metal Total Hip Arthroplasty. *The Journal of arthroplasty*. 2020.
 36. Brock TM, Sidaginamale R, Rushton S, Nargol AV, Bowsher JG, Savisaar C, Joyce TJ, Deehan DJ, Lord JK, Langton DJ. Shorter, rough trunnion surfaces are associated with higher taper wear rates than longer, smooth trunnion surfaces in a contemporary large head metal-on-metal total hip arthroplasty system. *Journal of orthopaedic research : official publication of the Orthopaedic Research Society*. 2015;33:1868-1874.
 37. Brown SA, Flemming CA, Kawalec JS, Placko HE, Vassaux C, Merritt K, Payer JH, Kraay MJ. Fretting corrosion accelerates crevice corrosion of modular hip tapers. *Journal of Applied Biomaterials (New York)*. 1995;6:19-26.
 39. Bryant M, Hu X, Farrar R, Brummitt K, Freeman R, Neville A. Crevice corrosion of biomedical alloys: a novel method of assessing the effects of bone cement and its chemistry. *Journal of biomedical materials research. Part B, Applied biomaterials*. 2013;101:792-803.
 41. Cartner J, Aldinger P, Li C, Collins D. Characterization of Femoral Head Taper Corrosion Features Using a 22-Year Retrieval Database. *HSS Journal*. 2017;13:35-41.
 42. Chana R, Esposito C, Campbell PA, Walter WK, Walter WL. Mixing and matching causing taper wear: corrosion associated with pseudotumour formation. *The Journal of bone and joint surgery. British volume*. 2012;94:281-286.

43. Chaplin RPS, Lee AJC, Hooper RM. Assessment of wear on the cones of modular stainless steel Exeter hip stems. *Journal of Materials Science: Materials in Medicine*. 2004;15:977-990.
46. Chiu YC, Kocagoz S, Larson JC, Brey EM. Evaluation of physical and mechanical properties of porous poly (ethylene glycol)-co-(L-lactic acid) hydrogels during degradation. *PLoS one*. 2013;8:e60728.
48. Clarke IC, Campbell PA, Kossovsky N. Debris-Mediated Osteolysis. A Cascade Phenomenon Involving Motion, Wear, Particulates, Macrophage Induction, and Bone Lysis In: St. John KR, ed. *STP 1144: Particulate Debris from Medical Implants: Mechanisms of Formation and Biological Consequences* Philadelphia, PA: American Society for Testing and Materials; 1992:7-26.
56. Cook RB, Bolland BJ, Wharton JA, Tilley S, Latham JM, Wood RJ. Pseudotumour formation due to tribocorrosion at the taper interface of large diameter metal on polymer modular total hip replacements. *The Journal of arthroplasty*. 2013;28:1430-1436.
59. Cook SD, Manley MT, Kester MA, Dong NG. Torsional resistance and wear of a modular sleeve-stem hip system. *Clinical materials*. 1993;12:153-158.
62. Crainic AM, Callisti M, Palmer MR, Cook RB. Investigation of nano-sized debris released from CoCrMo secondary interfaces in total hip replacements: Digestion of the flakes. *Journal of Biomedical Materials Research - Part B Applied Biomaterials*. 2019;107:424-434.
67. Danoff JR, Longaray J, Rajaravivarma R, Gopalakrishnan A, Chen AF, Hozack WJ. Impaction Force Influences Taper-Trunnion Stability in Total Hip Arthroplasty. *Journal of Arthroplasty*. 2018;33:S270-S274.
69. de Steiger RN, Hatton A, Peng Y, Graves S. What Is the Risk of THA Revision for ARMD in Patients with Non-metal-on-metal Bearings? A Study from the Australian National Joint Replacement Registry. *Clinical orthopaedics and related research*. 2020.
70. Del Balso C, Teeter MG, Tan SC, Howard JL, Lanting BA. Trunnionosis: Does Head Size Affect Fretting and Corrosion in Total Hip Arthroplasty? *Journal of Arthroplasty*. 2016;31:2332-2336.
71. Delaney LJ, MacDonald D, Leung J, Fitzgerald K, Sevit AM, Eisenbrey JR, Patel N, Forsberg F, Kepler CK, Fang T, Kurtz SM, Hickok NJ. Ultrasound-triggered antibiotic release from PEEK clips to prevent spinal fusion infection: Initial evaluations. *Acta biomaterialia*. 2019;93:12-24.
74. Dyrkacz RMR, Brandt JM, Ojo OA, Turgeon TR, Wyss UP. The influence of head size on corrosion and fretting behaviour at the head-neck interface of artificial hip joints. *Journal of Arthroplasty*. 2013;28:1036-1040.
76. English R, Ashkanfar A, Rothwell G. A computational approach to fretting wear prediction at the head-stem taper junction of total hip replacements. *Wear*. 2015;338-339:210-220.
77. Etkin CD, Springer BD. The American Joint Replacement Registry-the first 5 years. *Arthroplast Today*. 2017;3:67-69.
79. Falkenberg A, Dickinson EC, Morlock MM. Adapter sleeves are essential for ceramic heads in hip revision surgery. *Clinical Biomechanics January*. 2020;71:1-4.
80. Fallahnezhad K, Oskouei RH, Badnava H, Taylor M. An adaptive finite element simulation of fretting wear damage at the head neck taper junction of total hip replacement: The role of taper angle mismatch. *Journal of the mechanical behavior of biomedical materials*. 2017;75:58-67.

84. Gilbert JL. Electrochemical Behavior of Metals in the Biological Milieu. In: Ducheyne P, ed. *Comprehensive Biomaterials*: Elsevier; 2011:21-48.
85. Gilbert JL, Buckley CA, Jacobs JJ. In vivo corrosion of modular hip prosthesis components in mixed and similar metal combinations. The effect of crevice, stress, motion, and alloy coupling. *Journal of biomedical materials research*. 1993;27:1533-1544.
86. Gilbert JL, Buckley CA, Jacobs JJ, Bertin KC, Zernich MR. Intergranular corrosion-fatigue failure of cobalt-alloy femoral stems. A failure analysis of two implants. *The Journal of bone and joint surgery. American volume*. 1994;76:110-115.
89. Gilbert JL, Mali SA, Sivan S. Corrosion of Modular Tapers in Total Joint Replacements: A Critical Assessment of Design, Materials, Surface Structure, Mechanics, Electrochemistry, and Biology. In: Greenwald S, Kurtz SM, ed. *STP1591: Modularity and Tapers in Total Joint Replacement Devices*. West Conshohocken, PA: ASTM International; 2015.
90. Gilbert JL, Sivan S, Liu Y, Kocagöz SB, Arnholt CM, Kurtz SM. Direct in vivo inflammatory cell-induced corrosion of CoCrMo alloy orthopedic implant surfaces. *Journal of Biomedical Materials Research - Part A*. 2015;103:211-223.
91. Gill IP, Webb J, Sloan K, Beaver RJ. Corrosion at the neck-stem junction as a cause of metal ion release and pseudotumour formation. *The Journal of bone and joint surgery. British volume*. 2012;94:895-900.
94. Goldberg JR, Gilbert JL, Jacobs JJ, Bauer TW, Paprosky W, Leurgans S. A multicenter retrieval study of the taper interfaces of modular hip prostheses. *Clinical orthopaedics and related research*. 2002:149-161.
95. Hall DJ, McCarthy SM, Ehrich J, Urban RM, Fischer A, Jacobs JJ, Lundberg HJ, Pourzal R. Imprinting and Column Damage on CoCrMo Head Taper Surfaces in Total Hip Replacements. *ASTM Special Technical Publication*. 2018;STP 1606:131-155.
96. Hall DJ, Pourzal R, Della Valle CJ, Galante JO, Jacobs JJ, Urban RM. Corrosion of modular junctions in femoral and acetabular components for hip arthroplasty and its local and systemic effects. In: *ASTM Special Technical Publication*. 2015:410-427.
97. Hall DJ, Pourzal R, Jacobs JJ. What Surgeons Need to Know About Adverse Local Tissue Reaction in Total Hip Arthroplasty. *Journal of Arthroplasty*. 2020.
98. Hall DJ, Pourzal R, Lundberg HJ, Mathew MT, Jacobs JJ, Urban RM. Mechanical, chemical and biological damage modes within head-neck tapers of CoCrMo and Ti6Al4V contemporary hip replacements. *Journal of Biomedical Materials Research. Part B, Applied Biomaterials*. 2018;106:1672-1685.
99. Hallab NJ. Biologic Aspects of Implant Wear. *Materials for Medical Devices: ASM Handbooks*, ASM International; 2012.
100. Hallab NJ, Messina C, Skipor A, Jacobs JJ. Differences in the fretting corrosion of metal-metal and ceramic-metal modular junctions of total hip replacements. *Journal of orthopaedic research : official publication of the Orthopaedic Research Society*. 2004;22:250-259.
106. Haschke H, Konow T, Huber G, Morlock MM. Influence of flexural rigidity on micromotion at the head-stem taper interface of modular hip prostheses. *Medical engineering & physics*. 2019;68:1-10.
107. Heckmann ND, Sivasundaram L, Stefl MD, Kang HP, Basler ET, Lieberman JR. Total Hip Arthroplasty Bearing Surface Trends in the United States From 2007 to 2014: The Rise of Ceramic on Polyethylene. *Journal of Arthroplasty*. 2018;33:1757-1763.e1751.
108. Heiney J, Battula S, Vrabec G, Parikh A, Blice R, Schoenfeld A, Njus G. Impact magnitudes applied by surgeons and their importance when applying the femoral head onto the

- Morse taper for total hip arthroplasty. *Archives of orthopaedic and trauma surgery*. 2009.
109. Higgs GB, Hanzlik JA, MacDonald DW, Gilbert JL, Rimnac CM, Kurtz SM. Is increased modularity associated with increased fretting and corrosion damage in metal-on-metal total hip arthroplasty devices?: a retrieval study. *The Journal of arthroplasty*. 2013;28:2-6.
 111. Higgs GB, MacDonald DW, Gilbert JL, Rimnac CM, Kurtz SM, Implant Research Center Writing C. Does Taper Size Have an Effect on Taper Damage in Retrieved Metal-on-Polyethylene Total Hip Devices? *The Journal of arthroplasty*. 2016;31:277-281.
 112. Hothi HS, Berber R, Whittaker RK, Blunn GW, Skinner JA, Hart AJ. The Relationship Between Cobalt/Chromium Ratios and the High Prevalence of Head-Stem Junction Corrosion in Metal-on-Metal Total Hip Arthroplasty. *Journal of Arthroplasty*. 2016;31:1123-1127.
 117. Hui T, Kubacki GW, Gilbert JL. Voltage and wear debris from Ti-6Al-4V interact to affect cell viability during in-vitro fretting corrosion. *Journal of biomedical materials research. Part A*. 2018;106:160-167.
 118. Huk OL, Bansal M, Betts F, Rimnac CM, Lieberman JR, Huo MH, Salvati EA. Polyethylene and Metal Debris Generated by Non-articulating Surfaces of Modular Acetabular Components. *The Journal of Bone and joint surgery*. 1994;76-B:568-574.
 120. Huot Carlson JC, Van Citters DW, Currier JH, Bryant AM, Mayor MB, Collier JP. Femoral stem fracture and in vivo corrosion of retrieved modular femoral hips. *The Journal of arthroplasty*. 2012;27:1389-1396.e1381.
 121. Jacobs JJ. Corrosion at the Head-Neck Junction: Why Is This Happening Now? *Journal of Arthroplasty*. 2016;31:1378-1380.
 123. Jacobs JJ, Hallab NJ. Loosening and osteolysis associated with metal-on-metal bearings: A local effect of metal hypersensitivity? *The Journal of bone and joint surgery. American volume*. 2006;88:1171-1172.
 124. Jayasuriya RL, Buckley SC, Hamer AJ, Kerry RM, Stockley I, Tomouk MW, Wilkinson JM. Effect of sliding-taper compared with composite-beam cemented femoral prosthesis loading regime on proximal femoral bone remodeling: a randomized clinical trial. *The Journal of bone and joint surgery. American volume*. 2013;95:19-27.
 125. Kao YYJ, Koch CN, Wright TM, Padgett DE. Flexural Rigidity, Taper Angle, and Contact Length Affect Fretting of the Femoral Stem Trunnion in Total Hip Arthroplasty. *Journal of Arthroplasty*. 2016;31:254-258.
 126. Kim J, Gilbert JL. Cytotoxic effect of galvanically coupled magnesium-titanium particles. *Acta biomaterialia*. 2016;30:368-377.
 130. Kocagoz SB, Underwood RJ, MacDonald DW, Gilbert JL, Kurtz SM. Ceramic Heads Decrease Metal Release Caused by Head-taper Fretting and Corrosion. *Clinical orthopaedics and related research*. 2016;474:985-994.
 131. Kocagoz SB, Underwood RJ, Sivan S, Gilbert JL, Macdonald DW, Day JS, Kurtz SM. Does Taper Angle Clearance Influence Fretting and Corrosion Damage at the Head-Stem Interface? A Matched Cohort Retrieval Study. *Semin Arthroplasty*. 2013;24:246-254.
 132. Koch CN, Figgie M, Jr., Figgie MP, Elpers ME, Wright TM, Padgett DE. Ceramic Bearings with Titanium Adapter Sleeves Implanted During Revision Hip Arthroplasty Show Minimal Fretting or Corrosion: a Retrieval Analysis. *HSS Journal*. 2017;13:241-247.
 133. Krull A, Morlock MM, Bishop NE. The Influence of Contamination and Cleaning on the Strength of Modular Head Taper Fixation in Total Hip Arthroplasty. *Journal of Arthroplasty*. 2017;32:3200-3205.

134. Kubacki GW, Gilbert JL. The effect of the inflammatory species hypochlorous acid on the corrosion and surface damage of Ti-6Al-4V and CoCrMo alloys. *Journal of biomedical materials research. Part A*. 2018;106:3185-3194.
135. Kurtz SM, ed. *UHMWPE Biomaterials Handbook: Ultra-High Molecular Weight Polyethylene in Total Joint Replacement and Medical Devices*: Elsevier; 2009.
138. Kurtz SM, Greenwald S, Lemons J, Mihalko WM, ed. *STP 1301: Modularity of Orthopedic Implants*. West Conshohocken, PA: ASTM International; 1997.
139. Kurtz SM, Greenwald S, Lemons J, Mihalko WM, ed. *STP 1560: Metal-on-Metal Total Hip Replacement Devices*. West Conshohocken, PA: ASTM International; 2013.
140. Kurtz SM, Greenwald S, Lemons J, Mihalko WM, ed. *STP 1591: Modularity and Tapers in Total Joint Replacement Devices* West Conshohocken, PA: ASTM International; 2015.
141. Kurtz SM, Greenwald S, Lemons JE, Mihalko WM, ed. *STP 1606: Beyond the Implant - Retrieval Analysis Methods for Implant Surveillance* West Conshohocken, PA: ASTM International; 2018.
143. Kurtz SM, Kocagoz SB, Hanzlik JA, Underwood RJ, Gilbert JL, MacDonald DW, Lee GC, Mont MA, Kraay MJ, Klein GR, Parvizi J, Rimnac CM. Do ceramic femoral heads reduce taper fretting corrosion in hip arthroplasty? A retrieval study. *Clinical orthopaedics and related research*. 2013;471:3270-3282.
144. Kurtz SM, MacDonald DW, Gilbert JL, Mont MA, Klein G, Chen A, Kraay M, Hamlin B, Rimnac CM. Is Taper Fretting Corrosion a Threat to the Clinical Performance of Large-Diameter Hips with Highly Crosslinked Polyethylene Bearings? In: Greenwald S, Kurtz SM, ed. *STP1591: Modularity and Tapers in Total Joint Replacement Devices*. West Conshohocken, PA: ASTM International; 2015.
147. Laaksonen I, Donahue GS, Madanat R, Makela KT, Malchau H. Outcomes of the Recalled Articular Surface Replacement Metal-on-Metal Hip Implant System: A Systematic Review. *The Journal of arthroplasty*. 2017;32:341-346.
151. Langton DJ, Jameson SS, Joyce TJ, Gandhi JN, Sidaginamale R, Mereddy P, Lord J, Nargol AV. Accelerating failure rate of the ASR total hip replacement. *The Journal of bone and joint surgery. British volume*. 2011;93:1011-1016.
152. Langton DJ, Sidaginamale R, Lord JK, Nargol AV, Joyce TJ. Taper junction failure in large-diameter metal-on-metal bearings. *Bone & joint research*. 2012;1:56-63.
155. Lavernia CJ, Baerga L, Barrack RL, Tozakoglou E, Cook SD, Lata L, Rossi MD. The effects of blood and fat on Morse taper disassembly forces. *American journal of orthopedics (Belle Mead, N.J.)*. 2009;38:187-190.
156. Levine B, Della Valle CJ, Jacobs JJ. Applications of porous tantalum in total hip arthroplasty. *The Journal of the American Academy of Orthopaedic Surgeons*. 2006;14:646-655.
157. Levine BR, Sporer S, Poggie RA, Della Valle CJ, Jacobs JJ. Experimental and clinical performance of porous tantalum in orthopedic surgery. *Biomaterials*. 2006;27:4671-4681.
159. Lieberman JR, Rimnac CM, Garvin KL, Klein RW, Salvati EA. An analysis of the head-neck taper interface in retrieved hip prostheses. *Clinical orthopaedics and related research*. 1994:162-167.
160. Lim S-JMD, Jang S-PMD, Kim D-WMD, Moon Y-WMD, Park Y-SMDa. Primary Ceramic-on-ceramic Total Hip Arthroplasty Using a 32-mm Ceramic Head With a Titanium-alloy Sleeve. *Clinical Orthopaedics & Related Research*. 2015;473:3781-3787.
162. Lundberg HJ, Ha NQ, Hall DJ, Urban RM, Levine BR, Pourzal R. Contact mechanics and plastic deformation at the local surface topography level after assembly of modular

- head-neck junctions in modern total hip replacement devices. In: *ASTM Special Technical Publication*. 2015:59-82.
163. MacDonald DW, Chen AF, Lee GC, Klein GR, Mont MA, Kurtz SM, Taper Corrosion Writing C, Cates HE, Kraay MJ, Rimnac CM. Fretting and Corrosion Damage in Taper Adapter Sleeves for Ceramic Heads: A Retrieval Study. *The Journal of arthroplasty*. 2017;32:2887-2891.
165. Mali SA, Gilbert JL. Correlating fretting corrosion and micromotions in modular tapers: Test method development and assessment. In: *ASTM Special Technical Publication*. 2015:259-282.
166. Martin AJ, Jenkins DR, Van Citters DW. Role of corrosion in taper failure and head disassociation in total hip arthroplasty of a single design. *Journal of Orthopaedic Research*. 2018;36:2996-3003.
169. Mathew MT, Patel M, Royhman D, Runa M, Jacobs J, Wimmer MA, Hallab NJ. Tribocorrosion in hip modular taper junctions: Load-triggered transitions in electrochemical and mechanical behavior. In: *ASTM Special Technical Publication*. 2015:283-302.
173. Matthies AK, Racasan R, Bills P, Blunt L, Cro S, Panagiotidou A, Blunn G, Skinner J, Hart AJ. Material loss at the taper junction of retrieved large head metal-on-metal total hip replacements. *Journal of orthopaedic research : official publication of the Orthopaedic Research Society*. 2013;31:1677-1685.
179. Meyer H, Mueller T, Goldau G, Chamaon K, Ruetschi M, Lohmann CH. Corrosion at the cone/taper interface leads to failure of large-diameter metal-on-metal total hip arthroplasties. *Clinical orthopaedics and related research*. 2012;470:3101-3108.
180. Miller MA, Goodheart JR, Izant TH, Rimnac CM, Cleary RJ, Mann KA. Loss of cement-bone interlock in retrieved tibial components from total knee arthroplasties. *Clinical orthopaedics and related research*. 2014;472:304-313.
181. Miller MA, Terbush MJ, Goodheart JR, Izant TH, Mann KA. Increased initial cement-bone interlock correlates with reduced total knee arthroplasty micro-motion following in vivo service. *Journal of biomechanics*. 2014;47:2460-2466.
182. Moharrami N, Langton DJ, Sayginer O, Bull SJ. Why does titanium alloy wear cobalt chrome alloy despite lower bulk hardness: a nanoindentation study? *Thin Solid Films*. 2013.
183. Morlock MM, Dickinson EC, Günther KP, Bünthe D, Polster V. Head Taper Corrosion Causing Head Bottoming Out and Consecutive Gross Stem Taper Failure in Total Hip Arthroplasty. *Journal of Arthroplasty*. 2018;33:3581-3590.
185. Nassif NA, Nawabi DH, Stoner K, Elpers M, Wright T, Padgett DE. Taper design affects failure of large-head metal-on-metal total hip replacements. *Clinical orthopaedics and related research*. 2014;472:564-571.
186. Nassif NAMDa, Nawabi DHMD, Stoner KM, Elpers MBS, Wright TP, Padgett DEMD. Taper Design Affects Failure of Large-head Metal-on-metal Total Hip Replacements. *Clinical Orthopaedics & Related Research*. 2014;472:564-571.
187. Norman TL, Denen JE, Land AJ, Kienitz DM, Fehring TA. Taper-Trunnion Interface Stress Varies Significantly With Head Size and Activity. *Journal of Arthroplasty*. 2019;34:157-162.
189. Ouellette ES, Gilbert JL. Production and characterization of melt-spun Poly(Ether Ether Ketone) fibers for biomedical applications. *Polymer*. 2015;63:10-18.

190. Ouellette ES, Gilbert JL. Properties and Corrosion Performance of Self-reinforced Composite PEEK for Proposed Use as a Modular Taper Gasket. *Clinical Orthopaedics and Related Research*. 2016;474:2414-2427.
191. Ouellette ES, Mali SA, Kim J, Grostefon J, Gilbert JL. Design, Material, and Seating Load Effects on In Vitro Fretting Corrosion Performance of Modular Head-Neck Tapers. *The Journal of arthroplasty*. 2019;34:991-1002.
192. Ouellette ES, Shenoy AA, Gilbert JL. The seating mechanics of head-neck modular tapers in vitro: Load-displacement measurements, moisture, and rate effects. *Journal of Orthopaedic Research*. 2018;36:1164-1172.
193. Panagiotidou A, Cobb T, Meswania J, Skinner J, Hart A, Haddad F, Blunn G. Effect of impact assembly on the interface deformation and fretting corrosion of modular hip tapers: An in vitro study. *Journal of Orthopaedic Research*. 2018;36:405-416.
194. Panagiotidou A, Meswania J, Hua J, Muirhead-Allwood S, Hart A, Blunn G. Enhanced wear and corrosion in modular tapers in total hip replacement is associated with the contact area and surface topography. *Journal of orthopaedic research : official publication of the Orthopaedic Research Society*. 2013;31:2032-2039.
195. Panayotov IV, Orti V, Cuisinier F, Yachouh J. Polyetheretherketone (PEEK) for medical applications. *Journal of materials science. Materials in medicine*. 2016;27:118.
196. Panigrahi P, Liao Y, Mathew MT, Fischer A, Wimmer MA, Jacobs JJ, Marks LD. Intergranular pitting corrosion of CoCrMo biomedical implant alloy. *Journal of biomedical materials research. Part B, Applied biomaterials*. 2014;102:850-859.
197. Pennock AT, Schmidt AH, Bourgeault CA. Morse-type tapers: factors that may influence taper strength during total hip arthroplasty. *The Journal of arthroplasty*. 2002;17:773-778.
200. Pierre D, Swaminathan V, Scholl LY, TenHuisen K, Gilbert JL. Effects of Seating Load Magnitude on Incremental Cyclic Fretting Corrosion in 5degree40' Mixed Alloy Modular Taper Junctions. *Journal of Arthroplasty*. 2018;33:1953-1961.
201. Plummer DR, Berger RA, Paprosky WG, Sporer SM, Jacobs JJ, Della Valle CJ. Diagnosis and Management of Adverse Local Tissue Reactions Secondary to Corrosion at the Head-Neck Junction in Patients With Metal on Polyethylene Bearings. *The Journal of arthroplasty*. 2016;31:264-268.
202. Porter DA, Urban RM, Jacobs JJ, Gilbert JL, Rodriguez JA, Cooper HJ. Modern trunnions are more flexible: a mechanical analysis of THA taper designs. *Clinical orthopaedics and related research*. 2014;472:3963-3970.
203. Pourzal R, Hall DJ, Ehrich J, McCarthy SM, Mathew MT, Jacobs JJ, Urban RM. Alloy Microstructure Dictates Corrosion Modes in THA Modular Junctions. *Clinical orthopaedics and related research*. 2017;475:3026-3043.
204. Pourzal R, Hall DJ, Ha NQ, Urban RM, Levine BR, Jacobs JJ, Lundberg HJ. Does Surface Topography Play a Role in Taper Damage in Head-neck Modular Junctions? *Clinical Orthopaedics and Related Research*. 2016;474:2232-2242.
205. Pourzal R, Lundberg HJ, Hall DJ, Jacobs JJ. What Factors Drive Taper Corrosion? *Journal of Arthroplasty*. 2018;33:2707-2711.
206. Pruitt LA, Chakravartula AM. *Mechanics of Biomaterials: Fundamental Principles for Implant Design*. Cambridge University Press; 2011.
208. Rehmer A, Bishop NE, Morlock MM. Influence of assembly procedure and material combination on the strength of the taper connection at the head-neck junction of modular hip endoprostheses. *Clinical biomechanics (Bristol, Avon)*. 2012;27:77-83.

213. Shenoy AA, Gilbert JL. In vitro test methods for seating and fretting corrosion behavior of modular metal-on-metal acetabular tapers. *Journal of orthopaedic research : official publication of the Orthopaedic Research Society*. 2020;38:1089-1100.
217. Siljander MP, Gehrke CK, Wheeler SD, Sobh AH, Moore DD, Flierl MA, Baker EA. Does Taper Design Affect Taper Fretting Corrosion in Ceramic-on-Polyethylene Total Hip Arthroplasty? A Retrieval Analysis. *Journal of Arthroplasty*. 2019;34:S366-S372.e362.
224. *The Seventh Annual Report of the American Joint Replacement Registry on Hip and Knee Arthroplasty*, 2020.
226. Swaminathan V, Gilbert JL. Fretting corrosion of CoCrMo and Ti6Al4V interfaces. *Biomaterials*. 2012;33:5487-5503.
228. Tan SC, Lau ACL, Del Balso C, Howard JL, Lanting BA, Teeter MG. Tribocorrosion: Ceramic and Oxidized Zirconium vs Cobalt-Chromium Heads in Total Hip Arthroplasty. *Journal of Arthroplasty*. 2016;31:2064-2071.
229. Tan SC, Teeter MG, Del Balso C, Howard JL, Lanting BA. Effect of Taper Design on Trunnionosis in Metal on Polyethylene Total Hip Arthroplasty. *The Journal of arthroplasty*. 2015;30:1269-1272.
231. The National Joint Registry [NJR] for England W, Northern Ireland and the Isle of Man. *National Joint Registry 15th Annual Report 2018*.
236. Underwood RJ, Kocagoz SB, Smith R, Sayles RS, Siskey R, Kurtz SM, Cann PM. A Protocol to Assess the Wear of Head/Neck Taper Junctions in Large Head Metal-on-Metal (LHMoM) Hips. In: Kurtz SM, Greenwald AS, Mihalko WM, Lemons JE, ed. *Metal-on-Metal Total Hip Replacement Devices*; 2013:209-234.
237. Underwood RJ, Kocagoz SB, Smith R, Sayles RS, Siskey R, Kurtz SM, Cann PM. A protocol to assess the wear of head/neck taper junctions in large head metal-on-metal (LHMoM) hips. In: *ASTM Symposium on Metal-on-Metal Total Hip Replacement Devices, May 8, 2012 - May 8, 2012*. Phoenix, AZ, United states: ASTM International: 2013:209-234.
239. Urish KL, Hamlin BR, Plakseychuk AY, Levison TJ, Higgs GB, Kurtz SM, DiGioia AM. Trunnion Failure of the Recalled Low Friction Ion Treatment Cobalt Chromium Alloy Femoral Head. *The Journal of arthroplasty*. 2017;32:2857-2863.
240. Van Citters DW, Martin AJ, Currier JH, Park SH, Edidin AA. Factors Related to Imprinting Corrosion in Modular Head-Neck Junctions. In: Greenwald AS, Kurtz SM, Lemons JE, Mihalko WM, ed. *Modularity and Tapers in Total Joint Replacement Devices*; 2015:83-98.
243. Waly F, Abduljabbar FH, Gascoyne T, Turgeon TR, Huk O. Stem-Sleeve Junction Failure of a Modular Femoral Hip System: a Retrieval Analysis. *HSS Journal*. 2015;11:285-290.
245. Wauthle R, van der Stok J, Amin Yavari S, Van Humbeeck J, Kruth JP, Zadpoor AA, Weinans H, Mulier M, Schrooten J. Additively manufactured porous tantalum implants. *Acta biomaterialia*. 2015;14:217-225.
246. Weiser MCMDMa, Lavernia CJMDb. Trunnionosis in Total Hip Arthroplasty. *Journal of Bone & Joint Surgery - American Volume*. 2017;99:1489-1501.

Appendix

Table XIII: Patient and device information corresponding to the ceramic-metal cohort in Section 2.3.1

Case number	Implantation time (years)	Age at insertion (years)	Sex	BMI (kg/m ²)	Maximum UCLA score	Revision reason	Head size (mm)	Lateral offset (mm)	Manufacturer	Stem type	Stem alloy	Stem taper angle	Flexural rigidity 10 ⁹ ·Nm ²
1	0.5	75	M	27	7	Loosening	36	41.5	Stryker	Accolade	TMZF	V40	89
2	0.5	31	M	33	5	Infection	36	39	Stryker	Accolade	TMZF	V40	89
3	0.5	48	M	42	2	Loosening	36	50.3	Stryker	Accolade	TMZF	V40	89
4	0.6	N/A	M	N/A	N/A	Loosening	32	44	Stryker	Accolade	TMZF	V40	89
5	0.6	39	M	41	N/A	Infection	36	37	Stryker	Accolade	TMZF	V40	89
6	0.6	46	F	19	4	Infection	36	49	DePuy	Corail	Ti-6Al-4V	12/14	185
7	0.7	49	M	27	2	Loosening	32	40	Zimmer	M/L Taper	Ti-6Al-4V	12/14	202
8	0.8	52	M	38	6	Loosening	32	41	Zimmer	M/L Taper	Ti-6Al-4V	12/14	202
9	0.8	49	M	35	5	Loosening	32	48	Stryker	Accolade	TMZF	V40	89
10	0.9	49	M	N/A	N/A	Loosening	32	44.2	Stryker	Accolade	TMZF	V40	89
11	1.0	53	M	27	4	Infection	36	39	Stryker	Omnifit	Ti-6Al-4V	V40	185
12	1.0	53	M	28	7	Loosening	36	33.4	Stryker	Accolade	TMZF	V40	89
13	1.0	55	M	N/A	5	Loosening	36	39	Stryker	Accolade	TMZF	V40	89
14	1.1	43	M	21	8	Infection	36	58	DePuy	Corail	Ti-6Al-4V	12/14	185
15	1.2	68	F	39	4	Instability	32	38	Zimmer	M/L Taper	Ti-6Al-4V	12/14	202
16	1.2	50	M	34	6	Pain	32	38	DePuy	Tri-Lock	Ti-6Al-4V	12/14	185
17	1.2	55	F	31	8	Loosening	28	44	Stryker	Accolade	TMZF	V40	89
18	1.4	41	M	44	6	Loosening	32	34	Stryker	Accolade	TMZF	V40	89
19	1.5	57	M	30	3	Infection	32	42	Smith & Nephew	Anthology	Ti-6Al-4V	12/14	185
20	1.6	48	M	29	4	Infection	36	39	Stryker	Accolade	TMZF	V40	89
21	1.7	N/A	M	N/A	6	Loosening	32	49	Stryker	Accolade	TMZF	V40	89
22	1.7	50	F	N/A	N/A	Loosening	32	32.1	Stryker	Accolade	TMZF	V40	89
23	1.9	53	F	27	N/A	Malalignment	28	40	Stryker	Accolade	TMZF	V40	89
24	1.9	63	M	28	4	Loosening	36	49	Stryker	Accolade	TMZF	V40	89
25	2.0	53	M	N/A	N/A	Loosening	32	38	Stryker	Accolade	TMZF	V40	89
26	2.0	61	M	28	6	Loosening	36	48	Stryker	Accolade	TMZF	V40	89
27	2.1	50	F	26	7	Loosening	32	32	Stryker	Accolade	TMZF	V40	89
28	2.3	32	M	34	10	Loosening	32	49	Stryker	Accolade	TMZF	V40	89
29	2.3	72	F	22	N/A	Malposition	32	44	Zimmer	Versys FMT	Ti-6Al-4V	12/14	202
30	2.3	34	M	34	3	Infection	32	45	Smith & Nephew	Echelon	CoCr	12/14	358
31	2.4	71	M	N/A	N/A	Loosening	32	38	Stryker	Accolade	TMZF	V40	89
32	2.5	51	M	29	2	Infection	32	40	Smith & Nephew	Echelon	CoCr	12/14	353
33	2.5	57	F	21	6	Loosening	28	36	Encore	Linear	Ti-6Al-4V	12/14	220

Table XIII: continued

Case number	Implantation time (years)	Age at insertion (years)	Sex	BMI (kg/m ²)	Maximum UCLA score	Revision reason	Head size (mm)	Lateral offset (mm)	Manufacturer	Stem type	Stem alloy	Stem taper angle	Flexural rigidity 10 ⁹ ·Nm ²
34	2.5	49	M	24	6	Infection	32	27	DePuy	Tri-Lock	Ti-6Al-4V	12/14	185
35	2.9	N/A	F	25	5	Loosening	32	41	Zimmer	Versys FMT	Ti-6Al-4V	12/14	190
36	3.4	59	M	28	6	Loosening	36	52	Stryker	Accolade	TMZF	V40	89
37	3.5	48	F	32	7	Loosening	32	50	Stryker	Accolade	TMZF	V40	89
38	3.6	76	F	22	8	Periprosthetic fracture	28	32	Stryker	Accolade	TMZF	V40	89
39	4.5	56	M	52	N/A	Loosening	36	38	Stryker	Accolade	TMZF	V40	89
40	5.1	42	F	26	6	Malalignment	28	44	Wright Medical	Perfecta	Ti-6Al-4V	12/14	252
41	5.4	66	M	28	7	Loosening	28	34	Stryker	Accolade	TMZF	V40	89
42	5.6	46	M	18	2	Pain	36	59	DePuy	Corail	Ti-6Al-4V	12/14	179
43	5.9	58	M	37	7	Loosening	32	49	Stryker	Accolade	TMZF	V40	89
44	6.3	43	M	27	10	Osteolysis	32	35	Smith & Nephew, Richards	Spectron EF	CoCr	12/14	353
45	6.3	47	F	32	8	Infection	32	39	Stryker	Accolade	TMZF	V40	89
46	7.6	47	F	21	N/A	Infection	32	45	DePuy	Solution	CoCr	12/14	676
47	8.8	47	F	21	N/A	Infection	32	46	DePuy	Solution	CoCr	12/14	676
48	14.3	52	F	38	N/A	Femoral loosening	32	36	Wright Medical, Dow Corning Wright	Infinity	Ti-6Al-4V	12/14	226
49	14.6	64	F	34	N/A	Loosening	32	46	Zimmer	Muller modified	CoCr	12/14	385
50	17.8	48	M	33	8	PE wear	32	41	Smith & Nephew, Richards	Opti-Fix	Ti-6Al-4V	14/16	328

BMI = body mass index; N/A = not available; M = male; F = female; PE = polyethylene; CoCr = cobalt-chromium.

Table XIV: Patient and device information corresponding to the metal-metal cohort in Section 2.3.1

Case number	Implantation time (years)	Age at insertion (years)	Sex	BMI (kg/m ²)	Maximum UCLA score	Revision reason	Head size (mm)	Lateral offset (mm)	Manufacturer	Stem type	Stem alloy	Trunnion type	Flexural rigidity 10 ⁹ ·Nm ²
1	0.9	51	F	23	6	Infection	28	38	Stryker	Accolade	TMZF	V40	89
2	0.5	70	F	32	3	Loosening	32	38	Stryker	Accolade	TMZF	V40	89
3	0.6	79	F	N/A	N/A	Loosening	32	46	Stryker	Accolade	TMZF	V40	89
4	0.6	64	M	31	7	Loosening	40	44	Stryker	Accolade	TMZF	V40	89
5	0.7	46	M	37	8	Loosening	32	39	Stryker	Accolade	TMZF	V40	89
6	1.0	N/A	F	35	N/A	Infection	32	44	Zimmer	Versys FMT	Ti-6Al-4V	12/14	202
7	0.5	59	M	N/A	8	Infection	36	44	Zimmer	M/L Taper	Ti-6Al-4V	12/14	202
8	0.8	52	F	28	6	Infection	36	48	Zimmer	M/L Taper	Ti-6Al-4V	12/14	202
9	1.4	42	M	27	5	Infection	32	58	Stryker	Accolade	TMZF	V40	247
10	1.0	61	M	29	5	Loosening	36	55	Stryker	Accolade	TMZF	V40	89
11	1.1	65	F	33	4	Infection	36	39	Zimmer	Versys FMT	Ti-6Al-4V	12/14	202
12	1.1	59	F	22	N/A	Infection	36	32	Stryker	Accolade	TMZF	V40	89
13	0.8	67	M	38	4	Infection	36	33	Stryker	Accolade	TMZF	V40	89
14	1.2	47	F	40	2	Infection	36	65	DePuy	Corail	Ti-6Al-4V	12/14	196
15	1.0	65	M	26	5	Loosening	32	51	Zimmer	M/L Taper	Ti-6Al-4V	12/14	202
16	1.3	67	F	25	2	Loosening	32	40	DePuy	Tri-Lock	Ti-6Al-4V	12/14	185
17	1.0	56	M	30	8	Loosening	40	45	Stryker	Accolade	TMZF	V40	89
18	1.4	46	F	N/A	2	Loosening	28	34	Stryker	Accolade	TMZF	V40	89
19	1.5	83	M	23	8	Infection	32	49	Zimmer	M/L Taper	Ti-6Al-4V	12/14	202
20	0.8	53	F	N/A	7	Loosening	32	41	Stryker	Accolade	TMZF	V40	89
21	1.8	55	M	36	4	Loosening	36	46	Stryker	Accolade	TMZF	V40	89
22	1.8	82	M	27	3	Loosening	32	33	Stryker	Accolade	TMZF	V40	89
23	1.7	57	F	29	4	Infection	40	43	Stryker	Accolade	TMZF	V40	89
24	1.9	57	M	28	N/A	Loosening	32	48	Stryker	Accolade	TMZF	V40	89
25	1.0	76	F	31	4	Loosening	32	44	Stryker	Accolade	TMZF	V40	89
26	2.2	N/A	F	22	4	Loosening	28	47	Stryker	Accolade	TMZF	V40	236
27	2.0	59	F	43	6	Loosening	36	34	Stryker	Accolade	TMZF	V40	89
28	1.9	45	M	45	7	Loosening	32	44	Stryker	Accolade	TMZF	V40	89
29	2.0	63	M	35	6	Infection	32	49	Zimmer	Versys FMT	Ti-6Al-4V	12/14	202
30	2.5	N/A	M	23	2	Infection	40	42	Zimmer	Versys Beaded Fullcoat	CoCr	12/14	385
31	1.1	57	F	23	N/A	Infection	36	35	Stryker	Accolade	TMZF	V40	89
32	2.5	76	M	22	N/A	Infection	28	46	Zimmer	Harris Precoat	CoCr	6°	180

Table XIV: continued

Case number	Implantation time (years)	Age at insertion (years)	Sex	BMI (kg/m ²)	Maximum UCLA score	Revision reason	Head size (mm)	Lateral offset (mm)	Manufacturer	Stem type	Stem alloy	Trunnion type	Flexural rigidity 10 ⁹ ·Nm ²
33	2.3	49	F	35	6	Infection	40	65	DePuy	Corail	Ti-6Al-4V	12/14	202
34	2.2	61	F	23	7	N/A	28	42	DePuy	Tri-Lock	Ti-6Al-4V	12/14	185
35	2.3	63	F	51	4	Infection	32	39	Zimmer	Versys FMT	Ti-6Al-4V	12/14	202
36	2.7	55	M	29	6	Loosening	32	50	Stryker	Accolade	TMZF	V40	89
37	2.3	74	M	34	9	Loosening	32	48	Stryker	Accolade	TMZF	V40	89
38	3.6	50	M	20		Pain	36	38	Stryker	Accolade	TMZF	V40	89
39	4.0	49	F	30	6	Periprosthetic fracture	28	39	Stryker	Accolade	TMZF	V40	89
40	5.2	66	F	37	N/A	N/A	28	50	Biomet	Taperloc	Ti-6Al-4V	Type I	132
41	5.0	13	F	21	3	Infection	22.2	39	Stryker	Accolade	TMZF	V40	89
42	5.2	46	F	21	7	Periprosthetic fracture	28	64	DePuy	Corail	Ti-6Al-4V	12/14	207
43	5.0	48	M	24	2	Infection	28	45	Stryker	Accolade	TMZF	V40	89
44	5.2	51	F	N/A	2	Loosening	28	34	Smith & Nephew	Spectron	CoCr	12/14	353
45	9.5	48	F	21	3	Infection	36	35	Stryker	Accolade	CoCr	V40	236
46	9.3	53	M	33	8	Component fracture	28	66	DePuy	AML	CoCr	14/16, or 12/14	374
47	10.1	51	M	32	8	Loosening	32	40	DePuy	AML	CoCr	14/16, or 12/14	676
48	13.1	64	M	29	8	PE wear	28	43	Biomet	Taperloc	Ti-6Al-4V	Type I	112
49	15.0	49	M	35	8	Periprosthetic fracture	32	52	Zimmer	Anatomic	Ti-6Al-4V	12/14	116
50	17.4	16	M	32	9	Loosening	28	36	Zimmer	Harris-Galante	Ti-6Al-4V	6°	101

BMI = body mass index; N/A = not available; F = female; M = male; PE = polyethylene; CoCr = cobalt-chromium.

Matlab Code for Taper Material Loss

The following code is used to input a single axial trace. The user is prompted to manually select regions to include and exclude from the estimation of the as manufactured surface.

```

%This code performs the analysis of a single taper
trace. The output files
%can be used in conjunction with Taper2 to perform
the analysis
%incorporating all measurement traces of the
implant's taper.
%Proximal Inputs must be less than Distal Inputs!

%%%%%%%%%%%%%%%%%%%%%%%%%%%%%%%%%%%%%%%%%%%%%%%%%%%%%%%%%%%%%%%%%%%%%%%%
%%%%%%%%%%%%%%%%%%%%%%%%%%%%%%%%%%%%%%%%%%%%%%%%%%%%%%%%%%%%%%%%%%%%%%%%
%Hard code of the variables for development
purposes - To be deleted later
close all
clear all
clc

    Implant_ID = 'HUMC_H0738';

%       k=1;
%       % resol= 0.001; not used in current
version
%%%%%%%%%%%%%%%%%%%%%%%%%%%%%%%%%%%%%%%%%%%%%%%%%%%%%%%%%%%%%%%%%%%%%%%%
%%%%%%%%%%%%%%%%%%%%%%%%%%%%%%%%%%%%%%%%%%%%%%%%%%%%%%%%%%%%%%%%%%%%%%%%

current_dir=uigetdir; %ask user for a directory
if length(current_dir)<2,return; end;%check if the
directory name is valid, return otherwise
cd(current_dir); %go into the selected directory
%Look for .PRF files
PRF_directory_listing = dir('*.PRF'); %get
directory listing of PRF files
PRF_num_files = length(PRF_directory_listing);
%calculate total number of files in the directory
filenames = zeros(PRF_num_files,1); %make a matrix
the length of the number of PRF files

```

```

angle_increment = 360/PRF_num_files;
%measurement_angles = zeros(PRF_num_files,1);

%Set up matrices for metrics
Measurement_Angle = [0:angle_increment:360-
angle_increment]';
Wear_Area = zeros(1,PRF_num_files);
Max_Wear_Depth = zeros(1,PRF_num_files);
Average_Wear_Depth = zeros(1,PRF_num_files);
Taper_Angle = zeros(1,PRF_num_files);
Volume=zeros(1,PRF_num_files);

if PRF_num_files<1
    error('There are no PRF files in the current
directory.  Locate the proper directory.')
end; %check if there is at least one file.

MatMax = zeros(PRF_num_files,1);
MatMin = zeros(PRF_num_files,1);

for k=1:1:PRF_num_files
    % Read in file as Text
    %filename = PRF_directory_listing(k).name;
    fid = fopen(PRF_directory_listing(k).name,'r');
    %Header = fscanf(fid,'c',{1 inf});
    Header=textscan(fid,'%s','delimiter',' ');
    fclose (fid);
    %Get Spacing and start info from the header
    X_Spacing = str2num(Header{Abdullah, 2008
#303});%Double Check once file is read in!!!!
    Column_Y = str2num(Header{1,4});%Double Check
once file is read in!!!!
    Correction=str2num(Header{1,1}{16,1}); %Get
correction Factor
    R = str2num(Header{1,1}{41,1});
    clearvars Header; %Clear large dataset
    %Open actual y-data (Y - Data is actually X-
Data before convert to
    %Linear in Taly-Rond Software
    fid = fopen(PRF_directory_listing(k).name,'r');

```

```

    for skip_lines=1:20;fgetl(fid);end %skip
comment lines
    data=fscanf(fid,'%f',{1 inf})'; %read in the
data
    Y_Values = data * Correction*1000;
    %Calculate X - values
    Array_Size = size(data);%Find size of data
array
    %X_SP = str2num(X_Spacing);Spin_X =
str2num(Column_Y); %Convert header strings to
numbers
    X_Size = Array_Size(1)*X_Spacing;    %Find size
in mm of x axis
    X_End = X_Size + Column_Y; %Find end X value
    X_Values = [Column_Y:X_Spacing:X_End]';
    X_Values(end)=[];
    fclose(fid); %and close the file
    %Plot X and Y Data - This should be the trace
from the taly Rond

    maxX = max(X_Values);
    minX = min(X_Values);
    MatMax(k) = maxX;
    MatMin(k) = minX;

    if k==1;
plot(Y_Values,X_Values)
    end

end

mindist = min(MatMax)
maxprox = max(MatMin)
    distal = input('input X smaller than
mindist =');
    proximal = input('input X greater than
maxprox =');

for k=1:1:PRF_num_files
    % Read in file as Text

```

```

%filename = PRF_directory_listing(k).name;
fid = fopen(PRF_directory_listing(k).name, 'r');
%Header = fscanf(fid, 'c', {1 inf});
Header=textscan(fid, '%s', 'delimiter', ' ');
fclose (fid);
%Get Spacing and start info from the header
X_Spacing = str2num(Header{1,1}{26,1});%Double
Check once file is read in!!!!
Column_Y = str2num(Header{1,1}{44,1});%Double
Check once file is read in!!!!
Correction=str2num(Header{1,1}{16,1}); %Get
correction Factor
R = str2num(Header{1,1}{41,1});
clearvars Header; %Clear large dataset
%Open actual y-data (Y - Data is actually X-
Data before convert to
%Linear in Taly-Rond Software
fid = fopen(PRF_directory_listing(k).name, 'r');
for skip_lines=1:20;fgetl(fid);end %skip
comment lines
data=fscanf(fid, '%f', {1 inf})'; %read in the
data
Y_Values = data * Correction*1000;
%Calculate X - values
Array_Size = size(data);%Find size of data
array
%X_SP = str2num(X_Spacing);Spin_X =
str2num(Column_Y); %Convert header strings to
numbers IDID THIS UP HIGHER NOW
X_Size = Array_Size(1)*X_Spacing; %Find size
in mm of x axis
X_End = X_Size + Column_Y; %Find end X value
X_Values = [Column_Y:X_Spacing:X_End]';
X_Values(end)=[];
fclose(fid); %and close the file
%Plot X and Y Data - This should be the trace
from the taly Rond

scrsz = get(0, 'ScreenSize');
figure('Position', {1 scrsz(4) scrsz(3)
scrsz(4)});

```

```

%      set(f,'PaperPosition',[0.25 0.25 10.5 8]);
%fill the page

    [valDist,indDist] = min(abs(X_Values-distal));
    [valProx,indProx] = min(abs(X_Values-
proximal));

    R = R - Y_Values(indProx)*1e-3;

    X_Values = X_Values(indProx:indDist); %X values
in the unworn region, height
    Y_Values = Y_Values(indProx:indDist);

    Y_Values=(Y_Values-Y_Values(1)-(R*1e3))*1e-3;

%      scrsz = get(0,'ScreenSize');
%      figure
%      scatter (X_Values, Y_Values);
%      set(gca,'FontSize',14,'FontName','Arial');
%Make pretty
%      xlabel('Depth Height (mm)','FontSize',
16,'FontName','Arial');ylabel('X Distance
(um)','FontSize', 16,'FontName','Arial');
title(PRF_directory_listing(k).name,'FontSize',18,'
FontName','Arial');%Appropriately label the axes
%      set(gcf,'color','w'); box on;

plot(X_Values,Y_Values)
hold off
pause

    i = cursor_info(1,2).Position(1);
    ii = cursor_info(1,1).Position(1);

    [val_i,ind_i] = min(abs(X_Values-i));
    [val_ii,ind_ii] = min(abs(X_Values-ii));

figure
scatter (X_Values, Y_Values);

```

```

    set(gca, 'FontSize', 14, 'FontName', 'Arial');
%Make pretty
    xlabel('Depth Height (mm)', 'FontSize',
16, 'FontName', 'Arial'); ylabel('X Distance
(um)', 'FontSize', 16, 'FontName', 'Arial');
title(PRF_directory_listing(k).name, 'FontSize', 18, '
FontName', 'Arial'); %Appropriately label the axes
    set(gcf, 'color', 'w'); box on;

%%%%%%%%%%%%%%%%%%%%%%%%%%%%%%%%%%%%%%%%%%%%%%%%%%%%%%%%%%%%%%%%%%%%%%%%
%%%%%%%%%%%%%%%%%%%%%%%%%%%%%%%%%%%%%%%%%%%%%%%%%%%%%%%%%%%%%%%%%%%%%%%%
    %Find indices of end of unworn areas
    %This is a quick and dirty method of finding the
index of Proximal X_Value
    %Plot points
    Y_i = Y_Values(ind_i);
    X_i = X_Values(ind_i);
    Y_ii = Y_Values(ind_ii);
    X_ii = X_Values(ind_ii);

    %Plot proximal and distal stop points
    hold on
    scatter
(X_i, Y_i, 100, 'LineWidth', 3, 'MarkerEdgeColor', 'r');
    scatter
(X_ii, Y_ii, 100, 'LineWidth', 3, 'MarkerEdgeColor', 'r')
;

    range=[ind_ii:ind_i];

%%%%%%%%%%%%%%%%%%%%%%%%%%%%%%%%%%%%%%%%%%%%%%%%%%%%%%%%%%%%%%%%%%%%%%%%
%%%%%%%%%%%%%%%%%%%%%%%%%%%%%%%%%%%%%%%%%%%%%%%%%%%%%%%%%%%%%%%%%%%%%%%%
    %Take out "Wear Scar" Data
    %Zero out the values in the "Wear Scar"
    Y_Values_LF = Y_Values;
    for m=range;
        Y_Values_LF(m)=1e9;
    end

```



```

        %Y_Values_LF(ind0)=0;This was an earlier
hack
X_Values_LF = X_Values;
    for n=range;
        X_Values_LF(n)=1e9;
    end

    %Remove out 1e9's
    X_LF = X_Values_LF(X_Values_LF~=1e9);
    Y_LF = Y_Values_LF(Y_Values_LF~=1e9);

%%%%%%%%%%%%%%%%%%%%%%%%%%%%%%%%%%%%%%%%%%%%%%%%%%%%%%%%%%%%%%%%%%%%%%%%
%%%%%%%%%%%%%%%%%%%%%%%%%%%%%%%%%%%%%%%%%%%%%%%%%%%%%%%%%%%%%%%%%%%%%%%%
    %Fit a line to the "unworn" data using polyfit
(Uses Least Squares)
    Line_Fit = polyfit(X_LF,Y_LF,1); % Get slope
and intercept of least squares linear fit
    Xfit = min(X_Values):X_Spacing:max(X_Values);
%Make a matrix of the x-values
    Yfit = Line_Fit(1)*Xfit + Line_Fit(2); %Make
the matrix of correspondign y-values
    hold on
    scatter(Xfit',Yfit',3,'MarkerEdgeColor','k');

    %%Here I am trying to get an r-squard for the
linear least squares fit.

    %Output = polyval(Line_Fit,Xfit);
    %Correlation = corrcoef(Y_LF, Output);
% Write out equation and place on chart
    Line_Fit_Angle =
polyfit(X_LF,(Y_LF./1000),1);
    Slope = num2str(Line_Fit_Angle(1));
    Intercept = num2str(Line_Fit_Angle(2));
    Equation_Str = strcat('y = ',Slope,'x +
',Intercept);
    text(-5,180,Equation_Str);
    axis([min(X_Values) max(X_Values)
min(Y_Values) max(Y_Values)]);

```

```

    %Calculate Wear (This is for wear of the
entire trace; it is commented
    %out and replaced by slected region wear
calculations

%           Wear_Vector = Yfit'-Y_Values;
%           scatter(X_Values,Wear_Vector,2);
%           %Calculate and Display Metrics
%           Wear = sum(Wear_Vector(:));
%           Wear_Area(k) = Wear
*X_Spacing;%%%%%%%%%%
%%%%%%%%%%
%           Wear_Area = Wear_Area(Wear_Area~=0);
%           WearStr = num2str(Wear*X_Spacing);
Wear_Area_Str = strcat('Wear Area = ',WearStr,'
um^2'); %Make and plot a Wear Area Results String
%           text(-5,150,Wear_Area_Str);
%
%           Max_Wear_Depth(k) = max(Wear_Vector);
%           Max_Wear_Depth =
Max_Wear_Depth(Max_Wear_Depth~=0);
%           WDStr = num2str(max(Wear_Vector));
Depth_String = strcat('Maximum Wear Depth =
',WDStr,' um'); %Make and plot max wear depth
Results string
%           text(-5,120,Depth_String);

%%%%%%%%%%
%%%%%%%%%%
%                               Wear Metrics
%%%%%%%%%%
%%%%%%%%%%

%   Average Wear depth Calculations
        Wear_XValues= X_Values(range);
        Wear_YValues=Y_Values(range);
%   Fit Values
        Wear_Fit_XValues= Xfit(range);
        Wear_Fit_YValues=Yfit(range);
%   Wear

```

```

        Selected_Wear_Vector=Wear_YValues-
Wear_Fit_YValues';

scatter(Wear_XValues,Selected_Wear_Vector,2);
        Selected_Wear =
sum(Selected_Wear_Vector(:));
%   Wear Area
        Wear_Area(k) = Selected_Wear * X_Spacing;
        Wear_Area = Wear_Area(Wear_Area~=0);
        WearStr =
num2str(Selected_Wear*X_Spacing); Wear_Area_Str =
strcat('Wear Area = ',WearStr,' um^2'); %Make and
plot a Wear Area Results String
        text(-5,150,Wear_Area_Str);
%   Max Wear Depth
        Max_Wear_Depth(k) =
max(Selected_Wear_Vector);
        Max_Wear_Depth =
Max_Wear_Depth(Max_Wear_Depth~=0);
        WDStr =
num2str(max(Selected_Wear_Vector)); Depth_String =
strcat('Maximum Wear Depth = ',WDStr,' um'); %Make
and plot max wear depth Results string
        text(-5,120,Depth_String);
%   Average Wear Depth
        Average_Wear_Depth(k) =
mean(Selected_Wear_Vector);
        Average_Wear_Depth =
Average_Wear_Depth(Average_Wear_Depth~=0);
        Ave_Cat =
num2str(mean(Selected_Wear_Vector(:))); Average_Str
= strcat('Average Wear Depth = ',Ave_Cat,'
um');%Make and plot average wear depth Results
string
        text(-5,90,Average_Str);
%   Plot a datum at 0
        Y_Datum = zeros(size(X_Values));
scatter(X_Values,Y_Datum,1);
%   Taper Angle Analysis
        % Find slope of the line

```

```

        Taper_Angle(k) =
atan(Line_Fit_Angle(1))*180/pi; %Find angle of line
using trig and convert to degrees
        Taper_Angle = Taper_Angle(Taper_Angle~=0);
        Taper_Angle_Str =
num2str(atan(Line_Fit_Angle(1))*180/pi); Angle_Str
= strcat('Taper Angle = ',Taper_Angle_Str, '
degrees');%Make and plot Taper Angle Results string
        text(-5,60,Angle_Str);
%   Wear Volume Calculation (mm^3)
        Point_Volume = (pi*((Wear_Fit_YValues).^2
- (Wear_YValues).^2))*X_Spacing;
        Volume(k)=sum(Point_Volume(:));
        Volume_Str =
num2str(sum(Point_Volume(:))); Volume_String =
strcat('Wear Volume = ',Volume_Str, ' mm3');
        text(-5,30,Volume_String);
%%%%%%%%%%%%%%%%%%%%%%%%%%%%%%%%%%%%%%%%%%%%%%%%%%%%%%%%%%%%%%%%%%%%%%%%
%%%%%%%%%%%%%%%%%%%%%%%%%%%%%%%%%%%%%%%%%%%%%%%%%%%%%%%%%%%%%%%%%%%%%%%%
%   Save Figures
        Angle=num2str((k-1)*angle_increment);

saveas(gcf,strcat(Implant_ID,'_',Angle,'_Degrees'),
'fig');

saveas(gcf,strcat(Implant_ID,'_',Angle,'_Degrees'),
'png');
%           close;
end;

Average_Volume = mean(Volume)

%save the data to a file
results_str =
strcat(char(Implant_ID),'_results.csv');
fid=fopen([results_str],'wt'); %open a comma
separated file
header=['Measurement Angle,Maximum Wear Depth
[um],Wear Area [um2],Average Wear Depth [um],Taper
Angle [deg],Volume,\n'];

```

```

fprintf(fid,header);%print out the header
buffer= repmat(',',length(Wear_Area),1);%create a
column vector of commas for separation
save_string=[num2str(Measurement_Angle),
buffer,num2str(Max_Wear_Depth'),buffer,num2str(Wear
_Area'),buffer,num2str(Average_Wear_Depth'),buffer,
num2str(abs(Taper_Angle')),buffer,num2str(Volume')]
;
%save_string2=[num2str(Volume')];
%for i=1:length(save_string),
    %save_string;
%end

for J=1:size(save_string,1),%save all the strings
    fprintf(fid, '%s\n', save_string(J,:));
    %fprintf(fid, [save_string(J,:),'\n']);
    %K=1:size(save_string2,1)
    %fprintf(fid, [save_string2(K,:),'\n']);
end
%Need to save figures inside loop
% numfigs=gcf;
% for m=numfigs:-1:1
%     saveas
(gcf, strcat('Figure',num2str(gcf),'.tif'))
%     saveas
(gcf, strcat('Figure',num2str(gcf),'.fig'))
%     close(gcf)
% end

```

References

1. Abdullah KA. Finite element modelling of the neck-stem interface of a modular hip implant for micro-motion study. In: *19th IASTED International Conference on Modelling and Simulation, MS 2008, May 26, 2008 - May 28, 2008*. Quebec City, QC, Canada: Acta Press; 2008:364-369.
2. Agne MT, Underwood RJ, Kocagoz SB, MacDonald DW, Day JS, Parvizi J, Kraay MJ, Mont MA, Klein GR, Cates HE, Kurtz SM. Is there material loss at the backside taper in modular CoCr acetabular liners? *Clinical orthopaedics and related research*. 2015;473:275-285.
3. Aldinger P, Cartner J, Jones B. Validating a Simplified Method for Assessing Total Hip Arthroplasty Taper Corrosion Susceptibility with a 15-Year Retrieval Database. In: Greenwald AS, Kurtz SM, Lemons JE, Mihalko WM, ed. *Modularity and Tapers in Total Joint Replacement Devices*; 2015:113-131.
4. Arnholt C, Underwood R, MacDonald D, Higgs G, Chen A, Klein G, Hamlin B, Lee G, Mont M, Cates H, Malkani A, Kraay M, Rimnac C, Kurtz S. Microgrooved Surface Topography Does Not Influence Fretting Corrosion of Tapers in THA: Classification and Retrieval Analysis. *Modularity and Tapers in Total Joint Replacement Devices*. Conshohocken PA: American Society of Testing Materials (ASTM); 2015.
5. Arnholt C, Underwood R, MacDonald DW, Higgs GB, Chen AF, Klein G, Hamlin B, Lee GC, Mont M, Cates H, Malkani A, Kraay M, Rimnac C, Kurtz SM. Microgrooved surface topography does not influence fretting corrosion of tapers in total hip arthroplasty: Classification and retrieval analysis. In: *ASTM Special Technical Publication*. 2015:99-112.
6. Arnholt CM, MacDonald DW, Tohfafarosh M, Gilbert JL, Rimnac CM, Kurtz SM, Implant Research Center Writing C, Klein G, Mont MA, Parvizi J, Cates HE, Lee GC, Malkani A, Kraay M. Mechanically assisted taper corrosion in modular TKA. *Journal of Arthroplasty*. 2014;29:205-208.
7. Arnholt CM, MacDonald DW, Underwood RJ, Guyer EP, Rimnac CM, Kurtz SM, Implant Research Center Writing C, Mont MA, Klein GR, Lee GC, Chen AF, Hamlin BR, Cates HE, Malkani AL, Kraay MJ. Do Stem Taper Microgrooves Influence Taper Corrosion in Total Hip Arthroplasty? A Matched Cohort Retrieval Study. *Journal of Arthroplasty*. 2017;32:1363-1373.
8. Ashkanfar A, Langton DJ, Joyce TJ. Does a micro-grooved trunnion stem surface finish improve fixation and reduce fretting wear at the taper junction of total hip replacements? A finite element evaluation. *Journal of Biomechanics*. 2017;63:47-54.
9. Ashkanfar A, Langton DJ, Joyce TJ. A large taper mismatch is one of the key factors behind high wear rates and failure at the taper junction of total hip replacements: A finite element wear analysis. *Journal of the mechanical behavior of biomedical materials*. 2017;69:257-266.
10. Australian Orthopaedic Association. *Australian Orthopaedic Association National Joint Replacement Registry. Annual Report. Adelaide:AOA; 2019*.
11. Bal BS, Garino J, Ries M, Rahaman MN. A review of ceramic bearing materials in total joint arthroplasty. *Hip international : the journal of clinical and experimental research on hip pathology and therapy*. 2007;17:21-30.

12. Banerjee S, Cherian JJ, Bono JV, Kurtz SM, Geesink R, Meneghini RM, Delanois RE, Mont MA. Gross trunnion failure after primary total hip arthroplasty. *The Journal of arthroplasty*. 2015;30:641-648.
13. Bansal T, Aggarwal S, Dhillon MS, Patel S. Gross trunnion failure in metal on polyethylene total hip arthroplasty—a systematic review of literature. *International orthopaedics*. 2020;44:609-621.
14. Basgul C, MacDonald DW, Siskey R, Kurtz SM. Thermal Localization Improves the Interlayer Adhesion and Structural Integrity of 3D printed PEEK Lumbar Spinal Cages. *Materialia (Oxf)*. 2020;10.
15. Basgul C, Yu T, MacDonald DW, Siskey R, Marcolongo M, Kurtz SM. Structure-Property Relationships for 3D printed PEEK Intervertebral Lumbar Cages Produced using Fused Filament Fabrication. *J Mater Res*. 2018;33:2040-2051.
16. Basgul C, Yu T, MacDonald DW, Siskey R, Marcolongo M, Kurtz SM. Does annealing improve the interlayer adhesion and structural integrity of FFF 3D printed PEEK lumbar spinal cages? *Journal of the mechanical behavior of biomedical materials*. 2019;102:103455.
17. Baumann AP, Vesnovsky O, Topoleski LDT, Donaldson F, McMinn NLL, Vignola A, Di Prima MA. Specimen Specific Finite Element Models for Predicting Fretting Wear in Total Hip Arthroplasty Tapers. *J Biomech Eng*. 2020.
18. Baxmann M, Jauch SY, Schilling C, Blomer W, Grupp TM, Morlock MM. The influence of contact conditions and micromotions on the fretting behavior of modular titanium alloy taper connections. *Medical Engineering and Physics*. 2013;35:676-683.
19. Baykal D. Tribological Assessment of Hydrogels for Replacing Damaged Articular Cartilage. *Biomedical Engineering, Science and Health Systems: Drexel University*; 2013.
20. Baykal D, Siskey RS, Haider H, Saikko V, Ahlroos T, Kurtz SM. Advances in tribological testing of artificial joint biomaterials using multidirectional pin-on-disk testers. *Journal of the mechanical behavior of biomedical materials*. 2014;31:117-134.
21. Baykal D, Siskey RS, Underwood RJ, Briscoe A, Kurtz SM. The Biotribology of PEEK-on-HXLPE Bearings Is Comparable to Traditional Bearings on a Multidirectional Pin-on-disk Tester. *Clinical orthopaedics and related research*. 2016;474:2384-2393.
22. Bishop N, Witt F, Pourzal R, Fischer A, Rutschi M, Michel M, Morlock M. Wear patterns of taper connections in retrieved large diameter metal-on-metal bearings. *Journal of orthopaedic research : official publication of the Orthopaedic Research Society*. 2013;31:1116-1122.
23. Bitter T, Khan I, Marriott T, Lovelady E, Verdonschoff N, Janssen D. The effects of manufacturing tolerances and assembly force on the volumetric wear at the taper junction in modular total hip arthroplasty. *Computer Methods in Biomechanics and Biomedical Engineering*. 2019;22:1061-1072.
24. Bitter T, Khan I, Marriott T, Lovelady E, Verdonschot N, Janssen D. Finite element wear prediction using adaptive meshing at the modular taper interface of hip implants. *Journal of the mechanical behavior of biomedical materials*. 2018;77:616-623.
25. Bitter T, Khan I, Marriott T, Lovelady E, Verdonschot N, Janssen D. The effects of manufacturing tolerances and assembly force on the volumetric wear at the taper junction in modular total hip arthroplasty. *Computer Methods in Biomechanics and Biomedical Engineering*. 2019;22:1061-1072.
26. Bobbert FSL, Lietaert K, Eftekhari AA, Pouran B, Ahmadi SM, Weinans H, Zadpoor AA. Additively manufactured metallic porous biomaterials based on minimal surfaces: A

- unique combination of topological, mechanical, and mass transport properties. *Acta biomaterialia*. 2017;53:572-584.
27. Bobyn JD, Poggie RA, Krygier JJ, Lewallen DG, Hanssen AD, Lewis RJ, Unger AS, O'Keefe TJ, Christie MJ, Nasser S, Wood JE, Stulberg SD, Tanzer M. Clinical validation of a structural porous tantalum biomaterial for adult reconstruction. *The Journal of bone and joint surgery. American volume*. 2004;86-A Suppl 2:123-129.
 28. Bobyn JD, Stackpool GJ, Hacking SA, Tanzer M, Krygier JJ. Characteristics of bone ingrowth and interface mechanics of a new porous tantalum biomaterial. *The Journal of bone and joint surgery. British volume*. 1999;81:907-914.
 29. Bobyn JD, Tanzer M, Krygier JJ, Dujovne AR, Brooks CE. Concerns with modularity in total hip arthroplasty. *Clinical orthopaedics and related research*. 1994:27-36.
 30. Bone MC, Sidaginamale RP, Lord JK, Scholes SC, Joyce TJ, Nargol AVF, Langton DJ. Determining material loss from the femoral stem trunnion in hip arthroplasty using a coordinate measuring machine. *Proceedings of the Institution of Mechanical Engineers Part H-Journal of Engineering in Medicine*. 2015;229:69-76.
 31. Bonner B, Arauz P, Klemm C, Kwon YM. Outcome of Re-Revision Surgery for Adverse Local Tissue Reaction in Metal-on-Polyethylene and Metal-on-Metal Total Hip Arthroplasty. *The Journal of arthroplasty*. 2020.
 32. Boudeau N, Liksonov D, Barriere T, Maslov L, Gelin J-C. Composite based on polyetheretherketone reinforced with carbon fibres, an alternative to conventional materials for femoral implant: Manufacturing process and resulting structural behaviour. *Materials and Design*. 2012;40:148-156.
 33. Boutin P. [Total arthroplasty of the hip by fritted aluminum prosthesis. Experimental study and 1st clinical applications]. *Revue de chirurgie orthopedique et reparatrice de l'appareil moteur*. 1972;58:229-246.
 34. Boutin P, Blanquaert D. [A study of the mechanical properties of alumina-on-alumina total hip prosthesis (author's transl)]. *Revue de chirurgie orthopedique et reparatrice de l'appareil moteur*. 1981;67:279-287.
 35. Boutin P, Christel P, Dorlot JM, Meunier A, de Roquancourt A, Blanquaert D, Herman S, Sedel L, Witvoet J. The use of dense alumina-alumina ceramic combination in total hip replacement. *Journal of biomedical materials research*. 1988;22:1203-1232.
 36. Brock TM, Sidaginamale R, Rushton S, Nargol AV, Bowsher JG, Savisaar C, Joyce TJ, Deehan DJ, Lord JK, Langton DJ. Shorter, rough trunnion surfaces are associated with higher taper wear rates than longer, smooth trunnion surfaces in a contemporary large head metal-on-metal total hip arthroplasty system. *Journal of orthopaedic research : official publication of the Orthopaedic Research Society*. 2015;33:1868-1874.
 37. Brown SA, Flemming CA, Kawalec JS, Placko HE, Vassaux C, Merritt K, Payer JH, Kraay MJ. Fretting corrosion accelerates crevice corrosion of modular hip tapers. *Journal of Applied Biomaterials (New York)*. 1995;6:19-26.
 38. Brown SA, Simpson JP. Crevice and fretting corrosion of stainless-steel plates and screws. *Journal of biomedical materials research*. 1981;15:867-878.
 39. Bryant M, Hu X, Farrar R, Brummitt K, Freeman R, Neville A. Crevice corrosion of biomedical alloys: a novel method of assessing the effects of bone cement and its chemistry. *Journal of biomedical materials research. Part B, Applied biomaterials*. 2013;101:792-803.
 40. Cahoon JR, Paxton HW. Metallurgical Analyses of Failed Orthopedic Implants *Journal of biomedical materials research*. 1968;2:1-22.

41. Cartner J, Aldinger P, Li C, Collins D. Characterization of Femoral Head Taper Corrosion Features Using a 22-Year Retrieval Database. *HSS Journal*. 2017;13:35-41.
42. Chana R, Esposito C, Campbell PA, Walter WK, Walter WL. Mixing and matching causing taper wear: corrosion associated with pseudotumour formation. *The Journal of bone and joint surgery. British volume*. 2012;94:281-286.
43. Chaplin RPS, Lee AJC, Hooper RM. Assessment of wear on the cones of modular stainless steel Exeter hip stems. *Journal of Materials Science: Materials in Medicine*. 2004;15:977-990.
44. Charnley J. Arthroplasty of the hip. A new operation. *Lancet*. 1961;1:1129-1132.
45. Chevalier J. What future for zirconia as a biomaterial? *Biomaterials*. 2006;27:535-543.
46. Chiu YC, Kocagoz S, Larson JC, Brey EM. Evaluation of physical and mechanical properties of porous poly (ethylene glycol)-co-(L-lactic acid) hydrogels during degradation. *PLoS one*. 2013;8:e60728.
47. Clarke IC. Metastable Nature of Zirconia Femoral Heads From a 20-Year Perspective of Clinical and Simulator Wear Studies. *Seminars in Arthroplasty*. 2006:165-178.
48. Clarke IC, Campbell PA, Kossovsky N. Debris-Mediated Osteolysis. A Cascade Phenomenon Involving Motion, Wear, Particulates, Macrophage Induction, and Bone Lysis In: St. John KR, ed. *STP 1144: Particulate Debris from Medical Implants: Mechanisms of Formation and Biological Consequences* Philadelphia, PA: American Society for Testing and Materials; 1992:7-26.
49. Clarke IC, Green DD, Williams PA, Kuboc K, Pezzotti G, Lombardi AV. Hip-simulator wear studies of an alumina-matrix composite (AMC) ceramic compared to retrieval studies of AMC balls with 1–7 years follow-up. *Wear*. 2009;267:702-709.
50. Clarke IC, Manaka M, Green DD, Williams P, Pezzotti G, Kim YH, Ries M, Sugano N, Sedel L, Delauney C, Nissan BB, Donaldson T, Gustafson GA. Current status of zirconia used in total hip implants. *The Journal of bone and joint surgery. American volume*. 2003;85-A Suppl 4:73-84.
51. Cohen J, Lindenbaum B. Fretting corrosion in orthopedic implants. *Clinical orthopaedics and related research*. 1968;61:167-175.
52. Colangelo VJ, Greene ND. Corrosion and fracture of type 316 SMO orthopedic implants. *Journal of biomedical materials research*. 1969;3:247-265.
53. Collier JP, Mayor MB, Jensen RE, Surprenant VA, Surprenant HP, McNamar JL, Belec L. Mechanisms of failure of modular prostheses. *Clinical orthopaedics and related research*. 1992:129-139.
54. Collier JP, Mayor MB, Williams IR, Surprenant VA, Surprenant HP, Currier BH. The tradeoffs associated with modular hip prostheses. *Clinical orthopaedics and related research*. 1995:91-101.
55. Collier JP, Surprenant VA, Jensen RE, Mayor MB, Surprenant HP. Corrosion between the components of modular femoral hip prostheses. *The Journal of bone and joint surgery. British volume*. 1992;74:511-517.
56. Cook RB, Bolland BJ, Wharton JA, Tilley S, Latham JM, Wood RJ. Pseudotumour formation due to tribocorrosion at the taper interface of large diameter metal on polymer modular total hip replacements. *The Journal of arthroplasty*. 2013;28:1430-1436.
57. Cook SD, Barrack RL, Baffes GC, Clemow AJ, Serekian P, Dong N, Kester MA. Wear and corrosion of modular interfaces in total hip replacements. *Clinical orthopaedics and related research*. 1994:80-88.

58. Cook SD, Barrack RL, Clemow AJ. Corrosion and wear at the modular interface of uncemented femoral stems. *The Journal of bone and joint surgery. British volume.* 1994;76:68-72.
59. Cook SD, Manley MT, Kester MA, Dong NG. Torsional resistance and wear of a modular sleeve-stem hip system. *Clinical materials.* 1993;12:153-158.
60. Cooper HJ. The local effects of metal corrosion in total hip arthroplasty. *The Orthopedic clinics of North America.* 2014;45:9-18.
61. Cooper HJ, Della Valle CJ, Berger RA, Tetreault M, Paprosky WG, Sporer SM, Jacobs JJ. Corrosion at the head-neck taper as a cause for adverse local tissue reactions after total hip arthroplasty. *The Journal of bone and joint surgery. American volume.* 2012;94:1655-1661.
62. Crainic AM, Callisti M, Palmer MR, Cook RB. Investigation of nano-sized debris released from CoCrMo secondary interfaces in total hip replacements: Digestion of the flakes. *Journal of Biomedical Materials Research - Part B Applied Biomaterials.* 2019;107:424-434.
63. Cramer SD, Covino BS, Jr. 14. Corrosion of Cobalt and Cobalt-Base Alloys. *ASM Handbook, Volume 13B - Corrosion: Materials: ASM International; 2005.*
64. Cramer SD, Covino BS, Jr. 19. Corrosion of Titanium and Titanium Alloys. *ASM Handbook, Volume 13B - Corrosion: Materials: ASM International; 2005.*
65. Cuckler JM, Bearcroft J, Asgian CM. Femoral head technologies to reduce polyethylene wear in total hip arthroplasty. *Clinical orthopaedics and related research.* 1995:57-63.
66. Dalal A, Pawar V, McAllister K, Weaver C, Hallab NJ. Orthopedic implant cobalt-alloy particles produce greater toxicity and inflammatory cytokines than titanium alloy and zirconium alloy-based particles in vitro, in human osteoblasts, fibroblasts, and macrophages. *Journal of biomedical materials research. Part A.* 2012;100:2147-2158.
67. Danoff JR, Longaray J, Rajaravivarma R, Gopalakrishnan A, Chen AF, Hozack WJ. Impaction Force Influences Taper-Trunnion Stability in Total Hip Arthroplasty. *Journal of Arthroplasty.* 2018;33:S270-S274.
68. De Aza AH, Chevalier J, Fantozzi G, Schehl M, Torrecillas R. Crack growth resistance of alumina, zirconia and zirconia toughened alumina ceramics for joint prostheses. *Biomaterials.* 2002;23:937-945.
69. de Steiger RN, Hatton A, Peng Y, Graves S. What Is the Risk of THA Revision for ARMD in Patients with Non-metal-on-metal Bearings? A Study from the Australian National Joint Replacement Registry. *Clinical orthopaedics and related research.* 2020.
70. Del Balso C, Teeter MG, Tan SC, Howard JL, Lanting BA. Trunnionosis: Does Head Size Affect Fretting and Corrosion in Total Hip Arthroplasty? *Journal of Arthroplasty.* 2016;31:2332-2336.
71. Delaney LJ, MacDonald D, Leung J, Fitzgerald K, Sevit AM, Eisenbrey JR, Patel N, Forsberg F, Kepler CK, Fang T, Kurtz SM, Hickok NJ. Ultrasound-triggered antibiotic release from PEEK clips to prevent spinal fusion infection: Initial evaluations. *Acta biomaterialia.* 2019;93:12-24.
72. DeVilliers T, ed. *STP 144: Symposium on Fretting Corrosion.* Philadelphia, PA: American Society for Testing Materials; 1952.
73. Di Laura A, Hothi H, Henckel J, Swiatkowska I, Liow MHL, Kwon YM, Skinner JA, Hart AJ. Retrieval analysis of metal and ceramic femoral heads on a single CoCr stem design. *Bone & joint research.* 2017;6:345-350.

74. Dyrkacz RMR, Brandt JM, Ojo OA, Turgeon TR, Wyss UP. The influence of head size on corrosion and fretting behaviour at the head-neck interface of artificial hip joints. *Journal of Arthroplasty*. 2013;28:1036-1040.
75. Eichler D, Barry J, Lavigne M, Masse V, Vendittoli PA. No radiological and biological sign of trunnionosis with Large Diameter Head Ceramic Bearing Total Hip Arthroplasty after 5 years. *Orthopaedics & traumatology, surgery & research : OTSR*. 2020.
76. English R, Ashkanfar A, Rothwell G. A computational approach to fretting wear prediction at the head-stem taper junction of total hip replacements. *Wear*. 2015;338-339:210-220.
77. Etkin CD, Springer BD. The American Joint Replacement Registry-the first 5 years. *Arthroplast Today*. 2017;3:67-69.
78. Falkenberg A, Biller S, Morlock MM, Huber G. Micromotion at the head-stem taper junction of total hip prostheses is influenced by prosthesis design-, patient- and surgeon-related factors. *Journal of Biomechanics*. 2020;98.
79. Falkenberg A, Dickinson EC, Morlock MM. Adapter sleeves are essential for ceramic heads in hip revision surgery. *Clinical Biomechanics January*. 2020;71:1-4.
80. Fallahnezhad K, Oskouei RH, Badnava H, Taylor M. An adaptive finite element simulation of fretting wear damage at the head neck taper junction of total hip replacement: The role of taper angle mismatch. *Journal of the mechanical behavior of biomedical materials*. 2017;75:58-67.
81. Flemming CAC, Brown SA, Payer JH. Mechanical testing for fretting corrosion of modular total hip tapers. In: Kambic HE, Yokobori JAT, ed. *Biomaterials' Mechanical Properties*. Philadelphia: American Society for Testing and Materials; 1994.
82. Friedrich K, Kargerkocsis J, Lu Z. Effects of Steel Counterface Roughness and Temperature on the Friction and Wear of Pe(E)K Composites under Dry Sliding Conditions. *Wear*. 1991;148:235-247.
83. Fukui K, Kaneuji A, Sugimori T, Ichiseki T, Matsumoto T. Retrieval analysis of new-generation yttria-stabilized zirconia femoral heads after total hip arthroplasty. *European journal of orthopaedic surgery & traumatology : orthopedie traumatologie*. 2014;24:1197-1202.
84. Gilbert JL. Electrochemical Behavior of Metals in the Biological Milieu. In: Ducheyne P, ed. *Comprehensive Biomaterials*: Elsevier; 2011:21-48.
85. Gilbert JL, Buckley CA, Jacobs JJ. In vivo corrosion of modular hip prosthesis components in mixed and similar metal combinations. The effect of crevice, stress, motion, and alloy coupling. *Journal of biomedical materials research*. 1993;27:1533-1544.
86. Gilbert JL, Buckley CA, Jacobs JJ, Bertin KC, Zernich MR. Intergranular corrosion-fatigue failure of cobalt-alloy femoral stems. A failure analysis of two implants. *The Journal of bone and joint surgery. American volume*. 1994;76:110-115.
87. Gilbert JL, Jacobs JJ. The Mechanical and Electrochemical Processes Associated with Taper Fretting and Crevice Corrosion: A Review. In: Marlowe DE, Parr JE, Mayor MB, ed. *STP1301: Modularity of Orthopedic Implants*. West Conshohocken, PA: American Society for Testing and Materials; 1997.
88. Gilbert JL, Mali S, Urban RM, Silverton CD, Jacobs JJ. In vivo oxide-induced stress corrosion cracking of Ti-6Al-4V in a neck-stem modular taper: Emergent behavior in a new mechanism of in vivo corrosion. *Journal of biomedical materials research. Part B, Applied biomaterials*. 2011;100:584-594.
89. Gilbert JL, Mali SA, Sivan S. Corrosion of Modular Tapers in Total Joint Replacements: A Critical Assessment of Design, Materials, Surface Structure, Mechanics,

- Electrochemistry, and Biology. In: Greenwald S, Kurtz SM, ed. *STP1591: Modularity and Tapers in Total Joint Replacement Devices*. West Conshohocken, PA: ASTM International; 2015.
90. Gilbert JL, Sivan S, Liu Y, Kocagöz SB, Arnholt CM, Kurtz SM. Direct in vivo inflammatory cell-induced corrosion of CoCrMo alloy orthopedic implant surfaces. *Journal of Biomedical Materials Research - Part A*. 2015;103:211-223.
 91. Gill IP, Webb J, Sloan K, Beaver RJ. Corrosion at the neck-stem junction as a cause of metal ion release and pseudotumour formation. *The Journal of bone and joint surgery. British volume*. 2012;94:895-900.
 92. Goldberg JR, Gilbert JL. In vitro corrosion testing of modular hip tapers. *Journal of biomedical materials research. Part B, Applied biomaterials*. 2003;64:78-93.
 93. Goldberg JR, Gilbert JL. The electrochemical and mechanical behavior of passivated and TiN/AlN-coated CoCrMo and Ti6Al4V alloys. *Biomaterials*. 2004;25:851-864.
 94. Goldberg JR, Gilbert JL, Jacobs JJ, Bauer TW, Paprosky W, Leurgans S. A multicenter retrieval study of the taper interfaces of modular hip prostheses. *Clinical orthopaedics and related research*. 2002:149-161.
 95. Hall DJ, McCarthy SM, Ehrich J, Urban RM, Fischer A, Jacobs JJ, Lundberg HJ, Pourzal R. Imprinting and Column Damage on CoCrMo Head Taper Surfaces in Total Hip Replacements. *ASTM Special Technical Publication*. 2018;STP 1606:131-155.
 96. Hall DJ, Pourzal R, Della Valle CJ, Galante JO, Jacobs JJ, Urban RM. Corrosion of modular junctions in femoral and acetabular components for hip arthroplasty and its local and systemic effects. In: *ASTM Special Technical Publication*. 2015:410-427.
 97. Hall DJ, Pourzal R, Jacobs JJ. What Surgeons Need to Know About Adverse Local Tissue Reaction in Total Hip Arthroplasty. *Journal of Arthroplasty*. 2020.
 98. Hall DJ, Pourzal R, Lundberg HJ, Mathew MT, Jacobs JJ, Urban RM. Mechanical, chemical and biological damage modes within head-neck tapers of CoCrMo and Ti6Al4V contemporary hip replacements. *Journal of Biomedical Materials Research. Part B, Applied Biomaterials*. 2018;106:1672-1685.
 99. Hallab NJ. Biologic Aspects of Implant Wear. *Materials for Medical Devices: ASM Handbooks*, ASM International; 2012.
 100. Hallab NJ, Messina C, Skipor A, Jacobs JJ. Differences in the fretting corrosion of metal-metal and ceramic-metal modular junctions of total hip replacements. *Journal of orthopaedic research : official publication of the Orthopaedic Research Society*. 2004;22:250-259.
 101. Hallab NJ, Mikecz K, Vermes C, Skipor A, Jacobs JJ. Orthopaedic implant related metal toxicity in terms of human lymphocyte reactivity to metal-protein complexes produced from cobalt-base and titanium-base implant alloy degradation. *Molecular and cellular biochemistry*. 2001;222:127-136.
 102. Hamilton WG, McAuley JP, Dennis DA, Murphy JA, Blumenfeld TJ, Politi J. THA with Delta ceramic on ceramic: results of a multicenter investigational device exemption trial. *Clinical orthopaedics and related research*. 2010;468:358-366.
 103. Hampton C, Weitzler L, Baral E, Wright TM, Bostrom MPG. Do oxidized zirconium heads decrease tribocorrosion in total hip arthroplasty? A study of retrieved components. *Bone and Joint Journal*. 2019;101 B:386-389.
 104. Harper CA, Petrie EM. *Plastics Materials and Processes: A Concise Encyclopedia*: Wiley; 2003.
 105. Haschke H, Jauch-Matt SY, Sellenschloh K, Huber G, Morlock MM. Assembly force and taper angle difference influence the relative motion at the stem-neck interface of bi-

- modular hip prostheses. *Proceedings of the Institution of Mechanical Engineers, Part H: Journal of Engineering in Medicine*. 2016;230:690-699.
106. Haschke H, Konow T, Huber G, Morlock MM. Influence of flexural rigidity on micromotion at the head-stem taper interface of modular hip prostheses. *Medical engineering & physics*. 2019;68:1-10.
 107. Heckmann ND, Sivasundaram L, Stefl MD, Kang HP, Basler ET, Lieberman JR. Total Hip Arthroplasty Bearing Surface Trends in the United States From 2007 to 2014: The Rise of Ceramic on Polyethylene. *Journal of Arthroplasty*. 2018;33:1757-1763.e1751.
 108. Heiney J, Battula S, Vrabec G, Parikh A, Blice R, Schoenfeld A, Njus G. Impact magnitudes applied by surgeons and their importance when applying the femoral head onto the Morse taper for total hip arthroplasty. *Archives of orthopaedic and trauma surgery*. 2009.
 109. Higgs GB, Hanzlik JA, MacDonald DW, Gilbert JL, Rimnac CM, Kurtz SM. Is increased modularity associated with increased fretting and corrosion damage in metal-on-metal total hip arthroplasty devices?: a retrieval study. *The Journal of arthroplasty*. 2013;28:2-6.
 110. Higgs GB, Hanzlik JA, MacDonald DW, Kane WM, Day JS, Klein GR, Parvizi J, Mont MA, Kraay MJ, Martell JM, Gilbert JL, Rimnac CM, Kurtz SM. Method of characterizing fretting and corrosion at the various taper connections of retrieved modular components from metal-on-metal total hip arthroplasty. In: *ASTM Symposium on Metal-on-Metal Total Hip Replacement Devices, May 8, 2012 - May 8, 2012*. Phoenix, AZ, United states: ASTM International: 2013:146-156.
 111. Higgs GB, MacDonald DW, Gilbert JL, Rimnac CM, Kurtz SM, Implant Research Center Writing C. Does Taper Size Have an Effect on Taper Damage in Retrieved Metal-on-Polyethylene Total Hip Devices? *The Journal of arthroplasty*. 2016;31:277-281.
 112. Hothi HS, Berber R, Whittaker RK, Blunn GW, Skinner JA, Hart AJ. The Relationship Between Cobalt/Chromium Ratios and the High Prevalence of Head-Stem Junction Corrosion in Metal-on-Metal Total Hip Arthroplasty. *Journal of Arthroplasty*. 2016;31:1123-1127.
 113. Hothi HS, Eskelinen AP, Henckel J, Kwon YM, Blunn GW, Skinner JA, Hart AJ. Effect of Bearing Type on Taper Material Loss in Hips From 1 Manufacturer. *Journal of Arthroplasty*. 2018;33:1588-1593.
 114. Hothi HS, Kendoff D, Lausmann C, Henckel J, Gehrke T, Skinner J, Hart A. Clinically insignificant trunnionosis in large-diameter metal-on-polyethylene total hip arthroplasty. *Bone and Joint Research*. 2017;6:52-56.
 115. Hothi HS, Matthies AK, Berber R, Whittaker RK, Skinner JA, Hart AJ. The reliability of a scoring system for corrosion and fretting, and its relationship to material loss of tapered, modular junctions of retrieved hip implants. *The Journal of arthroplasty*. 2014;29:1313-1317.
 116. Huet R, Sakona A, Kurtz SM. Strength and reliability of alumina ceramic femoral heads: Review of design, testing, and retrieval analysis. *Journal of the mechanical behavior of biomedical materials*. 2011;4:476-483.
 117. Hui T, Kubacki GW, Gilbert JL. Voltage and wear debris from Ti-6Al-4V interact to affect cell viability during in-vitro fretting corrosion. *Journal of biomedical materials research. Part A*. 2018;106:160-167.
 118. Huk OL, Bansal M, Betts F, Rimnac CM, Lieberman JR, Huo MH, Salvati EA. Polyethylene and Metal Debris Generated by Non-articulating Surfaces of Modular Acetabular Components. *The Journal of Bone and joint surgery*. 1994;76-B:568-574.

119. Huo MH, Martin RP, Zatorski LE, Keggi KJ. Total hip replacements using the ceramic Mittelmeier prosthesis. *Clinical orthopaedics and related research*. 1996;143-150.
120. Huot Carlson JC, Van Citters DW, Currier JH, Bryant AM, Mayor MB, Collier JP. Femoral stem fracture and in vivo corrosion of retrieved modular femoral hips. *The Journal of arthroplasty*. 2012;27:1389-1396.e1381.
121. Jacobs JJ. Corrosion at the Head-Neck Junction: Why Is This Happening Now? *Journal of Arthroplasty*. 2016;31:1378-1380.
122. Jacobs JJ, Gilbert JL, Urban RM. Corrosion of Metal Orthopaedic Implants*. *Journal of Bone & Joint Surgery - American Volume*. 1998;80:268-282.
123. Jacobs JJ, Hallab NJ. Loosening and osteolysis associated with metal-on-metal bearings: A local effect of metal hypersensitivity? *The Journal of bone and joint surgery. American volume*. 2006;88:1171-1172.
124. Jayasuriya RL, Buckley SC, Hamer AJ, Kerry RM, Stockley I, Tomouk MW, Wilkinson JM. Effect of sliding-taper compared with composite-beam cemented femoral prosthesis loading regime on proximal femoral bone remodeling: a randomized clinical trial. *The Journal of bone and joint surgery. American volume*. 2013;95:19-27.
125. Kao YYJ, Koch CN, Wright TM, Padgett DE. Flexural Rigidity, Taper Angle, and Contact Length Affect Fretting of the Femoral Stem Trunnion in Total Hip Arthroplasty. *Journal of Arthroplasty*. 2016;31:254-258.
126. Kim J, Gilbert JL. Cytotoxic effect of galvanically coupled magnesium-titanium particles. *Acta biomaterialia*. 2016;30:368-377.
127. Kim YH, Park JW, Kim JS. There is no significant difference in fretting and corrosion at the trunnion of metal and ceramic heads. *Orthopedics*. 2019;42:e99-e103.
128. Knahr K, Bohler M, Frank P, Plenk H, Salzer M. Survival analysis of an uncemented ceramic acetabular component in total hip replacement. *Archives of orthopaedic and trauma surgery*. 1987;106:297-300.
129. Kocagöz S, Underwood R, MacDonald D, Day J, Kurtz S. What Is the Clinical Relevance of Visual Inspection of the Head/Stem Taper Junctions in Large Head Metal-on-Metal Hips? In: *American Academy of Orthopedic Surgeons*. New Orleans, LA, USA: 2014.
130. Kocagoz SB, Underwood RJ, MacDonald DW, Gilbert JL, Kurtz SM. Ceramic Heads Decrease Metal Release Caused by Head-taper Fretting and Corrosion. *Clinical orthopaedics and related research*. 2016;474:985-994.
131. Kocagoz SB, Underwood RJ, Sivan S, Gilbert JL, Macdonald DW, Day JS, Kurtz SM. Does Taper Angle Clearance Influence Fretting and Corrosion Damage at the Head-Stem Interface? A Matched Cohort Retrieval Study. *Semin Arthroplasty*. 2013;24:246-254.
132. Koch CN, Figgie M, Jr., Figgie MP, Elpers ME, Wright TM, Padgett DE. Ceramic Bearings with Titanium Adapter Sleeves Implanted During Revision Hip Arthroplasty Show Minimal Fretting or Corrosion: a Retrieval Analysis. *HSS Journal*. 2017;13:241-247.
133. Krull A, Morlock MM, Bishop NE. The Influence of Contamination and Cleaning on the Strength of Modular Head Taper Fixation in Total Hip Arthroplasty. *Journal of Arthroplasty*. 2017;32:3200-3205.
134. Kubacki GW, Gilbert JL. The effect of the inflammatory species hypochlorous acid on the corrosion and surface damage of Ti-6Al-4V and CoCrMo alloys. *Journal of biomedical materials research. Part A*. 2018;106:3185-3194.
135. Kurtz SM, ed. *UHMWPE Biomaterials Handbook: Ultra-High Molecular Weight Polyethylene in Total Joint Replacement and Medical Devices*: Elsevier; 2009.
136. Kurtz SM, ed. *PEEK Biomaterials Handbook*: William Andrew - Elsevier; 2012.

137. Kurtz SM, Devine JN. PEEK biomaterials in trauma, orthopedic, and spinal implants. *Biomaterials*. 2007;28:4845-4869.
138. Kurtz SM, Greenwald S, Lemons J, Mihalko WM, ed. *STP 1301: Modularity of Orthopedic Implants*. West Conshohocken, PA: ASTM International; 1997.
139. Kurtz SM, Greenwald S, Lemons J, Mihalko WM, ed. *STP 1560: Metal-on-Metal Total Hip Replacement Devices*. West Conshohocken, PA: ASTM International; 2013.
140. Kurtz SM, Greenwald S, Lemons J, Mihalko WM, ed. *STP 1591: Modularity and Tapers in Total Joint Replacement Devices* West Conshohocken, PA: ASTM International; 2015.
141. Kurtz SM, Greenwald S, Lemons JE, Mihalko WM, ed. *STP 1606: Beyond the Implant - Retrieval Analysis Methods for Implant Surveillance* West Conshohocken, PA: ASTM International; 2018.
142. Kurtz SM, Kocagoz S, Arnholt C, Huet R, Ueno M, Walter WL. Advances in zirconia toughened alumina biomaterials for total joint replacement. *Journal of the mechanical behavior of biomedical materials*. 2014;31:107-116.
143. Kurtz SM, Kocagoz SB, Hanzlik JA, Underwood RJ, Gilbert JL, MacDonald DW, Lee GC, Mont MA, Kraay MJ, Klein GR, Parvizi J, Rimnac CM. Do ceramic femoral heads reduce taper fretting corrosion in hip arthroplasty? A retrieval study. *Clinical orthopaedics and related research*. 2013;471:3270-3282.
144. Kurtz SM, MacDonald DW, Gilbert JL, Mont MA, Klein G, Chen A, Kraay M, Hamlin B, Rimnac CM. Is Taper Fretting Corrosion a Threat to the Clinical Performance of Large-Diameter Hips with Highly Crosslinked Polyethylene Bearings? In: Greenwald S, Kurtz SM, ed. *STP1591: Modularity and Tapers in Total Joint Replacement Devices*. West Conshohocken, PA: ASTM International; 2015.
145. Kurtz SM, MacDonald DW, Kocagoz S, Tohfafarosh M, Baykal D. Can pin-on-disk testing be used to assess the wear performance of retrieved UHMWPE components for total joint arthroplasty? *BioMed research international*. 2014;2014:581812.
146. Kurtz SM, Ong KL, Schmier J, Mowat F, Saleh K, Dybvik E, Karrholm J, Garellick G, Havelin LI, Furnes O, Malchau H, Lau E. Future clinical and economic impact of revision total hip and knee arthroplasty. *The Journal of bone and joint surgery. American volume*. 2007;89 Suppl 3:144-151.
147. Laaksonen I, Donahue GS, Madanat R, Makela KT, Malchau H. Outcomes of the Recalled Articular Surface Replacement Metal-on-Metal Hip Implant System: A Systematic Review. *The Journal of arthroplasty*. 2017;32:341-346.
148. Lancaster JG, Dowson D, Isaac GH, Fisher J. The wear of ultra-high molecular weight polyethylene sliding on metallic and ceramic counterfaces representative of current femoral surfaces in joint replacement. *Proceedings of the Institution of Mechanical Engineers. Part H, Journal of engineering in medicine*. 1997;211:17-24.
149. Langlois J, El Hage S, Madi F, Courpied JP, Kerboull M, Hamadouche M. Charnley-Kerboull total hip arthroplasty combining zirconia on polyethylene. A minimum eight-year follow-up prospective study. *International orthopaedics*. 2013;37:355-360.
150. Langton D, Ahmed I, Avery P, Bone M, Cooke N, Deehan D, Duffy P, Foguet P, Green S, Holland J, Jafri A, Longstaff L, Lord J, Loughhead J, Meek RMD, Murray H, Nanu A, Nargol AVF, Scholes SC, Sidaginamale RP, Waller S, Joyce T. Investigation of Taper Failure in a Contemporary Metal-on-Metal Hip Arthroplasty System Through Examination of Unused and Explanted Prostheses. *Journal of Bone and Joint Surgery-American Volume*. 2017;99:427-436.

151. Langton DJ, Jameson SS, Joyce TJ, Gandhi JN, Sidaginamale R, Mereddy P, Lord J, Nargol AV. Accelerating failure rate of the ASR total hip replacement. *The Journal of bone and joint surgery. British volume.* 2011;93:1011-1016.
152. Langton DJ, Sidaginamale R, Lord JK, Nargol AV, Joyce TJ. Taper junction failure in large-diameter metal-on-metal bearings. *Bone & joint research.* 2012;1:56-63.
153. Langton DJ, Wells SR, Joyce TJ, Bowsher JG, Deehan D, Green S, Nargol AVF, Holland JP. Material loss at the femoral head taper: a comparison study of the Exeter metal-on-polyethylene and contemporary metal-on-metal total hip arthroplasty. *The bone & joint journal.* 2018;100-B:1310-1319.
154. Laux KA, Schwartz CJ. Influence of linear reciprocating and multi-directional sliding on PEEK wear performance and transfer film formation. *Wear.* 2013;301:727-734.
155. Lavernia CJ, Baerga L, Barrack RL, Tozakoglou E, Cook SD, Lata L, Rossi MD. The effects of blood and fat on Morse taper disassembly forces. *American journal of orthopedics (Belle Mead, N.J.).* 2009;38:187-190.
156. Levine B, Della Valle CJ, Jacobs JJ. Applications of porous tantalum in total hip arthroplasty. *The Journal of the American Academy of Orthopaedic Surgeons.* 2006;14:646-655.
157. Levine BR, Sporer S, Poggie RA, Della Valle CJ, Jacobs JJ. Experimental and clinical performance of porous tantalum in orthopedic surgery. *Biomaterials.* 2006;27:4671-4681.
158. Liang B, Kawanabe K, Ise K, Iida H, Nakamura T. Polyethylene wear against alumina and zirconia heads in cemented total hip arthroplasty. *The Journal of arthroplasty.* 2007;22:251-257.
159. Lieberman JR, Rimnac CM, Garvin KL, Klein RW, Salvati EA. An analysis of the head-neck taper interface in retrieved hip prostheses. *Clinical orthopaedics and related research.* 1994:162-167.
160. Lim S-JMD, Jang S-PMD, Kim D-WMD, Moon Y-WMD, Park Y-SMDa. Primary Ceramic-on-ceramic Total Hip Arthroplasty Using a 32-mm Ceramic Head With a Titanium-alloy Sleeve. *Clinical Orthopaedics & Related Research.* 2015;473:3781-3787.
161. Lombardi AV, Jr., Mallory TH, Vaughn BK, Drouillard P. Aseptic loosening in total hip arthroplasty secondary to osteolysis induced by wear debris from titanium-alloy modular femoral heads. *The Journal of bone and joint surgery. American volume.* 1989;71:1337-1342.
162. Lundberg HJ, Ha NQ, Hall DJ, Urban RM, Levine BR, Pourzal R. Contact mechanics and plastic deformation at the local surface topography level after assembly of modular head-neck junctions in modern total hip replacement devices. In: *ASTM Special Technical Publication.* 2015:59-82.
163. MacDonald DW, Chen AF, Lee GC, Klein GR, Mont MA, Kurtz SM, Taper Corrosion Writing C, Cates HE, Kraay MJ, Rimnac CM. Fretting and Corrosion Damage in Taper Adapter Sleeves for Ceramic Heads: A Retrieval Study. *The Journal of arthroplasty.* 2017;32:2887-2891.
164. Mali SA. MECHANICALLY ASSISTED CORROSION PERFORMANCE OF METALLIC BIOMATERIALS: IMPLANT RETRIEVAL, MATERIAL ANALYSES AND DEVICE TESTING. Syracuse University; 2015.
165. Mali SA, Gilbert JL. Correlating fretting corrosion and micromotions in modular tapers: Test method development and assessment. In: *ASTM Special Technical Publication.* 2015:259-282.

166. Martin AJ, Jenkins DR, Van Citters DW. Role of corrosion in taper failure and head disassociation in total hip arthroplasty of a single design. *Journal of Orthopaedic Research*. 2018;36:2996-3003.
167. Martin AJ, McGrory BJ, Edidin AA, Van Citters DW. Using coordinate measuring machine validated with white light interferometry to identify contributors to material loss due to corrosion of total hip replacement modular junctions. In: *ASTM Special Technical Publication*. 2018:118-130.
168. Masonis JL, Bourne RB, Ries MD, McCalden RW, Salehi A, Kelman DC. Zirconia femoral head fractures: a clinical and retrieval analysis. *The Journal of arthroplasty*. 2004;19:898-905.
169. Mathew MT, Patel M, Royhman D, Runa M, Jacobs J, Wimmer MA, Hallab NJ. Tribocorrosion in hip modular taper junctions: Load-triggered transitions in electrochemical and mechanical behavior. In: *ASTM Special Technical Publication*. 2015:283-302.
170. Mathew MT, Patel M, Royhman D, Runa MJ, Jacobs JJ, Wimmer MA, Hallab NJ. Tribocorrosion in Hip Modular Taper Junctions: Load-Triggered Transitions in Electrochemical and Mechanical Behavior. In: Greenwald S, Kurtz SM, ed. *STP1591: Modularity and Tapers in Total Joint Replacement Devices*. West Conshohocken, PA: ASTM International; 2015.
171. Mathiesen EB, Lindgren JU, Blomgren GG, Reinholt FP. Corrosion of modular hip prostheses. *The Journal of bone and joint surgery. British volume*. 1991;73:569-575.
172. Matthies A, Underwood R, Cann P, Ilo K, Nawaz Z, Skinner J, Hart AJ. Retrieval analysis of 240 metal-on-metal hip components, comparing modular total hip replacement with hip resurfacing. *The Journal of bone and joint surgery. British volume*. 2011;93:307-314.
173. Matthies AK, Racasan R, Bills P, Blunt L, Cro S, Panagiotidou A, Blunn G, Skinner J, Hart AJ. Material loss at the taper junction of retrieved large head metal-on-metal total hip replacements. *Journal of orthopaedic research : official publication of the Orthopaedic Research Society*. 2013;31:1677-1685.
174. McKellop HA, Sarmiento A, Brien W, Park SH. Interface corrosion of a modular head total hip prosthesis. *The Journal of arthroplasty*. 1992;7:291-294.
175. Medel FJ, Shah P, Kurtz SM. Retrieval Analysis of Contemporary Alternative Femoral Head Materials: Oxinium and Biolox Delta. In: *Orthopedic Research Society*. 2009.
176. Mendenhall S. 2014 Hip and Knee Implant Review. *Orthopedic Network News*. 2014;25.
177. Mendenhall S. Hospital resources and implant cost management—a 2013 update. *Orthopedic Network News*. 2014;25:9-15.
178. Meneghini RM, Hallab NJ, Jacobs JJ. Evaluation and treatment of painful total hip arthroplasties with modular metal taper junctions. *Orthopedics*. 2012;35:386-391.
179. Meyer H, Mueller T, Goldau G, Chamaon K, Ruetschi M, Lohmann CH. Corrosion at the cone/taper interface leads to failure of large-diameter metal-on-metal total hip arthroplasties. *Clinical orthopaedics and related research*. 2012;470:3101-3108.
180. Miller MA, Goodheart JR, Izant TH, Rimnac CM, Cleary RJ, Mann KA. Loss of cement-bone interlock in retrieved tibial components from total knee arthroplasties. *Clinical orthopaedics and related research*. 2014;472:304-313.
181. Miller MA, Terbush MJ, Goodheart JR, Izant TH, Mann KA. Increased initial cement-bone interlock correlates with reduced total knee arthroplasty micro-motion following in vivo service. *Journal of biomechanics*. 2014;47:2460-2466.

182. Moharrami N, Langton DJ, Sayginer O, Bull SJ. Why does titanium alloy wear cobalt chrome alloy despite lower bulk hardness: a nanoindentation study? *Thin Solid Films*. 2013.
183. Morlock MM, Dickinson EC, Günther KP, Bunte D, Polster V. Head Taper Corrosion Causing Head Bottoming Out and Consecutive Gross Stem Taper Failure in Total Hip Arthroplasty. *Journal of Arthroplasty*. 2018;33:3581-3590.
184. Nassif NA, Nawabi DH, Stoner K, Elpers M, Wright T, Padgett DE. Taper Design Affects Failure of Large-head Metal-on-metal Total Hip Replacements. *Clinical orthopaedics and related research*. 2013.
185. Nassif NA, Nawabi DH, Stoner K, Elpers M, Wright T, Padgett DE. Taper design affects failure of large-head metal-on-metal total hip replacements. *Clinical orthopaedics and related research*. 2014;472:564-571.
186. Nassif NAMDa, Nawabi DHMD, Stoner KM, Elpers MBS, Wright TP, Padgett DEMD. Taper Design Affects Failure of Large-head Metal-on-metal Total Hip Replacements. *Clinical Orthopaedics & Related Research*. 2014;472:564-571.
187. Norman TL, Denen JE, Land AJ, Kienitz DM, Fehring TA. Taper-Trunnion Interface Stress Varies Significantly With Head Size and Activity. *Journal of Arthroplasty*. 2019;34:157-162.
188. Oonishi H, Kim SC, Kyomoto M, Iwamoto M, Ueno M. PE wear in ceramic/PE bearing surface in total knee arthroplasty: Clinical experiences of more than 24 years. In: Francesco Benazzo FF, Martin Dietrich, ed. *Bioceramics and Alternative Bearings in Joint Arthroplasty: 11th BIOLOX Symposium Proceedings*: Springer Science and Business Media; 2006:101-110.
189. Ouellette ES, Gilbert JL. Production and characterization of melt-spun Poly(Ether Ether Ketone) fibers for biomedical applications. *Polymer*. 2015;63:10-18.
190. Ouellette ES, Gilbert JL. Properties and Corrosion Performance of Self-reinforced Composite PEEK for Proposed Use as a Modular Taper Gasket. *Clinical Orthopaedics and Related Research*. 2016;474:2414-2427.
191. Ouellette ES, Mali SA, Kim J, Grostefon J, Gilbert JL. Design, Material, and Seating Load Effects on In Vitro Fretting Corrosion Performance of Modular Head-Neck Tapers. *The Journal of arthroplasty*. 2019;34:991-1002.
192. Ouellette ES, Shenoy AA, Gilbert JL. The seating mechanics of head-neck modular tapers in vitro: Load-displacement measurements, moisture, and rate effects. *Journal of Orthopaedic Research*. 2018;36:1164-1172.
193. Panagiotidou A, Cobb T, Meswania J, Skinner J, Hart A, Haddad F, Blunn G. Effect of impact assembly on the interface deformation and fretting corrosion of modular hip tapers: An in vitro study. *Journal of Orthopaedic Research*. 2018;36:405-416.
194. Panagiotidou A, Meswania J, Hua J, Muirhead-Allwood S, Hart A, Blunn G. Enhanced wear and corrosion in modular tapers in total hip replacement is associated with the contact area and surface topography. *Journal of orthopaedic research : official publication of the Orthopaedic Research Society*. 2013;31:2032-2039.
195. Panayotov IV, Orti V, Cuisinier F, Yachouh J. Polyetheretherketone (PEEK) for medical applications. *Journal of materials science. Materials in medicine*. 2016;27:118.
196. Panigrahi P, Liao Y, Mathew MT, Fischer A, Wimmer MA, Jacobs JJ, Marks LD. Intergranular pitting corrosion of CoCrMo biomedical implant alloy. *Journal of biomedical materials research. Part B, Applied biomaterials*. 2014;102:850-859.

197. Pennock AT, Schmidt AH, Bourgeault CA. Morse-type tapers: factors that may influence taper strength during total hip arthroplasty. *The Journal of arthroplasty*. 2002;17:773-778.
198. Pezzotti G, Saito T, Padeletti G, Cossari P, Yamamoto K. Nano-scale topography of bearing surface in advanced alumina/zirconia hip joint before and after severe exposure in water vapor environment. *Journal of orthopaedic research : official publication of the Orthopaedic Research Society*. 2010;28:762-766.
199. Piconi C, Maccauro G. Zirconia as a ceramic biomaterial. *Biomaterials*. 1999;20:1-25.
200. Pierre D, Swaminathan V, Scholl LY, TenHuisen K, Gilbert JL. Effects of Seating Load Magnitude on Incremental Cyclic Fretting Corrosion in 5degree40' Mixed Alloy Modular Taper Junctions. *Journal of Arthroplasty*. 2018;33:1953-1961.
201. Plummer DR, Berger RA, Paprosky WG, Sporer SM, Jacobs JJ, Della Valle CJ. Diagnosis and Management of Adverse Local Tissue Reactions Secondary to Corrosion at the Head-Neck Junction in Patients With Metal on Polyethylene Bearings. *The Journal of arthroplasty*. 2016;31:264-268.
202. Porter DA, Urban RM, Jacobs JJ, Gilbert JL, Rodriguez JA, Cooper HJ. Modern trunnions are more flexible: a mechanical analysis of THA taper designs. *Clinical orthopaedics and related research*. 2014;472:3963-3970.
203. Pourzal R, Hall DJ, Ehrich J, McCarthy SM, Mathew MT, Jacobs JJ, Urban RM. Alloy Microstructure Dictates Corrosion Modes in THA Modular Junctions. *Clinical orthopaedics and related research*. 2017;475:3026-3043.
204. Pourzal R, Hall DJ, Ha NQ, Urban RM, Levine BR, Jacobs JJ, Lundberg HJ. Does Surface Topography Play a Role in Taper Damage in Head-neck Modular Junctions? *Clinical Orthopaedics and Related Research*. 2016;474:2232-2242.
205. Pourzal R, Lundberg HJ, Hall DJ, Jacobs JJ. What Factors Drive Taper Corrosion? *Journal of Arthroplasty*. 2018;33:2707-2711.
206. Pruitt LA, Chakravartula AM. *Mechanics of Biomaterials: Fundamental Principles for Implant Design*. Cambridge University Press; 2011.
207. Randall NX. Tribological Characterization of Biomaterials. In: Narayan R, ed. *ASM Handbook, Volume 23: Materials for Medical Devices*: ASM International; 2012.
208. Rehmer A, Bishop NE, Morlock MM. Influence of assembly procedure and material combination on the strength of the taper connection at the head-neck junction of modular hip endoprostheses. *Clinical biomechanics (Bristol, Avon)*. 2012;27:77-83.
209. Rodrigues DC, Urban RM, Jacobs JJ, Gilbert JL. In vivo severe corrosion and hydrogen embrittlement of retrieved modular body titanium alloy hip-implants. *Journal of biomedical materials research. Part B, Applied biomaterials*. 2009;88:206-219.
210. Roualdes O, Duclos ME, Gutknecht D, Frappart L, Chevalier J, Hartmann DJ. In vitro and in vivo evaluation of an alumina-zirconia composite for arthroplasty applications. *Biomaterials*. 2010;31:2043-2054.
211. Santavirta S, Bohler M, Harris WH, Konttinen YT, Lappalainen R, Muratoglu O, Rieker C, Salzer M. Alternative materials to improve total hip replacement tribology. *Acta orthopaedica Scandinavica*. 2003;74:380-388.
212. Santos EM, Vohra S, Catledge SA, McClenny MD, Lemons J, Moore KD. Examination of surface and material properties of explanted zirconia femoral heads. *The Journal of arthroplasty*. 2004;19:30-34.
213. Shenoy AA, Gilbert JL. In vitro test methods for seating and fretting corrosion behavior of modular metal-on-metal acetabular tapers. *Journal of orthopaedic research : official publication of the Orthopaedic Research Society*. 2020;38:1089-1100.

214. Sheth NP, Lementowski P, Hunter G, Garino JP. Clinical applications of oxidized zirconium. *J Surg Orthop Adv*. 2008;17:17-26.
215. Shikata T, Oonishi H, Hashimoto Y. Wear Resistance of irradiated UHMW polyethylenes to Al₂O₃ ceramics in total hip prostheses. In: *Third Annual Meeting of the Society for Biomaterials*. 1977.
216. Siljander MP, Baker EA, Baker KC, Salisbury MR, Thor CC, Verner JJ. Fretting and Corrosion Damage in Retrieved Metal-on-Polyethylene Modular Total Hip Arthroplasty Systems: What Is the Importance of Femoral Head Size? *Journal of Arthroplasty*. 2018;33:931-938.
217. Siljander MP, Gehrke CK, Wheeler SD, Sobh AH, Moore DD, Flierl MA, Baker EA. Does Taper Design Affect Taper Fretting Corrosion in Ceramic-on-Polyethylene Total Hip Arthroplasty? A Retrieval Analysis. *Journal of Arthroplasty*. 2019;34:S366-S372.e362.
218. Siskey R, Ciccarelli L, Lui MK, Kurtz SM. Are PEEK-on-Ceramic Bearings an Option for Total Disc Arthroplasty? An In Vitro Tribology Study. *Clinical orthopaedics and related research*. 2016;474:2428-2440.
219. Sivan S, Rahman E, Weaver JD, Di Prima M. Comparison of ASTM F2129 and ASTM F746 for Evaluating Crevice Corrosion. *Journal of Testing and Evaluation*. 2019;47.
220. Sommer F, Landfried R, Kern F, Gadow R. Mechanical properties of zirconia toughened alumina with 10–24 vol% 1Y-TZP reinforcement. *Journal of the European Ceramic Society*. 2012;32:4177-4184.
221. Songur M, Calikkan H, Gokmese F, Simsek SA, Altun NS, Aksu ML. Electrochemical corrosion properties of metal alloys used in orthopaedic implants. *J Appl Electrochem*. 2009;39:1259–1265.
222. Stachowiak GW. 10. Fundamentals of Contact Between Solids. *Engineering Tribology*; 2014.
223. Stachowiak GW, Batchelor AW. 15. Fretting and Minor Wear Mechanisms. *Engineering Tribology*; 2014.
224. *The Seventh Annual Report of the American Joint Replacement Registry on Hip and Knee Arthroplasty*, 2020.
225. Swaminathan V. FRETTING CREVICE CORROSION OF METALLIC BIOMATERIALS: INSTRUMENT DEVELOPMENT AND MATERIALS ANALYSIS. *Biomedical and Chemical Engineering*. Syracuse, NY, USA: Syracuse University; 2012:224.
226. Swaminathan V, Gilbert JL. Fretting corrosion of CoCrMo and Ti6Al4V interfaces. *Biomaterials*. 2012;33:5487-5503.
227. Syrett BC, Acharya A, ed. *STP 684: Corrosion and Degradation of Implant Materials*. Philadelphia, PA: American Society for Testing and Materials; 1978.
228. Tan SC, Lau ACL, Del Balso C, Howard JL, Lanting BA, Teeter MG. Tribocorrosion: Ceramic and Oxidized Zirconium vs Cobalt-Chromium Heads in Total Hip Arthroplasty. *Journal of Arthroplasty*. 2016;31:2064-2071.
229. Tan SC, Teeter MG, Del Balso C, Howard JL, Lanting BA. Effect of Taper Design on Trunnionosis in Metal on Polyethylene Total Hip Arthroplasty. *The Journal of arthroplasty*. 2015;30:1269-1272.
230. Tateiwa T, Clarke IC, Williams PA, Garino J, Manaka M, Shishido T, Yamamoto K, Imakiire A. Ceramic total hip arthroplasty in the United States: safety and risk issues revisited. *American journal of orthopedics (Belle Mead, N.J.)*. 2008;37:E26-31.
231. The National Joint Registry [NJR] for England W, Northern Ireland and the Isle of Man. *National Joint Registry 15th Annual Report 2018*.
232. Thomas TR. *Rough Surfaces*: Imperial College Press; 1999.

233. Tkaczyk C, Tabrizian M. Biocompatibility, Metals Ions, and Corrosion Products. In: Narayan R, ed. *ASM Handbook, Volume 23: Materials for Medical Devices*: ASM International; 2012.
234. Tomlinson GA, Thorpe PL, Gough HJ. An Investigation of the Fretting Corrosion of Closely Fitting Surfaces. *Proceedings of the Institution of Mechanical Engineers*. 1939;141:223-249.
235. Underwood RJ, Fowell M, Sayles RS, Kurtz SM, PM C. *The Development of a Standard Method for Assessing Wear of Explanted Metal-on-Metal Hip Joints*. West Conshohoken, PA: American Society for Testing and Materials,; 2013.
236. Underwood RJ, Kocagoz SB, Smith R, Sayles RS, Siskey R, Kurtz SM, Cann PM. A Protocol to Assess the Wear of Head/Neck Taper Junctions in Large Head Metal-on-Metal (LHMoM) Hips. In: Kurtz SM, Greenwald AS, Mihalko WM, Lemons JE, ed. *Metal-on-Metal Total Hip Replacement Devices*; 2013:209-234.
237. Underwood RJ, Kocagoz SB, Smith R, Sayles RS, Siskey R, Kurtz SM, Cann PM. A protocol to assess the wear of head/neck taper junctions in large head metal-on-metal (LHMoM) hips. In: *ASTM Symposium on Metal-on-Metal Total Hip Replacement Devices, May 8, 2012 - May 8, 2012*. Phoenix, AZ, United states: ASTM International: 2013:209-234.
238. Urban RM, Gilbert JL, Jacobs JJ. Corrosion of modular titanium alloy stems in cementless hip replacement. *Journal of ASTM International*. 2005;2:357-366.
239. Urish KL, Hamlin BR, Plakseychuk AY, Levison TJ, Higgs GB, Kurtz SM, DiGioia AM. Trunnion Failure of the Recalled Low Friction Ion Treatment Cobalt Chromium Alloy Femoral Head. *The Journal of arthroplasty*. 2017;32:2857-2863.
240. Van Citters DW, Martin AJ, Currier JH, Park SH, Edidin AA. Factors Related to Imprinting Corrosion in Modular Head-Neck Junctions. In: Greenwald AS, Kurtz SM, Lemons JE, Mihalko WM, ed. *Modularity and Tapers in Total Joint Replacement Devices*; 2015:83-98.
241. Vingsbo O, Soderberg S. On Fretting Maps. *Wear*. 1988;126:131-147.
242. Walton K, Petrucci M, Racasan R, Blunt L, Hart A, Bills P. Focus variation measurement and advanced analysis of volumetric loss at the femoral head taper interface of retrieved modular replacement hips in replica. In: *Journal of Physics: Conference Series*. 2019.
243. Waly F, Abduljabbar FH, Gascoyne T, Turgeon TR, Huk O. Stem-Sleeve Junction Failure of a Modular Femoral Hip System: a Retrieval Analysis. *HSS Journal*. 2015;11:285-290.
244. Wang Q, Eltit F, Garbuz D, Duncan C, Masri B, Greidanus N, Wang R. CoCrMo metal release in metal-on-highly crosslinked polyethylene hip implants. *Journal of Biomedical Materials Research - Part B Applied Biomaterials*. 2020;108:1213-1228.
245. Wauthle R, van der Stok J, Amin Yavari S, Van Humbeeck J, Kruth JP, Zadpoor AA, Weinans H, Mulier M, Schrooten J. Additively manufactured porous tantalum implants. *Acta biomaterialia*. 2015;14:217-225.
246. Weiser MCDMa, Lavernia CJMDb. Trunnionosis in Total Hip Arthroplasty. *Journal of Bone & Joint Surgery - American Volume*. 2017;99:1489-1501.
247. Whittaker RK, Hothi HS, Eskelinen A, Blunn GW, Skinner JA, Hart AJ. Variation in taper surface roughness for a single design effects the wear rate in total hip arthroplasty. *Journal of Orthopaedic Research*. 2017;35:1784-1792.
248. Whittaker RK, Hothi HS, Meswania JM, Berber R, Blunn GW, Skinner JA, Hart AJ. The effect of using components from different manufacturers on the rate of wear and corrosion of the head–stem taper junction of metal-on-metal hip arthroplasties. *Bone and Joint Journal*. 2016;98B:917-924.

249. Wiegand MJ, Shenoy AA, Littlejohn SE, Gilbert JL. Sensing Localized Surface Corrosion Damage of CoCrMo Alloys and Modular Tapers of Total Hip Retrievals Using Nearfield Electrochemical Impedance Spectroscopy. *ACS Biomaterials Science & Engineering*. 2020;6:1344-1354.
250. Williams RL, Brown SA, Merritt K. Electrochemical studies on the influence of proteins on the corrosion of implant alloys. *Biomaterials*. 1988;9:181-186.

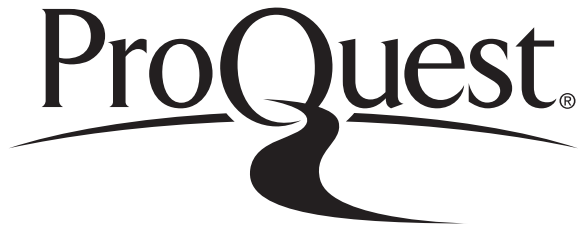
ProQuest Number:28022700

All rights reserved

INFORMATION TO ALL USERS

The quality of this reproduction is dependent on the quality of the copy submitted.

In the unlikely event that the author did not send a complete manuscript and there are missing pages, these will be noted. Also, if material had to be removed, a note will indicate the deletion.



ProQuest 28022700

Published by ProQuest LLC (2021). Copyright of the Dissertation is held by the Author.

All Rights Reserved.

This work is protected against unauthorized copying under Title 17, United States Code
Microform Edition © ProQuest LLC.

ProQuest LLC
789 East Eisenhower Parkway
P.O. Box 1346
Ann Arbor, MI 48106 - 1346